Raman, Infrared, X-ray, and EELS Studies of Nanophase Titania

Reinaldo J. Gonzalez

Dissertation submitted to the Faculty of the Virginia Polytechnic Institute and State University in partial fulfillment of the requirements for the degree of

Doctor of Philosophy
in
Physics

Richard Zallen, Chair
Richey M. Davis
James R. Heflin
Guy Indebetouw
Alfred Ritter

July 26, 1996
Blacksburg, Virginia

Keywords: Titania, Raman, Infrared, Nanocrystals, Phase Transitions, Anatase

Raman, Infrared, X-ray, and, EELS Studies of Nanophase Titania

Reinaldo J. Gonzalez

(ABSTRACT)

Sol-gel titania particles were investigated, primarily by optical techniques, by systematically varying synthesis, sample handling, and annealing variables. The material phases investigated were amorphous titania, anatase TiO_2, and rutile TiO_2. Annealing-induced phase transformations from amorphous TiO_2 to anatase to rutile were studied by Raman scattering, infrared reflectivity, infrared absorption, x-ray diffraction, and electron energy-loss spectroscopy (EELS). Detailed experiments were carried out on the effects of annealing on the Raman and infrared spectra of anatase nanocrystals. The frequencies of the zone-center transverse optical (TO) and longitudinal-optical (LO) phonons of anatase were determined and were used in analyzing the results obtained on composites consisting of annealed sol-gel particles

The TO and LO frequencies of anatase were obtained from polarization-dependent far-infrared reflectivity measurements on single crystals. These results, which determined the dielectric functions of anatase, were used to explain infrared (IR) reflectivity spectra of titania nanoparticles pressed into pellets, as well as the grazing-incidence IR reflectivity observed for titania thin films. Because of the polycrystalline character of the titania nanoparticles, the surface roughness of the pressed pellets, and the island-structure character of the thin films, effective-medium theories (appropriate for composites) were used, along with the anatase dielectric functions, to interpret the experimental results.

The titania nanoparticles were prepared by the hydrolysis/condensation of $Ti(OC_2H_5)_4$. A polymeric steric stabilizer was used in the sol-gel synthesis in order to prevent continued agglomeration during the condensation process. This yielded particles with a relatively narrow size distribution. The amount of water used in the reaction determines the final particle size. Particles as small as 80 nm and as large as 300 nm were used throughout this work. From the colloidal suspension, loose powders, pressed pellets, and thin films were formed. These samples were subjected to different annealing processes at temperatures ranging from room temperature up to 1000°C. Two different annealing atmospheres were used: air (oxygen-containing) and argon (no oxygen).

The amorphous to anatase transformation was followed by in-situ IR transmission measurements carried out during annealing. The particles as prepared are amorphous and the anatase phase could be detected, using this sensitive IR technique, at temperatures as low as 150°C. This phase transition was shown to be particle size dependent. It was also shown that

introducing the stabilizer by means of the alkoxide flask instead of the water flask (during the sol-gel synthesis) decreases the anatase to rutile transformation temperature. Loose powders were found to transform more readily than dense pellets, while island-structure films were found to be the hardest to transform. Even at 1000°C, most of these films did not transform to rutile.

X-ray diffraction experiments were used to determine nanocrystal sizes in anatase samples obtained by air and argon anneals at temperatures from 300 to 800°C. A correlation was found between Raman band shape (peak position and linewidth) and crystallite size, but this correlation was different for air anneals and for argon anneals. These experiments called for an interpretation based on a stoichiometric effect rather than a finite size effect. Based on this interpretation, the as-prepared particles are slightly oxygen-deficient, with a stoichiometry corresponding to $TiO_{1.98}$.

In the electron energy-loss experiments, a special data-analysis technique was used to extract the EELS spectrum of the titania nanoparticles from the observed substrate-plus-particles signal. This technique successfully resolved the titania absorption-edge peak. Which was found to be momentum independent. For low electron momentum, the results were consistent with the reported optical absorption edge.

Dedication

To my dearest wife and children:
Gladys, Diana, Andrea, and Camille.

Acknowledgments

First and foremost, I would like to thank to our Father in Heavens for all His support and guidance during these years. To my wife and my kids (Mi Gatita, Dianita, Andrea, and Camille). Gladys, I cannot thank you enough for all your patience and understanding and taken care of me and our growing family all these years. "Tu amor y tu afecto me han ayudado a culminar con este trabajo. He sido afortunado de tenerte de companiera de mi vida". And to my little ones, thank you for your patience and love to your dad. This thesis is for you, my dear family.

I am grateful to my advisor, Prof. Richard Zallen, whose guidance and insightful suggestions made this work meaningful and a success. To Prof. Rick Davis and Prof. Jimmy Ritter for always having the time needed to help me understand sol-gel processes and the propagation of electron through matter. Thanks a lot for your patience.

I would also like to express my sincere thanks to Francis Webster for introducing me to the field of infrared spectroscopy, and mostly for becoming such a great friend; and to Anne Gaynor for introducing me to the field of sol-gel chemistry. To Calvin Doss another great friend and co-worker.

Millions of thanks to Dale Schut, Roger Link and Grayson Wright, of the electronic shop, and Bob Ross, Melvin Shaver, and Dave Miller, of the machine shop for their outstanding technical support.

I would like to thank as well to Dr. Girma Biresaw for his guidance and encouragement while an intern at Alcoa Technical Center. To Dr. Richard Hoffman of the Alcoa Technical Center for depositing the alumina films on the salt and platinum substrates. These films made possible the electron energy-loss experiments. Special thanks to Vidhu Nagpal for providing the continuous titania film.

I am grateful to Helmut Berger to providing the anatase single crystal, to Brenda Kutz of the Dept. of Geological Sciences for her help in orienting, cutting, and polishing the anatase crystals. To Prof. R. J. Bodnar for making the Dilor XY Raman spectrometer available to us and to Frank Harrison for helping us with the use. I also thank T. N. Solberg for very valuable help with the x-ray experiments and Dr. G. Chen for the TEM work.

I would like to thank my father and mother, Cesar Aurelio and Dolores Catalina, for giving me the freedom and support in choosing a non-conventional career. He is a very hard working man and I have always been inspired by his enthusiasm and dedication to work. "Papi, Mami, gracias por siempre apoyarme en mi carrera. Xavito, Monica, Charito, Anita Lucia, y Katita gracias por sus oraciones y por cuidar de nuestros padres".

Table of Contents

List of Figures

List of Tables

CHAPTER ONE

1. INTRODUCTION

1.1 Introductory Remarks

Sol-gel technology is a method to synthesize nanophase metal oxide particles in a colloidal suspension. Primary concerns in this process are the control of the size, the chemical composition, and the microstructure of the ultrafine particles. For application purposes, these particles are handled as powders, pellets, and thin films, and they are subject to a variety of heat treatments. Many efforts have been sought to produce small particles with controlled size and shape owing to their optical, electronic, and densification properties for their use as thin films, ceramics, composites, and catalysts. The sol-gel process can be varied through changes in solution chemistry and stabilization techniques to produce the desired particle morphologies. Sol-gel processes are very complex and only partially understood.[1]

The aim of this dissertation was to contribute to the understanding of the effects of the different parameters involved in the synthesis and the sample-handling steps, especially the effects on particle properties after experiencing different annealing processes. Throughout these annealing steps, the samples were characterized in several ways: (1) Their surface appearance and agglomeration state were studied by electron microscopy, (2) Their internal structure (crystallite size, phases present) was studied by infrared spectroscopy, x-ray diffraction and Raman scattering, and (3) Their optical properties (from 20 meV to 20 eV) were studied by infrared (IR) absorption, infrared reflectivity, and electron-energy loss spectroscopy (EELS). The metal oxide investigated in this work is titania (TiO_2). Titania is a highly ionic compound with interesting properties that make it useful for many applications. Among its properties are polymorphism (three crystal phases coexist at ordinary conditions), high dielectric constant, transparency in the visible, and complete non-toxicity. Among its uses are as a white pigment (more than 10^9 kg/year is made for print), as a whitener additive to toothpaste, as an ultraviolet-absorbing optical filter, and as a dielectric in thin-film capacitors. The last-mentioned application is potentially very important for future microelectronics, because miniaturization may require thinner dielectric films and TiO_2 (with its high dielectric constant) is being considered as a candidate to replace the silicon oxide and silicon nitride films that are currently used.

In this chapter, the sol-gel synthesis mechanism will be reviewed, stressing the parameters that are believed to control the particle morphology and aggregation state. Besides these titania nanoparticles and the annealed powders, pellets and films formed from them, bulk anatase (one of the crystal phases of titania) crystals were characterized in the far-infrared region, the region where the optical phonons are active. This information was previously unavailable for single-crystal anatase, and it is needed to understand the optical properties of the sol-gel nanoparticles. For that work, which involves the use of the complex dielectric function for characterizing the IR optical properties, an analysis procedure (called the

factorized form for the dielectric function) was used which is different from the usual analysis for highly ionic crystals, and background about it is included in this chapter. Spin-coated thin films were prepared for this study from the colloidal suspensions, and these films were found to have an island-structure character. The infrared spectra of these films are affected by their surface quality and morphology. To understand these results, it was necessary to use a recently developed version of the effective medium approximation. The effective medium approximation is a mathematical technique for estimating the dielectric function of a nanocomposite (in our case, an air/titania nanocomposite) from the dielectric function of the individual components. A brief review of this theory is presented.
The use of Raman scattering, as a technique for identifying amorphous and crystalline phases and for revealing finite-size (nanocrystallinity-induced) and stoichiometry effects, is also briefly reviewed.

1.2 Sol-Gel Synthesis of Titania Particles

Metal alkoxides are particularly useful precursors for the synthesis of the oxides. Structurally, a metal alkoxide consists of a M-O-R linkage, where M is the metal, O is the oxygen and R is an alkyl group. A polarization takes place in the M-O bond due the opposite charges of M and O. This polarization makes the alkoxide receptive to a nucleophilic reagent such as water. In the presence of water the alkoxide will go through a nucleophilic addition-substitution reaction in which the alkoxy groups (OR) are replaced by hydroxyl groups (OH) provided by water. This process is called hydrolysis. The metal hydroxide groups link up by different mechanisms, generating a hydrated metal-oxide network which eventually will form small nuclei (2-3 nm). This process is called condensation. In this work, the alkoxide used is titanium tetraethoxide, $Ti(OC_2H_5)_4$, also called tetraethylorthotitanate (TEOT). The hydrolysis-condensation reactions, written in abbreviated form, are as follows:[1]

$$Ti(OC_2H_5)_4 + 4H_2O \rightarrow Ti(OH)_4 + 4C_2H_5OH \quad \text{hydrolysis} \quad (1.1)$$

$$Ti(OH)_4 \rightarrow TiO_2 \cdot xH_2O + (2-x)H_2O \quad \text{condensation} \quad (1.2)$$

Barringer et. al.[2] reported the formation of titania particles following this mechanism. A crucial parameter in controlling the hydrolysis reaction is the amount of water, defined as the molar ratio with respect to the alkoxide: $R=[H_2O]/[TEOT]$. They reported that $R>2.5$ is required for particle formation. The largest R value reported was 7 which correspond to particles with average size 300 nm. Edelson and Glaeser[3] modified this procedure with the addition of the water-soluble polymeric surfactant hydroxypropylcellulose (HPC). They were

---

[1] C. J. Brinker and G. W. Scherer, *Sol-Gel Science: The physics and chemistry of sol-gel processing*, Academic Press, San Diego Ca, 1990 (Chap. 4)

[2] E. A. Barringer and H. K. Bowen, J. Am. Ceram. Soc. **65**, C-199 (1982); E. A. Barringer and H. K. Bowen, Langmuir, **1**, 414 (1985).

[3] L. H. Edelson and A. M. Glaeser, J. Am. Ceram. Soc., **71**, C-198 (1988)

able to obtain a better control of the particle size distribution (better monodispersity). They used [TEOT]=0.15 M and R=3, which corresponded to 350 nm particle size. The polymer adsorbed onto the particles as they formed, generating repulsive steric forces and preventing further aggregation. Jean and Ring[4] measured the adsorption of HPC on titania particles, and showed that this in-situ steric force is the stabilization mechanism during particle formation.

Nagpal et. al.[5], in work carried out at Virginia Tech, followed the same synthesis procedure but grew titania particles using a wide range of R values, from 5.3 up to 60. They studied the effect of water concentration on particle size and HPC adsorption. The synthesis of the particles used in the present dissertation followed Nagpal's procedure. The main results found by Nagpal will be summarized. These are important because they define some of the parameters that were studied in this dissertation. The main factor is the effect of water concentration on particle size, this is shown in Fig. 1.1. The particle size was measured from TEM micrographs. There is a strong dependence of particle size on water concentration up to R values of 60; from then on there is little effect. Nagpal showed that this is due to an increase of HPC adsorption and nucleation rates with increasing R value. A mechanism suggested for the adsorption is a water bridge between the TiO_2 particle surface and HPC via hydrogen bonding.

Nagpal studied these synthesis procedures by using dynamic light scattering to monitor the particle growth rate as shown in Fig. 1.2. The three procedures used: (1) suspensions prepared without HPC, (2) "standard" suspensions prepared by dissolving HPC in the water-ethanol solution prior to reaction with TEOT, and (3) "premix" suspensions prepared by dissolving HPC in the TEOT-ethanol solution prior to reaction with water. Two parameters can be extracted from the graph: (1) the induction time which is the time required for the condensation reaction to form detectable particles (2-3 nm); and (2) growth rate: which is given by the slope of the curves of particle size vs. time. The induction time for premix suspensions was 10 min, compared to 16 min for standard suspensions; and the subsequent particle growth rate was much slower, 3.3 Å/sec, compared to 16 Å/sec for standard suspensions. These results indicate a bonding of the Ti-O-Ti nuclei with HPC chains that generates steric forces which retard the growth rate. It was suggested that this bonding results from an alcoholysis reaction according to the following equation:

$$Ti(OC_2H_5)_4 + HOC_3H_7\text{ - HPC} \rightarrow Ti(OC_2H_5)_3\text{ - }OC_3H_7\text{ - HPC} + C_2H_5OH \ .$$

1.3 The Process Variables

Summarizing the above, the particle synthesis procedure has two main process variables. One relates to the polymer: whether it is absent or present, and, if present, whether it is introduced

[4] J. H. Jean and T. A. Ring, Colloids Surfaces, **29**, 273 (1988).

[5] V. J. Nagpal, R. M. Davis, and J. S. Riffle, Colloids and Surfaces A, **87**, 25 (1994); V. J. Nagpal, PhD Thesis, Virginia Tech, Blacksburg, VA (1993).

by the standard method or by the premix method. The other relates to the water concentration used (R); the larger is R, the smaller is the particle size. The type of sample prepared from the particles is another form of process variable related to particle aggregation: whether they are studied in the form of a loose powder, an island-structure film made by spin coating, or a dense pellet made by compression. The final process variables are those which characterize the final thermal treatment: anneal temperature (which varied from room temperature to 1000°C) and annealing atmosphere (air or argon, i.e. an oxygen-containing atmosphere and an inert atmosphere). All of these were studied in this dissertation.

1.4 Factorized Form of the Dielectric Function

The classical-oscillator form (Eq. 1.3) of the dielectric function is the form that is usually used to analyze infrared reflectivity in the fundamental lattice-vibration (one-phonon) region:

$$e(n) = e_1(n) - ie_2(n) = e_\infty + \sum_n h_n \frac{n_{TOn}^2}{n_{TOn}^2 - n^2 + ig_n n} \qquad (1.3)$$

Here $\varepsilon(\nu)$ is the dielectric constant at frequency ν, ε_1 and ε_2 are its real and imaginary parts, h_n is the oscillator strength of the infrared-active (dipole-induced) mode, ν_{TOn} is the mode frequency, and γ_n is the damping factor.

This function provides a good fit when the reflectivity band is narrow, because then the transverse optical (TO) and longitudinal optical (LO) frequencies are close, and the same decay constant γ_n is expected for both modes. When the crystal is very ionic and the TO and LO frequencies are not close, difficulties in fitting reflectivity data have been reported. Barker and Hopfield[6] introduced an extra parameter for each mode to improve the fit in $BaTiO_3$, $SrTiO_3$, and $KTaO_3$. Spitzer et al.[7] reported a relatively poor fit to the reflection spectrum of the E_u mode of the rutile form of TiO_2. The same difficulty was encountered with the E_u-mode reflection spectrum of anatase TiO_2 (discussed in Chap. 4). In Fig. 1.3, this experimental spectrum and its best fit with the use of the classical-oscillator dispersion formula is presented (two oscillators were used); a relative poor fit was the result. All these spectra have, as a common characteristic, wide reflectivity bands (large TO-LO splittings).

To overcome this difficulty, Berreman and Unterwald[8] proposed that when dealing with wide reflectivity bands, independently adjustable damping parameters should be used for the TO and LO modes, and instead of the classical oscillator expression, they proposed a factorized form in which the TO modes are the poles and the LO modes are the zeros of the dielectric dispersion function (a requirement of Maxwell equation $e\vec{\nabla}.\vec{E} = 0$). This

---

[6] A. S. Barker Jr. and J. J. Hopfield, Phys. Rev. **135**, A1732 (1964).

[7] W. G. Sptizer, R. C. Miller, D. A. Kleiman, and L. E. Howarth, Phys. Rev. **126**, 1710 (1962).

[8] D. W. Berreman and F. C. Unterwald, Phys. Rev. **174**, 791 (1968).

expression was also proposed by others[9] as an extension of the Lyddane-Sachs-Teller relation, (which is what the factorized form reduces to at zero frequency). The factorized form is given by:

$$e(n) = e_1(n) - ie_2(n) = e_\infty \prod_n \frac{n_{LOn}^2 - n^2 + ig_{LOn}n}{n_{TOn}^2 - n^2 + ig_{TOn}n} \qquad (1.4)$$

Here e_∞ is the high-frequency (visible region) dielectric constant. For each mode (n), a TO and an LO frequency, and a TO and an LO damping constant, are included.

Figure 1.3 contains the fit obtained using the factorized form (with two factors), the superiority of this fit compared to the classical-oscillator fit is evident. This factorized form has been widely used by F. Gervais et al.[10] working with corundum, rutile, niobium dioxide, and several ferroelectric materials. The factorized form uses four adjustable parameters per reflection band: the TO and LO frequencies and their corresponding damping constants. The additional parameter (relative to the three-parameters-per-band classical oscillator form) is one reason that a better fit is attained. Another advantage of the factorized form is that the TO and LO frequencies are direct results of the fit, while in the oscillator expression only the TO frequency is directly obtained. The fitting itself is easier, since the first attempt to a fit can be guessed rather well from the experimental data, because the TO and LO frequencies are located at the low- and high-frequency edges of the observed reflection bands and the damping parameters correspond to the slopes at these edges. It is harder to get a first good guess with the oscillator form, because the oscillator strength parameter is related to the TO-LO splitting in a somewhat complex way. For these several reasons, the analysis of the IR results for single-crystal anatase (to be reported in chapter four) will be primarily based on the factorized form of Eq. (1.4).

1.5 Effective Medium Approximation

The sol-get titania particles, when crystallized, are made of nanocrystallites. Depending on annealing history, the average nanocrystal size ranges from 15 to 80 nm (for the anatase phase). This means that the particles themselves are polycrystalline (made up of several nanocrystals), since the average particle size ranges from 80 to 300 nm. From the sample preparation procedure, no prefered orientation is expected in the pressed pellets and thin

---

[9] A. S. Barker Jr., Phys. Rev. **136**, A1290 (1964); A. S. Chaves and S. P. S. Porto, Sol. State Commun. **13**, 865 (1973); R. P. Lowdnes, Phys. Rev. B **1**, 2754 (1970); C. Perry, in *"Far Infrared Spectroscopy"*, edited by K. D. Moller and W. G. Rothschild, (Wiley, New York) pp. 557 (1971).

[10] F. Gervais and B. Piriou, J. Phys. C **7**,2374 (1974); F. Gervais and B. Piriou, Phys. Rev. B **10**, 1642 (1974); F. Gervais and J. F. Baumard, J. Phys. C **12**, 1977 (1979); J. L. Servoin, Y. Luspin, and F. Gervais, Phys. Rev. B **22**, 5501 (1980); F. Gervais, J-L Servoin, A. Baratoff, J. G. Bednorz, and G. Binnig, Phys. Rev. B **47**, (1993).

films; the nanocrystals should be randomly oriented. When studying the optical properties of the pellets or films for a given polarization (electric-field direction) of incident light, we can (crudely speaking) expect to find twice as many nanocrystals oriented with their c-axis perpendicular to the polarization direction as there are nanocrystals oriented with their c-axis parallel to the polarization. (Both anatase and rutile are tetragonal; the independent polarization directions are // c and $\perp$ c. In other words, we can consider a polycrystalline anatase or rutile sample to be a composite made up of crystals in only two orientations, with two-thirds of the crystals oriented so that E$\perp$c and one-third of the crystals oriented so that E//c. Such a composite is optically equivalent to a composite made up of fictitious optically isotropic particles, two-thirds of which have a dielectric function given by the $\varepsilon_{\perp}$ of the crystal and one-third of which have a dielectric function given by the $\varepsilon_{//}$ of the crystal. To calculate the optical properties of a such composite, we need to make use of the Bruggeman effective medium approximation (B-EMA).

When studying the island-structure films, the first approach is to consider all the islands to be spheres. This is also a composite, one consisting of spheres randomly distributed in a matrix (the matrix, in this case, is air). The optical properties of such spheres-in-a-matrix composites are described by the Maxwell-Garnett effective medium approximation (MG-EMA). D. E. Aspnes[11] has presented a comprehensive derivation of both the B-EMA and MG-EMA theories (along with the Clausius-Mossotti relation) on a unified basis. I will summarize his main results.

We consider a simple cubic infinite lattice. Each lattice point ($\vec{R}_i$) has a polarizability (α). An external electric field ($\vec{E}_{\text{int}}$) is applied. First we have to find the resulting electric field [$\vec{E}(\vec{r})$] and the dipole distribution [$\vec{p}(\vec{r})$] of the system. $\vec{E}_{loc}$ is the electric field at a lattice point, and $\vec{E}(\vec{p},\vec{r}) = [3(\vec{p}.\hat{r})\hat{r} - \vec{p}]/r^3$ is the electric field at $\vec{r}$ of a dipole $\vec{p}$ located a the origin.

The induced dipole is $\vec{p}_i = a\vec{E}(\vec{R}_i) = \vec{E}_{loc}$ because of symmetry. The resulting fields are:

$$\vec{E}(\vec{r}) = \vec{E}_{loc} + \sum_i \vec{E}(a\vec{E}_{loc}, \vec{r} - \vec{R}_i) \tag{1.5}$$

$$\vec{p}(\vec{r}) = \sum_i a\vec{E}_{loc} d(\vec{r} - \vec{R}_i) \tag{1.6}$$

$$\text{and} \quad \vec{E}_{loc} = \vec{E}_{\text{int}} \tag{1.7}$$

We need to relate these results to the macroscopic field quantitites;:

$$\vec{D} = e\vec{E} = \vec{E} + 4p\vec{P} \tag{1.8}$$

[11] D. E. Aspnes, Am. J. Phys. **50**, 704 (1982).

The volume average of (1.6) is $\vec{P} = na\vec{E}_{loc}$, where *n* is the lattice-point density (number of polarizable points per unit volume).

The volume average of (1.5) is $\vec{E} = \vec{E}_{loc} - (4p/3)na\vec{E}_{loc}$. Plugging these results into Eq. (1.8), we obtain:

$$\frac{e-1}{e+2} = \frac{4p}{3}na \qquad \text{(Clausius-Mossoti relation)} \qquad (1.9)$$

Now we generalize the problem to include a random mixture of lattices having two different polarizabilities, α_a and α_b, and let the surrounding medium be (instead of vacuum) a dielectric with dielectric constant ε_m. Following the same schedule we obtain[12]:

$$\frac{e-e_m}{e+2e_m} = \frac{4p}{3e_m}(n_a a_a + n_b a_b),$$

where n_a and n_b are the volume densities of points a and b. If the dielectric constants ε_a and ε_b of each pure phase are known, then we can rewrite it:

$$\frac{e-e_m}{e+2e_m} = f_a\frac{e_a-e_m}{e_a+2e_m} + f_b\frac{e_b-e_m}{e_b+2e_m} \qquad \text{(Lorentz-Lorenz EMA)} \qquad (1.10)$$

where f_a is the volume fraction of phase (a): $f_a = n_a/(n_a+n_b)$. This is called the Lorentz-Lorenz effective-medium expression.

Now suppose that the microscopic regions are small compare to the wavelength of light but large enough to possess their own dielectric identity, and suppose these elements are spheres. Following the derivation of Genzel and Martin,[13] the average (macroscopic) field in our system is going to be a volume average of the field inside the spheres and the average field outside the spheres: $\vec{E} = f\vec{E}_o + (1-f)\vec{E}_m$. Here f is the volume fraction occupied by the spheres. Similarly the average polarization, using the macroscopic relation (1.8) is

$$\vec{P} = (1-f)\frac{e_m-1}{4p}\vec{E}_m + f\frac{e_o-1}{4p}\vec{E}_o.$$

The field inside the sphere in the presence of an external field is given by[14]:

$$\vec{E}_o = \frac{3e_m}{e_o+2e_m}\vec{E}_m.$$

Using again the macroscopic relation (1.8), we obtain:

$$\frac{e-e_m}{e+2e_m} = f\frac{e_o-e_m}{e_o+2e_m} \qquad \text{(Maxwell-Garnett EMA)} \qquad (1.11)$$

---

[12] R. W. Cohen, G. D. Dody, M. D. Coutts, and B. Abeles, Phys. Rev. B **8**, 3689 (1973).
[13] L. Genzel and T. P. Martin, Phys. Stat. Sol. (b) **51**, 91 (1972).
[14] J. D. Jackson, *Classical Electrodynamics* (Wiley, N.York, 1975), Sec. 4.4.

We can see that MG Effective Medium Approximation is a special case of the Lorentz-Lorenz Effective Medium Approximation. Looking back again to the Lorentz-Lorenz expression of Eq. (1.10) we see that if the two media (a) and (b) occupy all of the space, then ε_m, the dielectric function of the immersion medium, becomes ε the dielectric function of the composite material itself. Setting $\varepsilon=\varepsilon_m$ in Eq. (1.10) yields the following equation:

$$0 = f_a \frac{e_a - e}{e_a + 2e} + f_b \frac{e_b - e}{e_b + 2e} \qquad \text{(Bruggeman EMA)} \qquad (1.12)$$

To summarize, equations (1.11) and (1.12) allow us to estimate the dielectric function of a composite from the dielectric functions of the components. The Mawell-Garnett EMA of Eq. (1.11) is applied when spheres (dielectric function = ε_0) are completely surrounded by a matrix medium (here assumed to be air, ε=1). The Bruggeman EMA of Eq. (1.12) is applied when two randomly-intermixed phases are more properly treated on an equal footing: when each particle is surrounded by particles of both (ε_a, ε_b) types.

1.6 Generalized Effective Medium Approximation

Hayashi et al.[15] generalized the MG-EMA to include ellipsoidal-shape crystallites. They followed the procedure of Genzel and Martin, with the corresponding modification to take into account the particle shape. Take the principal axes of the ellipsoid to correspond to the principal axis of the dielectric tensor of the crystal. The electric field inside an ellipsoid immersed in an external electric field is given by[16]: $E_{oi} = \frac{e_m}{g_i(e_i - e_m) + e_m} E_{mi} = \hat{e}_i E_{mi}$, where i = x, y, z are the ellipsoid body coordinates, and the polarization induced inside the ellipsoid is given by: $P_{oi} = \frac{1}{4p}(e_i - 1)\hat{e}_i E_{mi} = \tilde{e}_i E_{mi}$. Here g_i is the depolarization factor and the inverse of g_i is approximately proportional to the ellipsoidal axis length; varying this parameter correspond to varying the crystallite shape (for spheres g_i=1/3). For uniaxial crystals, $\varepsilon_1 = \varepsilon_{//}$ and $\varepsilon_2 = \varepsilon_3 = \varepsilon_\perp$ and $g_{//} + 2\, g_\perp = 1$. Following the Genzel-Martin steps, the volume average of the electric field and polarization are taken and using the macroscopic relation (1.8) we obtain the following expression:

$$e - 1 = \frac{3(1-f)(e_m - 1) + f(\hat{e}_{//} + 2\hat{e}_\perp)}{3(1-f) + f(\tilde{e}_{//} + 2\tilde{e}_\perp)} \qquad (1.13)$$

This is called the generalized effective medium approximation (also called theory of the average dielectric constant (TADC)), in which the depolarization factor $g_{//}$ allow us to vary

---

[15] S. Hayashi, N. Nakamori, H. Kanamori, J. Phys. Soc. of Japan **46**, 176 (1979).

[16] C. F. Bohren and D. R. Huffman, *Absorption and Scattering of Light by Small Particles,* (Wiley, New York) Sec. 5.3.

the departure from sphericity (i.e. the ellipsoidal axis ratio) of the particles. The name "generalized EMA" is not completely accurate, since this theory applies only to the Maxwell-Garnett situation.

1.7 Finite-Size Effects and Raman Spectra

In silicon[17,18] and several other semiconductor crystals,[19, 20, 21] there is a well-documented finite-size effect observed in Raman-scattering experiments on nanocrystalline samples; the Raman bands broaden and shift with decreasing nanocrystal size L. This effect has also recently been seen in an oxide insulator, AlO(OH).[22] The gist of the mechanism is as follows.[17, 20] For a nanocrystal of size L, the strict "infinite-crystal" k-space selection rule is replaced by a relaxed version characterized by a k-space uncertainty of order (1/L). Here, k is the phonon wavevector. Instead of only the k=0 mode of a phonon branch being Raman-active (for a Raman-allowed mode symmetry), now all modes of the phonon branch within a range of k values [roughly from k=0 to k=(1\L)] are Raman-active. Because the phonon dispersion curve $\nu(k)$ is not flat, the observed Raman band shifts and broadens. The smaller the L, the larger is the shift and broadening of the Raman band.

If the phonon dispersion relation is known, it is possible to estimates crystallite sizes from the Raman shift and broadening. That is not usually the case, for anatase TiO_2 there is no available data on this matter. But for rutile TiO_2, the phonon dispersion curves are known[23] from inelastic neutron scattering measurements. The low frequency E_g anatase Raman line (144 cm^{-1})[24] is very close in frequency to the B_{1g} rutile Raman line (143 cm^{-1}).[25] We want to estimate the broadening and shifting of the B_{1g} rutile Raman band as a function of crystallite size, in order to have some estimate for the corresponding finite-size effects on the low-frequency E_g anatase line. This calculation will then be available for possible application to

---

[17] H. Richter, Z. P. Wang, and L. Ley, Solid State Commun. **39**, 624 (1981)
[18] Z. Iqbal and S. Veprek, J. Phys C **15**, 377 (1982).
[19] K. K. Tiong, P. M. Amirthara, F. H. Pollak, and D. E. Aspnes, Appl. Phys. Lett. **44**, 122 (1984); M. Holtz, R. Zallen, O. Brafman, and S. Matteson, Phys Rev. B **37**, 4609 (1988); I. H. Campbell and P. M. Fauchet, Solid State Commun. **58**, 739 (1986); M. Gargouri, B. Prevot, and C. Schwab, J. Appl. Phys. **62**, 3902 (1987); T. Kanata, H. Murai, and K. Kubota, J. Appl. Phys. **61**, 969 (1987); S. J. Yu, H. Asahi, S. Emura, H. Sumida, S. Gonda, and J. Tanoue, J. Appl. Phys. **66**, 856 (1989); R. Zallen, J. Non-Cryst. Solids **141**, 227 (1992).
[20] R. J. Nemanich, S. A. Solin, and R. M. Martin, Phys. Rev. B **23**, 6348 (1981).
[21] K. Nakamura, M. Fujitsuka, and M. Kitajima, Phys. Rev. B **41**, 12260 (1990).
[22] C. J. Doss and R. Zallen, Phys. Rev. B **48**, 15626 (1993).
[23] J. G. Traylor, H. G. Smith, R. M. Nicklow, and M. K. Wilkinson, Phys. Rev. B **3**, 3457 (1971).
[24] T. Ohsaka, F. Izumi, and Y. Fujiki, J. Raman Spectrosc. **7**, 321 (1978).
[25] S. P. S. Porto, P. A. Fleury and T. C. Damen, Phys. Rev. **154**, 522 (1966).

the studies of Raman lineshape changes with temperature during the annealing of the anatase nanoparticles (to be reported in chapter five).

The phonon dispersion curve[23] along the (110) direction in q-space was used for the calculation; the dispersion curves along the (100) and (001) direction have similar shapes and (especially) similar slopes near q = 0. Following the work done on semiconductors[19] we fit the dispersion curve with the following expression: $w(q) = A + B\cos(pq)$. We found A = 257.8 cm^{-1} and B = -113.5 cm^{-1}; the fit is shown in Fig. 1.4. A crystallite of spherical shape is assumed, with diameter L, and the phonon wave function is limited to this size through a Gaussian attenuation factor, $\exp(-2r^2/L^2)$. In q-space the corresponding weighting factor is $\exp(-q^2L^2/4)$. Now we can calculate the Raman intensity I(ω) as an integral in q-space of a Lorentzian peak attenuated by the finite crystal size factor:

$$I(w) \quad a \quad \int_0^1 \exp(\frac{-q^2 L^2}{4}) \frac{d^3 q}{[w - w(q)]^2 + [\Gamma_0 / 2]^2} \tag{1.14}$$

Here Γ_0 is the bulk-crystal Raman line width, and the integral is done assuming a spherical Brillouin zone. The results of this calculation, for nine different diameters, are shown in Fig. 1.5. Comparing these results with the ones found in semiconductors and aluminum oxide we see the following interesting points: (1) Because of the positive slope of the dispersion curve the rutile 143 cm^{-1} Raman line blueshifts with decreasing crystallite size, in opposite direction of the silicon-family semiconductors and aluminum oxide results. Our results, described in chapter five, of Raman measurements on anatase particles annealed to different temperatures show a blueshifting with decreasing crystallite size. (2) The same order of magnitude of Raman-line broadening and shifting in rutile and semiconductors corresponds to a different order of magnitude of crystallite size. The semiconductor crystallites are roughly 10 times smaller, for similar broadening and shiftingn. We assume this is because the dispersion curve of rutile has a larger curvature near q=0. than for example, GaAs.[19] Again, our Raman results on annealed anatase particles (described in chapter five) show crystallite sizes of the order calculated here for rutile crystallites.

1.8 Nonstoichiometry and Raman Spectra

Parker and Siegel[26,27] investigated nanophase titania formed by oxidizing titanium particles made by gas-phase condensation. Their particles had a range of stoichiometries (thermogravimetrically determined) ranging from $TiO_{1.89}$ to TiO_2, with the as-prepared samples being oxygen-deficient and the more stoichiometric samples obtained by subsequent anneals in air. Nonstoichiometric samples were dark blue, consistent with earlier work on

[26] J. C. Parker and R. W. Siegel, J. Mater. Res. **5**, 1246 (1990).
[27] J. C. Parker and R. W. Siegel, Appl. Phys. Lett. **57**, 943 (1990)

vacancy-induced optical absorption in reduced (oxygen-deficient) rutile.[28] Grain sizes, not monitored in detail, were about 12 nm for the as-prepared material and increased to 24 after one of their air anneals. Both rutile and anatase were present on their as-prepared (unannealed) samples. Parker and Siegel observed shifts in the main Raman peaks of rutile and anatase as the stoichiometry changed, and ascribed these effects entirely to stoichiometry.

Parker and Siegel presented Raman peak position measurements of the 144 cm^{-1} anatase line, the 447 and 612 cm^{-1} rutile lines. Similar to the size-effect results (calculated in rutile) the anatase line blueshifts with nonstoichiometry. The 447 cm^{-1} (E_g) rutile line, according to lattice vibration calculations[23] are oxygen out-of-phase motions along the z-direction. The dispersion curve for this mode[23] along the (001) direction has a large negative curvature. This means that size effects should cause redshifting of the Raman line. Parker and Siegel results are also redshifted with increasing nonstoichiometry. Finally, the 612 cm^{-1} (A_{1g}) rutile line corresponds to a Ti-O stretch mode; its dispersion curve is flat in the (100) direction and has negative slope in the (110) direction. We expect size effects to cause a small redshifting of this Raman line. Parker and Siegel reported no shifting at all with increase of nonstoichiometry. It is interesting to note that the same shift directions occur for effects arising from both small crystallite size and nonstoichiometry, and that a small predicted finite-size effect corresponds to a negligible observed nonstoichiometry effect.

1.9 Dissertation Outline

Chapter two is detail oriented. Here, specifics of the materials synthesis procedures are treated in enough detail to be useful for other researchers. In addition, details of the infrared measurements are described. Procedures for data collection for the infrared in-situ annealing experiment are included. Software needed for data analysis, involving Raman peak position correction, Raman peak position and width determination, fitting algorithms for the bulk anatase reflection data, some aspects on fitting the x-ray diffraction data, and general software for data manipulation such as smoothing and calculating derivatives are covered. This chapter is not a prerequisite for reading the rest of the chapters in the dissertation. It is primarily for researchers desiring to reproduce some of the results.

Chapter three presents a morphological and spectroscopic characterization of the sol-gel titania particles as a function of steric stabilizer presence, amount of water used, particle packing, and sample preparation mixing procedure. Morphology is characterized through electron microscopy (transmission electron microscopy, TEM, and scanning electron microscopy, SEM). The spectroscopic techniques concentrate on the phase-transition issue, especially the transformation from anatase to rutile. Raman intensities were calibrated to yield relative phase concentrations, specifically the relative anatase and rutile content.

---

[28] R. G. Breckernridge and W. R. Hosler, Phys. Rev. **91**, 793 (1953).

Chapter four presents polarization-dependent far-infrared reflectivity measurements on single crystals of anatase. The TO and LO modes of the infrared active phonons were determined. The large TO-LO splittings were used to estimate effective charges. Measurement on pressed pellets of anatase nanocrystals were interpreted in terms of effective medium theory and surface roughness.

Chapter five describes experiments carried out in order to see if finite-size effects could be observed in anatase nanocrystals through the evolution of the Raman band shape (peak position and linewidth) with annealing temperature (which determines average crystallite size). In order to be able to discriminate against possible effects of nonstoichiometry in the Raman spectra, anneals were done in both air (oxygen-containing) and argon (no oxygen) atmospheres. X-ray linewidths were used to estimate the crystallite sizes.

Chapter six presents infrared results on anatase nanoparticles thin films, infrared transmission results using KBr pellets, and Raman measurements on anatase pellets. The KBr pellets contained 0.5% wt/wt of titania nanoparticles, and were annealed inside the infrared spectrometer. These in-situ annealing experiments showed very clearly the amorphous to anatase transformation and the dependence of this transformation on particle size. Annealed anatase island-structure thin films were investigated in the infrared using grazing-incidence reflection measurements. The influence of nanocrystal size on the infrared spectra is reported here. Measurements of transmission and reflection at oblique incidence on anatase continuous thin films are also reported. Most of the TO and LO frequencies were measured and compared with results from bulk crystals. Finally, results on anatase-to-rutile transformations in thin films and pellets are reported.

Chapter seven presents the electron-energy loss (EELS) experimental results on titania thin films annealed to different temperatures. Electron diffraction results show the crystalline phases present. A simple subtraction technique is developed to eliminate the substrate features from the EELS spectra. The momentum dependence of the electron-energy loss spectra is reported.

Chapter eight briefly summarizes the results and provides suggestions for further study.

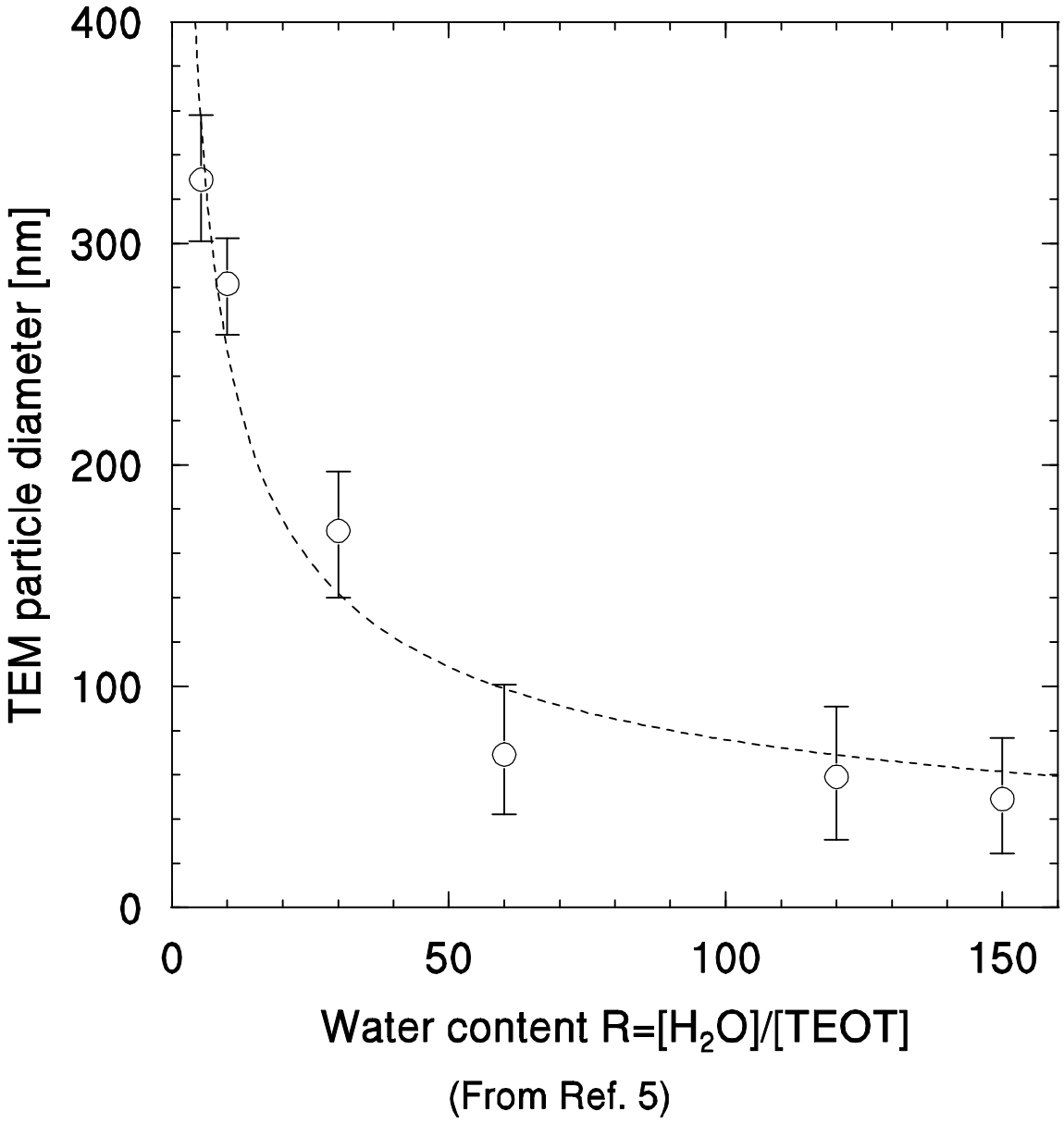

Figure 1.1. Sol-gel titania particles size (as measured from TEM micrographs) versus amount of water used during the hydrolysis reaction (the dashed line is an eyeball fitting).

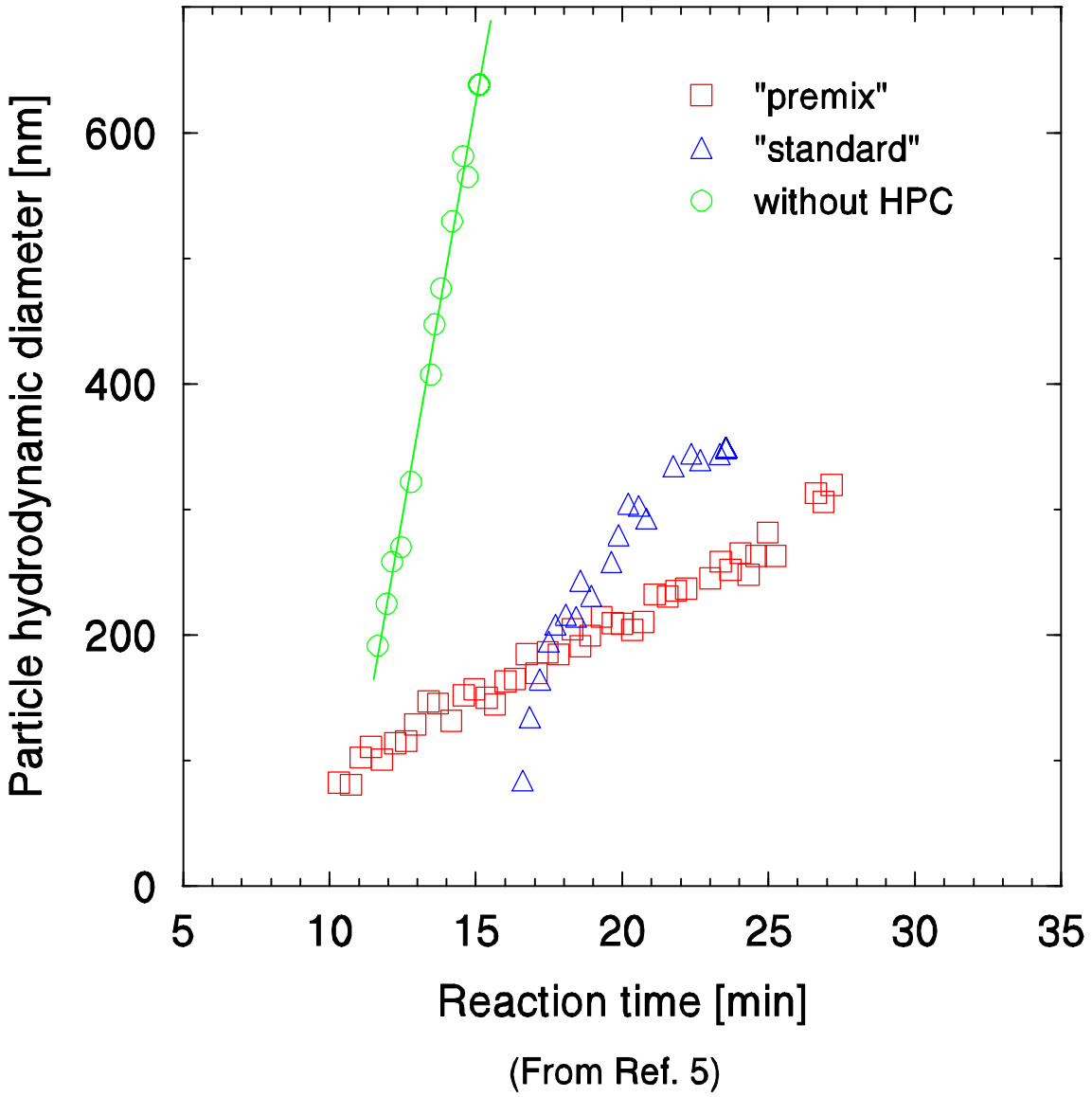

Figure 1.2. Sol-gel titania particle size (as determined through dynamic light scattering measurements in the colloidal suspensions during the particle synthesis) versus the reaction time for three different preparation procedures. The induction time and growth rate are two measurable parameters.

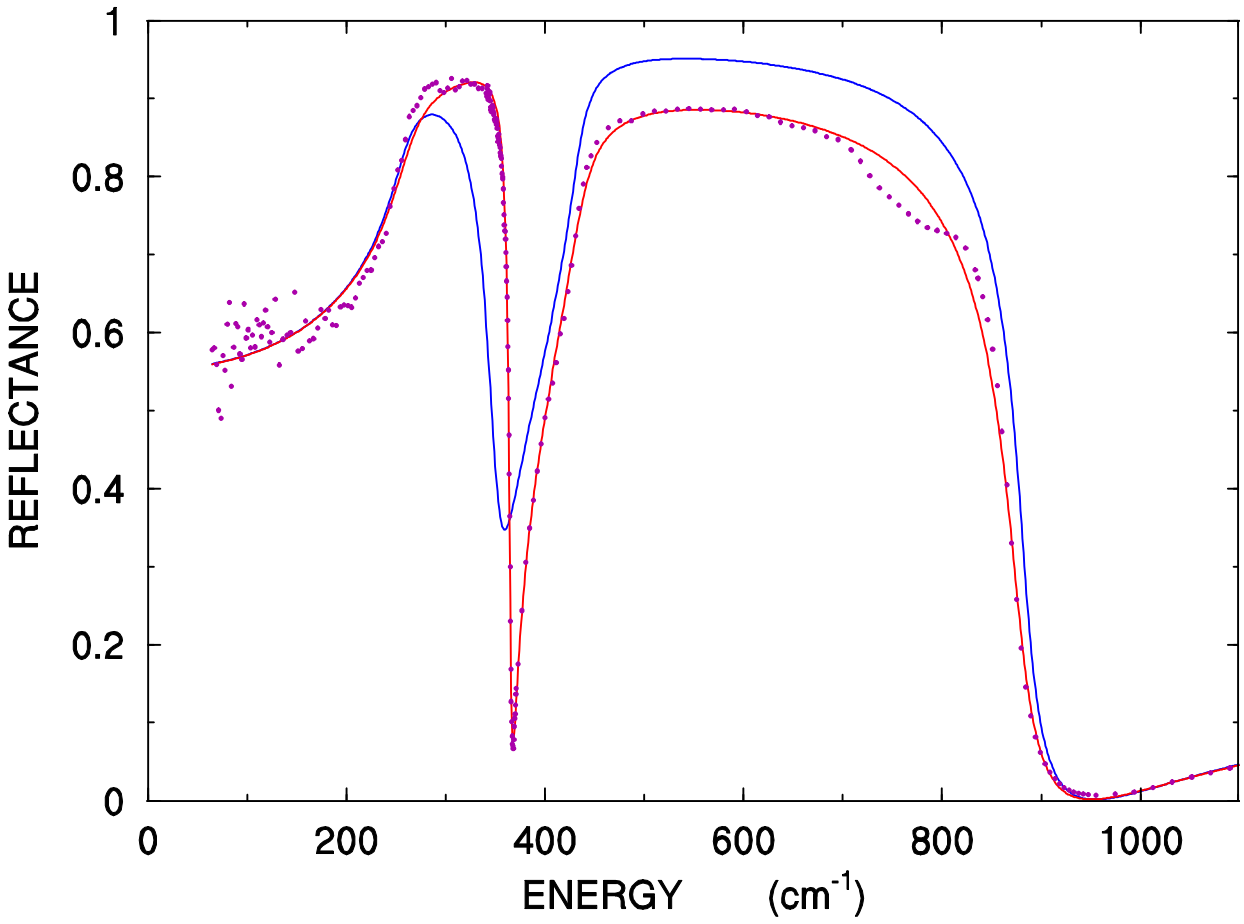

Figure 1.3. Near-normal infrared reflection spectrum on anatase single crystals, with the surface cut perpendicular to the optical c-axis. The fitting results using the factorized form (continuous line) and the classical-oscillator form (dashed line) of the dielectric function are presented.

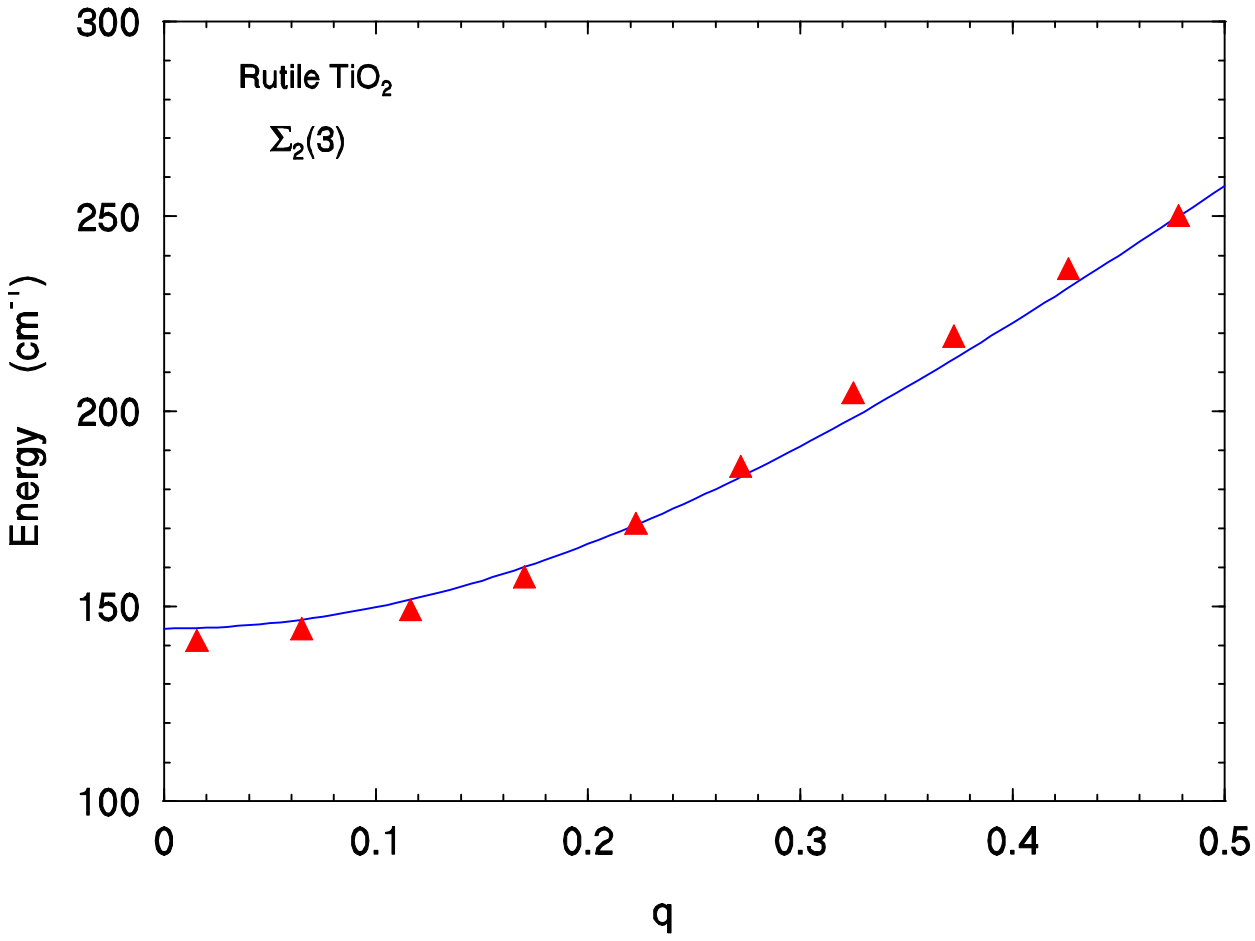

Figure 1.4 Rutile phonon dispersion curve $\Sigma_2(3)$ along the (110) direction (taken from ref. 23). The momentum axis is in units of $(2\pi/a)$, where a is the lattice constant. A fitted curve is also presented, $\omega(q) = 257.8 - 113.5 \cos(\pi q)$.

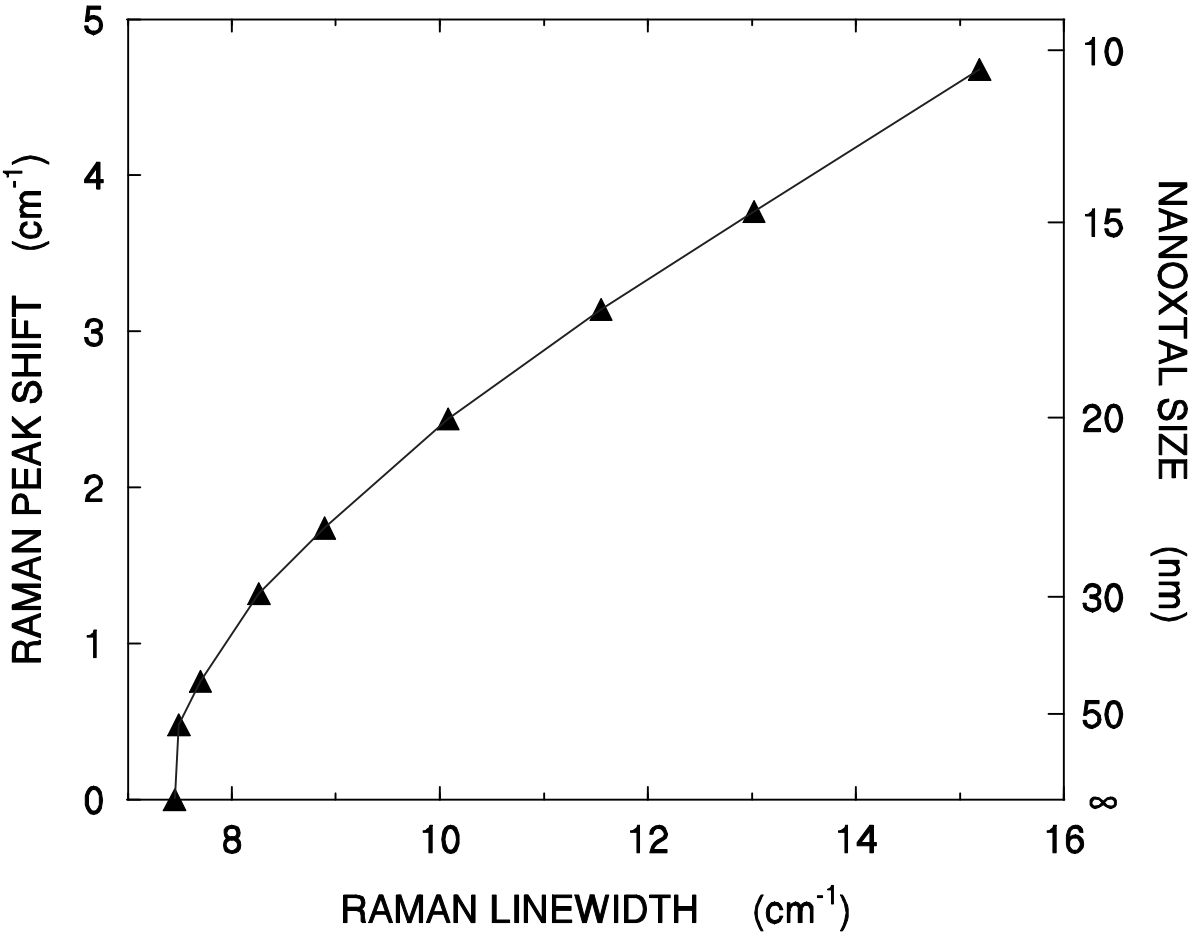

Figure 1.5. 143 cm^{-1} rutile Raman peak position versus linewidth as a function of nanocrystal size. These results were calculated using the equation 1.14 and the phonon dispersion curve reported in Fig. 1.4

CHAPTER TWO

2. EXPERIMENTAL: MATERIALS AND METHODS

2.1 Introduction

The details of the materials synthesis and the methods of analysis are discussed in this chapter. It is not necessary to read this chapter in order to understand the following chapters. However, this chapter should prove helpful to anyone interested in reproducing any of these experiments, or anyone attempting to carry out similar experiments. The data collection and data analysis sections are general and not restricted to sol-gel titania only. Section 2.2 details the process for making sol-gel titania particles, powders, pellets, and films. Section 2.3 details the experiments carried out in the infrared spectrometer; it includes details of the software developed for the fitting of reflectivity data and theoretical calculations of reflection of thin films. Section 2.4 is dedicated to Raman scattering experiments. Details about data collection using the Dilor spectrometer are included, as well as data analysis software for obtaining Raman peak parameters. Section 2.5 describes modifications of the data collection and data analysis software in the EELS experiments. Some comments about fitting x-ray diffraction data to extract line widths are presented. Also some general software for data analysis is described. Additional fine detail about processes, along with source codes for the software described, are listed in the appendices.

2.2 Sol-Gel Titania Synthesis

The process for making sol-gel titania using HPC consists of preparing two ethanol solutions: one of water and HPC (standard method) and the other of TEOT. These procedures are similar to the ones described by Nagpal[29], with some variations. Specific details follow:

2.2.1 Washing the glassware

Glassware that has been in contact with titania should be etched clean for 24 hours by filling them with an alcohol solution of KOH (2 liters of isopropanol + a handful of KOH pellets). A second bath is needed to neutralize the base; fill the glassware with a 2 M HNO_3 solution and leave at least for 1 hour. Rinse with deionized water. Glassware that has only come in contact with HPC ethanol solution should be cleaned with soapy water and rinsed with deionized water. All glassware should be put in an oven to dry completely. The cleaning solutions should periodically be remade.

Most of the preparation should be done in a nitrogen bag. For this purpose, the scale should be inside the bag. All the flasks should be covered with septums, except the ethanol flask. The instructions are general to prepare any amount of titania suspensions, but figures are given here for preparing 200 ml of sol-gel titania. All the dry ethanol to be used should be

[29] V. J. Nagpal, PhD Dissertation, Dept. of Chemical Engineering, Virginia Tech (1993).

filtered through a 0.2 μm membrane. Nagpal suggested filtering the TEOT and the HPC solutions as well. Schalz[30] found that filtering only the ethanol does not harm the experiments. Filtering HPC is really hard; Schalz found that HPC clogged the membrane pores, making it necessary to change filters every 15 ml of filtered solution. In this study we found the same difficulty, so we opted to filter the TEOT solution but not the HPC one.

2.2.2 HPC/ethanol solution

The final concentration of HPC in the suspension is 1.7 g/l. We prepare first a stock which has a higher concentration, 20 g/l (2.485% wt/wt). Prior to preparing this solution, the HPC is dried: Put 1 gram in the vacuum oven at room temperature. Every two hours increase the oven temperature to 40°C, 60°C, and 80°C, leaving it at this temperature for two hours. Then let it cool to room temperature under vacuum. Take a weighed septum-covered flask, which has been purged with nitrogen, to the oven. Add the HPC as quickly as possible and again cover the flask. Reweigh to determine the weight of HPC, finally, under nitrogen, add 50 ml of dry ethanol (0.785 g/ml) per gram of HPC, add stirrer and stir for a few hours.

2.2.3 TEOT/ethanol solution

A stock solution of TEOT should be prepared to be used for several syntheses.
The final concentration of TEOT (228 g/mol) in the suspension is 0.075 M. TEOT is dissolved initially in half of the final volume, so in the TEOT/ethanol flask, the concentration should be 0.15 M (34.2 g/l). To prepare two 200 ml titania suspensions, roughly 220 ml of this solution should be prepared. Remember that, since TEOT is 95% concentrated in ethanol, it is important to take into account the small amount of ethanol present to obtain accurate concentrations. Remember that the solution must be prepared inside a nitrogen bag. Use a syringe (without a needle) to pour TEOT (it is highly viscous) into the flask.

2.2.4 Water+HPC/ethanol solution

Determine first the amount of water needed based on the desired R value. Remember that the molarities are calculated for the final solution, which has twice the volume of this solution. As an example consider the preparation of 200 ml suspension at R=15. This R value means a water concentration of 1.125 M. In half the volume the molarity should be twice as high, 2.25 M = 40.5 g/l or 4.05 g of water in 100 ml of solution.

Determine the amount of HPC solution needed. Remember that the final concentration should be 1.7 g/l, in 200 ml, and the HPC stock solution has a concentration of 20 g/l. Finally, determine the amount of ethanol needed to make 100 ml, take into account the volume of water and the ethanol present in the HPC solution.

[30] M. L. Schalz, MS Thesis, U. of California, Berkeley (1991).

2.2.5 Mixing

Uncap the water/ethanol and the TEOT/ethanol flasks. Pour the water solution all at once into the TEOT solution, and mix for five seconds. It should turn milky white after a minute. Let the suspension sit for 24 hours.

2.2.6 Powders, pellets, and films

Roughly 20 ml of the final suspension is set aside for use for TEM samples and films. The rest is divided in four parts and centrifuged at 13000 RPM (19,000 g-force) for 20 minutes. The supernatant is decanted and the tubes are placed in an oven at 60°C, for 48 hours. After this process, chunks of titania fall off the tube walls. These chunks are gently ground with mortar and pestle. Half of the resulting powder is pressed into pellets at a pressure of 0.74 GPa for 3 minutes; each pellet is made with 100 mg of powder. The films are made by spin coating the suspension, at 1800 RPM for one minute,. Several coats can be repeated, if needed, to make a thicker film.

2.3 Infrared Spectroscopy

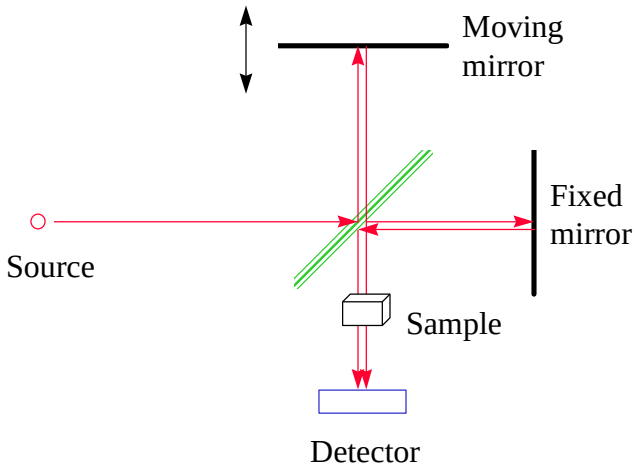

Figure 2.1. Michelson interferometer scheme

Infrared spectra were obtained in a BOMEM DA3-0.02 Fourier Transform Infrared (FTIR) Spectrometer. The spectrometer has a frequency range from 10 to 7000 cm^{-1}. This range could be extended to the uv-visible region with the right combinations of detectors and beamsplitters (not available at the present time). In what follows, a short description of the physical principle that governs the spectrometer will be presented; for details refer to the

instrument manual or to Griffiths and de Haseth.[31] The Fourier transform infrared spectrometers are computer-controlled Michelson interferometers. The source beam is divided by a beamsplitter into two components. One beam continues straight ahead to a fixed mirror and the other beam (perpendicular to the first) goes to a movable mirror. The reflected beams, after going again through the beamsplitter (which recombines them into a single beam) reach the sample and finally the detector (see Fig 2.1). This means that the signal at the detector is a space (or time)-dependent interferogram of the two incoming beams. The Fourier transform of this space (or time)-dependent interferogram provides the desired spectrum, the frequency-dependent signal. Two main factors affect the quality of a spectrum, its signal-to-noise ratio (s/n) and its spectral resolution. The resolution is proportional to the reciprocal of the path length of the moving mirror. High-resolution spectra take longer to collect. In the infrared experiments described in this dissertation, the resolution was not an issue. The maximum resolution needed was 1 cm^{-1}, and the system is capable of achieving a resolution of 0.02 cm^{-1}. The step size in the spectrum has a value that is half of the spectral resolution. The s/n ratio depends on the number of scans (N). A scan is the motion of the moving mirror from one end of its path to the other end. N is set by the chosen resolution, the sample area, and the analog-to-digital (ADC) bit resolution. In general, the only variable under control is N, and the s/n ratio increases as $\sqrt{N}$.

Table 2.1. Standard combination of sources, beamsplitters, and detectors for the BOMEM DA3.02, to cover a frequency range from 10 to 7000 cm^{-1}

Energy Range	Sources	Beamsplitter	Detector
500-7000	globar	KBr or KCl	dtgs/kbr or mct
200-700	(S# 1)	3 μm mylar	
125-400		3 μm mylar	
40-200	mercury	12 μm mylar	dtgs/poly
15-100	(S# 3)	25 μm mylar	
10-50		50 μm mylar	

There is no single beamsplitter or detector that can cover all of the IR region. For this reason a specific combination of these elements is used for each frequency range. Table 2.1 summarizes the standard combinations of detector/source/beamsplitter.
Table 2.2 presents the frequency range of each source, detector and beamsplitter available at the present time.

[31] P. R. Griffiths and J. A. de Haseth, *Fourier Transform Infrared Spectrometry*, (Wiley, New York, 1986), chap 1 and 3.

Table 2.2 Frequency range (cm^{-1}) of all sources, beamsplitters and detectors available for the FTIR BOMEM-DA3.02

Source	Range	Beamsplitter	Range	Detector	Range
globar(S#1)	200-10000	KBr	400-7000	DTGS/KBr	400-7000
quartz(S#2)	3000-25000	KCl	500-5000	MCT	600-5000
mercury(S#3)	5-800	Mylars	(See Table 2.1)	DTGS/poly	10-700

The quartz source (visible) is very useful for alignment. The mercury source overlaps with the globar source in the 200-700 cm^{-1} region. If the signal is strong enough and no polarizer is used, it is convenient to use the combination mercury/mylar-3µm/DTGS-poly that covers the frequency region from 125 to 700 cm^{-1}. The DTGS-KBr and MCT detectors have overlapping-working-frequency regions. The MCT detector has a shorter range but it has a higher sensitivity, and it needs liquid nitrogen to operate. The MCT detector maximum sensitivity is at moving-mirror speeds of 0.5 to 1 cm/s. The sensitivity is not constant over its working frequency region, it has a maximum value at 660 cm^{-1}. From 660 down to 600 cm^{-1}, it decreases abruptly, and from 660 up to 5000 cm^{-1}, the sensitivity decreases linearly. The DTGS detectors have maximum sensitivity when the moving mirror is operated at speeds ≤ 0.2 cm/s, and the sensitivity is constant over its working frequency region. On the other hand, KBr and KCl are two beamsplitters with overlapping working-frequency regions. Both are hydroscopic (keep under vacuum or in dry air). The only difference between them is that the KCl beamsplitter is newer. A polarizer is also available. The substrate is made of KRS-5 which determines the polarizer working-frequency region. In this case, it is from 200 to 16000 cm^{-1}. The polarizer is very delicate, never touch or blow on its surface.

2.3.1 Data collection:

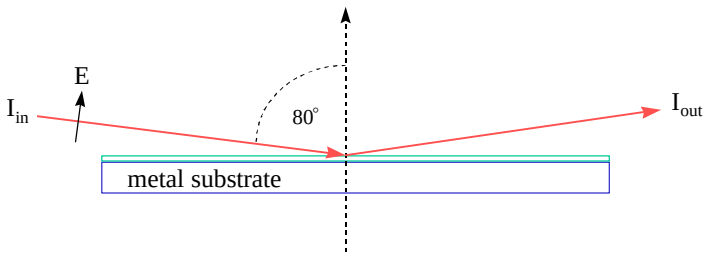

Figure 2.2 Schematics of grazing-incidence reflectivity, with p-polarized light (parallel to the plane of incidence).

The Bomem DA3 spectrometer is kept under rough pump vacuum (0.3 Torr). It can be run in a purge mode (with nitrogen) or in a vacuum mode. In the work described here, it was used in the vacuum mode. The spectrometer is controlled by a PDP-11 computer. The standard procedure is to collect spectra with this computer and then transfer the spectra files to a personal computer for data analysis. The files are transferred in Bomem format (*.DA) using KERMIT. To obtain ASCII files, the data analysis package LabCalc™ (Galactic, Inc.) is used. The *.DA files are imported into LabCalc, and then exported as ASCII files (*.PRN) (see Appendix A for further details). Spectra from different frequency regions can be patched into a single file; this is done with the program PATCH (Appendix A). The main concern when patching is to preserve continuity up to the first derivative of the two spectra. Since the overlapping region is usually large (>50 cm^{-1}), this is not an issue.

2.3.2 Grazing-incidence reflectivity

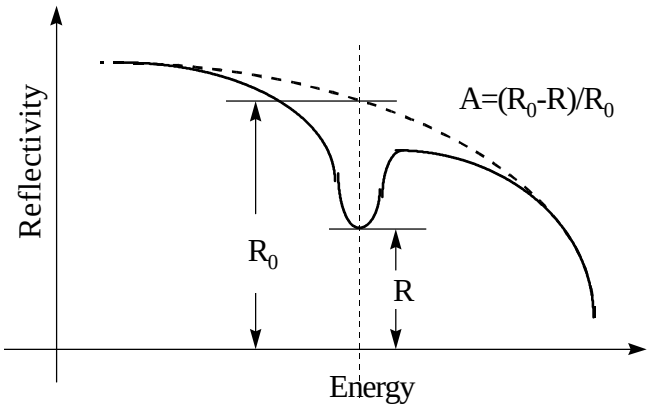

Figure 2.3. Reflectivity spectrum. It shows an absorption peak and the definition of the Absorption factor (A)

R. G. Greenler[32] established the grazing angle infrared reflection technique that allows the study of very thin layers (even molecules) deposited on a metal surface. Based on theoretical calculations of wave propagation through stratified media, he determined that measuring infrared reflection at very large angles (≈ 80°) and with light polarized parallel to the plane of incidence (this plane is defined by the incoming and outgoing beam), p-polarized light, the infrared absorption of an angstroms thick layer deposited on a metal could be detected (see Fig. 2.2). A convenient measure of the depth of an infrared absorption band is the absorption factor $A=(R_0-R)/R_0$ (see Fig. 2.3), where R_0 is the reflectivity when (absorption coefficient) of the film equals zero.

[32] R. G. Greenler, J. Chem. Phys. **44**, 310 (1966); R. G. Greenler, J. Vac. Sci. Technol. **12**, 1410 (1975).

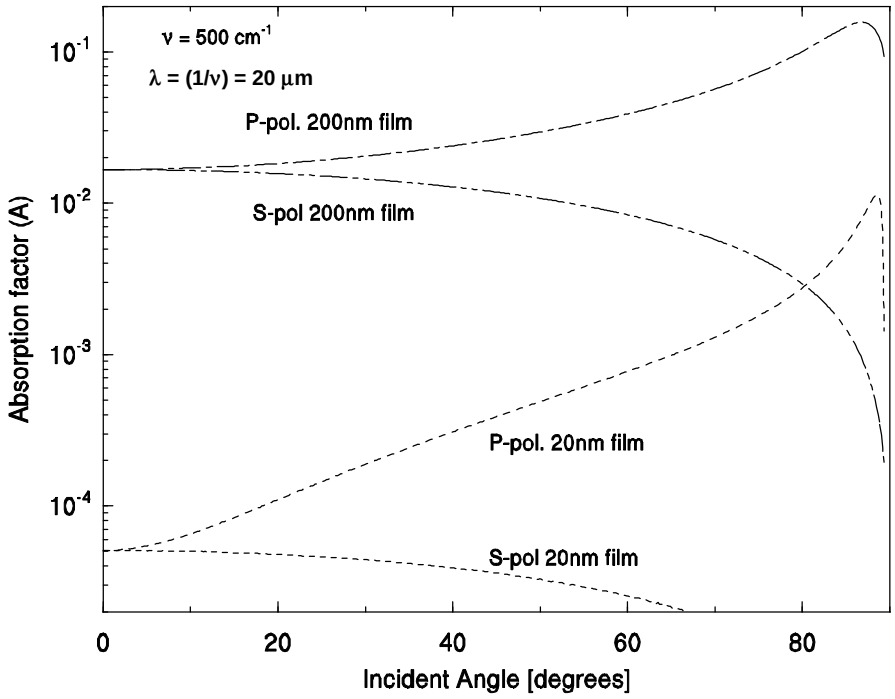

Figure 2.4 Calculated absorption factor as a function of incident angle for $\lambda = 20\ \mu m$ ($\nu = 500\ cm^{-1}$). The 200 nm film corresponds to $d/\lambda = 0.01$ and the 20 nm film corresponds to $d/\lambda = 0.001$. The film optical constants used here are n = 3.64, k = 6.12 (these correspond to anatase at this frequency). The metal substrate optical constants are n = 59 , k = 144 (these correspond to aluminum at this frequency).

Calculated results for A (absorption factor), as a function of incident angle for different d/λ ratios, are shown in Fig 2.4. Here d is the film thickness, which appears in the wave propagation expressions only in the ration d/λ. The results in Fig 2.4 show that only grazing angle measurements, with p-polarized light, give high absorption factors. Under these experimental conditions, the electric field is almost perpendicular to the metal substrate, and the wave vector is almost tangent to the film surface. This is similar to measuring transmission along (instead of through) the film, and intuitively explains the high sensitivity of the technique. This technique is also orientation selective; because of the electric field direction, only molecular vibrations or phonon modes polarized perpendicular to the substrate will be excited.

The results of Fig. 2.4 were obtained by using one of a set of programs developed on wave propagation through stratified media. Because of their usefulness, a short description of these will be presented in next section.

2.3.3 Wave propagation through stratified media

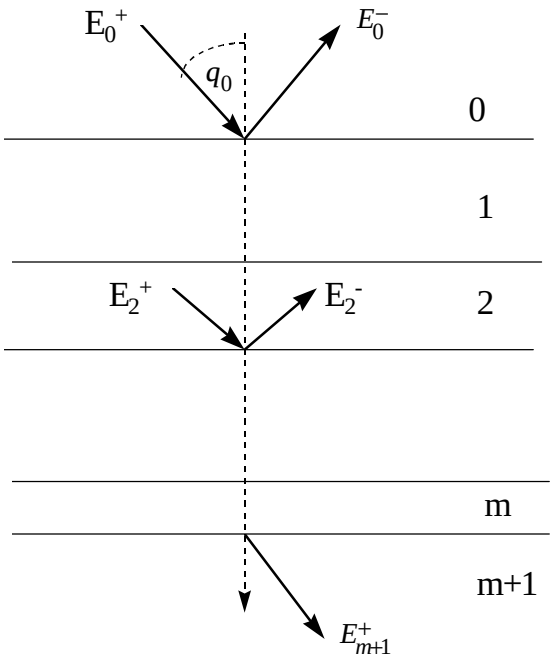

Figure 2.5. Schematics of wave propagation through stratified media

Algorithms for wave propagation through stratified media (see Fig 2.5) have been developed, with certain variations, by several authors.[33] The simple approach is a 2x2 matrix formalism. In each layer we assume two electric field components: a propagating (+) field and a reflected (-) one. Interfaces are represented by 2x2 matrices, as follows.

$$I_{ij} = \frac{1}{t_{ij}}\begin{pmatrix} 1 & r_{ij} \\ r_{ij} & 1 \end{pmatrix} \qquad \text{[Interface matrix between layer (i) and (j)].}$$

Each layer k (with thickness d_k) is represented by a propagation matrix

$$P_k = \begin{pmatrix} e^{ib_k \hat{n}_k \cos\hat{q}_k} & 0 \\ 0 & e^{-ib_k \hat{n}_k \cos\hat{q}_k} \end{pmatrix} \qquad \text{[Propagation matrix through layer (k)],}$$

where r_{ij} and t_{ij} are Fresnel coefficients and $b_k = \frac{2p}{l} d_k$.

For p-polarization (parallel to plane of incidence), the Fresnel coefficients are

$$r_{ij} = \frac{\hat{n}_j \cos\hat{q}_i - \hat{n}_i \cos\hat{q}_j}{\hat{n}_j \cos\hat{q}_i + \hat{n}_i \cos\hat{q}_j} \quad , \quad t_{ij} = \frac{2\hat{n}_i \cos\hat{q}_i}{\hat{n}_j \cos\hat{q}_i + \hat{n}_i \cos\hat{q}_j} \quad .$$

[33] W. N. Hansen, J. Opt. Soc. Am. **58**, 380 (1968); D. W. Berreman, J. Opt. Soc. Am. **62**, 502 (1972); K. Ohta and H. Ishida, Appl. Optics **29**, 1952 (1990).

For s-polarization (perpendicular to plane of incidence), they are

$$r_{ij} = \frac{\hat{n}_i \cos\hat{q}_i - \hat{n}_j \cos\hat{q}_j}{\hat{n}_i \cos\hat{q}_i + \hat{n}_j \cos\hat{q}_j} \quad , \quad t_{ij} = \frac{2\hat{n}_i \cos\hat{q}_i}{\hat{n}_i \cos\hat{q}_i + \hat{n}_j \cos\hat{q}_j} \quad .$$

Here $\hat{n} = n - ik$ is the complex refractive index. The complex $\cos\hat{q}$ function is defined by the Snell refraction law: $n_0 \sin q_0 = \hat{n}_k \sin\hat{q}_k$ for all k layers (θ_0 is the incident angle).
And, for all k layers.

Now we can find the propagated and reflected electric field components,

$$\begin{pmatrix} E_0^+ \\ E_0^- \end{pmatrix} = I_{01} \prod_{k=1}^{m} P_k I_{k,k+1} \begin{pmatrix} E_{m+1}^+ \\ 0 \end{pmatrix} \quad , \text{ for a m-layer system.}$$

Finally, the reflection (R) and transmission (T) coefficients are given by:

$$R = \frac{\left|E_0^-\right|^2}{\left|E_0^+\right|^2}, \text{ and} \qquad T = \frac{\mathrm{Re}(\hat{n}_{m+1} \cos\hat{q}_{m+1})}{n_0 \cos q_0} \frac{\left|E_{m+1}^+\right|^2}{\left|E_0^+\right|^2} \quad .$$

Appendix B contains the source code for the programs implemented for calculating R and T as function of incident angle and frequency. Also included in Appendix B is the code for calculating electric field intensities as a function of depth and some other codes.

2.3.4 In-situ infrared absorption, during annealing

The amorphous to anatase phase transformation takes place at a temperature that is low enough for simple commercial heated transmission cells (Spectra Tech, Inc.) to be used. The Bomem sample compartment was modify to include a vacuum-tight electric feedthrough with four leads (two for the heater and two for the electric signal from the thermometer). The sample (KBr pellet with 0.5% by weight of titania powder) was placed between two stainless-steel plates with holes at the center for the light passage. The plates were placed at the center of the heating unit. The temperature was monitored with a type K thermocouple mounted between the plates. The analog output signal of a digital thermometer (Omega, Inc.) was sent to a personal computer (PC) via a ADC/DAC (analog-to-digital and digital-to-analog) converter (VPI Physics Electronics Shop - Z8SVM). A program written in QuicBasic[34] (Microsoft Inc) was used to monitor and control the temperature, through a solid-state relay. The program incorporates proportional , integral, and derivative control features and allows multiple set points and ramp rates.

[34] The first version of this program was written by F. Webster, PhD Dissertation, Dept. of Chemistry,Virginia Tech (1992). The program was modify to make compatible with our equipment. The source code can be found in Webster's dissertation.

This experiment involved data collection with two computers (It was not possible to control and monitor the temperature and at the same time collect spectra with the PDP-11. In the future, after upgrading to a personal computer, one PC will do the job.) The PDP-11 collected spectra continuously and stored data as spectrum number versus time. Temperature information was collected using the personal computer and stored data as temperature versus time. To ensure equivalent time for both instruments, the PC internal clock was synchronized with the PDP-11 clock before each run. With these two sets of data, it was possible to establish the temperature that corresponds to each spectrum number.

2.3.5 Infrared reflectivity at near-normal incidence

In this section, details on the data collection and data analysis will be presented for infrared reflectivity of bulk crystals. The main experimental difficulty is small sample size. In our work on anatase crystals, this was roughly 2x2 mm^2. Before running the actual experiment, the right beam diameter should be determined. A very small beam size, just covering the sample area, will generate noisy spectra. A beam size covering an area much larger than the sample will show artifacts in the spectrum that result from reflection off the sample holder. The procedure consists of taking several spectra with different beam diameters from a mirror placed in the sample position and from the holder without any sample. Measure the maximum intensity of these spectra and ratio the maximum intensity of a mirror spectrum to the maximum intensity of a holder spectrum, both spectra taken with the same beam size. The beam diameter that corresponds to the largest ratio should be used for the actual experiment.

The incident angle is 11°, this is small enough to use the 0° (normal-incidence) approximation for reflectivity

$$R(n) = \left| \frac{\sqrt{e(n)} - 1}{\sqrt{e(n)} + 1} \right|^2 \quad .$$

Where ε(ν) is the factorized form of the dielectric function (refer to chapter four for details). This function is used to fit the reflectivity spectra. The fitting algorithm is a standard non-linear procedure based on the Levenberg-Marquardt method.[35] The user must provide the model function and its first derivative. Because of the complexity of the function, it is recommended that a symbolic software package be used to calculate the first derivative. Derive™, Mathematica™, or MathCad™ are suitable. In our calculations, Derive™ was used because of its simplicity. The source codes of the programs implemented to fit reflectivity data with the factorized form of the dielectric function are presented in Appendix C. This non-linear method works quite well in practice. The only problem that seems to arise regularly is the importance of the first guess. If the initial guess at the parameters is very far off, the program tends to wander far from the minimum, never to return. For this reason, the

[35] W. H. Press, S. A. Teukolsky, W. T. Vetterling, and B. P. Flannery, *Numerical Recipes*, (Cambridge University Press, 2nd ed. 1992) Section 15.5.

programs have implemented a visual iterative procedure that allows the user to change one parameter at a time to see on the screen what its effect is. Once a reasonable good guess is found the program runs the Levenberg-Marquardt algorithm.

2.3.6 Effective medium approximation

The programs implemented for the Bruggeman, the Maxwell-Garnett, and the generalized effective medium approximation (EMA) are presented in Appendix D. There are three different generalized-EMA programs: (1) One is applied to transmission experiments, (2) another is applied to reflectivity experiments, and (3) a third performs calculations where one of the parameters is varied (either the filling factor or the shape factor). The tables generated by this program are used to make graphs that allow us to find the right set of parameters, when comparing the theoretical and experimental results (refer to chapter six for details).

2.4 Raman Scattering Measurements

The Raman scattering measurements were performed, at room temperature, with two instruments: a SPEX 1403 Raman spectrometer and a DILOR XY Raman microprobe. The main features of the SPEX instrument are described by Holtz[36]; some experimental details on the instrumental bandwidth and the shift of the laser line with temperature and time are described by Doss.[37]
The SPEX spectrometer is equipped with a GaAs photomultiplier and photon counting electronics. A CW argon ion laser operating at 488.0 nm or 514.5 nm, and a CW krypton ion laser operating at 647.1 nm or 676.4 nm, were the excitation sources. We used an instrumental bandwidth of 4.0 cm^{-1} and a 2 cm^{-1} step size, unless otherwise indicated. The powder samples were contained in capillary tubes and spectra were obtained in the 90° scattering configuration, collecting both polarizations of scattered light.

The 514.5 nm was the laser line mostly used. The others were tried when difficulties in measuring a detectable Raman signal arouse. Most such difficulties involved the presence of luminescence in the spectrum. Changing the laser line did not always solve the problem of luminescence bands. In these cases, we used the Raman microprobe which can focus to a small area (small enough so that the luminescence could be discriminated against, when it arose from identifiable inclusions).

Raman linewidth, peak position, and peak height were determined by fitting the Raman peak with two Gaussian functions and a baseline. We used Labcalc™ to perform the non-linear fit. The Gaussian parameters do not have any physical meaning; they are simply used to obtain a convenient representation of the experimental data.

---

[36] M. Holtz, PhD Dissertation, Dept. of Physics, Virginia Tech (1987).
[37] C. Doss, PhD Dissertation, Dept. of Physics, Virginia Tech (1994).

2.4.1 Raman microprobe

The DILOR XY spectrometer is equipped with a microscope attachment. That allows the user to focus the laser on a 5x5 μm^2 area (with the 100X lens). The spectrometer is equipped with a multichannel detector (EG&G charged-couple detector), making the data collection rather fast. A CW argon ion laser operating at 514.5 nm was the excitation source, and spectra were collected in backscattering geometry. Some precautions should be taken in the spectra collection. The instrument is very sensitive to alignment, which is usually done by the technician in charge of the equipment. The signal has to be focussed on a large area, on all the detector channels (~ 1000), and the signal should have the same intensity on each channel, so that the response from every channel is uniform. Sometimes this is not the case. For this reason , compare a spectrum taken on a known sample (with the SPEX) with a spectrum taken with the DILOR. Choose a sample that has several Raman peaks over the frequency region of interest. This is very important when we are measuring relative peak heights, and more so with different spectrometers.

Two techniques were used to calibrate the laser line in the DILOR spectrometer. We took advantage (sometimes this could be a disadvantage) that the plasma line filter was ineffective, so some plasma lines appear in the spectrum. Knowing the absolute position of these lines allowed us to calibrate the Raman shift energies using data from a single spectrum (very convenient). Plasma lines can usually be a nuisance if they overlap with the Raman lines you are looking for. The standard procedure to calibrate the DILOR spectrometer is to use a neon source and take a spectrum every 2 to 3 hours, measure the peak positions of several Raman lines in the frequency range of interest, and find the calibration factors to correct the spectrum. Appendix E lists the source code of the programs used to perform this calibration.

2.5 Electron Energy-Loss Programs

The data acquisition programs for the EELS spectrometer were modified. Some elements of the new version that interact with a personal computer instead of the PDP-11 were developed. The data analysis package were compiled in a single program, making it user friendly. The source code of these programs are presented in Appendix F.

CHAPTER THREE

3. CHARACTERIZATION OF NANOPHASE TITANIA PARTICLES SYNTHESIZED USING IN-SITU STERIC STABILIZATION

3.1 introduction

Metal oxide particles under 100 nm in linear dimension can be synthesized through room-temperature hydrolysis of metal alkoxides.[38, 39] Many efforts have sought to produce small particles with controlled size, shape and porosity for use in thin films, ceramics, composites, and catalysts. The sol-gel process can be varied through changes in solution chemistry and stabilization techniques to produce different particle morphologies. Titanium tetraethoxide, $Ti(OC_2H_5)_4$, (also called tetraethylorthotitanate, or TEOT) has been hydrolyzed and condensed under various conditions to obtain dispersed submicron particles.[40]The reactions in an aqueous ethanol solution can be written in abbreviated form as:[38]

$Ti(OC_2H_5)_4 + 4H_2O$	$\rightarrow$	$Ti(OH)_4 + 4C_2H_5OH$	hydrolysis	(3.1)
$Ti(OH)_4$	$\rightarrow$	$TiO_2 \cdot xH_2O + (2\text{-}x)H_2O$	condensation	(3.2)

During hydrolysis, gel networks reach a critical size and condense into nuclei. These nuclei further aggregate to form particles. Previous work has shown that increases in initial water concentration, expressed by the molar ratio $R = [H_2O]/[TEOT]$, produced higher nucleation rates which resulted in a decrease in average particle size.[41, 42] If the reactions occur in the presence of the polymer hydroxypropylcellulose, HPC, the polymer can adsorb onto the surface of the TiO_2 particle through hydrogen bonding, creating a steric barrier which leads to smaller particle size and porous agglomerates.[43, 44] Titania particles less than 100 nm in diameter have been formed when the TEOT reacted in the presence of HPC.[40, 42]

---

[38] C.J. Brinker and G.W. Scherer *Sol-Gel Science* (Academic Press, San Diego, 1990), Chapter 4.

[39] J. Livage, M. Henry, J.P. Jolivet, and C. Sanchez, MRS Bulletin, **15(1)**, 18 (1990).

[40] J.-L. Look and C.F. Zukoski, J. Colloid Interface Sci., **153(2)**, 461 (1992); J. L. Look and C. F. Zukoski, J. Am. Ceram. Soc. **75**, 1587 (1992); J.H. Jean and T.A. Ring, Colloids and Surfaces, **29**, 273 (1988); V.J. Nagpal, R.M. Davis, and S.B. Desu, Journal of Materials Research, **10(12)**, 3068 (1995); T.E. Mates, and T.A. Ring, Colloids and Surfaces, **24**, 299 (1987).

[41] J. H. Jean and T. A. Ring, Colloids and Surfaces **29**, 273 (1988).

[42] V.J. Nagpal, J.S. Riffle, and R.M. Davis, Colloids and Surfaces, **87(1)**, 25 (1994).

[43] L.H. Edelson and A.M. Glaeser, J. Am. Ceram. Soc., **71(4)**, 225 (1988).

[44] L.H. Edelson and A.M. Glaeser, J. Am. Ceram. Soc., **71(4),** C198 (1988).

Understanding the kinetics of hydrolysis and condensation of metal alkoxides during particle formation and the role of polymer absorption at the particle surface are critical in attempting to produce metal-oxide particles with tailored microstructures and properties. Some studies have been carried out using Raman and FTIR spectroscopy. Raman measurements[45] can usually detect only relatively high reactant concentrations. Infrared measurements[46] using continuous flow techniques were used to follow the kinetics of acid-catalyzed hydrolysis and condensation of titanium alkoxide. For low water concentration (with no HPC present), a quarter of the $Ti(OR)_4$ ligands hydrolyzed within 80 ms and about half were gone at the end of the condensation step. Most studies have focused on TiO_2 particle formation at relatively low water concentrations where the reaction kinetics were slow enough to permit measurements and where well-defined, nearly spherical particles were formed with relatively narrow particle size distributions.

The sintering characteristics of titania spheres made at low water concentrations with HPC have been investigated.[43, 44] As the sintering temperature was increased, considerable shrinkage was observed which correlates to water loss, phase transformations, and densification within and between particles.[43] A recent study showed that phase transformations of sol-gel titania - phase concentrations and crystallite size - made at a constant R = 16 depended on the hydrolysis catalysts.[47] However, no detailed study has been done on the effect of HPC or high water concentrations on the phase transformations during sintering of TiO_2 particles.

This present chapter describes new results on morphological, aggregation, sintering, and annealing behavior of TiO_2 particles synthesized with and without HPC and for a wide range of water concentration. Prior to annealing the particles are amorphous with an octahedrally coordinated network that has been reported to resemble the brookite structure.[48] Typical particle sizes made with HPC were found to be in the range of 80 to 300 nm. Electron microscopy, x-ray diffraction, Raman spectroscopy, and infrared absorption were used to characterize the particles and their phase-transformation behavior under thermal annealing. The annealing behavior was found to be dependent on the initial water concentration and the presence or absence of HPC.

---

[45] T.M. Che, J.J. Rafalko, and P.B. Dorian, *Ultrastructure Processing of Advanced Ceramics* (John Wiley & Son, New York, 1988).

[46] J.L. Look and M.T. Harris, to be published in Materials Chemistry and Physics.

[47] Bokhimi, A. Morales, O. Novaro, T. Lopez, E. Sanchez, and R. Gomez, J. Mater. Res., **10**, 2788 (1995).

[48] Q.J. Wang, S.C. Moss, M.L. Shalz, A.M. Glaeser, H.W. Zandbergen, and P. Zschack, *Physics and Chemistry of Finite Systems: From Clusters to Crystals, Vol II* (Kluwer Academic Publishers, The Netherlands, 1992).

3.2 Experimental

3.2.1 Materials

Hydroxypropylcellulose polymer (HPC) was obtained from Aqualon, a subsidiary of Hercules Chemical Co. HPC consists of a cellulose backbone with an average of three hydroxypropyl units per anhydroglucose unit. The average molecular weight was 60 kg $mole^{-1}$. Tetraethylorthotitanate (95 weight % TEOT, 5% ethanol) was obtained from the Alfa Chemical Co. Anhydrous ethanol (200 proof) was purchased from the Aaper Alcohol and Chemical Co. Deionized water with a specific resistance of (16-18) x 10^{-6} mhos. All solutions were filtered through (0.2 μm) PTFE hydrophobic syringe filters. Glassware was cleaned with solutions of alcoholic KOH followed by 2M HNO_3, then thoroughly rinsed with deionized water and dried at 60°C. Experiments were conducted at 25±2°C under dry nitrogen.

3.2.2 Particle synthesis

In our work, we used [TEOT] = 0.075 M. These water concentrations were used: R = 5.5 (low), 15, 30, 60, and 155 (high). Under nitrogen, mixing was done with equal volume solutions. Two mixing procedures were followed. For the standard method, one flask contained either deionized water and 200 proof ethanol (when no HPC was used) or it contained deionized water, 200 proof ethanol, and HPC that had been previously dissolved in ethanol (when HPC was included in the synthesis). A second flask contained TEOT dissolved in ethanol. Both solutions were filtered through syringes before use. The two flasks were mixed together quickly, stirred for 5 seconds, and then allowed to stand for 24 hours.

In the second mixing procedure, the premix method, HPC-containing samples were prepared by premixing the HPC and TEOT ethanol solutions and allowing the mixed solution to stand for periods of 100 minutes before addition of an equal volume of an ethanol-water solution. After the addition of the ethanol-water solution, the mixtures were left to react for 24 hours. In both mixing methods, experiments conducted with HPC were done at a polymer concentration of 1.7 g l^{-1} in the reaction mixture.

3.2.3 Sintering

After the solutions were centrifuged for 20 minutes at 19,000 g-force, the supernatant was removed and the wet powder was dried in air at 60°C for 48 hours. The dried powders were gently ground with a mortar and pestle. Some samples were pressed into pellets at a pressure of 0.74 GPa for 3 minutes. Most of the samples (including all of the pellets) were annealed in air using the following schedule. Slow heating (1.5°C min^{-1}) was done up to 300°C, followed by a dwell time of 2 hours at that temperature. Then the sample was heated at 20°C min^{-1} up to the desired anneal temperature, and then held at that temperature for a 2-hour dwell time. This was followed by slow cooling back to room temperature. The slow heating to 300°C and the long dwell times were found to be an effective method for avoiding cracking of the

pellets. Anneal temperatures from 300°C to 1000°C were used at intervals of 100°C. For some of the powder samples, a simpler procedure was used: heating at 20°C min^{-1} to the anneal temperature, followed by a 40-minute dwell time, and slow cooling to room temperature.

3.2.4 Characterization

Scanning and transmission electron microscopy, SEM and TEM, were performed with a Phillips Model 420T electron microscope. SEM samples were placed in the form of a dry powder on a copper substrate using double-sided conductive tape and were then sputter-coated with gold. TEM samples were prepared by placing a drop of the sample solution (diluted tenfold with ethanol) onto a 150 mesh Cu grid with a Formvar film. X-ray diffraction data were obtained at room temperature, using a Scintag XDS-200 powder diffractometer and CuKα radiation with a wavelength of 1.54 Å. The x-ray measurements were carried out on powder samples placed on oriented quartz substrates.

Raman spectroscopy was performed with a SPEX 1403 Raman spectrometer with a GaAs-photocathode photomultiplier and photon-counting electronics. A CW argon ion laser operating at 514.5 nm was the excitation source. The laser power at the sample was approximately 30 mW. We used an instrumental bandwidth of 4 cm^{-1} and data were taken at every wavenumber. Spectra were taken in the 90° scattering configuration. A few low-temperature-anneal samples (whose Raman spectra are included in Fig. 3.8) contained black organic residual material. A micro-Raman instrument (DILOR XY spectrometer with a CCD detector) was used in the backscattering geometry to capture Raman spectra of organic-free regions of these samples. All Raman spectra were taken at room temperature.

Infrared spectroscopy was performed with a BOMEM DA 0.02 FTIR spectrometer. The infrared results reported here, unlike the Raman results, are in-situ measurements taken while the sample was at elevated temperature. Powder samples were diluted in KBr (0.5% wt/wt) and pressed into pellets. The pellet was mounted in a special optically accessible heater located within the evacuated sample space of the spectrometer. A heating rate of 1.25°C min^{-1} was used to scan the temperature range from room temperature to 550°C. Spectra were taken continuously in the 230 to 700 cm^{-1} range with 2 cm^{-1} resolution and coadding every 50 scans while the temperature was increasing. It took approximately 4 min to collect one spectral scan.

3.3 Results and Discussion

3.3.1 Particle characterization

3.3.1.1 Electron microscopy

For particles made with the standard method at the low water concentration (R = 5.5), HPC has a noticeable effect on the resulting particle morphology, as shown in Figures 3.1 and 3.2. The unheated titania particles made without HPC are 1 to 5 μm in diameter, agglomerated, and have relatively smooth surfaces (Figure 3.1). The surface features are indicative of aggregation of 2 to 10 nm units after nucleation. The particles made with HPC have a narrower size distribution (mean diameter ~ 400 nm), are discrete and show an underlying substructure of irregular spheres 10 to 40 nm in size. As the nuclei aggregate, ongoing polymer adsorption at their surfaces generates repulsive steric forces that provide a barrier to further aggregation. These small aggregates are then welded into larger, more uniform spheres by further hydrolysis and condensation.

Similar structural differences were observed for particles made with and without HPC at R=60. The particles made with HPC exhibited intraparticle substructures with the same dimensions as those made at the lower water concentration, but the average particle size was smaller at R = 60. A previous study showed a systematic decrease of average TiO_2 particle diameter with increasing water concentration up to R = 60 for particles grown in the presence of HPC. [42] This was due to an increasing nucleation rate and to increased HPC adsorption on the growing particles.

Particles obtained at high water concentrations (R = 155) are shown in Figure 3.3. They are loosely aggregated irregular, spheres 20 to 70 nm in diameter whose substructure closely resembles that of the R = 5.5 samples above. The appearance was identical for samples made with and without HPC. This similarity may be caused by the relatively slow rate of polymer adsorption at the surface compared to the relatively rapid formation rate of particle surface area by the hydrolysis and condensation reactions. This morphology was observed for all particles made at water concentrations of R = 120 and higher.

For the premix method, the R = 5.5 sample had a fine sediment and a flocculated region which filled 80% of the suspension volume, quite similar to the R = 5.5 sample made by the standard method. Samples made by the premix method at R = 60 and 155 were gelled until they separated into chunks upon shaking. These samples had a reddish cast when viewed by transmission. By comparison, the corresponding samples made by the standard method were quite turbid. SEM pictures (Figure 3.4) of particles made by the premix method at R = 5.5 showed the particles to be interconnected. Particles made at R = 60 and = 155 were made up of chains and loose agglomerates of 10 to 50 nm units.

3.3.1.2 Spectroscopy

Raman and X-ray spectroscopy showed that all unheated particles as prepared using this sol-gel technique were amorphous. This is consistent with previous work.[42, 43]

3.3.2 Sintering of titania powder

3.3.2.1 Electron Microscopy

As the sintering temperature increases, those particles made by the standard method with HPC at R = 5.5 displayed substructure coarsening and a moderate decrease in average diameter with no interparticle necking observed until annealed at 1000°C (see Figure 3.5). By contrast, the particles without HPC did not change in appearance except for interparticle necking which occurred at 600°C, as shown in Figure 3.6.

3.3.2.2 Spectroscopy

Raman scattering and x-ray diffraction were used to assess the crystallinity of the annealed powders. Figure 3.7 shows typical Raman spectra for the various forms of titania. Figure 3.8, for a powder sample made by the premix method at R = 5.5, shows that Raman spectroscopy can be used to track the evolution of phase composition of the titania with annealing temperature. Upon heating, amorphous titania particles convert to anatase at about 250°C and then from anatase to rutile at about 800°C. The low temperature phase conversion was also followed by measuring the infrared absorption of titania powders, dissolved in a KBr matrix, while they were being heated (in-situ annealing). Figure 3.9 shows the results for a powder sample made by the standard method at R = 5.5. At about 200°C, the main absorption feature of anatase is visible. To determine phase transformations (anatase to rutile) at higher temperatures, x-ray and Raman peak intensity ratios were used. Figure 3.10 shows x-ray spectra for powder samples at R = 5.5 annealed to different temperatures using the 40-minute anneal time. The intensity ratio of the (101) anatase peak to the (110) rutile peak has been used to determined phase composition.[49]

$$[\text{anatase}]/[\text{rutile}] = 0.79\ (I_{101}/I_{110}) \qquad (3.3)$$

Likewise the intensity ratio of the 141 cm^{-1} anatase peak to the 440 cm^{-1} rutile Raman peak is used to determined phase composition. Samples of known phase composition (as determined by x-ray diffraction) were used to calibrated the Raman spectra. Figure 3.11 shows the calibration curve:

[49] R.A. Spurr and H. Myers, Analytical Chemistry, **29(5)**, 761 (1957).

$$[\text{anatase}]/[\text{rutile}] = 0.038\ (I_{141}/I_{440}) \qquad (3.4)$$

The small value of the numerical factor in (3.4) is a consequence of the great intensity of the 141 cm^{-1} anatase line.
Figure 3.12 shows the results of samples annealed using the 2-hour anneal time. These samples were prepared by the standard method . Powders transform more readily than pellets. Conversion increased markedly with water concentration for powders and pellets made with HPC. Conversion also increased markedly in the presence of the HPC for both powders and pellets. Similar trends are seen in Figure 3.13 for particles made by both mixing methods. Samples were annealed using the 2-hour anneal time. Both methods show the same trend of conversion with respect to water concentration (particle size). There is a step increase until a plateau is reached at R = 60. Particles prepared by the premix method show higher conversion than particles prepared by the standard method. The premix method mixes HPC more intimately with TiO_2 than does the standard method. There is a strong likelihood that a transesterification reaction occurs between the hydroxypropyl side groups on the HPC chain and the ethoxide groups on the TEOT. This reaction would be favored in the premix method. We hypothesize that the effective surface area per unit mass of the TiO_2 made by the premix method is greater than obtained with the standard method and that the larger surface area provides more nucleation sites to facilitate the transition to the rutile form.

3.4 Conclusions

The size and morphology of ultrafine titania particles synthesized by the hydrolysis and condensation of TEOT can be controlled by varying initial water concentration and the solution concentration of the polymeric stabilizer HPC. Solutions having larger water concentrations produced particles with smaller average diameters, from 1-5 μm without HPC to less than 70 nm with HPC. Increases in water content led to particles which converted earlier (at lower temperature), during sintering, from anatase to rutile. The extent of aggregation of particles formed at the low (R = 5.5) and medium (R = 60) water concentrations were greatly affected by the presence of HPC in solution. The polymer adsorbed at the surfaces of growing nuclei, resulting in a repulsive steric barrier to aggregation and a narrow size distribution. Conversion from anatase to rutile increased markedly with water concentration and with the presence of HPC during particle formation. At 800^{o}C, the transformation from anatase to rutile was more than 95% complete for particles grown at the highest water concentration (R = 155) and with HPC premixed with TEOT. Conversely, particles made at the lowest water concentration (R = 5.5) without HPC showed no detectable conversion to rutile at this temperature. A possible mechanism for HPC's role is proposed in enhancing conversion.

Figure 3.1.- (a) Transmission electron microscopy (TEM) micrograph and (b) scanning electron microscopy (SEM) micrograph of particles made at low water concentration (R=5.5) without HPC by the standard method .(fig31.jpg) (27Kbytes)

Figure 3.2.- (a) TEM and (b) SEM micrographs of particles made at low water concentration (R=5.5) with HPC by the standard method .(fig32.jpg) (45Kbytes)

Figure 3.3.- (a) TEM and (b) SEM micrographs of particles made at high water concentration (R=155) with HPC by the standard method .(fig33.jpg) (28Kbytes)

Figure 3.4.- (a) Low magnification and (b) high magnification SEM micrographs of particles made at low water concentration (R=5.5) by the premix method . (fig34.jpg) (28Kbytes)

Figure 3.5.- SEM micrographs of particles made at low water concentration (R=5.5) with HPC by the standard method and annealed using the 40-minute anneal time: (a) room temperature, (b) annealed to 600°C, (c) annealed to 800°C and (d) annealed to 1000°C. (fig35.jpg) (42Kbytes)

Figure 3.6.- SEM micrograph of particles made at low water concentration (R=5.5) without HPC by the standard method and annealed to 600°C using the 40-minute anneal time.(fig36.jpg) (21Kbytes)

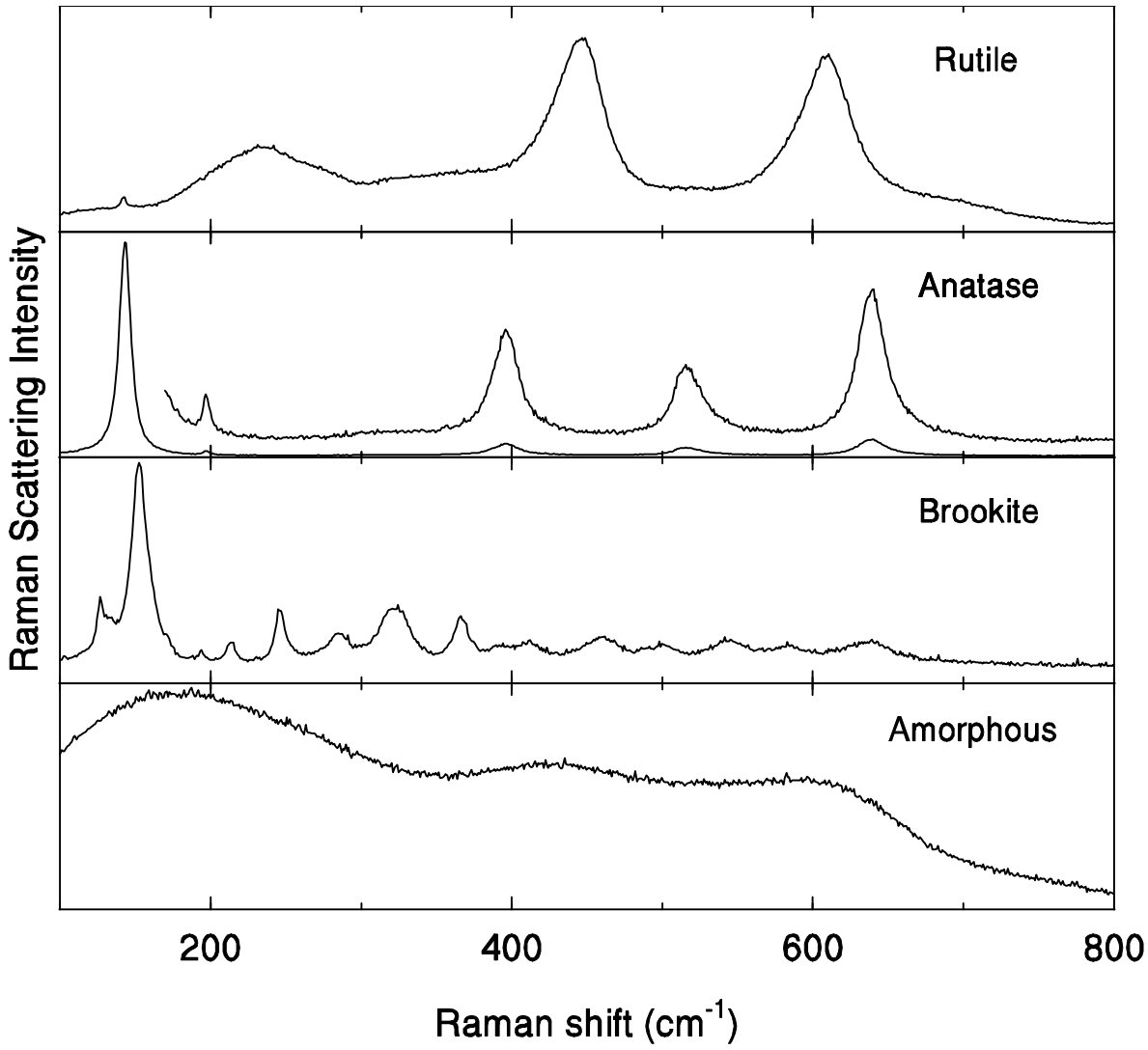

Figure 3.7.- Raman spectra of the various phases of titania. Data were taken at room temperature on powder samples with the 90° scattering configuration.

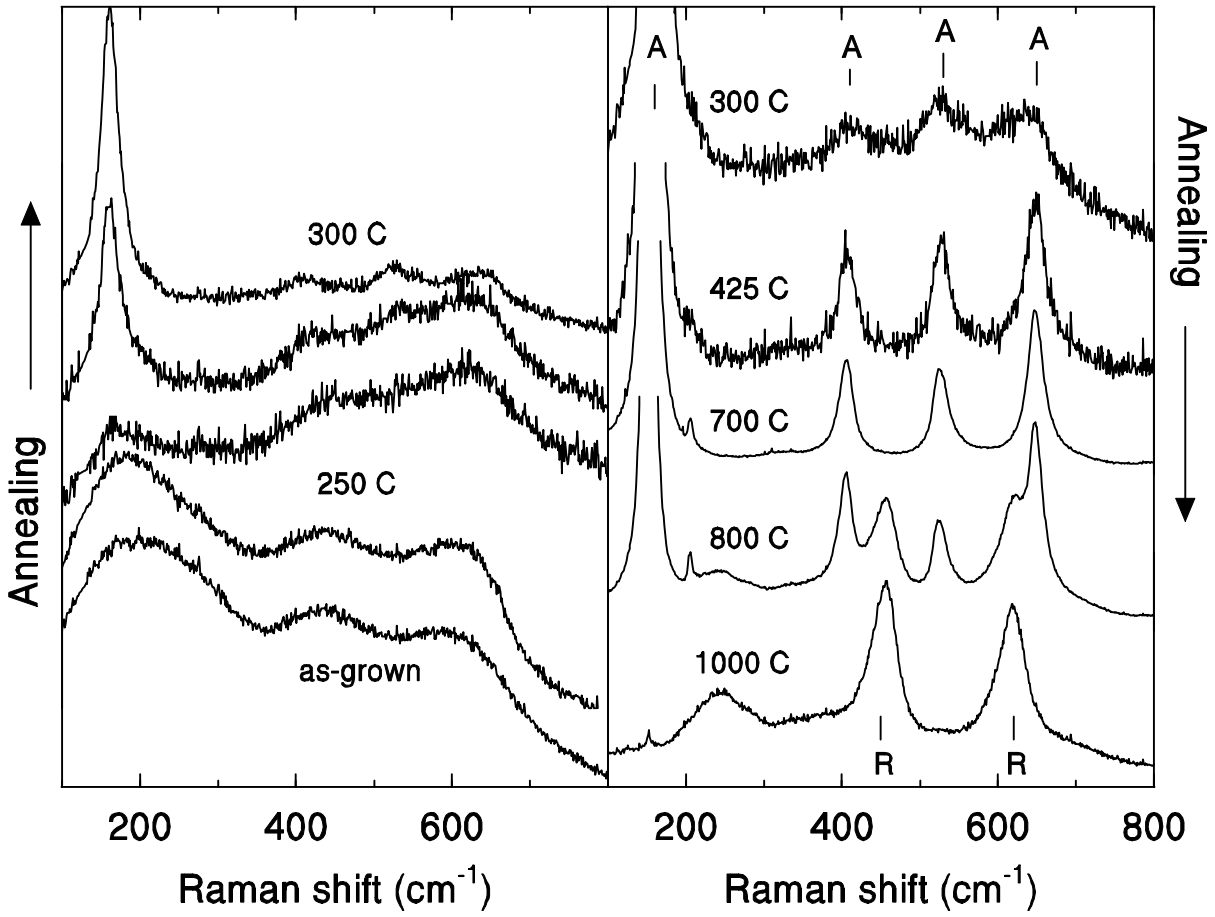

Figure 3.8.- Room temperature Raman spectra of powder samples (prepared by the premix method at R = 5.5) after annealing to different temperatures using the 40-minute anneal time. As grown particles are amorphous. At about 250°C, the 141 cm^{-1} anatase peak starts to grow and by 400°C conversion to anatase is complete. The anatase to rutile transformation is clearly visible at 800°C, where approximately 50% conversion of anatase to rutile has occurred (see Fig. 13). At 1000°C the conversion to rutile is complete. The 250°C spectra were taken with a micro-Raman instrument because of the presence of residual organic carbon which produced luminescence that obscured the anatase Raman peaks. With the microscope attachment (80 to 100X), we could focus on relatively organic-free parts of the sample.

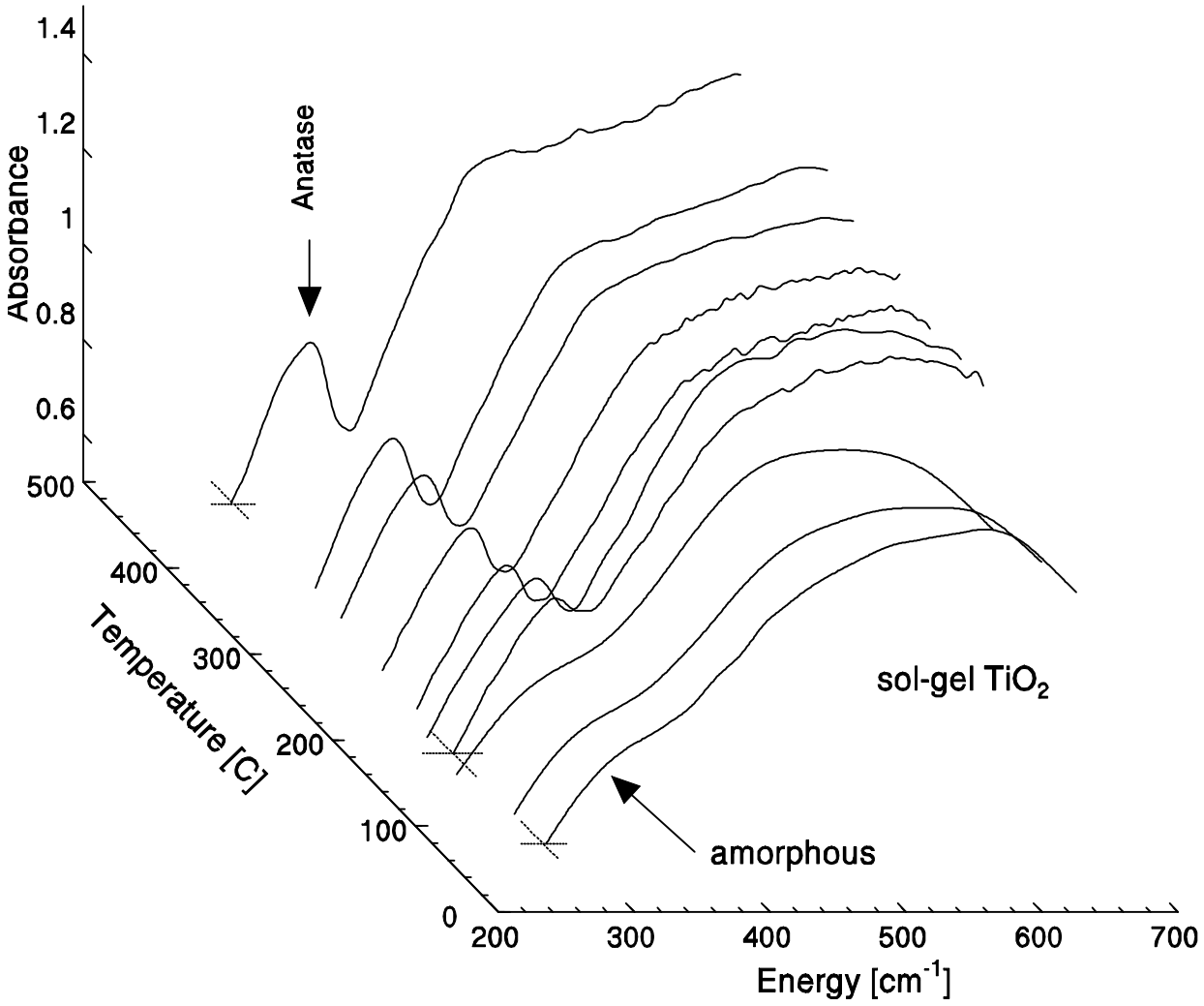

Figure 3.9.- Infrared spectra of powder samples made at low water concentration (R=5.5) without HPC (prepared by the standard method) diluted in KBr and pressed into pellets. These are in-situ temperature-dependent measurements; the sample was being annealed while taking data in infrared transmission mode. The characteristic anatase infrared band at 348 cm^{-1} clearly makes its appearance by 200°C.

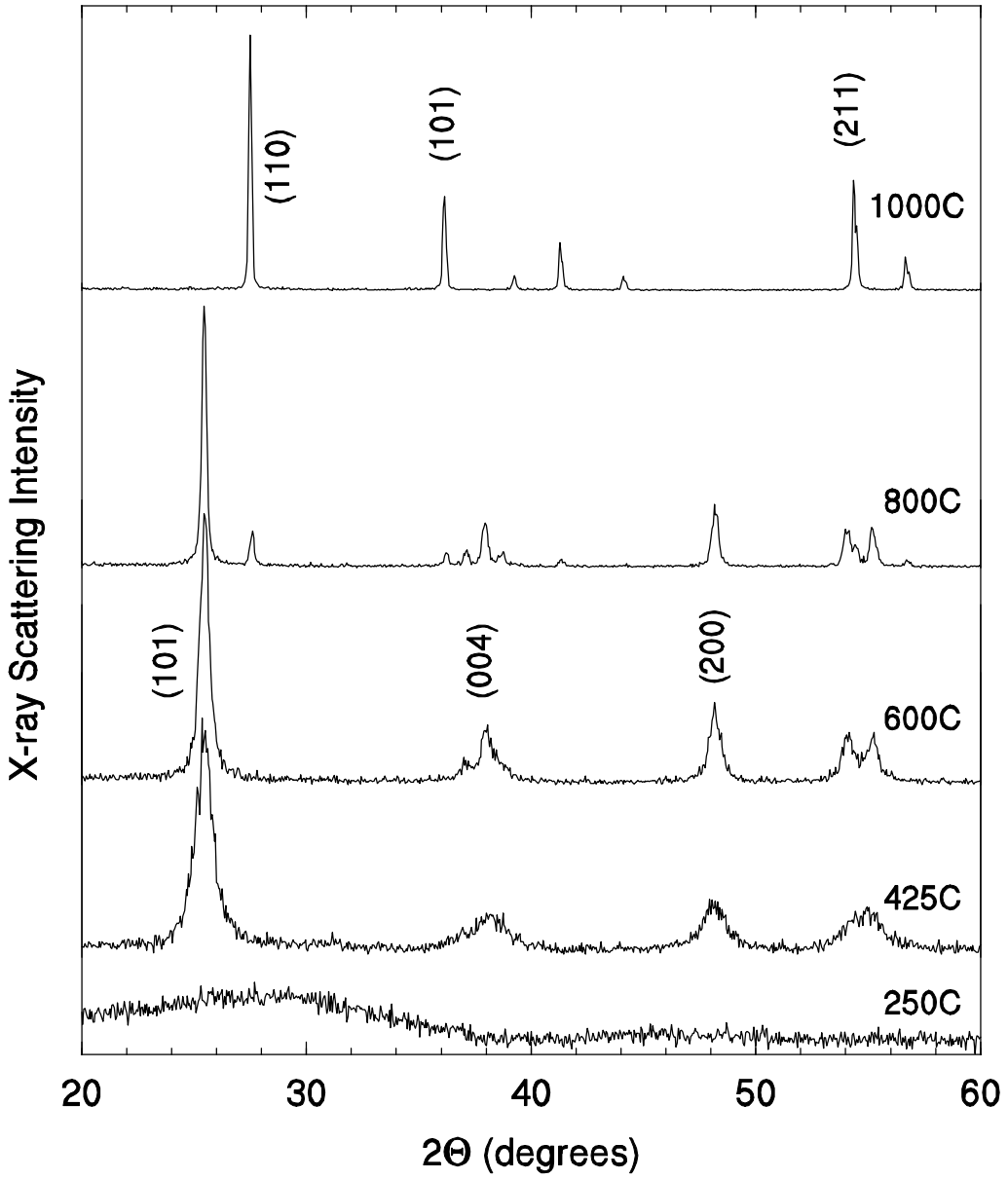

Figure 3.10.- X-ray diffraction data taken on powder samples (prepared by the standard method with R = 5.5) annealed to different temperatures using the 40-minute anneal time. The 425°C and 600°C curves show only anatase features, the 800°C curve shows mixed anatase and rutile features, and the 1000°C curve shows only rutile features. Samples annealed to 300°C did not show any anatase features.

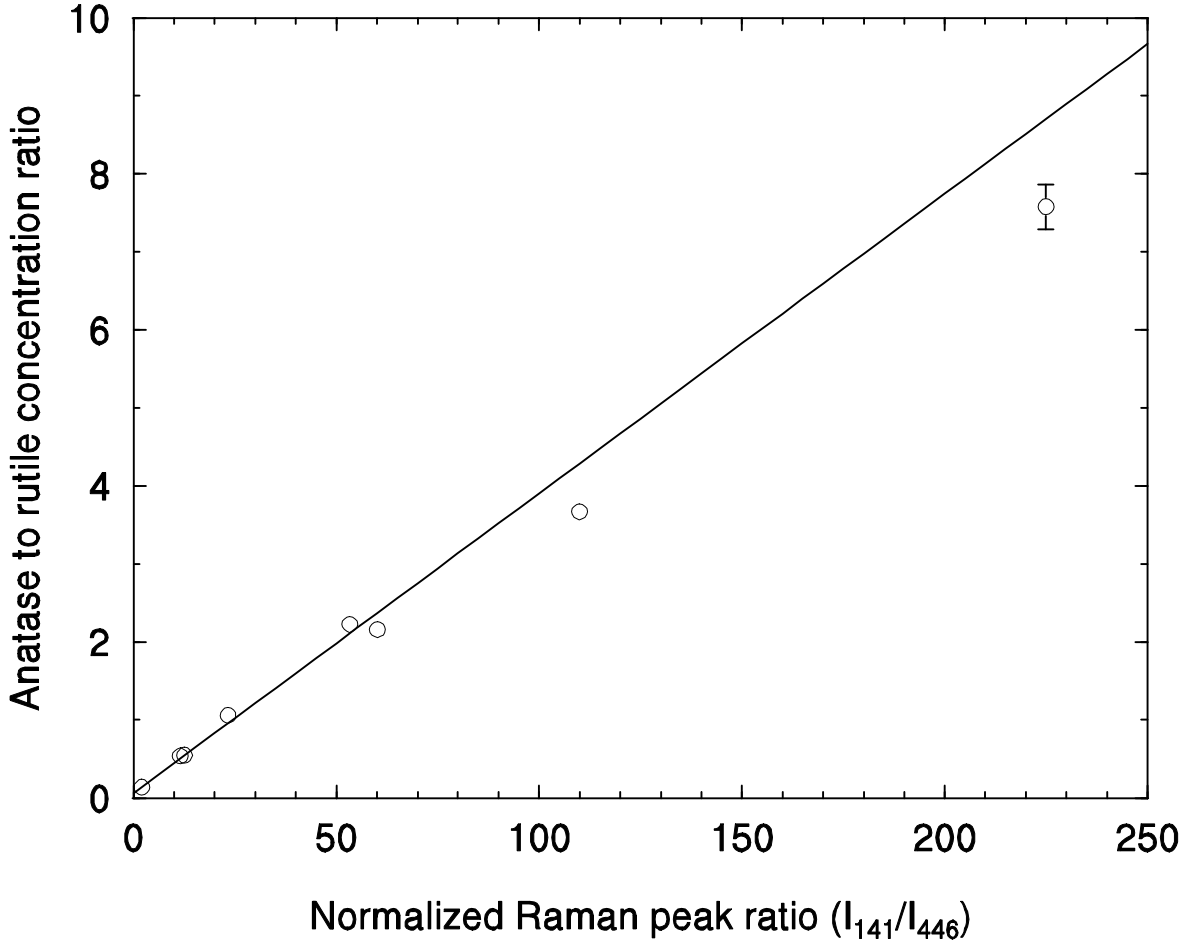

Figure 3.11.- Raman calibration curve. The anatase to rutile concentration ratio (as determined by x-ray measurements) is plotted versus the intensity ratio of the 141 cm^{-1} anatase peak to the 440 cm^{-1} rutile peak.

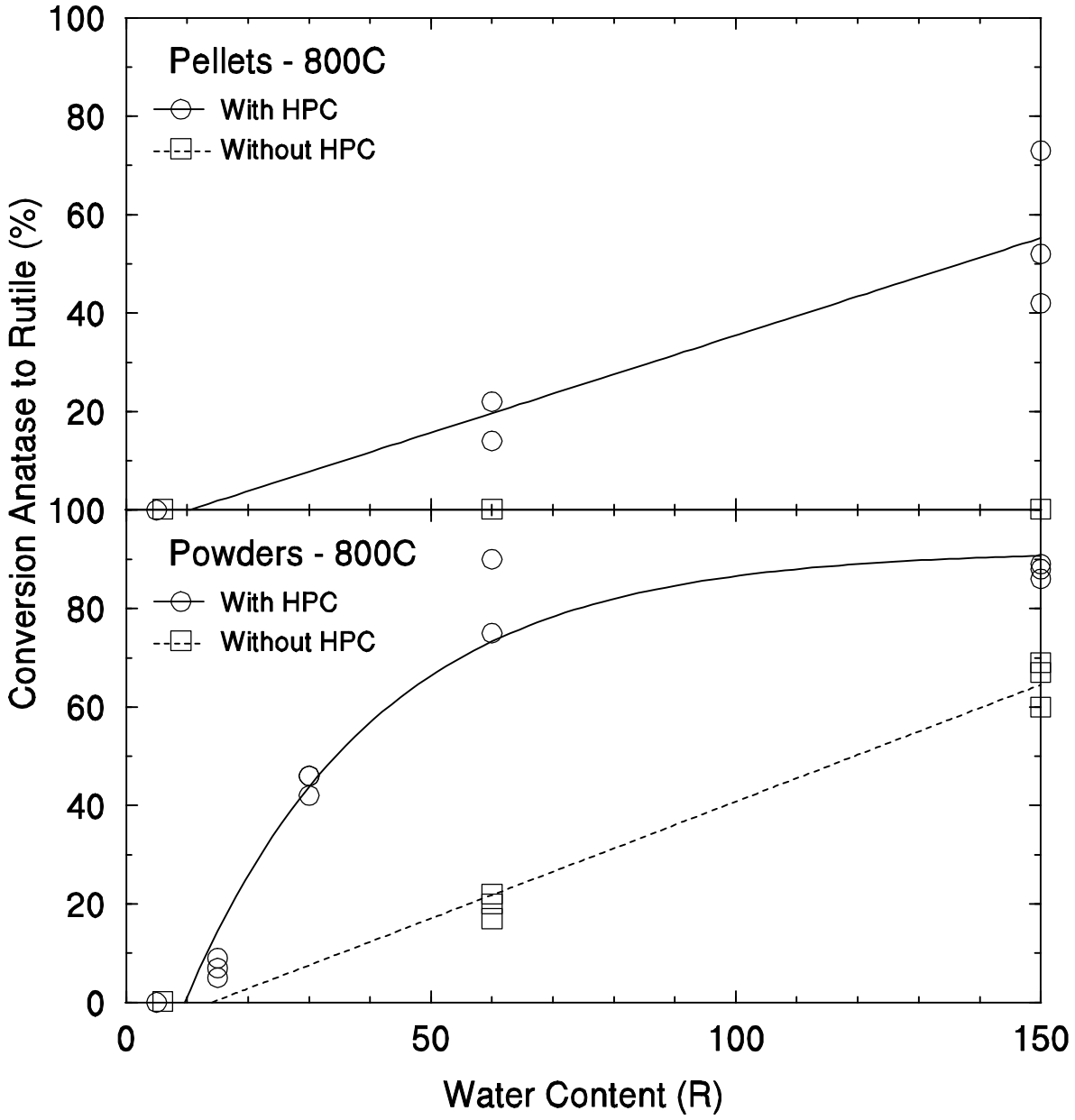

Figure 3.12.- Conversion of anatase to rutile as a function of water content (particle size) for powder samples prepared by the standard method and annealed to 800°C using the 2-hour anneal time: (a) powders prepared with and without HPC were pressed into pellets at a pressure of 0.74 GPa for 3 minutes prior to annealing, (b) powders prepared with and without HPC were ground with mortar and pestle prior to annealing.

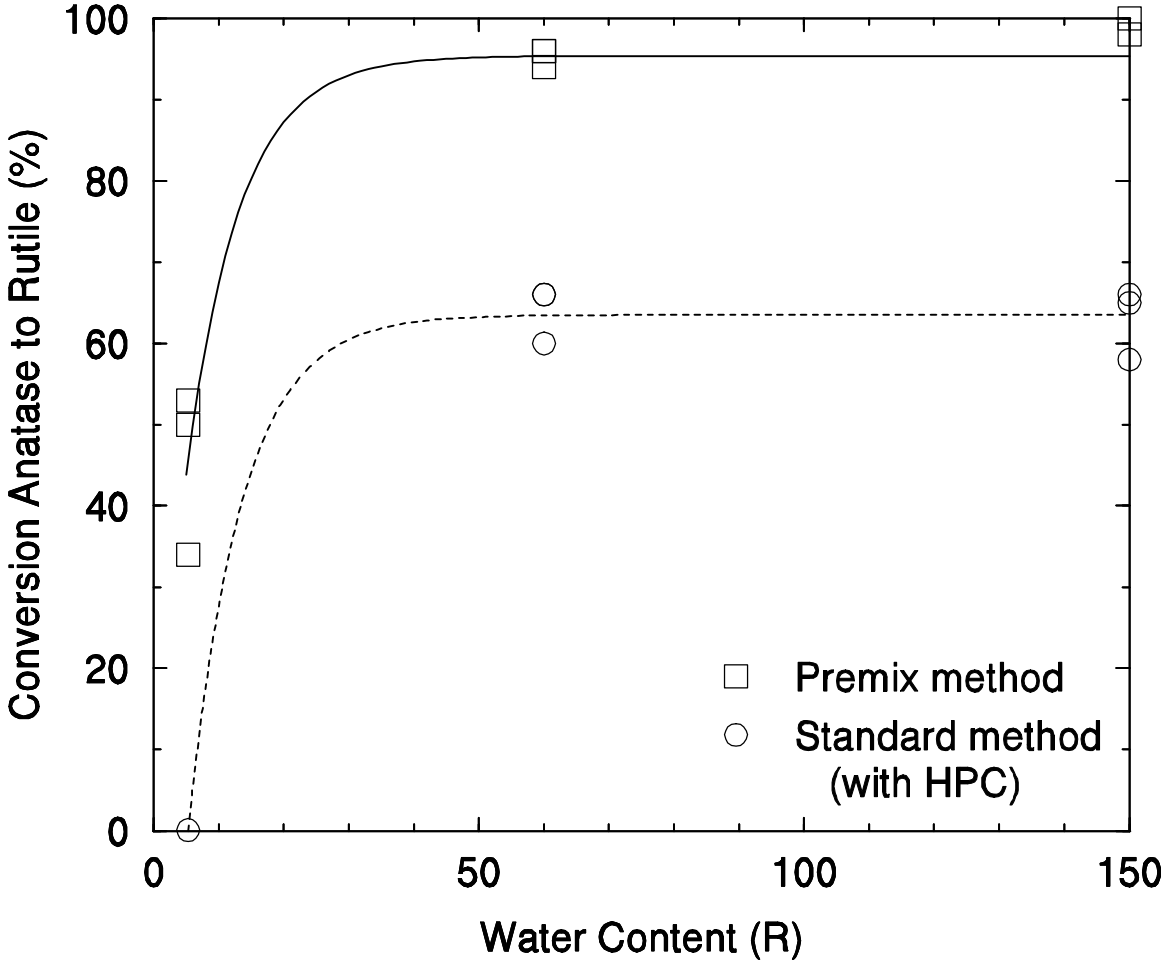

Figure 3.13.- Conversion of anatase to rutile as a function of water content (particle size) for powder samples prepared by the standard method and the premix method and annealed to 800°C using the 40-minute anneal time.

CHAPTER FOUR

4. INFRARED REFLECTIVITY AND LATTICE FUNDAMENTALS IN ANATASE TiO_2

4.1 Introduction

The crystal forms of titanium dioxide (titania) are rutile, anatase, and brookite. They are wide-bandgap semiconductors, transparent in the visible, with high refractive indices. Rutile is the stable phase at high temperature and is by far the most-studied and best-understood phase. Because large single crystals of rutile have long been available, the lattice dynamics of rutile TiO_2 in the lattice-fundamentals regime has been studied by polarization-dependent far-infrared reflectivity measurements[50, 51] and by neutron scattering measurements as well.[52] To our knowledge, no similar work has yet been reported for anatase TiO_2, although there have been studies of the Raman-active lattice fundamentals.[53] The near-bandgap optical absorption edge of anatase has recently been measured.[54]

In this chapter, we present the results of far-infrared reflectivity measurements on two types of anatase samples: single crystals and nanocrystalline pressed pellets. The polarization-dependent single-crystal results are analyzed to yield the zone-center transverse-optical (TO) and longitudinal-optical (LO) phonon frequencies, effective charges, and polariton dispersion curves of anatase. The nanocrystal spectra are analyzed by means of an effective medium theory that incorporates the effect of surface roughness in addition to the bulk TO and LO frequencies

4.2 Experimental

Anatase crystals were grown by chemical transport reactions.[55] As-grown single crystals were up to 5 mm in size, with an octahedral shape limited by (101) natural faces. Two crystals were used in this study. These were cut and polished; one to yield a surface containing the tetragonal c-axis, the other to yield a surface perpendicular to the c-axis. Alumina powder was used for polishing, the final grit size being 0.1 μm. The area of the optical surface was about 8 mm^2 for the parallel-to-c surface and about 9 mm^2 for the perpendicular-to-c surface.

---

[50] W. G. Spitzer, R. C. Miller, D. A. Kleinman, and L. E. Howarth, Phys. Rev. **126**, 1710 (1962).
[51] F. Gervais and B. Piriou, J. Phys. C. **7**, 2374 (1974).
[52] J. G. Traylor, H. G. Smith, R. M. Nicklow, and M. K. Wilkinson, Phys. Rev. B **3**, 3457 (1971).
[53] T. Ohsaka, F. Izumi, and Y. Fujiki, J. Raman Spectrosc. **7,** 321 (1978).
[54] H. Tang, F. Levy, H. Berger, and P. E. Schmid, Phys. Rev. B **52**, 7771 (1995).
[55] H. Berger, H. Tang, and F. Levy, J. of Crystal Growth, **130**, 108 (1993).

Ultrafine titania particles were synthesized by the hydrolysis and condensation of titanium tetraethoxide ethanol solutions, using hydroxypropylcellulose polymer as a steric barrier in order to form particles with relatively narrow size distribution compared to particles synthesized in the absence of the polymer.[56, 57] The amount of water used in hydrolysis controls the particle size, which ranged from 80 to 300 nm. The resulting colloidal sol was centrifuged and dried to yield a white powder, which was then pressed into a pellet using 0.74 GPa for 3 minutes. Since the as-prepared sol-gel titania particles are amorphous, the pellets were annealed at a temperature between 300 and 800°C to yield anatase.[8] The crystallite size, as estimated by x-ray peak widths, increased from 15 to 80 nm as anneal temperature increased from 300 to 800°C.

The infrared measurements were performed with a BOMEM DA-3 FTIR spectrometer. A pyroelectric detector was used to cover the wavenumber region from 50 to 700 cm^{-1}; a HgCdTe detector was used from 600 to 5000 cm^{-1}. Spectra were collected with a 1 cm^{-1} resolution. At least 400 interferometer sweeps were added for each spectrum. For measurements with light polarized parallel to the crystal c-axis, a wire-grid polarizer was used. (The low-frequency cutoff, determined by the polarizer substrate, KRS-5, was 200 cm^{-1}) Reflectivity was measured at an angle of incidence of 11°, and was determined by comparison to an aluminum mirror standard.

4.3 Infrared-active modes of anatase

Anatase is tetragonal, with two TiO_2 formula units (six atoms) per primitive cell. The space group is D_{4h}^{19} (I4/amd), number 141 in the standard listing. The structure is shown at the left side of Fig. 4.1. The c-axis is vertical, small circles denote Ti atoms, large circles denote O atoms. Oxygen atoms labeled with the same number are equivalent. The octahedral coordination of the titanium atoms is seen to be significantly distorted.

The 18-dimensional reducible representation generated by the atomic displacements contains the zone-center (*k=0)* modes: 3 acoustic modes and 15 optical modes. The irreducible representations corresponding to the 15 optical modes are[4] $1A_{1g} + 1A_{2u} + 2B_{1g} + 1B_{2u} + 3E_g + 2E_u$. Three modes are infrared active, the A_{2u} mode and the two E_u modes. (The B_{2u} mode is silent.) The A_{2u} mode is active for light polarized parallel to the c-axis (E ∥ c); the E_u modes are active for light polarized perpendicular to the c-axis (E ⊥ c).

---

[56] V. J. Nagpal, J. S. Riffle, and R. M. Davis, Colloids and Surfaces, **87(1)**, 25 (1994); V. J. Nagpal, R. M. Davis, and S. B. Desu, J. Materials Research **10**, 3068 (1995).
[57] A. Gaynor, R. J. Gonzalez, R. M. Davis, and R. Zallen, (submitted to the Journal of Materials Research).

The vibrational eigenvector for the A_{2u} is symmetry-determined; it is shown in Fig. 4.1. Symmetry coordinates for the E_u modes are also shown. The actual E_u eigenvectors are mutually orthogonal combinations of these.

4.4 Polarization-dependent reflectivity, dielectric function, and polariton dispersion

Figure 4.2 presents our results for the far-infrared reflectivity of single-crystal anatase, for E||c and for E⊥c. (The frequency or photon-energy scale used throughout this paper is in terms of wavenumber, $\bar{n} = \lambda^{-1}$.) The E||c results, obtained for a surface containing the c-axis, required the use of a polarizer which cut off below 200 cm^{-1}. The E⊥c results, obtained for a surface normal to the c-axis, required no polarizer and extended down to 50 cm^{-1}. (The 50-100 cm^{-1} range, not shown in Fig. 4.2, contained no discernible structure.)
The theoretical curves included in Fig. 4.2 are based on the factorized form of the dielectric function[51, 58, 59, 60]

$$e(n) = e_1(n) - ie_2(n) = e_\infty \prod_n \frac{n_{LOn}^2 - n^2 + ig_{LOn}n}{n_{TOn}^2 - n^2 + ig_{TOn}n} \qquad (4.1)$$

The factorized form is more elegant than the classical-oscillator form,[58, 59] and it is especially appropriate to highly ionic crystals (such as anatase) which have large TO-LO splittings. When ν_{LO} is much larger than ν_{TO}, a single damping parameter γ (as is used in oscillator analysis) is inadequate and the factorized-form analysis is more successful.[51, 60] We carried out both oscillator and factorized-form analyses of the data shown in Fig. 4.2. Both methods give good fits (and essentially identical results for ν_{TO} and ν_{LO}) for E||c. But for E⊥c, only the factorized form gives a good fit to the measured reflectivity spectrum.

Table 4.1 lists the TO and LO frequencies corresponding to the fitted curves shown in Fig 4.2. Also included in the table are the corresponding damping parameters and two sets of published calculations for the TO and LO frequencies using rigid-ion[61] and GF-matrix[53] models. The calculations tend to overestimate the vibrational frequencies and underestimate the TO-LO splittings (oscillator strengths)

The e_∞ values in Table 4.1, for frequencies well above the lattice-fundamental regime, correspond to ε's at frequencies below the electronic interband regime. Using $\varepsilon = n^2$ where n is

---

[58] T. Kurosawa, J. Phys. Soc. Japan **16**, 1298 (1961). Setting $\nu = 0$ in the factorized form yields the Lyddane-Sachs-Teller relation.
[59] D. W. Berreman and F. C. Unterwald, Phys. Rev. **174**, 791 (1968).
[60] F. Gervais and B. Piriou, Phys. Rev. B **10**, 1642 (1974); J. F. Baumard and F. Gervais, Phys. Rev. B **15**, 2316 (1977).
[61] N. Krishnamurthy and T. M. Haridasan, Indian J. of Pure and Appl. Phys. **17**, 67 (1979).

the refractive index, our e_∞ values correspond to refractive indices of 2.33 (E||c) and 2.41 (E⊥c). Reported values of *n* in the visible region are[62] 2.49 (E||c) and 2.56 (E⊥c), indicating that our *n* values are about 6% low. This does not affect our results for the TO and LO frequencies, which are predominantly determined by the shape of the reflectivity spectrum. We estimate the probable error in our frequency values to be no more than ±3 cm^{-1} for the TO and E||c LO frequencies, and ±5 cm^{-1} for the E⊥c LO frequencies.

Table 4.1. TO and LO Phonon Frequencies of Anatase TiO_2

Mode		Dielectric function fit to R($\bar{n}$)		Published Calculations	
		Frequency	Damping	Rigid-Ion[12]	GF-matrix[4]
		$\bar{n}$ (cm^{-1})	γ (cm^{-1})	$\bar{n}$ (cm^{-1})	$\bar{n}$ (cm^{-1})
E // c-axis	**TO**	**367**	**68**	566	654
(A_{2u})	**LO**	**755**	**79**	844	
E ⊥ c-axis	**TO**	**262**	**36**	329	169
(E_u)	**LO**	**366**	**4.1**	428	
	TO	**435**	**32**	644	643
	LO	**876**	**33**	855	
e_∞ (E//c) = 5.41		**ε_0(E//c)=22.7**			
e_∞ (E⊥c) = 5.82		**ε_0(E⊥c)=45.1**			

From the experimental values given in Table 4.1 and the ε(ν) expression of equation (1), it is straightforward to determine the following spectroscopic quantities in the far infrared: the real and imaginary parts of the dielectric function *e*, the real and imaginary parts of the complex refractive index n^c, the optical absorption coefficient, and the polariton dispersion curves $n(q_1)$, where q_1 is the real part of the complex propagation vector describing the coupled photon-phonon wave in the crystal.[63] We limit our discussion of spectroscopic quantities to the dielectric function and the polariton dispersion.

Figure 4.3 shows the results derived for the E||c and E⊥c dielectric functions for anatase, in the far infrared. The shaded bars highlight the TO-LO splittings, which are large.

[62] *Handbook of Chemistry and Physics*, 68th ed. (CRC Press, Boca Raton, 1987-88), p. B-193.
[63] R. Zallen, G. Lucovsky, W. Taylor, A. Pinczuk, and E. Burstein, Phys. Rev. B **1**, 4058 (1970); R. Zallen, M. L. Slade, and A. T. Ward, Phys. Rev. B **3**, 4257 (1971).

Polariton dispersion curves are shown in Fig. 4.4. The steps from $\varepsilon(\bar{n})$ to $\bar{n}(q_1)$ are[63]: $n^c(\bar{n}) = \sqrt{e(\bar{n})}$; $q^c(\bar{n}) = 2p\bar{n}n^c(\bar{n})$; $q_1(\bar{n}) = \mathrm{Re}\left[q^c(\bar{n})\right]$. The solid curves correspond to the experimental factorized-form parameters of Table 4.1. The dashed curves result from setting the damping parameters equal to zero; they display the classical coupled-wave form with $q=0$ intercepts at LO frequencies and $q \to \infty$ asymptotes at TO frequencies.[64] The light lines show the asymptotic slopes, which are inversely proportional to the optical refractive index (long line) and static refractive index (short line).

4.5 Effective charges

The vibrational eigenvector of the lone A_{2u} optical mode in anatase is fully determined by symmetry: the atomic displacements x_{Ti} and x_O are parallel to the c-axis and $(x_{Ti} / x_O) = -0.67$. (The mass ratio (m_{Ti}/m_O) is 2.994.) This presents us with an opportunity to estimate effective charges, using the approach of Kurosawa.[58] Since TiO_2 is highly ionic, we assign static charges (e_{Ti}* and e_O*) to the ions and assume these charges move with the ions. This is a rigid-ion model, with dynamic charge[65] neglected. The E||c dielectric function can then be written[58]:

$$e(w) = e_\infty + 4pV^{-1}\left[\sum_i e_i^* x_i\right]^2\left[\sum_i m_i x_i^2\right]^{-1}\left(w_{TO}^2 - w^2\right)^{-1} \quad , \tag{4.2}$$

where $w = 2pn$ is the angular frequency. V is the volume per TiO_2 unit, x_i is the displacement of ion i, e_i^* is the ion's charge, and m_i is its mass. From (2) and $(x_{Ti} / x_O) = -0.67$ and $(e_{Ti}^* / e_O^*) = -2$ (crystal neutrality) and $(m_{Ti}/m_O)=2.994$, it follows that

$$e_0 - e_\infty = 4pV^{-1}(e_O^*)^2(0.30m_O)^{-1}w_{TO}^{-2} \quad . \tag{4.3}$$

Every quantity in equation (4.3) is known except for e_O^*, which is thus determined: $e_O^* = -2.8e$, where e is the magnitude of the electron charge and the negative sign is chosen for the oxygen ion. The result is reasonable, but somewhat large; we do not expect the oxygen ion to be more highly charged than O^{--}, and any contribution from dynamic charge

[64] K. Huang, Proc. Roy. Soc. (London) **A208**, 352 (1951).
[65] W. Cochran, Nature (London) **191**, 60 (1961); E. Burstein, M. H. Brodsky, and G. Lucovsky, Int. J. Quantum Chem. **15**, 759 (1967); R. Zallen, R. M. Martin, and V. Natoli, Phys. Rev. B **49**, 7032 (1994).

would be expected to reduce the size of the observed effective charge.[66] Szigeti's introduction of the local-field correction in the case of a cubic crystal[67] reduces the effective charge by the factor $3/(e_\infty + 2)$. TiO_2 is not cubic, but the TO-LO splittings of Fig. 4.3 are larger than the anisotropy shifts so neglecting anisotropy may not be a terrible approximation. Doing this yields a Szigeti effective charge, for the oxygen ion, of $-1.1e$.

4.6 Nanophase anatase

We have studied annealing-induced phase transformations[57, 68] (amorphous → anatase → rutile) in nanophase titania prepared by a polymerically stabilized sol-gel technique.[7] Anatase dominates for anneal temperatures between 300 and 800°C. Figure 4.5 shows the infrared reflectivity of a pressed pellet prepared from particles annealed at 600°C. The x-ray-determined average nanocrystallite size is 50 nm.[69]

We have analyzed this reflectivity spectrum with a combination of:

(1) effective medium theory;
(2) bulk crystal data;
(3) surface roughness.

The Bruggeman effective-medium model[70] of item (1) is implemented by determining the nanocomposite dielectric function e_{pellet} from

$$0 = \frac{1}{3}\left(\frac{e_{//} - e_{pellet}}{e_{//} + 2e_{pellet}}\right) + \frac{2}{3}\left(\frac{e_{\perp} - e_{pellet}}{e_{\perp} + 2e_{pellet}}\right) \quad . \qquad (4.4)$$

The bulk anatase properties of item (2) enter equation (4.4) in the form of $e_{//}(\bar{n})$ and $e_{\perp}(\bar{n})$, the dielectric functions of Fig. 4.3. Equation (4.4) assumes the pellet to be a nanocomposite of two fictitious isotropic materials, one having dielectric function $e_{//}$ and the other having dielectric function $e_{\perp}$. The volume fractions are assumed to be 1/3 for $e_{//}$ material and 2/3 for $e_{\perp}$ material. The $e_{pellet}(\bar{n})$ thus determined from equation (4) determines the calculated reflectivity $R(\bar{n})$ corresponding to this model.

---

[66] B. G. Dick and A. W. Overhauser, Phys. Rev. **112**, 90 (1958); R. Zallen and G. Lucovsky, in *Selenium*, edited by R. A. Zingaro and W. C. Cooper (Van Nostrand Reinhold, New York, 1976), p. 148.
[67] B. Szigeti, Trans. Faraday Soc. **45**, 155 (1949).
[68] R. J. Gonzalez, A. Gaynor, R. Zallen, and R. M. Davis, unpublished results on annealing-induced phase transformations in titania particles.
[69] B. Szigeti, Trans. Faraday Soc. **45**, 155 (1949).
[70] D. A. G. Bruggeman, Ann. Phys. (Leipzig) **24**, 636 (1935); R. Landauer, J. Appl. Phys. **23**, 779 (1952); D. E. Aspnes, Am. J. Phys. **50**,704 (1982).

The result of this exercise, which incorporates the first two of the three items listed above, is the dashed curve shown in Fig. 4.5. Although the main qualitative features of the measured reflectivity spectrum are present in the theoretical curve, the quantitative fit is not close.

We now introduce the third item, the effect of surface roughness.[71] The dashed curve discussed above corresponds to the assumption of the usual abrupt air/pellet interface. The continuous curve shown in Fig. 4.5 corresponds to the assumption of a graded surface layer of thickness 1.5 μm. (Other thicknesses were tried; this one gave the best fit.) Within the graded layer, effective medium theory is used as before, but now the two materials are assumed to be the nanocomposite (with dielectric function equal to e_{pellet}) and air (with $e_{air} = 1.$). The volume fraction is linearly graded from 100% nanocomposite at the inner boundary to 30% nanocomposite at the outer boundary. Figure 4.5 indicates that this model is rather successful in reproducing the pellet's reflectivity spectrum. Conversely, it suggests that the reverse route — attempting to derive information about the crystal from pressed-pellet data — may not be impractical.

4.7 Summary

Single crystals of anatase, grown by transport reactions, were studied by far-infrared reflectivity. Clean polarization-dependent spectra were observed (Fig. 4.2), and the results were analyzed to yield the dielectric dispersion properties in the lattice fundamentals regime (Figs. 4.3 and 4.4). The TO (and LO) frequencies of the zone-center phonons were determined to be (in units of cm^{-1}): 367 (755) for the A_{2u} mode; 262 (366) and 435 (867) for the E_u modes. The large TO-LO splitting was analyzed in terms of effective charges for the A_{2u} mode, whose vibrational eigenvector is symmetry-determined. The bulk-crystal dielectric properties were used to analyze infrared reflectivity measurements made on pressed pellets of anatase nanocrystals, using effective-medium theory. It was found that the incorporation of surface roughness allowed a reasonable quantitative fit to the pellet reflectivity spectrum.

[71] V. Hopfe, E. H. Korte, P. Klobes, and W. Grahlert, Applied Spectroscopy **47**, 423 (1993).

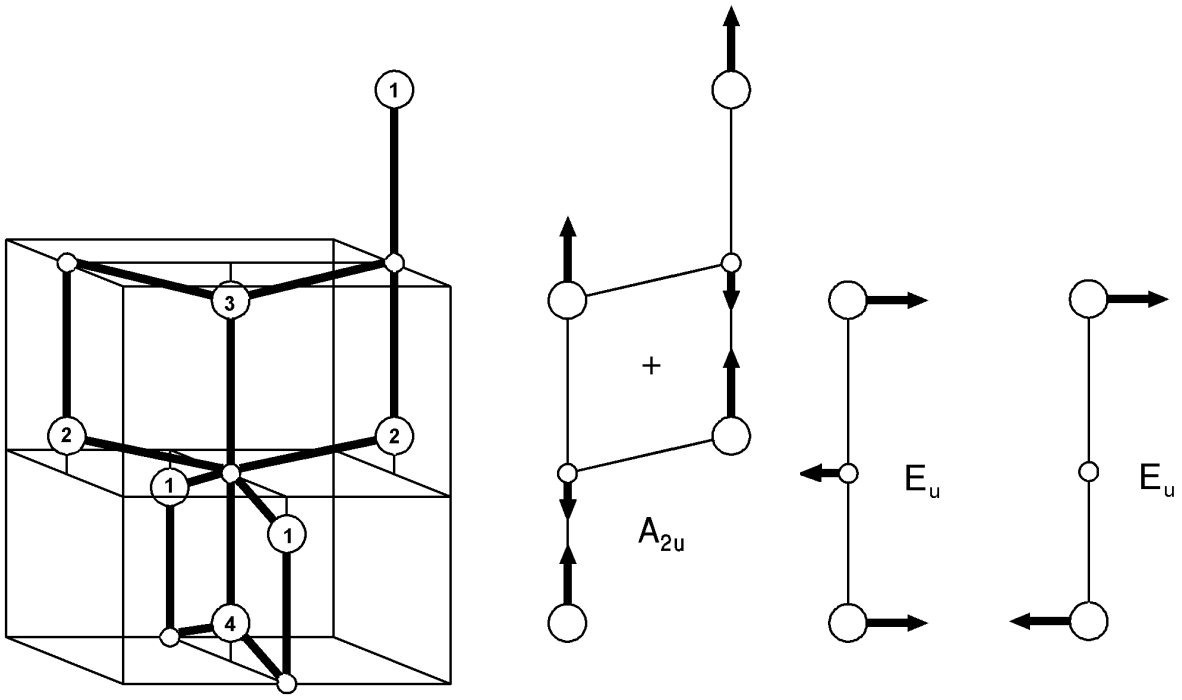

Figure 4.1. The structure of the anatase primitive cell is shown at the left. The c-axis is vertical, small circles denote Ti atoms, large circles denote O atoms. Oxygen atoms labeled with the same number are equivalent. The center figure shows (+) the position of the inversion center and the vibrational eigenvector for the A_{2u} mode. Symmetry coordinates for the E_u modes are shown at the right.

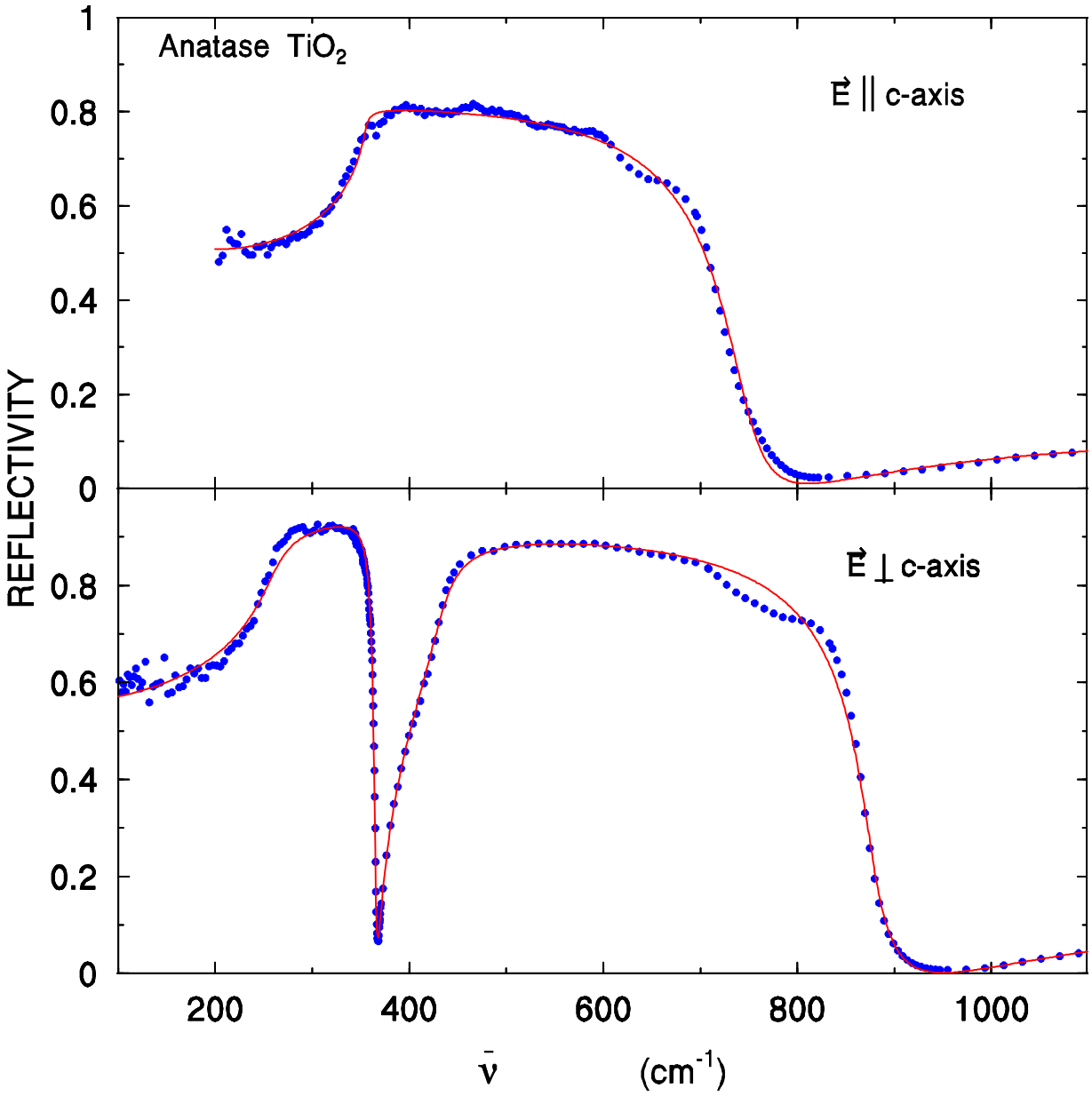

Figure 4.2. The polarization-dependent far-infrared reflectivity of single-crystal anatase. The E||c results, obtained for a surface containing the c-axis, required the use of a polarizer which cut off below 200 cm^{-1}. The E⊥c results, obtained for a surface normal to the c-axis, required no polarizer and extended down to 50 cm^{-1}. (The 50-100 cm^{-1} range, not shown, contained no discernible structure.) The continuous curves included in this figure are fits based on the factorized form of the dielectric function (Eq. 4.1).

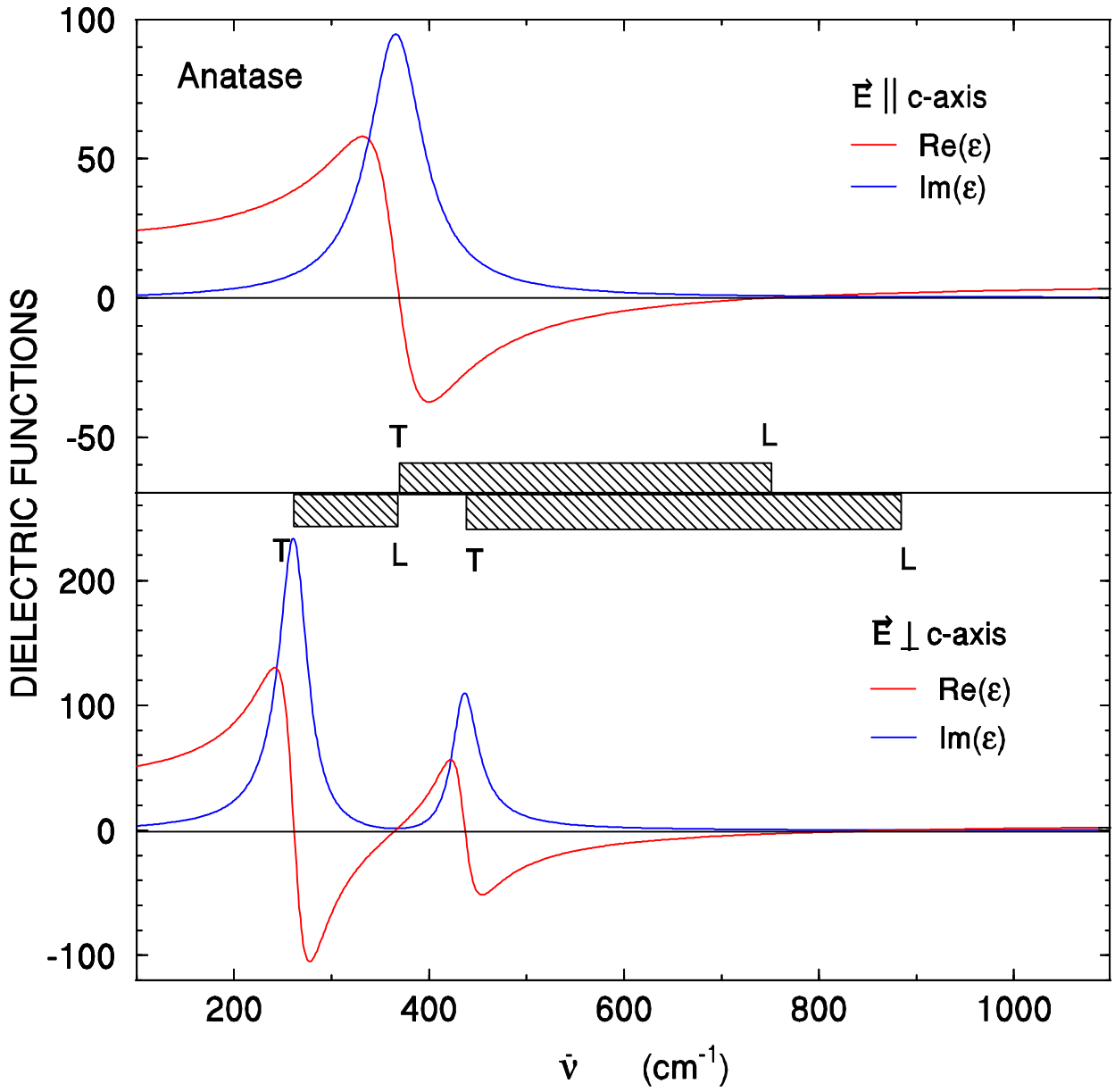

Figure 4.3. The dielectric functions of anatase TiO_2. These curves correspond to the fits obtained with the factorized form of the dielectric function. The shaded bars highlight the TO-LO splittings.

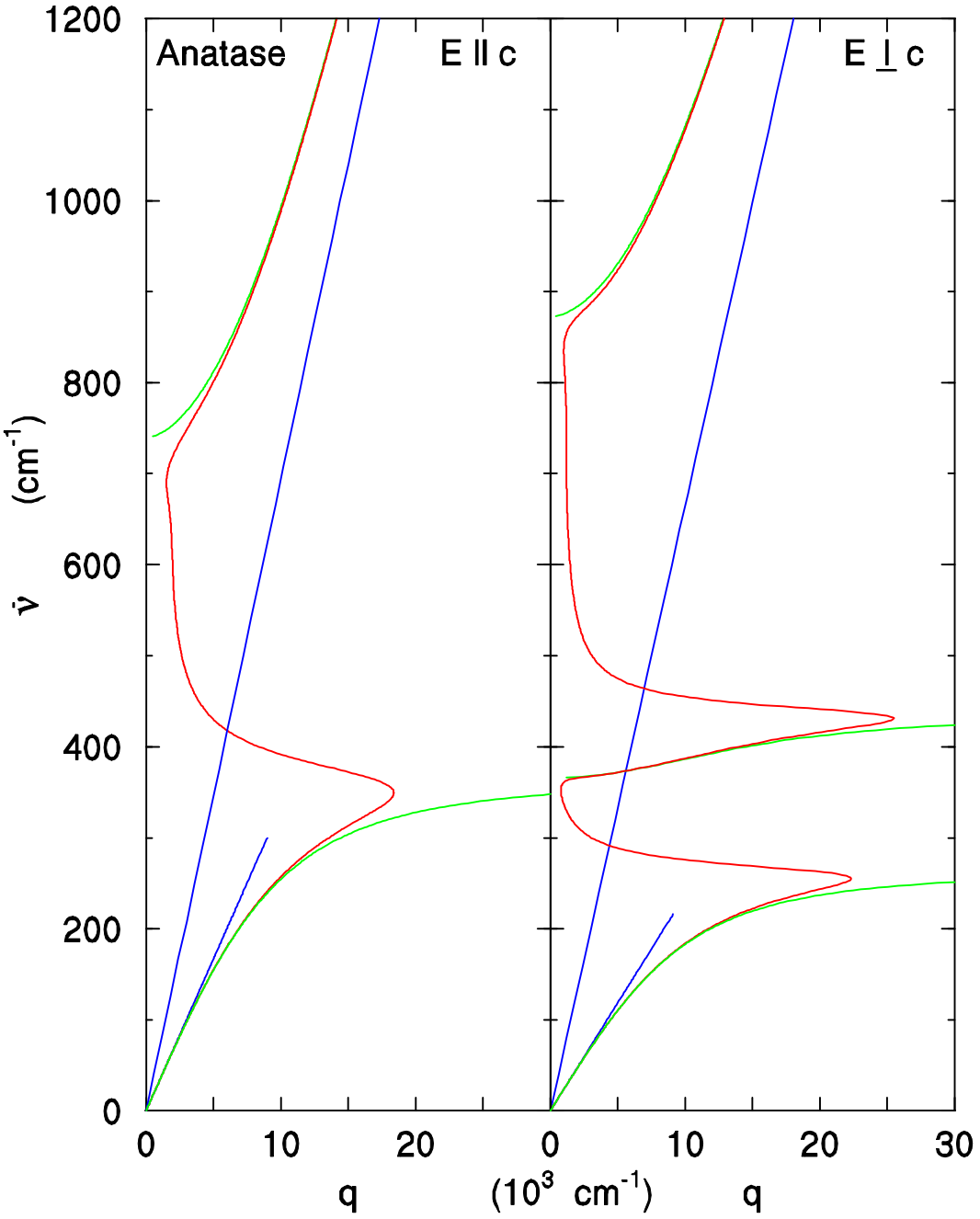

Figure 4.4. Polariton dispersion curves for anatase TiO_2. The solid curves correspond to the experimental parameters of Table 4.1. The dashed curves result from setting the damping parameters equal to zero. The light lines show the asymptotic slopes, which are inversely proportional to the optical refractive index (long line) and static refractive index (short line).

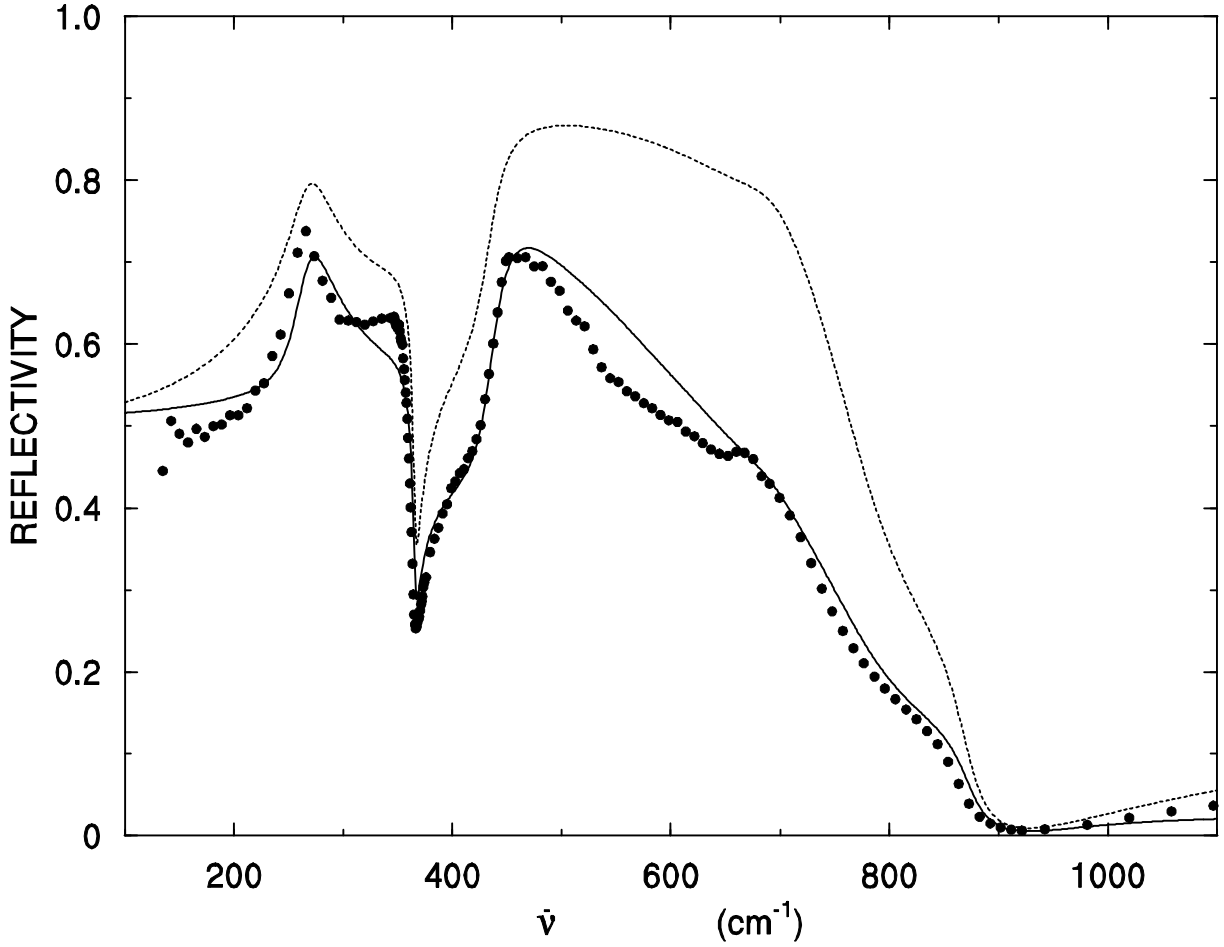

Figure 4.5. The infrared reflectivity of a pressed pellet prepared from sol-gel titania particles annealed at 600°C. We have analyzed this reflectivity spectrum with a combination of effective medium theory, bulk crystal data, and surface roughness. The dashed curve corresponds to the assumption of an abrupt air/pellet interface, the continuous curve corresponds to the assumption of a graded surface layer of thickness 1.5 μm.

CHAPTER FIVE

5. SEARCH FOR FINITE-SIZE EFFECTS IN RAMAN SCATTERING FROM NANOCRYSTALLINE ANATASE

5.1 Introduction

In Silicon[72,73] and several other semiconductor crystals,[74, 75, 76] there is a well-documented finite-size effect observed in Raman-scattering experiments on nanocrystalline samples; the Raman bands broaden and shift with decreasing nanocrystal size L. This effect has also recently been seen in an oxide insulator, AlO(OH).[77] The gist of the mechanism is as follows.[72, 75] For a nanocrystal of size L, the strict "infinite-crystal" k-space selection rule is replaced by a relaxed version characterized by a k-space uncertainty of order (1/L). Here, k is the phonon wavevector. Instead of only the k=0 mode of a phonon branch being Raman-active (for a Raman-allowed mode symmetry). Now all modes of the phonon branch within a range of k values [roughly from k=0 to k=(1\L)] are Raman-active. Because the phonon dispersion curve $\nu(k)$ is not flat, the observed Raman band shifts and broadens. The smaller the L, the larger is the shift and broadening of the Raman band.

This chapter describes experiments carried out in order to see if such finite-size effects could be observed in the anatase titania nanocrystals that are formed by annealing sol-gel nanophase titania at temperatures between 300 and 800°C. Anneals were done in both air and argon atmospheres, and x-ray linewidths were used for estimiting crystallite sizes. The use of two different annealing atmospheres was necessary because it is known that stoichiometry changes can influence the Raman spectra of TiO_2 materials.[78, 79, 80]

---

[72] H. Richter, Z. P. Wang, and L. Ley, Solid State Commun. **39**, 624 (1981)
[73] Z. Iqbal and S. Veprek, J. Phys C **15**, 377 (1982).
[74] K. K. Tiong, P. M. Amirthara, F. H. Pollak, and D. E. Aspnes, Appl. Phys. Lett. **44**, 122 (1984); M. Holtz, R. Zallen, O. Brafman, and S. Matteson, Phys Rev. B **37**, 4609 (1988); I. H. Campbell and P. M. Fauchet, Solid State Commun. **58**, 739 (1986); M. Gargouri, B. Prevot, and C. Schwab, J. Appl. Phys. **62**, 3902 (1987); T. Kanata, H. Murai, and K. Kubota, J. Appl. Phys. **61**, 969 (1987); S. J. Yu, H. Asahi, S. Emura, H. Sumida, S. Gonda, and J. Tanoue, J. Appl. Phys. **66**, 856 (1989); R. Zallen, J. Non-Cryst. Solids **141**, 227 (1992).
[75] R. J. Nemanich, S. A. Solin, and R. M. Martin, Phys. Rev. B **23**, 6348 (1981).
[76] K. Nakamura, M. Fujitsuka, and M. Kitajima, Phys. Rev. B **41**, 12260 (1990).
[77] C. J. Doss and R. Zallen, Phys. Rev. B **48**, 15626 (1993).
[78] C. A Melendres, A. Narayanasamy, V. A. Maroni, and R. W. Siegel, J. Mater. Res. **5**, 1246 (1990).
[79] J. C. Parker and R. W. Siegel, J. Mater. Res. **5**, 1246 (1990).
[80] J. C. Parker and R. W. Siegel, Appl. Phys. Lett. **57**, 943 (1990).

5.2 Experimental

The preparation of the sol-gel titania powders using a polymer for steric stabilization, as well as the SPEX and the DILOR instruments used for the Raman measurements, were described in chapter two. A short review of the preparation procedure follows. The titania particles were synthesized through the hydrolysis and condensation of titanium tetraethoxide (TEOT) [$Ti(OC_2H_5)_4$] in the presence of a steric stabilizer, hydroxypropylcellulose (HPC), which leads to a narrow particle size distribution.[81] The particle size is controlled through the amount of water used in the reaction. $R=[H_2O]/[TEOT]$ is a measure of the relative water concentration. The following R values were used: 5.3, 15, 30, and 60 and they correspond to particle size ranging from 80 nm (for R=60) to 300 nm (for R=5.3). Figure 5.1 shows some TEM micrographs of the resulting particles. After the colloidal suspensions were dried, the powders were gently ground and subjected to heating treatments in air and in argon. For annealing in air, a Lindberg 51542 box furnace was used. For annealing in argon, a Lindberg 54353 three-zone tube furnace was used, the argon was 99.998% pure and flew at a partial pressure of 1.2 Torr during all the annealing process. Each sample was taken from room temperature to desired anneal temperature at 20°C min^{-1}, held at the anneal temperature for 2 hr, then slowly cooled back to room temperature. X-ray diffraction measurements were carried out with a Scintag XDS-2000 powder diffractometer using radiation with 1.54Å wavelength. The substrate was an oriented quartz disk. Crystallite sizes were estimated from the Scherrer equation[82]

$$L = \frac{(0.94)\,l}{B\cos q} \qquad (1)$$

where L is the nanocrystallite, λ is the x-ray wavelength, θ is the peak position, and $B=B(2\theta)$ is the linewidth on the 2θ plot (after correcting for the instrumental linewidth, which was determined by measuring the diffraction pattern of a coarse powder of larger-than-micron-size anatase crystals). Three diffraction scans (at 0.2°/min, points taken every 0.005°) were taken for each sample.

5.3 Effects of Anneals on the Raman Bands of Anatase Nanocrystals

As discussed in chapter three and six, Raman, infrared, and x-ray results show that the as-prepared sol-gel titania particles are amorphous, and the crystalline phase which results from anneals in the range from 300 to 800°C is anatase.[83] Anatase is tetragonal, belongs to space

---

[81] J. H. Jean and T. A. Ring, Colloids and Surfaces **29**, 273 (1988); V. J. Nagpal, J. S. Riffle, and R. M. Davis, Colloids and Surfaces **87**, 25 (1994); V. J. Nagpal, R. M. Davis, and S. B. Desu, J. Mater. Res. **10**, 3068 (1995).

[82] H. P. Klug and L. E. Alexander, *X-ray Diffraction Procedures for Polycrystalline and Amorphous Materials*, (John Wiley & Sons, New York, 1973), pp. 635 and 687.

[83] A. G. Gaynor, R. J. Gonzalez, R. M. Davis, and R. Zallen, submitted to the Journal of Materials Research.

group D_{4h}^{19} (I4/amd), and has two TiO_2 units per primitive cell. It has six Raman-active modes,[84] corresponding to symmetries $A_{1g} + 2B_{1g} + 3E_g$. Figure 5.2 shows a Raman spectrum obtained on an anatase crystal; it is similar to the results reported by Ohsaka et al.,[84] whose symmetry assignments are shown (the A_{1g} and B_{1g} peaks near 515 cm^{-1} are not resolved at room temperature).
Also included in Fig. 5.2 is the spectrum obtained by annealing (in air, at 300°C) a sol-gel ultrafine powder prepared using R=5.3. Significant spectral changes are evident, relative to the spectrum of the bulk anatase. The distinctive, strong, sharp, bulk-anatase line at 141 cm^{-1} broadens and blue-shifts. The 638 cm^{-1} line broadens and red-shifts. The broad background is caused by residual organic from the sol-gel synthesis; it is subtracted (in what follows) prior to estimates of peak positions and linewidths.

The 300°C anneal temperature of Fig. 5.2 is the lowest T_{anneal}, that we measured, at which anatase appears. Anatase then remains the dominant form of TiO_2 present until about 800°C, when rutile takes over. Thus we were able to follow the evolution of the anatase Raman spectrum over a wide range of anneal temperatures. We followed the dominant 141 cm^{-1} band in most detail, although the 638 cm^{-1} band was also tracked. The peak position and linewidth (full width at half maximum) were used to characterize the bands. The linewidths were corrected for the instrumental linewidth. The results, for the 141 cm-1 band, are presented in Figs 5.3 and 5.4.
Figure 5.3 shows the influence of anneal temperature on the main Raman band for particles annealed in air. Figure 5.4 shows the corresponding results for particles annealed in argon. The Raman-spectrum value corresponding to the bulk crystal is shown at the left side of each panel. Both figures contain results obtained on two types of initial particles: particles synthesized with a relative low water concentration (R=5.3) during the sol-gel hydrolysis, and particles synthesized at high water concentration (R=60). Data points for the two particle types are denoted by circles and squares, respectively.

It is immediately evident that the annealing atmosphere strongly influences the observed behavior, supporting a key role for stoichiometry considerations as proposed previously by Parker and Siegel.[79, 80] The main observations about the overall behavior revealed in Figs. 5.3 and 5.4 may be stated as follows: For the oxygen anneals, the final Raman values attained with high-temperature anneals are close to the bulk-crystal values, and most of the change is completed quickly—at low values of T_{anneal}. For the argon anneals, there is some movement toward the bulk-crystal values, but there is no close approach to the bulk-crystal lineshape and no rapid change at low T_{anneal}. Similar behavior was also observed for the 638 cm^{-1} anatase Raman band, though the effects were more difficult to follow in this case because the band is weaker and the nanocrystal/bulk differences are less pronounced than for the 141 cm^{-1} band. Before discussing these observations and the question of whether finite-size effects also enter here, we first need to examine the results of the x-ray diffraction experiments.

---

[84] T. Ohsaka, F. Izumi, and Y. Fujiki, J. Raman spectrosc. **7**, 321 (1978).

5.4 Finite-Size Effects versus Stoichiometry

Estimates of L, the characteristic nanocrystal size for each set of anneal particles, were obtained from the Scherrer formula and measurements of the width of the (101) anatase diffraction peak. X-ray diffraction results for two sets of air-anneal particles are shown in Fig. 5.5. With increasing anneal temperature the diffraction peak sharpens, as L increases with T_{anneal}. Figure 5.6 shows the crystallite sizes for particles anneal to different temperatures. It is evident that large particles (R=5.3) have larger crystallites, and that this difference is more pronounced when the particle are annealed in argon. For particles annealed in air, the difference is rather small. It seems that the unburned organics left (when annealed in argon) in the particles have an effect on the crystallite growth depending on the particle size. This could be due to the highly porous character of these particles, which means the particles have a large surface area.

Figure 5.7 shows a re-statement of the results of Fig. 5.3 and 5.4 in terms of L (instead of T_{anneal}). For the lowest T_{anneal} of 300°C, only a fraction of the sol-gel amorphous titania samples had crystallized; the Raman spectrum is still dominated by the broad bands of the amorphous unannealed material.[82] By using the Raman microprobe to locate small regions for which the anatase lines were stronger (e.g. Fig. 5.2), it was possible to obtain reliable anatase-nanocrystal Raman signals for these partially crystalline samples and to thus include the measured Raman parameters (for T_{anneal} = 300°C) in Figs. 5.3 and 5.4. However, we were unable to obtain reliable anatase x-ray diffraction peaks—and thereby L estimates—for the nanocrystals in these low-temperature samples. But it is clear that L must be smaller than the L values observed at T_{anneal} = 400°C. For the air-annealed material, L=15 nm for T_{anneal} = 400°C. A reasonable (and generous) range in which to expect L, for T_{anneal} = 300°C, is from 3 to 12 nm. Using this range for L, along with the measured Raman values, results for low-temperature air-annealed sample have thus been included in Fig. 5.7; these are the heavy horizontal bars at the upper left of each panel.

Despite the considerable scatter, all of the argon-annealed samples (both R=5.3 and R=60 starting particles) lie close to a single curve in each panel of Fig. 5.7. A similar statement applies to the air-annealed samples. But the argon and air curves, for the L dependence of the Raman peak position and the L dependence of the Raman linewidth, are clearly different from each other. The argon curves progress only part way to the bulk-crystal values for the largest nanocrystal sizes observed; the air curves quickly approach them, becoming indistinguishable from the bulk-crystal values by L = 40 nm. If L was the only physical quantity responsible for the changes in the Raman spectra, then each panel of Fig. 5.7 would contain only a single curve. But this is not the case.

Parker and Siegel[79, 80] investigated nanophase titania formed by oxidizing titanium particles made by gas-phase condensation. Their particles had a range of stoichiometries (thermogravimetrically determined) ranging form $TiO_{1.89}$ to TiO_2, with the as-prepared samples being oxygen-deficient and the more stoichiometric samples obtained by subsequent

anneals in air. Nonstroichiometric samples were dark blue, consistent with earlier work on vacancy-induced optical absorption in reduced (oxygen-deficient) rutile.[85] Grain sizes, not monitored in detail, were about 12 nm for the as-prepared material and increased to 24 after one of their air anneals. Both rutile and anatase were present on their as-prepared (unannealed) samples. Parker and Siegel observed shifts in the main Raman peaks of rutile and anatase as the stoichiometry changed, and ascribed these effects entirely to stoichiometry. Those authors also carried out some argon anneals, which did not affect their spectra.

Our experiments differ from those of Parker and Siegel in the use of sol-gel titania rather than oxidation-prepared titania, a larger range of anneal temperatures, and a detailed tracking of nanocrystal sizes (using x-ray diffraction linewidths). Also, our as-prepared samples are white, amorphous and, as discussed below, are more stoichiometric.
Stoichiometry does, in fact, provide an adequate explanation of the curves shown in Fig. 5.3, 5.4, 5.7. The interpretation of the air/argon differences is as follows. The initial rapid approach to the bulk-crystal values, observed for the air anneals, is interpreted as uptake of oxygen and approach-to-stoichiometry of initially oxygen-deficient samples. Argon anneals produce little effect, because stoichiometry is not affected.

Stoichiometry measurements were not carried out on our samples. They are certainly much closer to stoichiometry than the as-prepared samples of Parker and Siegel ($TiO_{1.9}$), since they exhibit no trace of oxygen-vacancy-induced blue coloration. Parker and Siegel[80] present a linewidth-stoichiometry "calibration" curve for the 141 cm^{-1} line. The largest linewidth observed for our samples is 25 cm^{-1}. Using their curve would suggest a stoichiometry of $TiO_{1.98}$.
If stoichiometry changes provide the main factor determining the curves in Fig. 5.7, does there remain any indication of a contribution from finite-size effects? One indication might be found in the relationship between the Raman peak position $\overline{n}$ and the Raman linewidth Γ. Figure 5.8 shows this correlation, for all of our samples. The $\overline{n}$-Γ relation is roughly linear. Although linear $\overline{n}$-Γ relation have been observed in some well-documented finite-size-effect studies[75, 77], other effects could yield this simple relation. Parker and Siegel found approximate proportionality between $\Delta\overline{n}$ and $\Delta\Gamma$ in their stoichiometry study.[80]

The argon-anneal curves of Fig. 5.7 are not flat, the Raman parameters do change with L. Is this interpretable as a finite-size effect? The answer is no. For all documented finite-size effects, the nanocrystallinity-induced Raman parameter changes scale as L^{-a}, where the scaling exponent α is in the range[77] of 1.0 to 1.5. Thus the changes are most rapid at small L. But for the argon-anneal curves of Fig 5.7, the size of the slope is smallest at small L. The most likely explanation of the argon curves of Fig. 5.7 is some (again) approach to stoichiometry, since the argon atmosphere is not completely oxygen-free. Thus we conclude

[85] R. G. Breckernridge and W. R. Hosler, Phys. Rev. **91**, 793 (1953).

that the nanocrystal sizes studied here (down to 15 nm) were not small enough to produce observable finite-size effects, effects large enough to be competitive with those produced by the stoichiometry changes. In an earlier oxide-nanoparticle study in which finite-size effects were definitely observed[77], nanocrystal sizes down to 3 nm were available.

5.5 Summary

A systematic Raman-scattering and x-ray diffraction investigation has been carried out on sol-gel
titania particles subjected to air and argon anneals from 300 to 800°C. The phase investigated over this wide range of anneal temperatures was anatase, which the x-ray work showed to be nanocrystalline — with nanocrystal sizes growing from 15 nm (at low anneal temperature) to 80 nm (at high anneal temperature). Systematic sharpening and shifting, with increasing anneal temperature, was observed for the dominant anatase Raman band. But with different characteristic behavior for air and argon anneals. The results could be interpreted entirely on the basis of stoichiometry changes; no definite finite-size effects were observed. Comparison to earlier work on nonstoichiometric anatase indicates that our sol-gel titania may be close to $TiO_{1.98}$. Based on this interpretation, the argon anneal results (see Fig. 5.7 and 5.8) are showing that the as-prepared large particles (R=5.3) are less nonstoichiometric than small particles (R=60).

Figure 5.1. TEM micrographs of sol-gel titania particles synthesized with different water concentrations, R is a measure of the water concentration.(fig51.jpg) (49Kbytes)

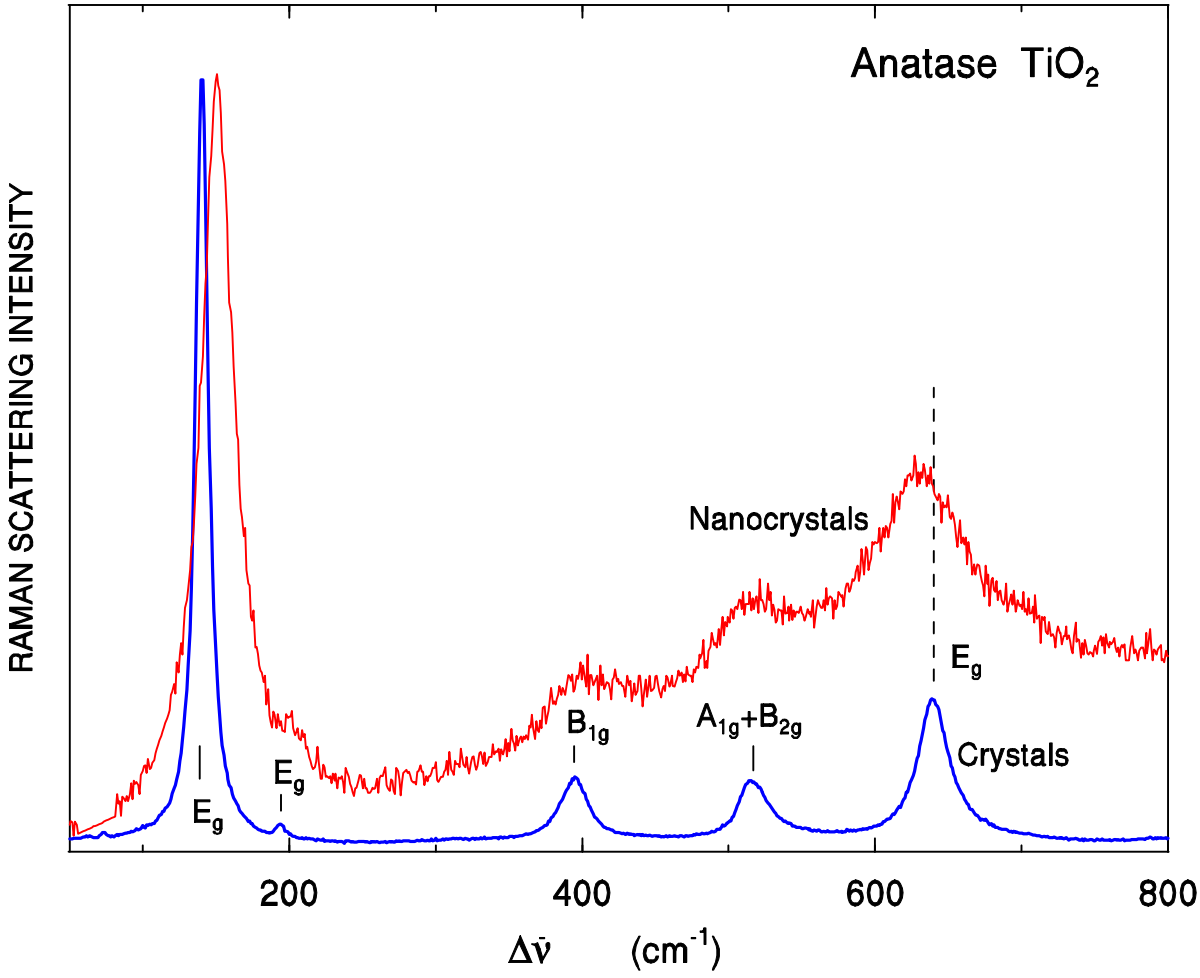

Figure 5.2. Comparison of the Raman spectrum of a nanocrystalline powder with that obtained from a powder of micron-size anatase crystals. The nanocrystalline sample was obtained by annealing R=5.3 sol-gel particles in air at 300°C.

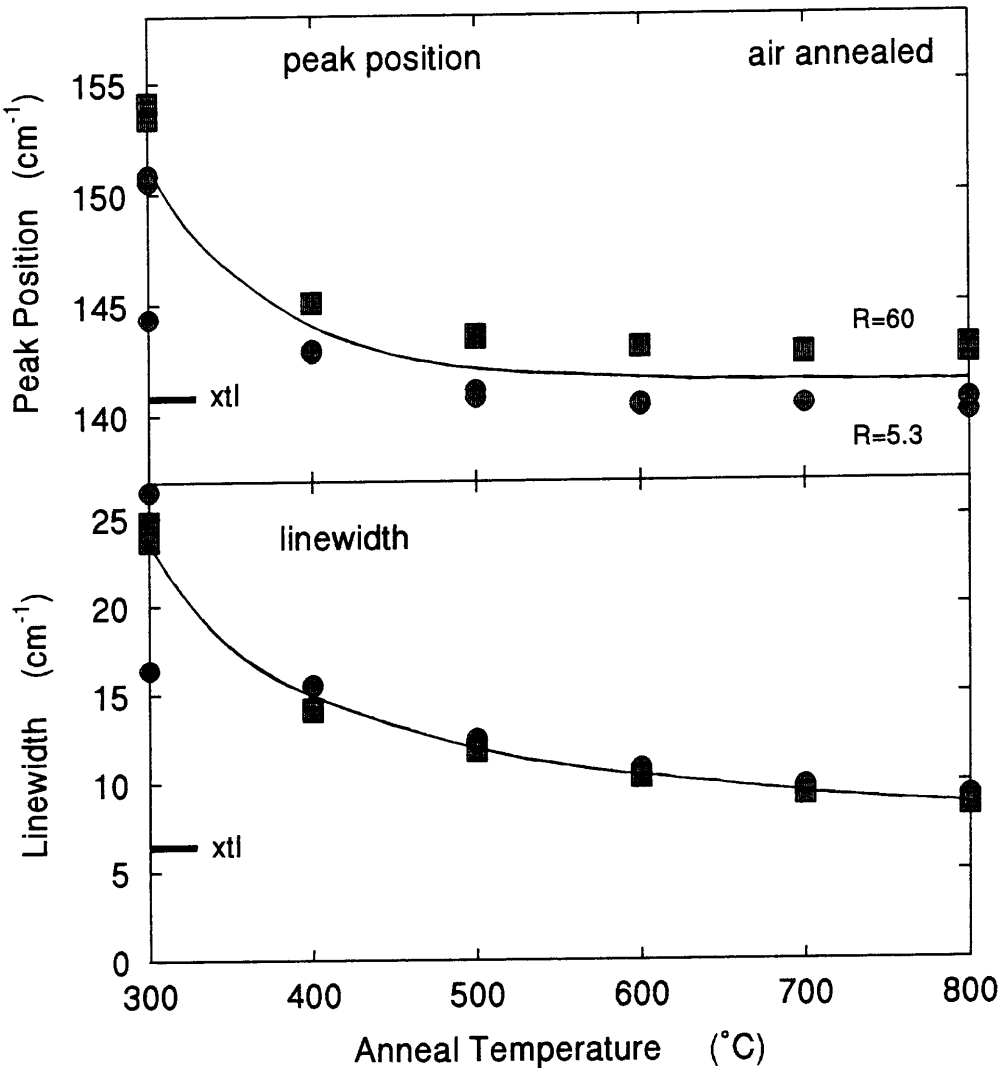

Figure 5.3. The effect of air anneals on the main anatase Raman band of the nanoparticles. Xtl stands for bulk crystal.

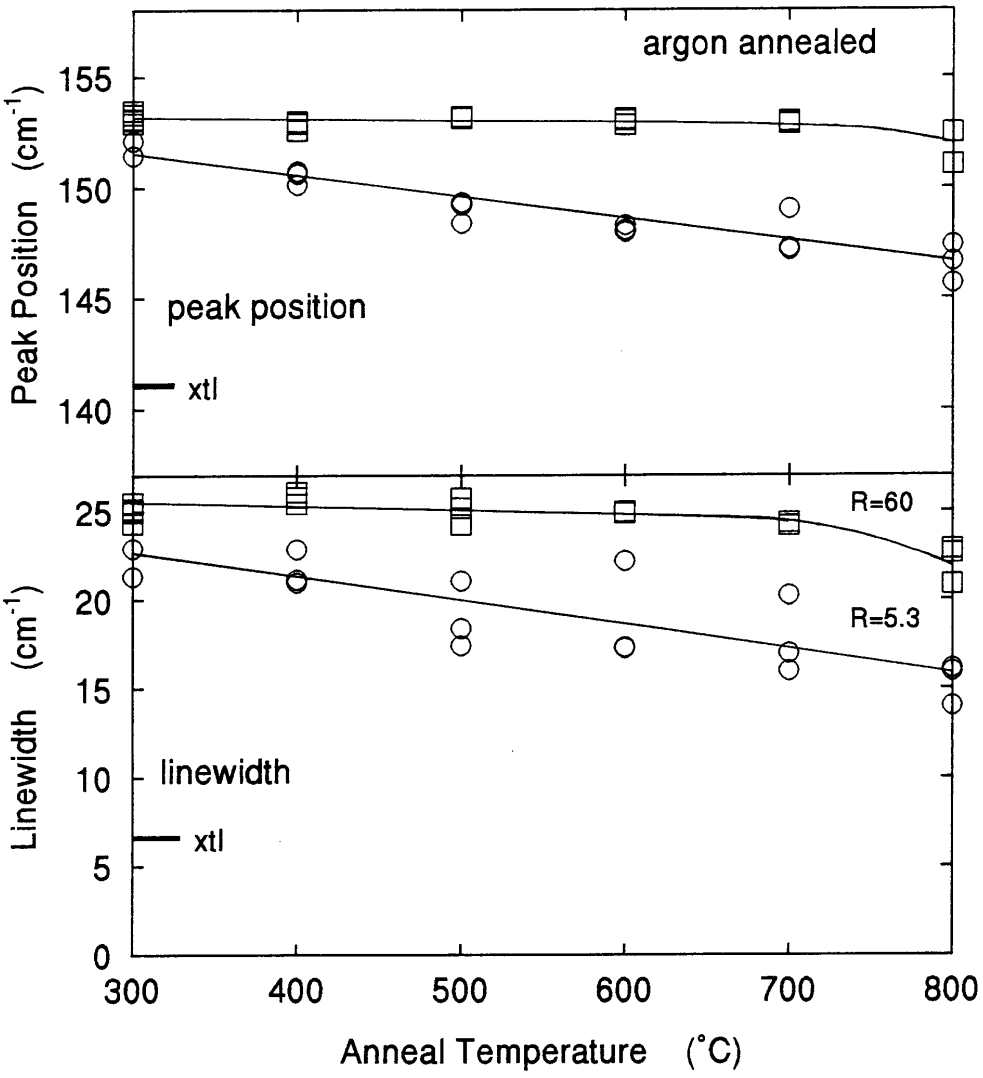

Figure 5.4 The effect of argon anneals on the main anatase Raman band of the nanoparticles.

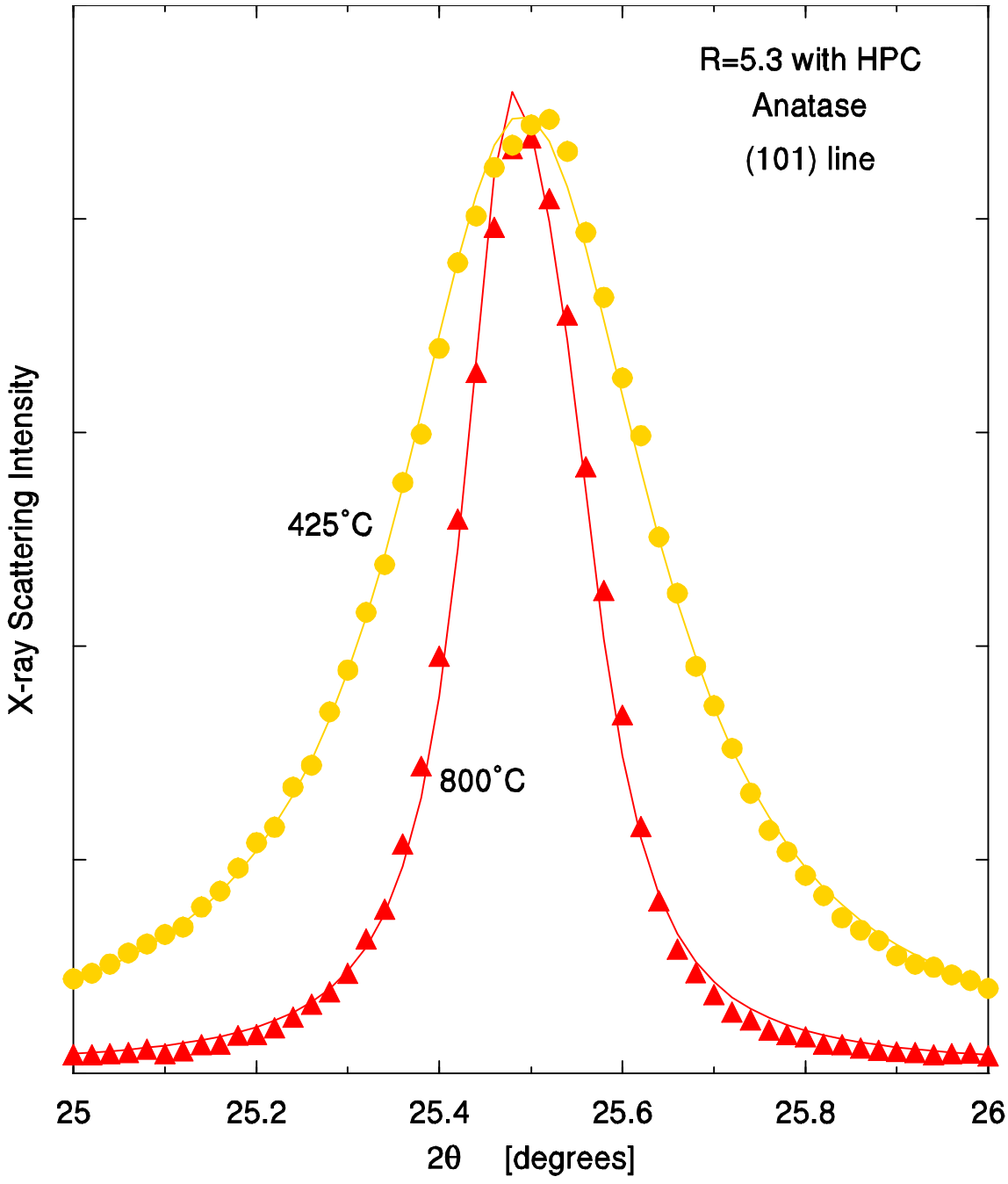

Figure 5.5. The anatase (101) x-ray diffraction peak for particles air-annealed at two temperatures.

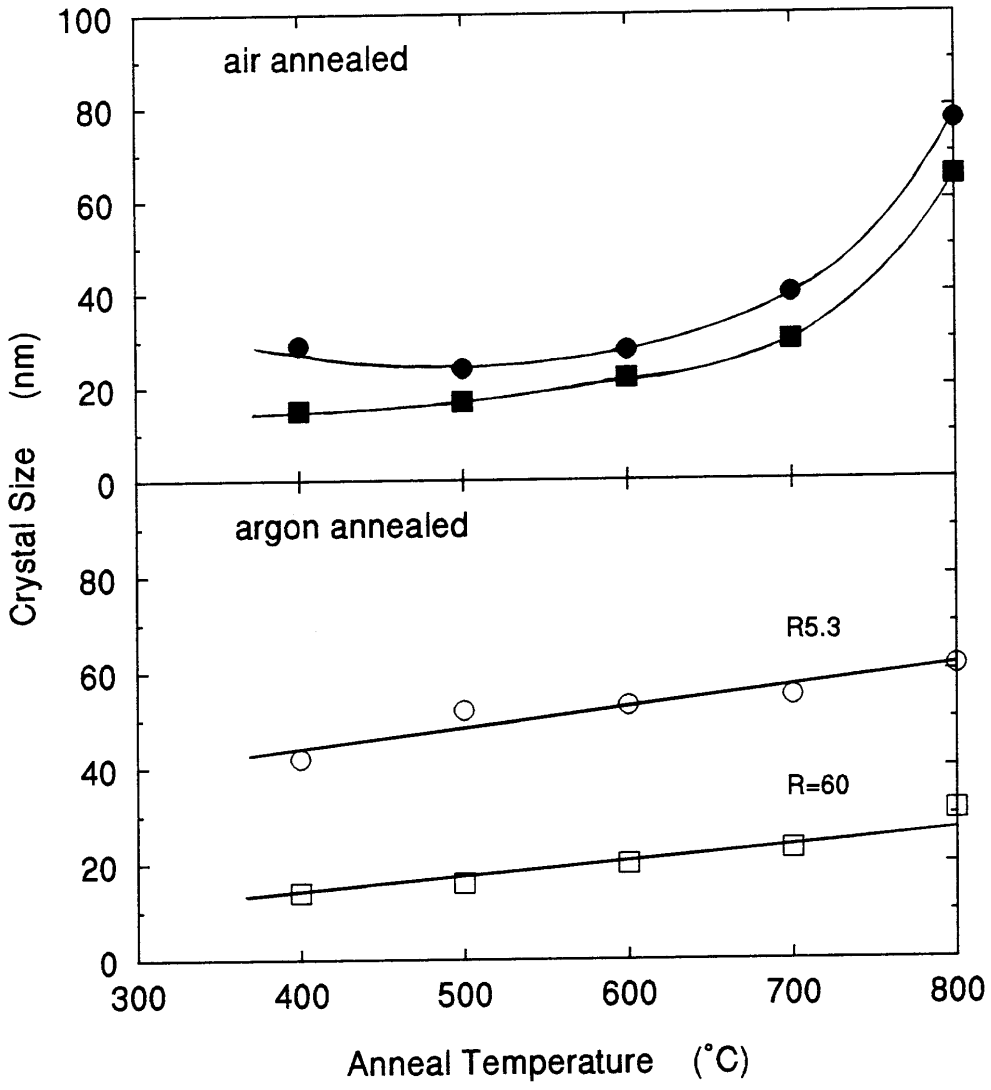

Figure 5.6. Nanocrystal-size growth with annealing temperature for particles anneal in argon and in air. □ for high water content particles (R=60) and ○ for low water content particles (R=5.3)

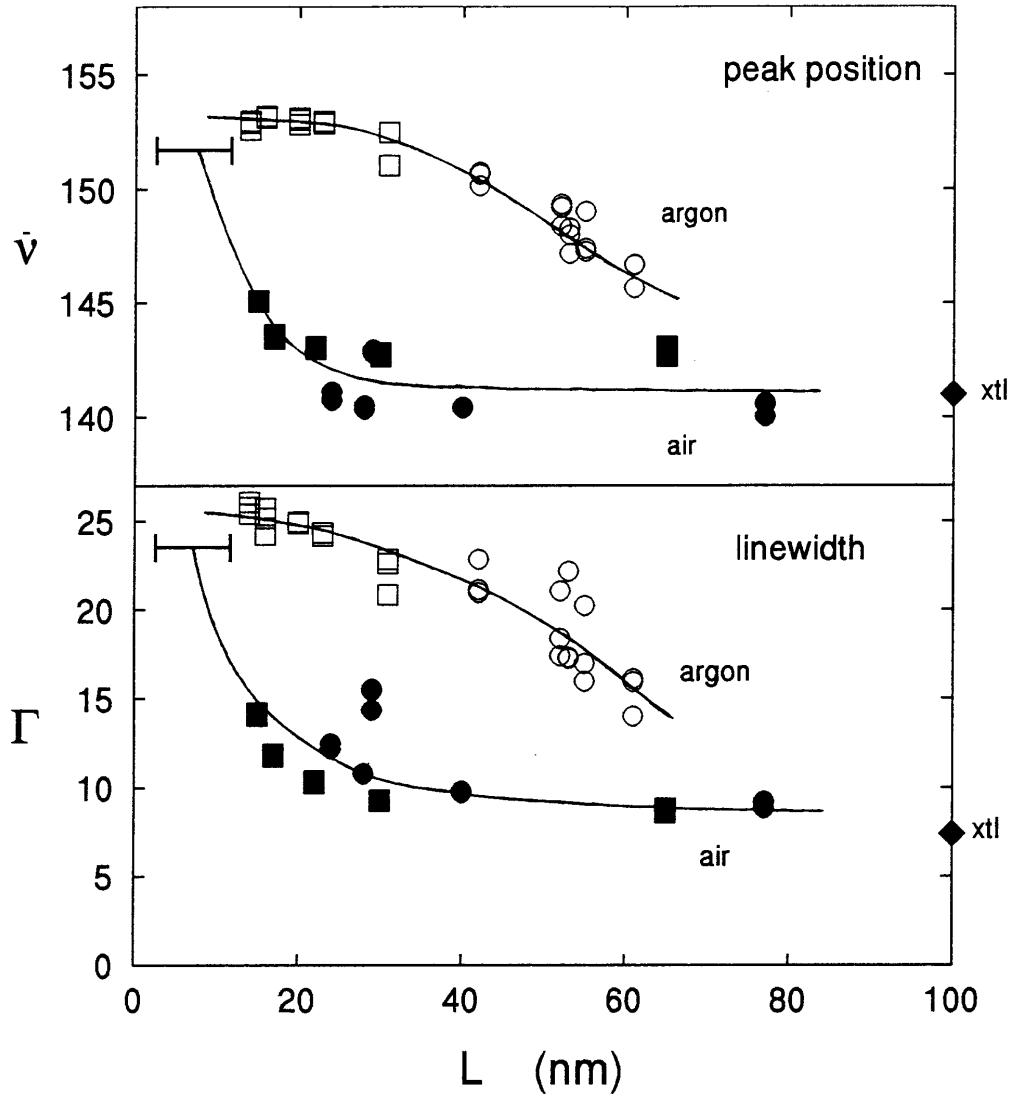

Figure 5.7. Raman lineshape versus nanocrystal size for the main anatase band of the annealed nanoparticles.

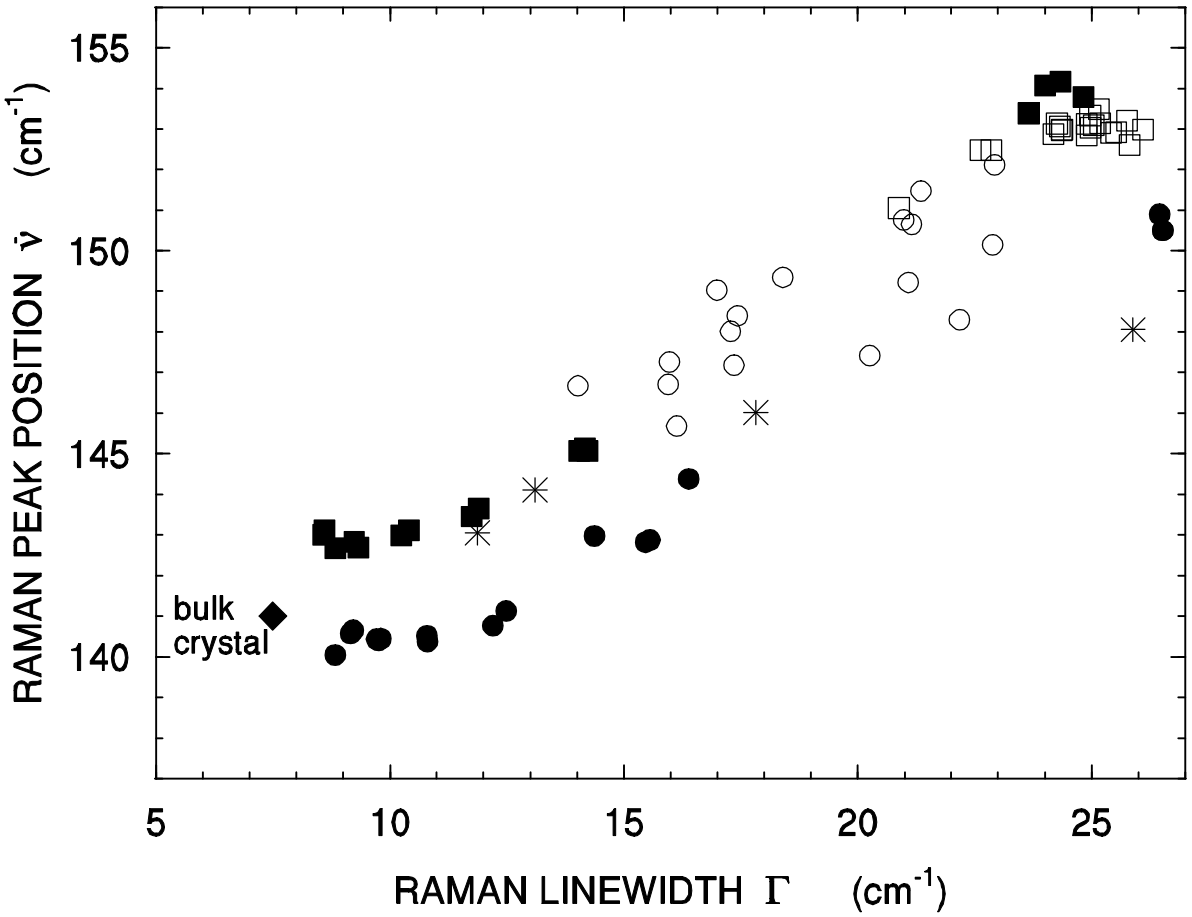

Figure 5.8. The correlation between peak position and linewidth for anatase Raman band (141 cm^{-1}) observed in sol-gel titania particles during the annealing to different temperatures. Results are shown for particles annealed in Argon and in air, and for small, R = 60, (O) and large, R = 5.3, ( ) particles. The results of stoichiometry effects on the Raman lineshape (∗) are also shown. (taken from ref. 80)

CHAPTER SIX

6. INFRARED AND RAMAN STUDIES OF NANOPHASE TITANIA THIN FILMS AND PELLETS

6.1 Introduction

Many efforts have sought to produce small titania particles with controlled size and shape for use in thin films, ceramics, composites, and catalysts. Through a sol-gel process, colloidal suspensions of metal oxides particles can be synthesized[86]. The hydrolysis and condensation of titanium tetraethoxide, in the presence of a steric stabilizer (hydroxypropylcellulose (HPC)) has been shown to produce a narrow particle size distribution with controlled particle size.[87, 88, 89] The particle size is controlled through the amount of water used in the reaction. During hydrolysis, gel networks reach a critical size and condense into nuclei. These nuclei further aggregate to form particles. The polymer present during the reaction can adsorb onto the particle surfaces through hydrogen bonds and becomes a barrier to prevent further agglomeration.

The sintering characteristics of titania particles have been investigated.[90, 91, 92] These studies were done mostly on loose powders and on pressed pellets. Their main effort was to study the factors that affect the anatase to rutile phase transformation temperature, through electron microscopy, x-ray diffraction, and Raman scattering. The rutile phase has been widely studied. The anatase phase has received a lot of attention only lately: The Raman-active fundamentals have been studied[93], the near-bandgap optical absorption edge has been studied,[94] and the infrared-active phonon frequencies[95] have been measured. Most of these studies have been carried out on bulk crystals. Studies on anatase powders and on some

---

[86] C. J. Brinker and G. W. Scherer, *Sol-Gel Science* (Academic Press, San Diego, 1990), chap. 4.
[87] E. A. Barringer and H. K. Bowen, J. Am. Ceram. Soc. **65**, C199 (1982).
[88] L. H. Edelson and A. M. Glaeser, J. Am. Ceram. Soc. **71**, 225 (1988).
[89] V. J. Nagpal, J. S. Riffle, and R. M. Davis, Colloid and Surfaces, **87**, 26 (1994).
[90] E.A. Barringer and H.K. Bowen, Langmuir, **1**, 414 (1985).
[91] R.A. Spurr and H. Myers, Analytical Chemistry, **29(5)**, 761 (1957).
[92] A. Gaynor, R. J. Gonzalez, R. M. Davis, and R. Zallen, (submitted to the Journal of Materials Research)
[93] T. Ohsaka, F. Izumi, and Y. Fujiki, J. Raman Spectrosc. **7,** 321 (1978).
[94] H. Tang, F. Levy, H. Berger, and P. E. Schmid, Phys. Rev. B **52**, 7771 (1995).
[95] R. J. Gonzalez, R. Zallen, and H. Berger (Submitted to Phys. Rev. B).

pellets, with respect to morphology[96] , nanocrystal size[97] , and oxygen deficiency[98] have been reported. Studies of titania thin films[99, 100], with respect to optical properties, are mostly in the uv-visible region.

In this chapter, I present the results of in-situ infrared absorption measurements, during annealing, on titania particles dispersed in a KBr matrix. These results show clearly the amorphous to anatase phase transformation and the dependence of this transformation on particle size. The annealing of island-structure anatase thin films was studied by grazing-incidence infrared (IR) reflectivity measurements. The effect of nanocrystal size on the infrared spectra is reported. To understand these infrared spectra, because of the special structure of the films, a generalized effective medium approximation was used, in which another parameter, besides the filling factor, is needed to incorporate the effect of particle shape. Annealing of continuous titania films, deposited on infrared transparent substrates, transforms them to anatase. This allows us to measure most of the infrared active TO and LO phonon modes and compare these results to our reflectivity-derived values.[95] The transformation, or lack of transformation, to the rutile phase upon annealing island-structure anatase films and 100%-anatase pellets to temperatures above 800°C, was studied through infrared and Raman measurements.

6.2 Particle Synthesis and Sintering

Ultrafine titania particles were synthesized by the hydrolysis and condensation of titanium tetraethoxide [TEOT] ethanol solutions, using hydroxypropylcellulose (HPC) polymer as a steric barrier in order to form monodisperse particles[89, 92]. The procedure was as follows: In a nitrogen atmosphere a flask containing deionized water, HPC, and ethanol was mixed with an equal volume flask containing TEOT dissolved in ethanol. The flasks were mixed together quickly, stirred for 5 seconds, and then allowed to stand for 24 hours. The size of the resulting colloidal particles can be controlled by the amount of water used in the reaction. It has been shown[89, 101] that increases in water concentration, expressed by the molar ratio R = $[H_2O]/[TEOT]$, produce higher nucleation rates which result in a decrease in average particle

---

[96] G. Busca, G. Ramis, J. M. Gallardo, V. Sanchez, and P. Plaggio, J. Chem. Soc. Faraday Trans. **90**, 3181 (1994).

[97] R. J. Gonzalez, and R. Zallen, unpublished resuts on the role of finite-size effects in the Raman spectra of titania nanocrystals.

[98] J. C. Parker and R. W. Siegel, J. Mater. Res. **5**, 1246 (1990); J. C. Parker and R. W. Siegel, Appl. Phys. Lett. **57**, 1246 (1990).

[99] N. Ozer, H, Demiryont and J. H. Simmons, Appl. Optics **30**, 3661 (1991); K. Bange, C. R. Otterman, O. Anderson, U. Jeschkowski, M Laube, and R. Feile, Thin Sol. Films, **197**, 279 (1991).

[100] V. J. Nagpal, R. M. Davis, and S. B. Desu, J. of Mater. Res., **10**, 1 (1995).

[101] J. H. Jean and T. A. Ring, Colloids and Surfaces, **29**, 273 (1988).

size. When HPC is used, the polymer adsorbs on to the surface of the TiO_2 particles through hydrogen bonding, creating a steric barrier which leads to smaller particle size and porous agglomerates. In our work, we used [TEOT] = 0.075M. The relative water concentrations used were R=5.3, 15, 30, 60, and 155 which resulted in TEM-determined particle sizes that ranged from 300 nm (for R=5.3) down to 80 nm (for R = 155) (refer to chapter one).

Three kinds of samples were prepared out of the colloidal sols: (1) films were formed by spin coating the colloidal sol on different substrates, including platinum, molybdenum, silicon, and aluminum oxide. The substrate rotation was 1800 RPM. The resulting films consisted of a single layer of nanoparticles uniformly distributed over the spinning area. (2) Part of the colloidal sol was centrifuged and dried (in a low heat oven (65°C)) to yield a white powder. (3) Some of this white powder was pressed into pellets using 0.74 GPa for 3 minutes. A small amount of it was dispersed in KBr (0.5% wt/wt) and then pressed into pellets. A few high-density films were made by spin coating (four times) concentrated suspensions on double-side polished silicon wafers. Concentrated sols are obtained when the titania suspensions are subject to a concentration step[100]. The concentration is done in a Buchi 461 rotavaporator at 70°C, until the solid concentration is 4% by weight. The aluminum oxide substrate used for the film deposition consisted of a 300 to 400 nm layer of aluminum oxide e-beam evaporated on a platinum substrate.

The loose powders, the spin-coated films and the 100%-titania pellets were annealed following this schedule: First slow heating (1.5°C/min) was done up to 300°C, followed by a dwell time of 2 hours at that temperature. Then the samples were heated at 20°C/min up to the desired anneal temperature, and then held at that temperature for a 2-hour dwell time. This was follow by slow cooling back to room temperature. Anneal temperatures from 300°C to 1000°C were used, at intervals of 100°C. Most of the samples were annealed in air. The films coated on molybdenum substrates needed to be annealed in an inert atmosphere to prevent oxidation of the substrate, which would have reduced the substrate IR reflectivity. For comparison purposes, some powders and pellets were also annealed in an inert atmosphere. Our inert atmosphere consisted of a flow of high-purity (99.998%) argon gas through a three-zone tube furnace at a pressure of 1.2 Torr during the annealing process.

6.3 Characterization

Scanning electron microscopy, SEM, was performed with a Phillips Model 420T electron microscope on the films spin-coated on silicon. The films were sputter-coated with gold prior to the electron-beam exposure.

The infrared measurements were performed with a BOMEM DA3-0.02 FTIR spectrometer. A pyroelectric detector was used to cover the region from 125 to 700 cm^{-1} (far-infrared region); a HgCdTe detector was used to cover the region from 600 to 5000 cm^{-1} (mid-infrared region). Spectra were collected with a 2 cm^{-1} resolution. At least 400 interferometer scans

were added for each spectrum. For the thin films, reflectivity was measured at an angle of incidence of 80° (grazing incidence), since the films were too thin to be detected in normal-incidence reflectivity. To increase the signal sensitivity p-polarized light (parallel to the plane of incidence, which here means nearly perpendicular to the surface) was used.[102] The polarizer was a wire-grid polarizer whose substrate had a low frequency cutoff of 200 cm^{-1}. For the 100%-titania pellets, reflectivity was measured at near-normal incidence, which in our instrument corresponds to an incident angle of 11°. For the dilute titania/KBr pellets, infrared transmission was measured. The pellets were placed in an optically accessible heater and were annealed while spectra were being collected. Details of the experimental set-up have been described in chapter two.

Raman spectroscopy was performed with a SPEX 1403 Raman spectrometer with a GaAs-photocathode photomultiplier and photon-counting electronics. A CW argon ion laser operating at 514.5 nm was the excitation source. The laser power at the sample was approximately 5 mW. Spectra were taken in the 90° scattering configuration. All Raman spectra were taken at room temperature.

6.4 Calculations

During the annealing process, the titania nanoparticles go through different crystalline phases. The particles as prepared are amorphous[92]; upon annealing the anatase phase nucleates. In most of the cases studied, this phase dominates for annealing temperatures between 300 and 800°C. Annealing to higher temperatures induces transformation to rutile. To understand our infrared and Raman results, a knowledge of the fundamental bulk crystal modes is needed. In Table 6.1 and 6.2, we summarize the fundamental infrared and Raman modes of anatase and rutile reported in the literature. In the case of the infrared-active modes in anatase, the values are those obtained in chapter four of this thesis.

Table 6.1. Infrared Active Phonons for Anatase and Rutile TiO_2

		ANATASE[1]		RUTILE[2]	
Mode		Frequency $\bar{n}$ (cm^{-1})	Damping γ (cm^{-1})	Frequency $\bar{n}$ (cm^{-1})	Damping γ (cm^{-1})
E // c-axis	TO	367	68	172	76
(A_{2u})	LO	755	79	796	38
E ⊥ c-axis	TO	262	36	189	27
(E_u)	LO	366	4.1	367	10
	TO	435	32	381.5	16.5
	LO	876	33	443.5	21.5

[102] R. G. Greenler, J. Chem. Phys. **44**, 310 (1966).

TO			508	24
LO			831	50
	ε_∞ (E//c)	= 5.41	ε_∞ (E//c)	= 7.8
	ε_∞ (E⊥c)	= 5.82	ε_∞ (E⊥c)	= 6.0

[1] Taken from chapter four.
[2] F. Gervais and B. Piriou, Phys. Rev. B **10**, 1642 (1974)

For particles crystallized to the anatase phase, the nanocrystallite size, as determined by x-ray peak widths (Scherrer formula), increased from 15 to 80 nm as the anneal temperature increased from 300°C to 800°C.[97] Since the TEM-determined particle sizes range from 80 to 300 nm, this means that the particles are polycrystalline. With the use of the Bruggeman effective-medium expression and bulk crystal optical data, it is possible to calculate dielectric functions for polycrystalline solids.[103]

Table 6.2 Raman Active Phonons for Anatase and Rutile TiO_2

ANATASE[1]		RUTILE[2]	
Mode	Frequency (cm^{-1})	Mode	Frequency (cm^{-1})
E_g	144	B_{1g}	143
E_g	197	E_g	447
B_{1g}	399	A_{1g}	612
A_{1g}	514	B_{2g}	826
B_{1g}	514		
E_g	639		

[1] T. Ohsaka, F. Izumi, and Y. Fujiki, J. Raman Spectrosc. **7,** 321 (1978).
[2] S. P. S. Porto, P. A. Fleury and T. C. Damen , Phys. Rev. **154**, 522 (1966).

This polycrystalline dielectric function will allow us to explain our 100%-titania-pellet and concentrated film infrared results. However, most of our films were made with a single coating, using the unconcentrated colloidal suspension (made without the concentration step). Figure 6.1 shows two characteristic thin films, one made from a sol synthesized with the polymer present and other made from a sol synthesized without the polymer.. The film made without HPC contains relatively large chunks ranging in size from 1 to 10 μm. A comparison of the two films shows the importance of HPC as a steric stabilizer. The majority of the films were made from sols containing HPC; these spin-coated films revealed a very discontinuous discrete structure. In fact, these are scarcely "films" at all. The structure consists of isolated islands formed by one particle or clusters of two to ten particles. Most of the clusters appear

[103] V. Hopfe, E. H. Korte, P. Klobes, and W. Grahlert, Applied Spectroscopy **47**, 423 (1993).

as linear chains of particles. Because of this discrete structure, we expect these island-structure films to behave more like very loose powders than true thin films.

The titania particles are much smaller than the wavelength of the incident light, so that the effective medium approximation (EMA) can be used. The early theory of Maxwell-Garnett EMA[104] assumes spherical particles with isotropic dielectric constants. Figure 6.2 shows some experimental results along with two calculations for comparison purposes. The continuous-film and the spherical particle calculations exhibit the 360 cm^{-1} band. Both calculations also have a wide LO band around 800 cm^{-1}, but fail to match the observed broad band at 700 cm^{-1}. The isolated-particle Maxwell-Garnett calculation is expected to be more appropriate for our particulate films than the continuous film calculation. This is indeed the case. The continuous-film calculation exhibits two pronounced TO bands that are not seen in the experiment, or in the Maxwell-Garnett calculation.

In the titania island-structure films, there are elongated agglomerated clusters in addition to isolated spherical particles. Genzel and Martin[105] and Hayashi, et. al.[106] generalized the Maxwell-Garnett EMA to include the effects of nonspherical (elliptical) particle shape and optical anisotropy of the particles. This generalized effective medium approximation can be used to calculate an effective dielectric function for our island-structure films as a function of the bulk crystal dielectric constants, the shape of the particles (g), the filling factor (f) i.e. the fraction of the total volume occupied by the particles, and the dielectric constants of the matrix (the media in which the particles are suspended). In our case, the matrix is air and its dielectric function (ε_m) is 1.

The resulting expression is as follows:

$$e_{avg} = 1 + \frac{3(1-f)(e_m - 1) + \sum_k f_k(\tilde{e}_1^k + \tilde{e}_2^k + \tilde{e}_3^k)}{3(1-f) + \sum_k f_k(\hat{e}_1^k + \hat{e}_2^k + \hat{e}_3^k)} \qquad (6.1)$$

where f_k is the volume fraction of the particles of shape-k, $f = \sum_k f_k$, and:

$$\hat{e}_j = \left[1 + g_j\left(\frac{e_j}{e_m} - 1\right)\right]^{-1} \qquad (6.2)$$

$$\tilde{e}_j = (e_j - 1)\hat{e}_j \qquad j=1,2,3 \qquad (6.3)$$

---

[104] D. E. Aspnes, Am. J. Phys. **50**,704 (1982).
[105] L. Genzel and T. P. Martin, Phys. Status Solidi (b), **51**, 91 (1972); L Genzel and T. P. Martin, Surf. Sci. **34**, 33 (1973).
[106] S. Hayashi, N. Nakamori, and H. Kanamori, J. Phys. Soc. Japan, **46**, 176 (1979).

where e_j are the single crystal dielectric functions and e_m is the matrix dielectric parameters. For uniaxial crystals $g_1 = g_2 = g_\wedge$ and $g_3 = g_{II}$. $g_{//} \to 0$ represents long prolates (cigars) and $g_{//} \to 0.5$ represents flat oblates (pancakes). A value of 0.333 corresponds to spherical particles.

This theory has been applied only to particles dispersed in infrared transparent matrices like KBr, where spectra are collected in the transmission configuration.[107] Because of the discontinuous character of our films, they resemble isolated particles and agglomerates dispersed in a matrix (air), so we have applied this same theory to our experimental reflectivity results.

The filling and shape factors along with the bulk and matrix dielectric functions, are needed for the calculations. From the micrographs, we can estimate the total filling factor and the partial factors corresponding to the different particle or agglomerate shapes. The main effect of the filling factor f is to change the total intensity of the infrared reflectivity bands, while the shape factor g affects the peak positions. Using equation (6.1) to determine the dielectric function of the effective medium corresponding to the particles-in-air composite, along with the reflectivity expression corresponding to the (composite) film thickness, the substrate dielectric function, and the experiment geometry, we can calculate theoretical reflectivity spectra from which we can determine peak positions and heights for the g used in Eq. (6.1). By changing the values of g we can determine curves of peak position and peak height as a function of this shape factor, as shown in Fig. 6.3. The experimental results determine the peak positions of the bands. With these experimental values, the curves in Fig. 6.3 then determine g. Whenever we have two candidates, the peak height curves helps to determine the right candidate. For the experimental results of Fig 6.2 and the intersection of the corresponding horizontal lines in Fig. 6.3 with the calculated g-dependent curves of Fig. 6.3, three values of g are obtained. These are given in Fig. 6.4, along with the calculated reflectivity curves that they lead to when combined with the f values given in the figure.

These combinations of particle shapes and filling factors provide the right peak positions in our calculated spectrum, but the absolute heights and widths are off, being larger and sharper respectively. This is usual for nanoparticles. Nanoparticle spectra usually show broad absorption bands, presumably due to the anharmonicity (or damping) larger than in the bulk crystal.[108] This effect of anharmonicity is treated only in a qualitative manner. In our calculations we multiply the bulk damping constants by a factor (>1, usually 2 or 3). Figure 6.5 shows our final calculation, which fits the experimental results fairly well. The parameters used for this fit are given in Table 6.4, they correspond to the 600°C sample.

---

[107] M. Ocana, V. Fornes, J. V. Garcia, and C. J. Serna, J. Sol. St. Chem., **75**, 364 (1988); J. E. Iglesias, M. Ocana, and C. J. Serna, Appl. Spect. **44**, 418 (1990).
[108] S. Hayashi and H. Kanamori, J. Phys. C: Solid St. Phys., **13**, 1529 (1980).

6.5 Amorphous to Anatase Transformation

Raman and x-ray spectroscopy have shown[92] that the unheated particles, as prepared using this sol-gel technique, were amorphous. The phase conversion to anatase was followed by measuring the infrared absorption of titania particles dispersed in KBr, while they were being heated. Figure 6.6 shows the results for particles synthesized with a low concentration of water and without HPC polymer. The 348 cm^{-1} anatase absorption band starts to appear as a weak shoulder around 150°C. We quantified the phase transition by fitting this band with a log-normal function[109] and tracking the peak height. (The log-normal width did not vary appreciably.) Figure 6.7 shows the 348 cm^{-1} band peak height as a function of temperature for particles synthesized with and without HPC and with low (R = 5.3) and high (R = 150) water concentrations. Sterically-stabilized particles exhibit a lower transition temperature by about 20°C. For most of the cases the peak height reaches a plateau in a transition interval of about 60°C. The peak height is an estimate of the relative concentration of anatase in the particles. It is not an absolute measurement, because the featureless amorphous-phase spectrum is overridden by the crystal absorption peaks and the amount of amorphous phase present is difficult to determine. It is interesting to notice that large particles (low R values) exhibit a stronger band-peak height than small (high R value) particles. Measurements[92] of this phase transition by Raman and x-ray spectroscopy (chapter three) lacked the sensitivity shown here by infrared absorption and were unable to detect any signal of anatase at these low anneal temperatures.

6.6 Annealing of Island-Structure Anatase Thin "Films"

6.6.1 Introduction

As has been demonstrated in the previous section, the titania nanoparticles readily transform to anatase when annealed to temperatures above 200°C. It was shown in chapter three, for pellets and loose powders, that they remain in this phase until the anneal temperature reaches 800°C. This is the average temperature at which they transform into rutile. During annealing from 200 to 800°C the anatase crystallites are increasing in size as determined by x-ray diffraction peak width measurements (see Fig. 5.6). In this section we will present our results of annealing our island-structure films from 300 to 800°C.

6.6.2 Scanning electron microscopy

Figure 6.8 shows SEM micrographs of titania films spin-coated on silicon for different R values, revealing the characteristic particle sizes of the films. The particle size determines the film thickness because a single layer of particles are deposited during the coating. The filling factor (the fraction of the total volume occupied by the particles) can be estimated, from the

[109] D. E. Metzler, C. M. Harris, R. J. Johnson, D. B. Siano, and J. A. Thomson, Biochemistry **12**, 5377 (1973).

micrographs, for R = 5.3 and R = 15 films. The filling factor of the other films was estimated by observing the particle size and assuming that the same amount of titania is present in every film (this assumption is acceptable because the extent of conversion of TEOT is almost 100% for R values ≥ 30[110]). The results are presented in Table 6.3.

6.6.3 The effect of annealing on the grazing-incidence infrared reflectivity

Annealing of the island-structure films induces changes in its characteristic infrared spectra as seen in Fig. 6.9. Two main bands are observed, a small but sharp peak at 360 cm^{-1} and a strong broad band at 700 cm^{-1}. The two peaks become narrower as the film is annealed to higher temperatures. Figure 6.10 shows detailed grazing-incidence reflectivity spectra at two different temperatures. The peak narrowing is clearly seen. Two morphological phenomena take place during the annealing to higher temperatures. The particles shrink and become smoother[88, 92], and the crystallites increase in size (Fig. 5.6).[92] The particle shrinkage will decrease the total filling factor f by a small fraction. Our calculations showed that this small change in f does not affect the spectra linewidth. On the other hand, we argue that the crystallite-size increase will decrease the nanocrystal anharmonicity (or damping). Our effective-medium calculations supported this view, because decreasing the damping-constant multiplier generated narrower peaks. A summary of the parameters used for the generalized-EMA calculations of Fig. 6.10 are presented in table 6.4. A correlation between the infrared-peak linewidths and the nanocrystal size is expected. For this reason, we determined the linewidth of the 360 cm^{-1} band by fitting this peak with an asymmetric Lorentzian function, and this Lorentzian linewidth was obtained as one of the fitting parameters. Figure 6.11 presents our results for the correlation between this linewidth and the crystallite size. Despite the scattering, there is a definite decrease in linewidth with nanocrystal size. The correlation is not affected by the substrate used, but the particle size does have an effect, as seen by the different rates of decrease for R = 5.3 and R = 60.

Table 6.3. Island-structure film parameters

Water content (R)	Film thickness[1] (nm)	Total filling factor f (%)
5.3	380	2
15	210	8
30	145	11
60	100	17

[1] V. J. Nagpal, J. S. Riffle, and R. M. Davis, Colloid and Surfaces **87**, 26 (1994)

[110] V. J. Nagpal, Ph D dissertation, Chemical Engineering Dept., Virginia Tech (1993).

Similar behavior was observed on particles deposited on molybdenum. The results are presented separately in Fig. 6.12. These films needed to be annealed in an inert atmosphere to avoid oxidation of the substrate. As a result unburned organics remain from the sol-gel synthesis, leaving a black residue on the particles. For this reason, we could not get an infrared signal from single-layer films so four spin-coated layers were deposited to yield thicker films. The 360 cm^{-1} band was then observable in grazing-incidence reflectivity and, as seen in Fig.6.12, it narrowed with increasing anneal temperature

6.7 Annealing of Continuous Anatase Thin Films

The concentration step when it is used, in the particle synthesis procedure, not only increases the particle concentration in the sol, it also breaks the titania aggregates into smaller particles.[100] Prior to the concentration step, the particles are 80 to 100 nm in size. After this step, the particles are 30 to 50 nm in size.[100] The increase in sol concentration and decrease in particle size leads to spin-coated films of higher density than the ones described in the previous section. We have studied such concentrated films that were made by spin-coating four times and then annealing in air for two hours at 800°C. Previous work indicated such films to have a filling factor of about 80%[100], so that they may resemble continuous films.

Table 6.4. Parameters used in the calculations of the infrared spectra of island-structure thin films (a water concentration of R = 15, and HPC were used in the colloidal suspension synthesis)

Temperature (°C)	Thickness (nm)	Damping factor multiplier	Filling fact.-1 (%)	Shape fact.-1	Filling fact.-2 (%)	Shape fact.-2	Filling fact.-3 (%)	Shape fact.-3
600	250	3	2	.17	1	.34	1	.44
800	200	2	1.8	.19	0.8	.35	0.8	.45

At normal incidence, transmission measurements in the infrared exhibit the transverse-optical (TO) phonon modes as absorption lines, but the longitudinal-optical (LO) modes are hidden. In oblique incidence, however, both the TO and LO modes show up as absorption lines. [111, 112] The zone-center TO and LO frequencies are usually obtained from Kramers-Kronig analysis, or from dielectric function analysis of normal-incidence reflectivity measurements on bulk samples, as done in this dissertation for single-crystal anatase in chapter four. Berreman[111] showed that in thin films, LO phonons are excited by oblique-incidence p-polarized light,

[111] D. W. Berreman, Phys. Rev., **130**, 2193 (1963).
[112] R. M. Almeida, Phys. Rev. B, **45**, 161 (1992); K. Yamamoto and H. Ishida, Appl. Spect. **48**, 775 (1994); K. Yamamoto and H. Ishida, Appl. Optics, **34**, 4177 (1995).

because the light's electric field has a component perpendicular to the surface and this couples to the LO mode. Figure 6.13 shows the electric-field intensity perpendicular to the film surface for two configurations: (1) grazing-incidence (80°) reflectivity from an island-structure anatase thin film deposited on a metal substrate, (2) oblique-incidence (60°) reflectivity or transmission from a continuous anatase thin film deposited on silicon. It can be seen that for these configuration the two E_u LO modes can be excited.

The concentrated film was deposited, by spin-coating, on a polished (both sides) silicon wafer appropriate for transmission measurements. A titania film sputtered on a polished silicon wafer, annealed at 425°C, was available from the Materials Science Dept., at Virginia Tech, and it was appropriate for reflectivity measurements. The annealing step was necessary because the as-prepared film was amorphous. Figure 6.14 presents results of transmission measurements at 60° incidence and reflectivity measurements at 40° incidence, both taken with p-polarized light (electric field in the plane of incidence). Together with the experimental spectra, theoretical calculations are shown. These calculations assume that the film has the polycrystalline anatase dielectric function of chapter four and that the film/air interface is abrupt. The positions of the measured peaks and predicted peaks from calculations agree very well. The extra peak (1075 cm^{-1}), in the transmission spectrum, correspond to a substrate (silicon) feature. There is some disagreement between the 825 cm^{-1} measured peak and 864 cm^{-1} predicted peak. Measuring transmission spectra on films with several thicknesses, ranging from angstrom to micron order, would bring more information to understand the source of this disagreement. The transmission spectrum has weaker peaks than the predicted one. That is because the titania film is not entirely continuous, it has a filling factor of about 80%.

6.8 Anatase to Rutile Transformation

Annealing the island structure thin films to temperatures above 800°C did not induce the expected transformation to rutile. Figure 6.15 shows two reflectance spectra: (1) from a single-layer film on platinum annealed to 900°C in air and (2) from a multiple-layer film on molybdenum anneal to 1000°C in argon. Both spectra show only anatase vibrational features. This result is somewhat surprising. For anatase pellets and powders[92], 800°C is the observed transition temperature. Figure 6.16 shows the transformation of the infrared spectra of a 100%-titania pellet annealed in argon. At 800°C, the rutile band near 460 cm^{-1} has clearly made its appearance. The particle size and the use of the steric stabilizer have an effect on the transition temperature. Raman spectra were taken on 100%-titania pellets annealed in air to different temperatures. The ratio of the 141 cm^{-1}-anatase peak to the 440 cm^{-1}-rutile peak is a measure of the relative phase concentrations, as shown in chapter four. Figures 6.17 and 6.18 show the conversion of anatase to rutile, calculated from the ratio of the Raman peaks. Results in Fig. 6.17 are for steric stabilized particles and in Fig. 6.18 for particles grown without polymer. We can see that conversion increases with the decrease in particle size regardless of the presence or absence of the steric stabilizer. For pellets made with particles of the same size, the ones synthesized with polymer show a higher conversion rate.

6.9 Summary

Titania nanoparticles, grown by a sol-gel process with a steric stabilizer, have been studied by far-infrared spectroscopy and Raman scattering. Titania particles dispersed in a KBr matrix were placed in an optically accessible heater and so were annealed while spectra was collected. By measuring the 348 cm^{-1} band peak height as a function of anneal temperature, we established that the transformation to anatase starts at, as low as, 150°C. Sterically-stabilized particles exhibit a lower transition temperature by about 20°C. For most of the samples, crystallization is complete in a temperature interval of about 60°C. Figure 6.7 summarizes these results.

Single-particle layer films were obtained by spin coating the colloidal suspensions on different substrates. These films have an island-structure rather than a true thin film character. The measured infrared spectra were different from that of a continuous film. To understand these infrared results, a generalized effective medium approximation was used. In this generalized form, an extra parameter is included to take into account the particle shape. Annealing these films in the anatase temperature region induce changes in the infrared spectra. In general, the infrared absorption peaks become sharper (decrease in linewidth) with increasing annealing temperature. We established that this change is due to a decrease in damping constant. During annealing the nanocrystallite size increases. Figure 6.11 exhibits these results.

Continuous titania films were deposited on infrared transparent substrates (silicon). These films were transformed to the anatase phase by appropriate annealing. Transmission and reflectivity infrared experiments at oblique incidence allowed us to measure anatase TO like and LO like peaks. These measurements were compared with calculations using the polycrystalline anatase dielectric function of chapter four and assuming that the film/air interface is abrupt. All the measured values agreed very well with the predicted ones except one high frequency LO-like peak.

Finally, the anatase to rutile transformation was investigated, by infrared measurements, in the island-structure films and in 100%-titania pellets. The island-structure thin films did not exhibit any rutile features even upon annealing to 1000°C. It seems that a packing effect (having other particles nearby) is necessary, besides temperature, to induce nucleation of the new phase. Pellet results showed that conversion increases with decrease in particle size and that sterically-stabilized particles have a higher conversion rate.

Figure 6.1. Optical photographs (100X) of island-structure thin films. The colloidal suspensions used to spin coat the films were synthesized with low water content (R=5.3), with steric stabilizer (A) and without it (B). (fig61.jpg) (50Kbytes)

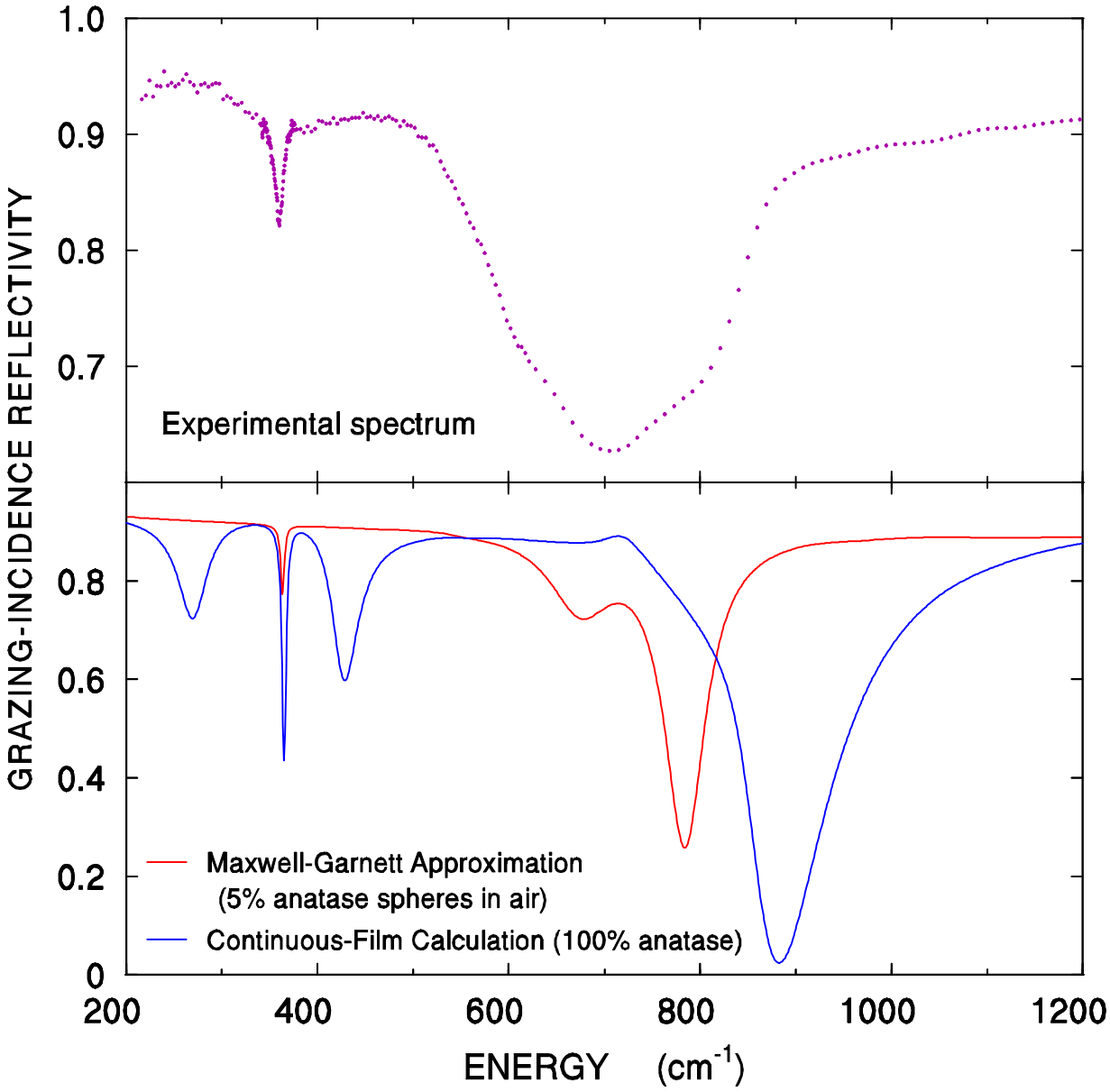

Figure 6.2. Grazing-incidence infrared reflectivity of an island-structure anatase film, made from a suspension synthesized using HPC and a water concentration of R=15. The sol was spin-coated on a platinum substrate and annealed in air at 600°C. The theoretical curves in the lower panel use the dielectric functions of bulk-crystal anatase obtained in chapter four. The Maxwell-Garnett calculation assumes spherical anatase particles in an anatase/air composite that is 95% air.

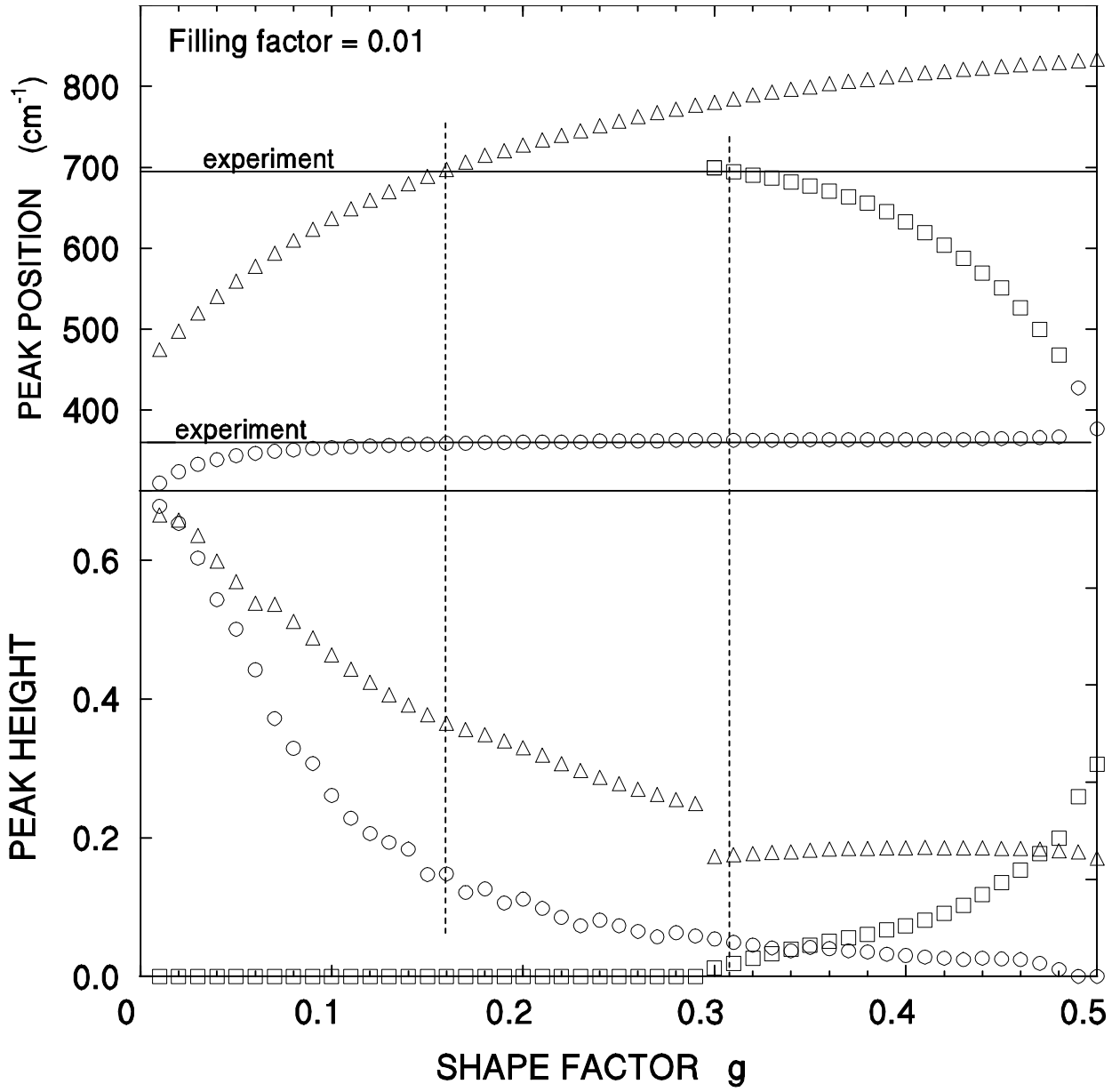

Figure 6.3. Calculated grazing-incidence infrared-reflectivity peak positions and heights as a function of shape factor, for an island-structure film with 1% volume fraction of anatase. Calculations were done using anatase parameters from chapter four and using the generalized effective medium approximation (ref. 106). The experimental peak positions are represented by the horizontal lines, and their intersections with the theoretical points are marked by vertical lines. These intersections provide values of the shape factor g that were included in the model used to fit the experimental results.

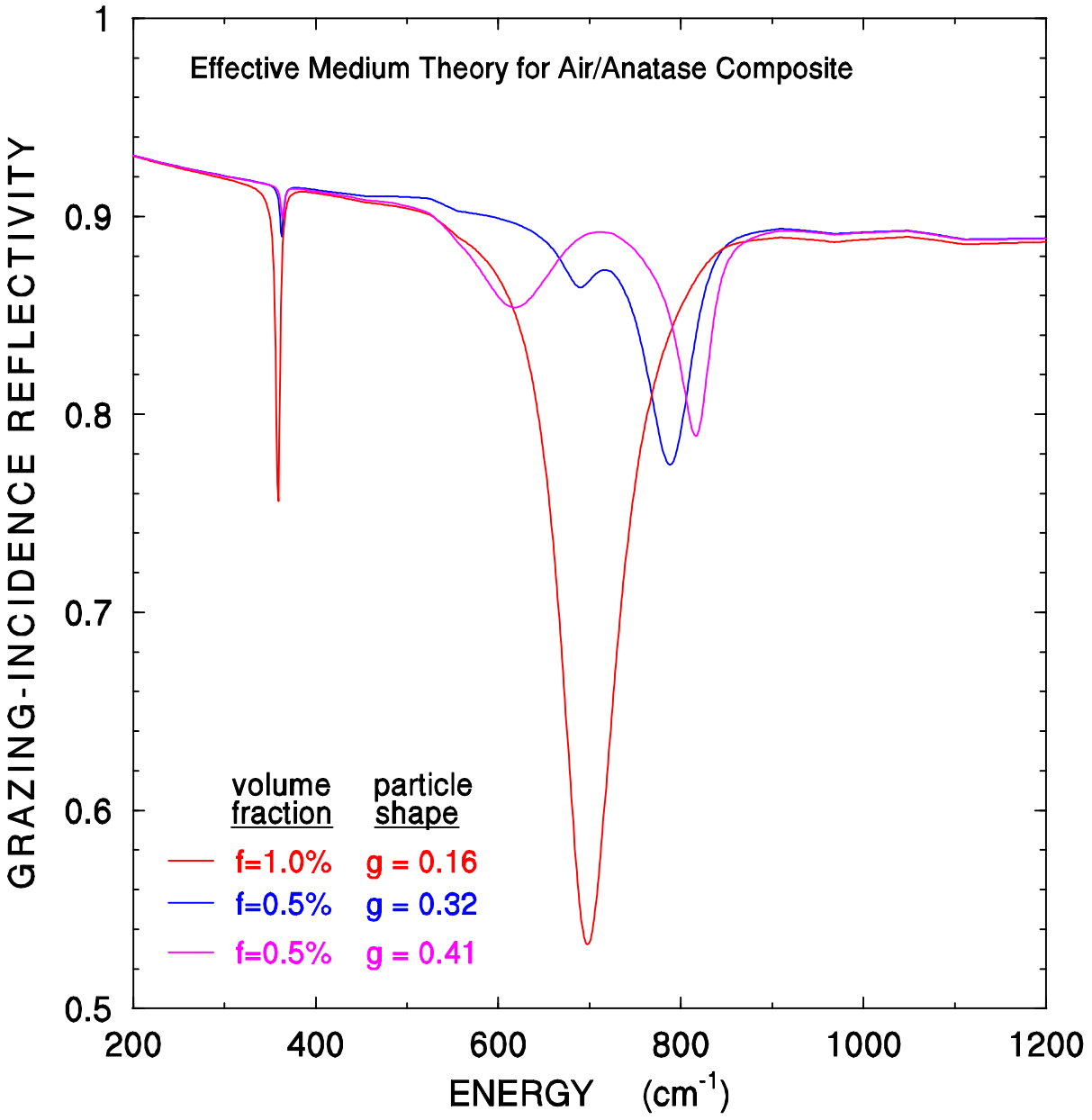

Figure 6.4. Theoretical grazing-incidence reflectivity spectra based on the generalized effective medium approximation. The three curves correspond to three pairs of (f, g) values, where g specifies the particle shape and f is the volume fraction occupied by the anatase particles. The solid curve corresponds to cigar-shape anatase agglomerates that occupy 1% of the volume in an air/anatase composite medium.

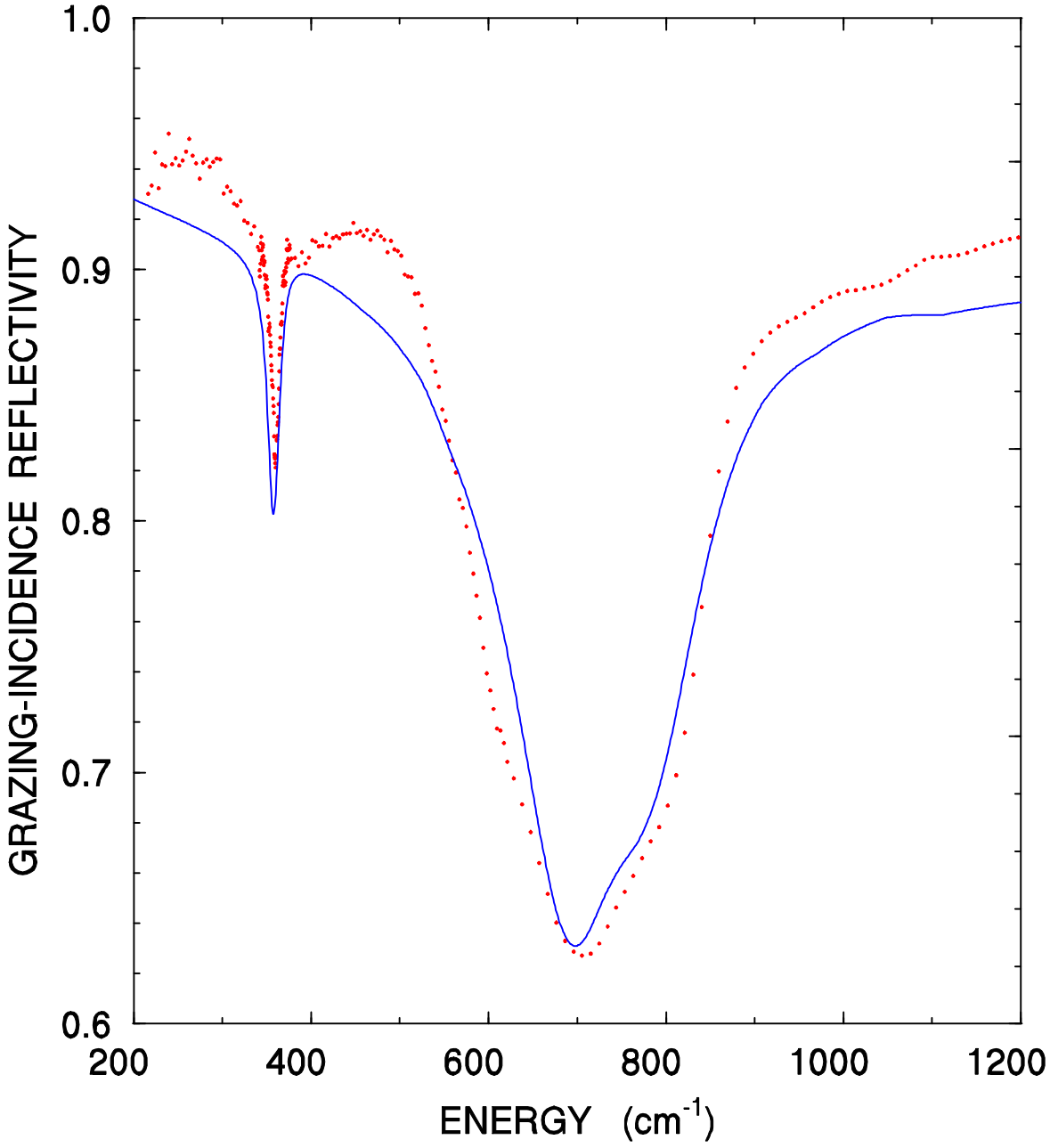

Figure 6.5. The observed spectrum of Fig. 6.3 (points) compares to a calculated spectrum (curve) which corresponds to the generalized effective medium approximation with three types of anatase particles present. The anatase/air composite is assumed to be 2% anatase (by volume), and the three particle types have the shape and volume fractions specified on Fig. 6.4. For this fit, the bulk-crystal anatase dielectric functions are modified by multiplying their damping constants by 3.

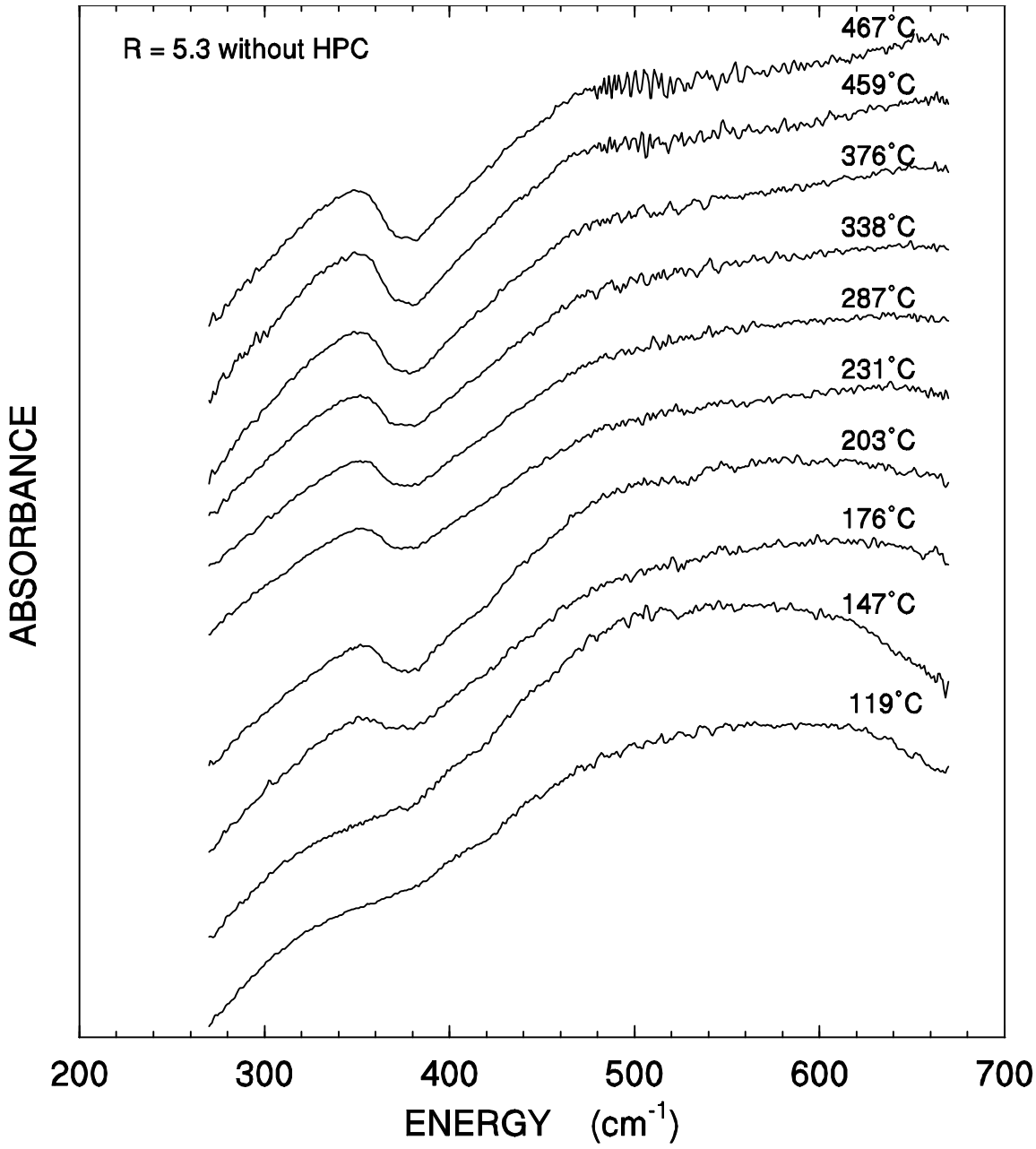

Figure 6.6. Infrared absorption spectra of titania particles dried out of suspensions made with low water (R= 5.3) and without polymer. The particles were dispersed in KBr and pressed into pellets. These are in-situ temperature-dependent measurements; the sample was being annealed while taking data in infrared transmission mode.

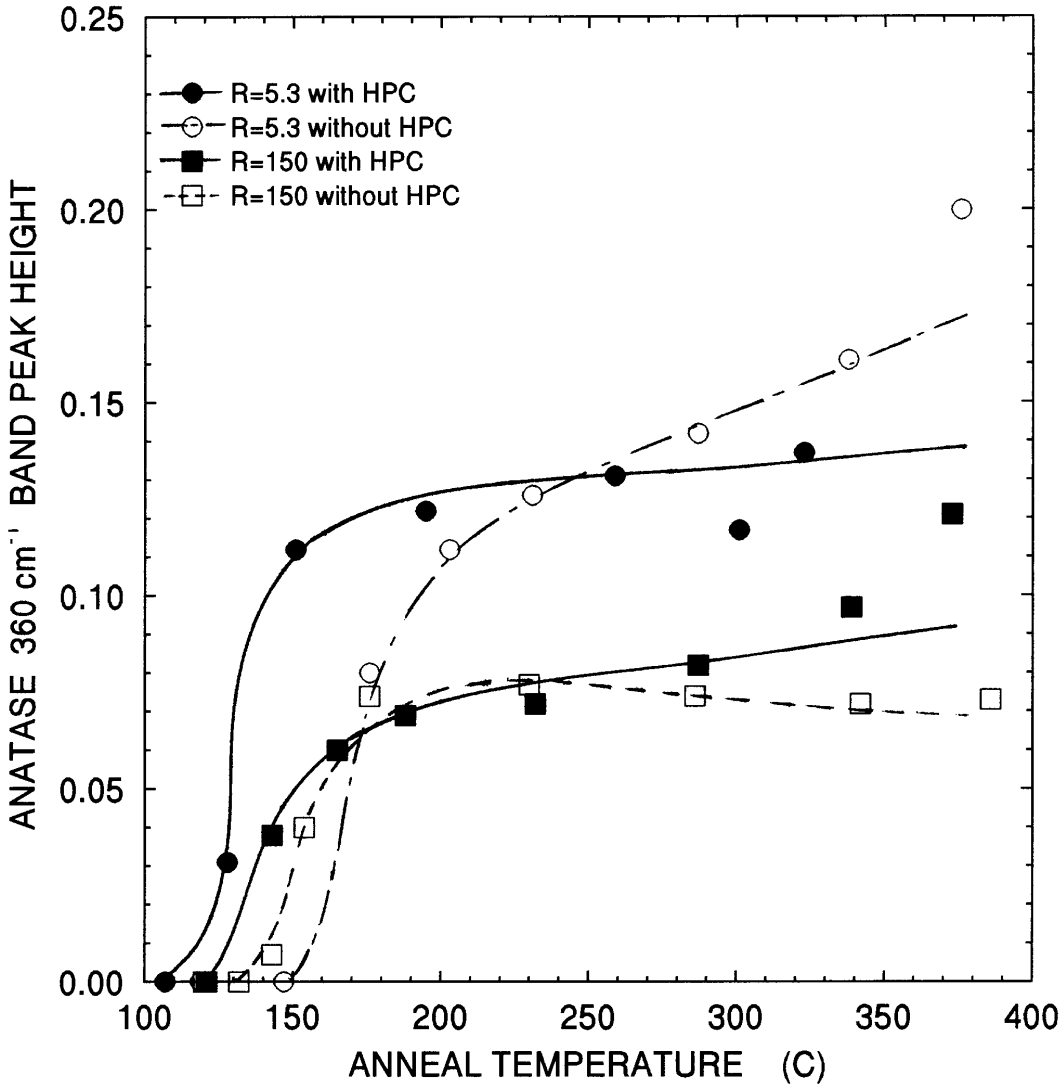

Figure 6.7. Anatase 348 cm^{-1} band peak height as a function of annealed temperature. These data were measured by fitting the 348 cm^{-1} band with a log-normal function, which provided the peak height.

Figure 6.8. SEM micrographs of the island-structure films. The suspensions, used to make the films, have different water contents (R values) which yields different particle sizes. (fig68.jpg) (138Kbytes)

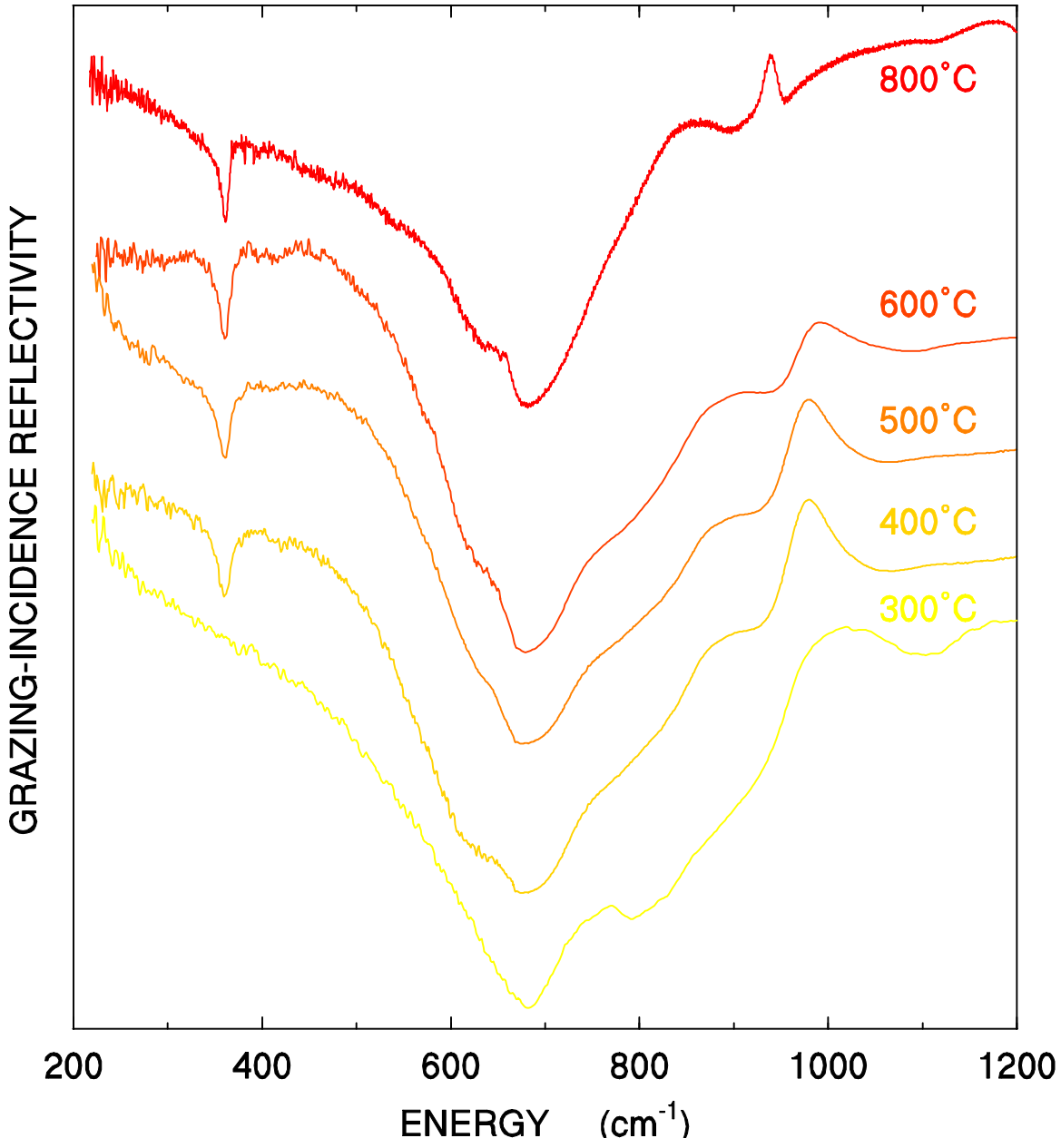

Figure 6.9. Grazing-incidence reflectivity spectra of island-structure films annealed to different temperatures. The suspension used for the films was a low water content (R = 5.3) with polymer. The substrate used is aluminum oxide. The feature seen around 1000 cm^{-1} corresponds to the substrate. The annealing process was done in air.

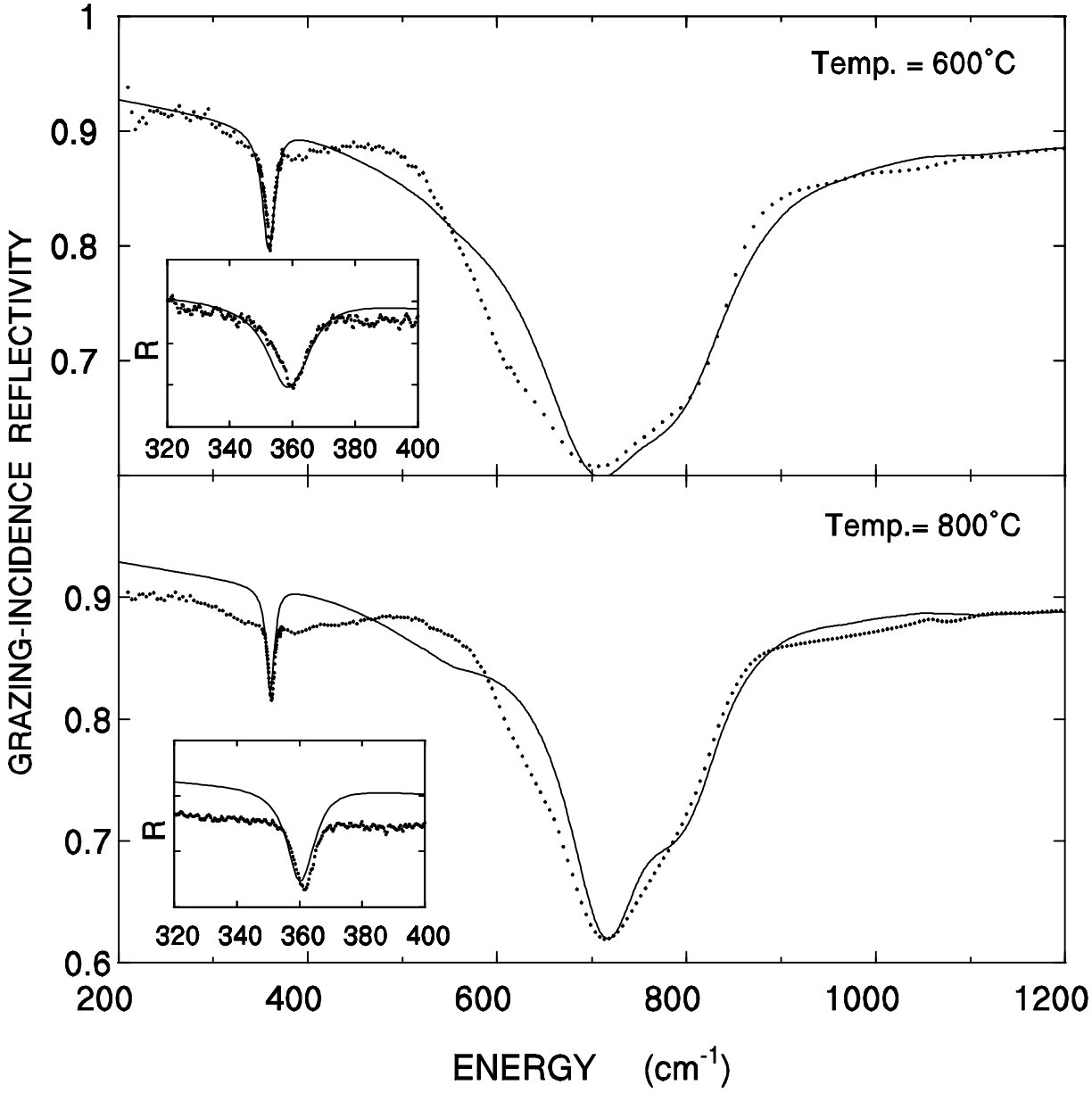

Figure 6.10. Grazing-incidence IR reflectivity spectra of two island-structure films, made from a R = 15, HPC-containing suspension that was spin-coated on platinum and annealed in air to 600°C and 800°C. The curves correspond to calculations based on the generalized effective medium approximation. The inserts demonstrate the narrowing, with increasing anneal temperature, of the 360 cm^{-1} line.

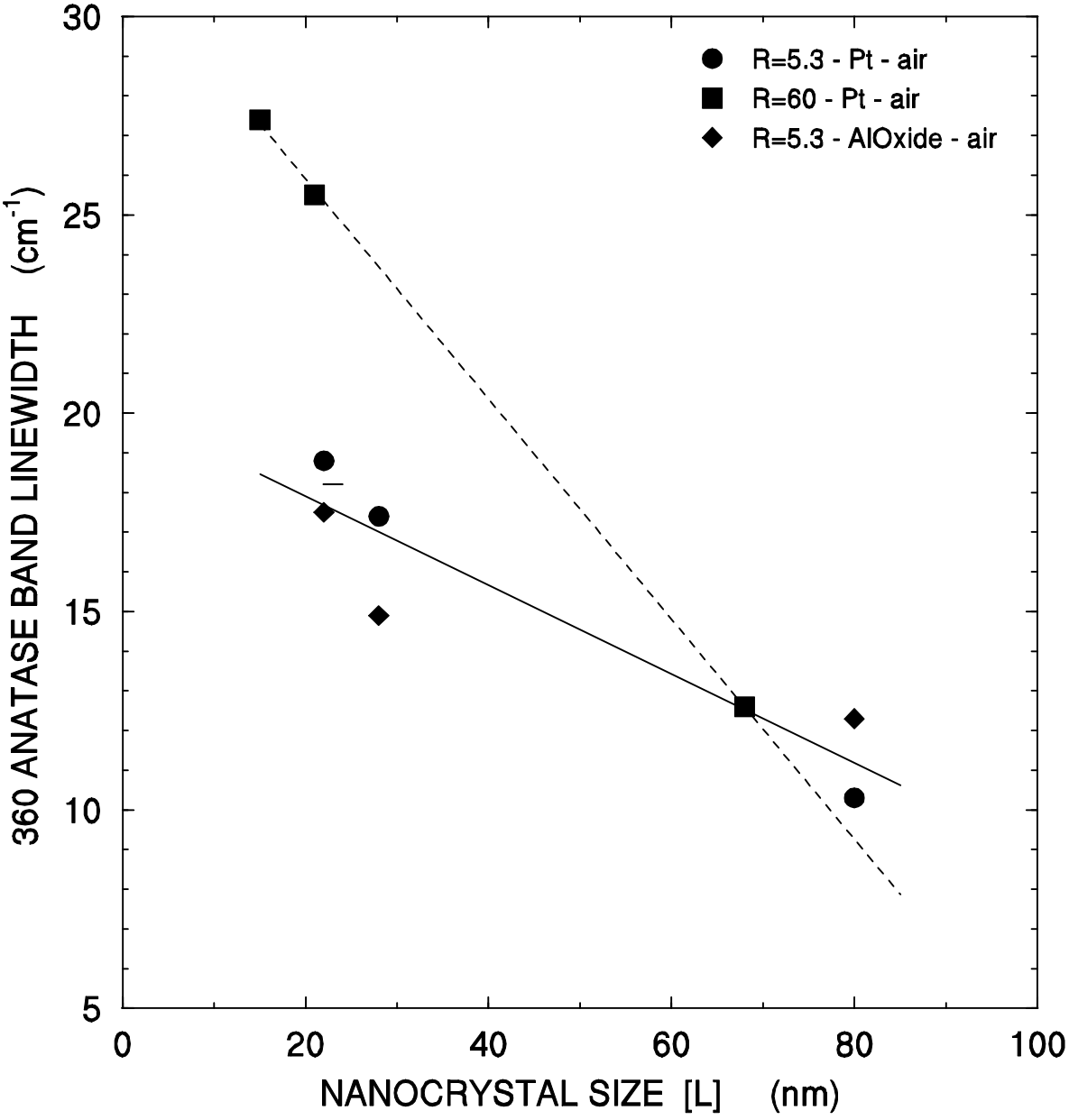

Figure 6.11. Anatase 360 cm^{-1} band linewidth change with nanocrystallite size. The linewidth was determined from fitting with asymmetric-Lorentzian functions to the 360 cm^{-1} infrared reflection band. The crystallite sizes were determined by x-ray diffraction on powders annealed under the same conditions as the films.

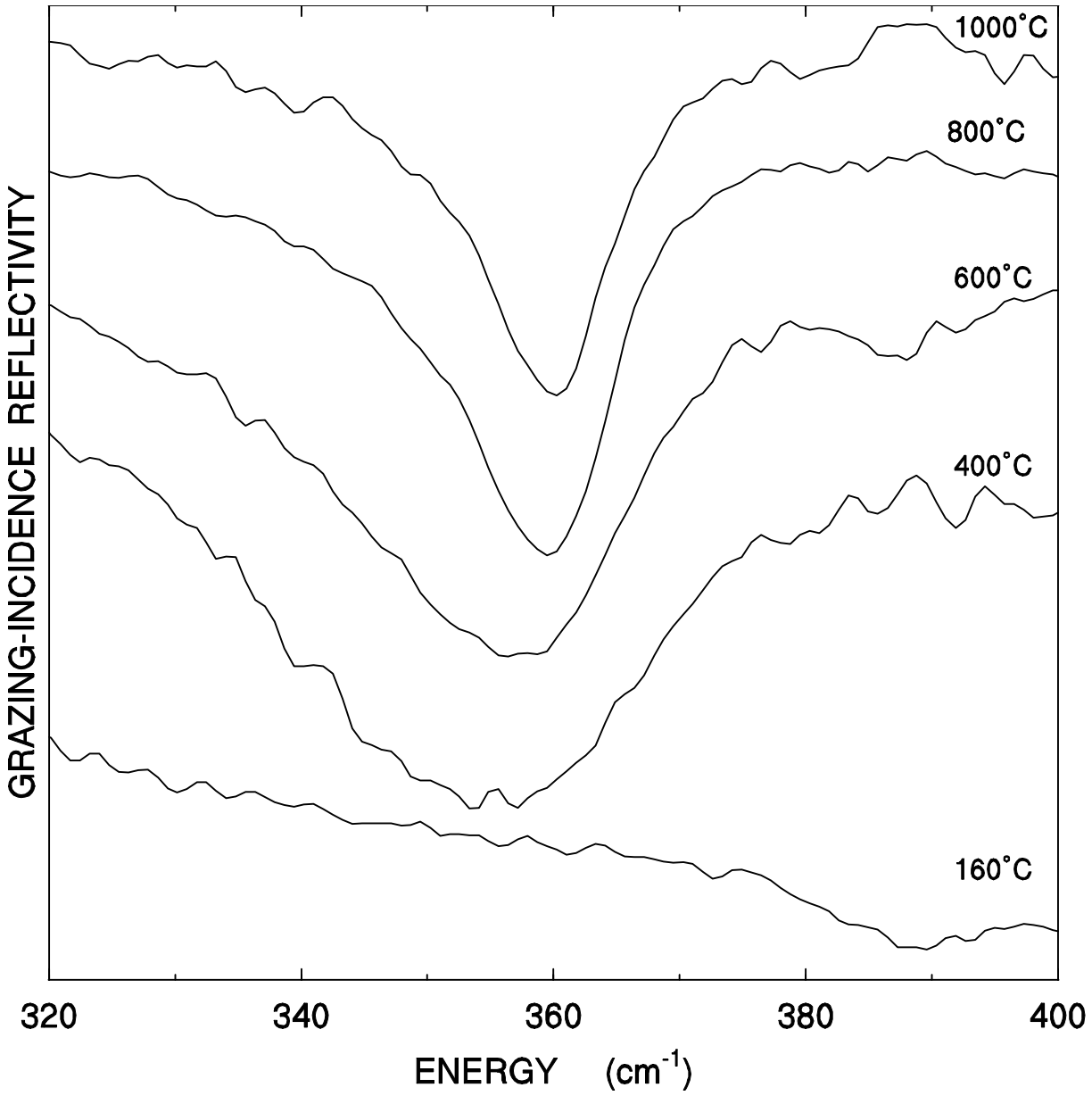

Figure 6.12. Grazing-incidence IR reflectivity spectra of an island-structure film, made with a R = 5.3, HPC-containing suspension that was spin-coated four times on molybdenum and annealed in argon to 400°C, 600°C, 800°C and 1000°C.

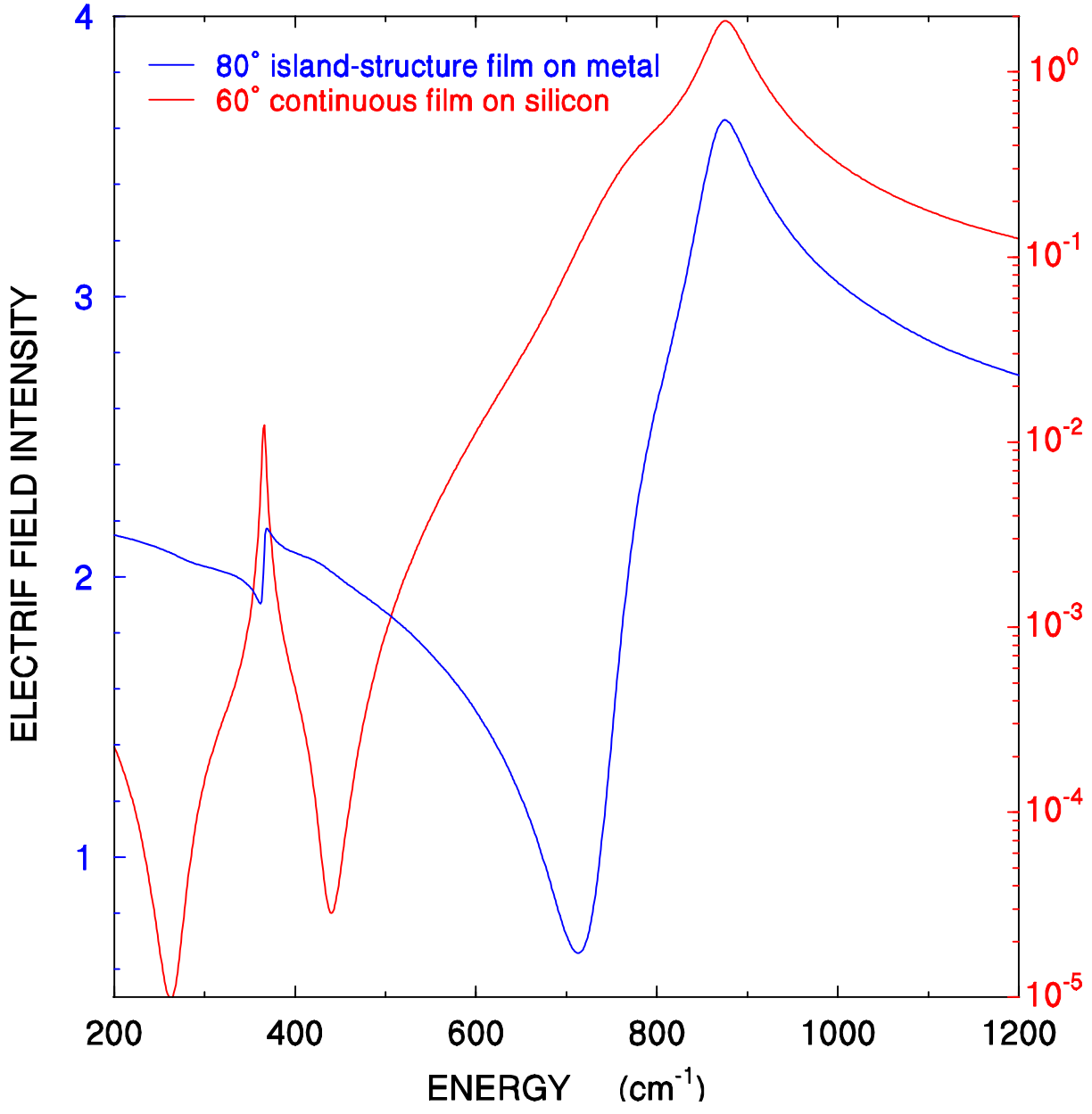

Figure 6.13. Electric field intensity perpendicular to the surface of thin anatase films as a function of frequency.

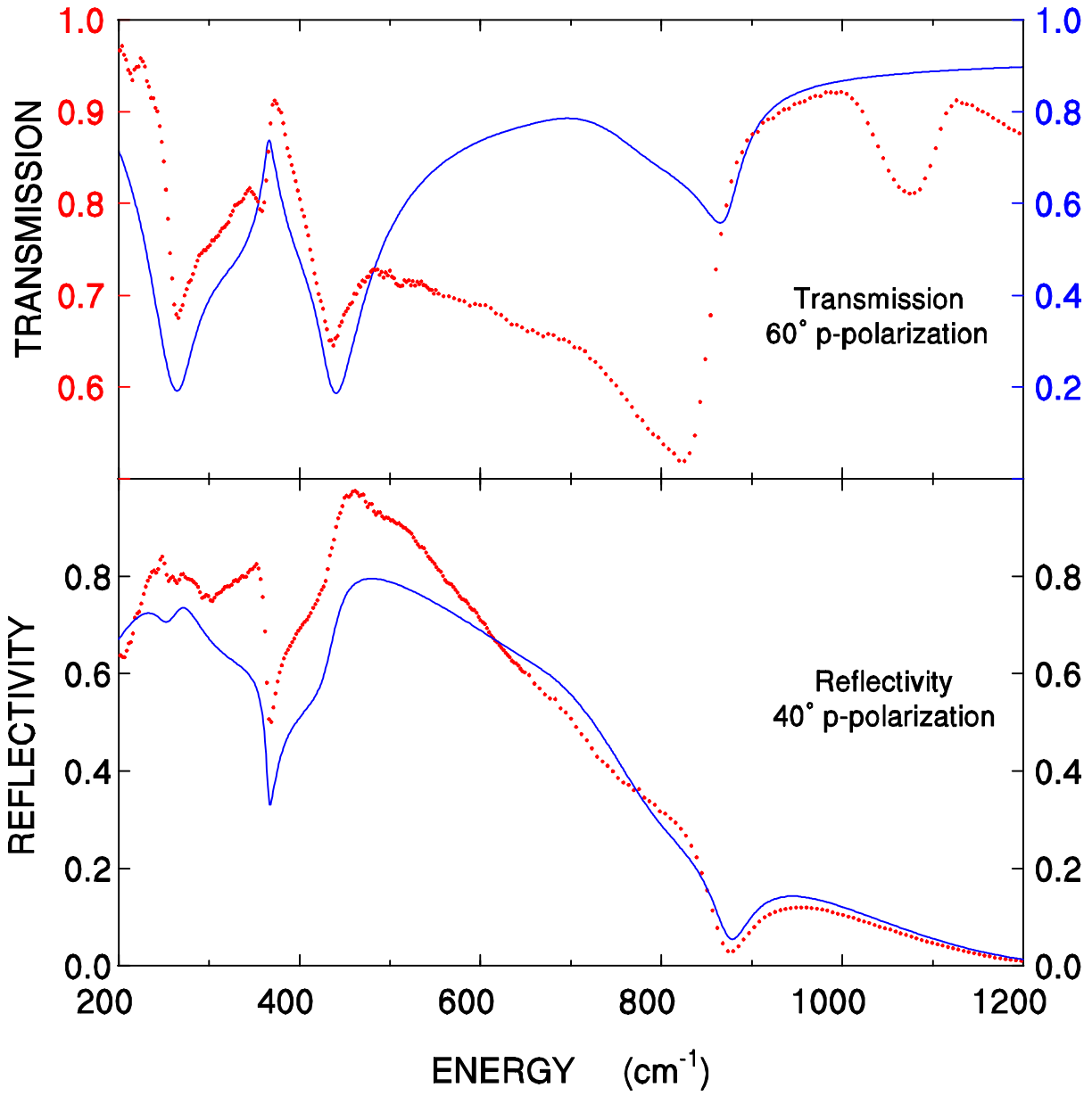

Figure 6.14. Infrared reflectivity and transmission at oblique incidence of continuous anatase films deposited on silicon (points). Theoretical spectra are based on the polycrystalline anatase dielectric function of chapter four (curves).

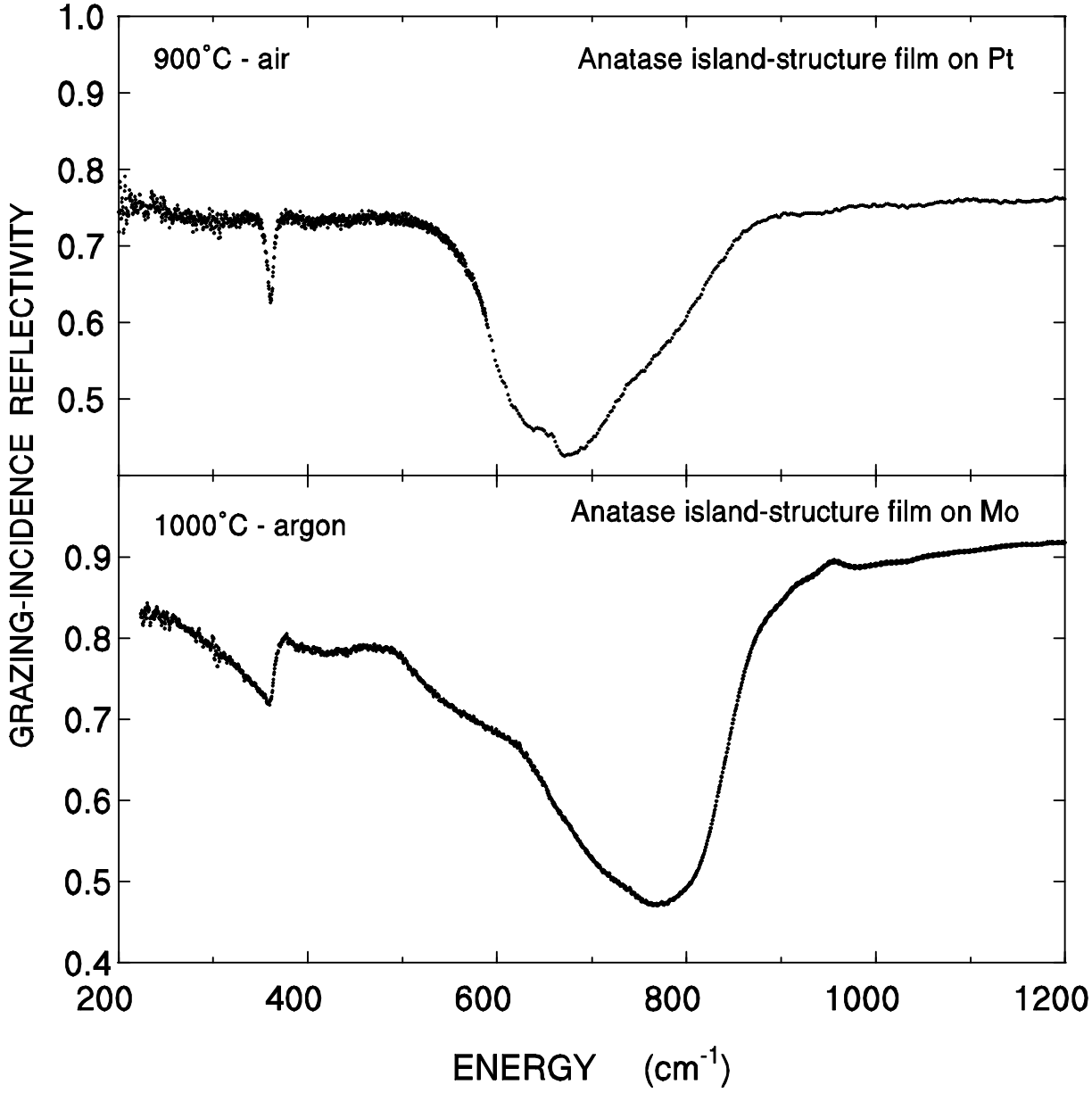

Figure 6.15. Grazing-incidence IR-reflectivity spectra of island-structure films. Upper spectrum from films made with R5.3 with HPC suspension spin coated on platinum and annealed to 900°C in air. Bottom spectrum from films made with R=60 with HPC suspensions spin coated (four times) on molybdenum and annealed to 1000°C in argon.

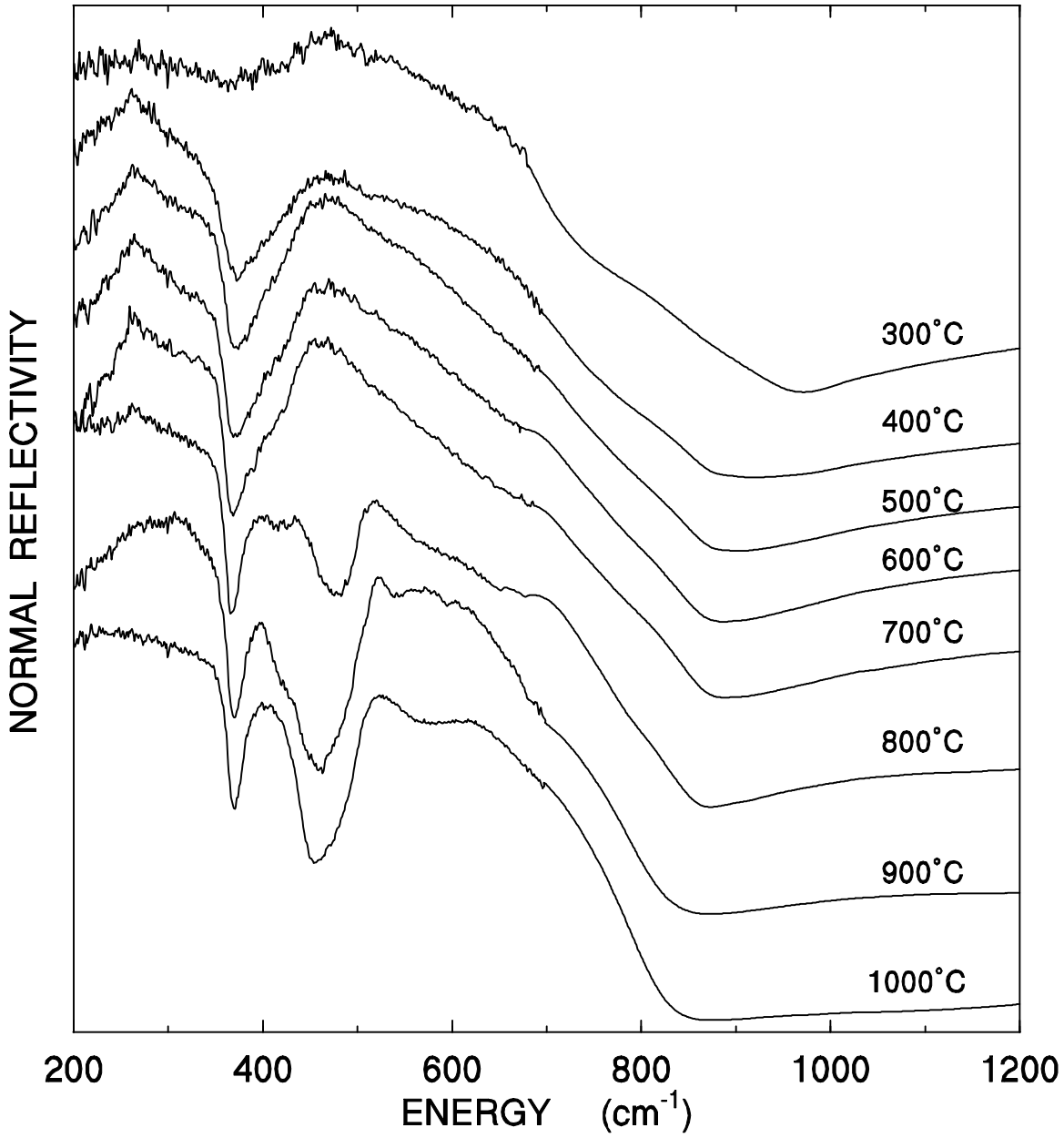

Figure 6.16. Near-normal reflectivity from 100%-titania pellets made out of particles dried out from suspensions with R=150 and HPC. The pellets were annealed in argon.

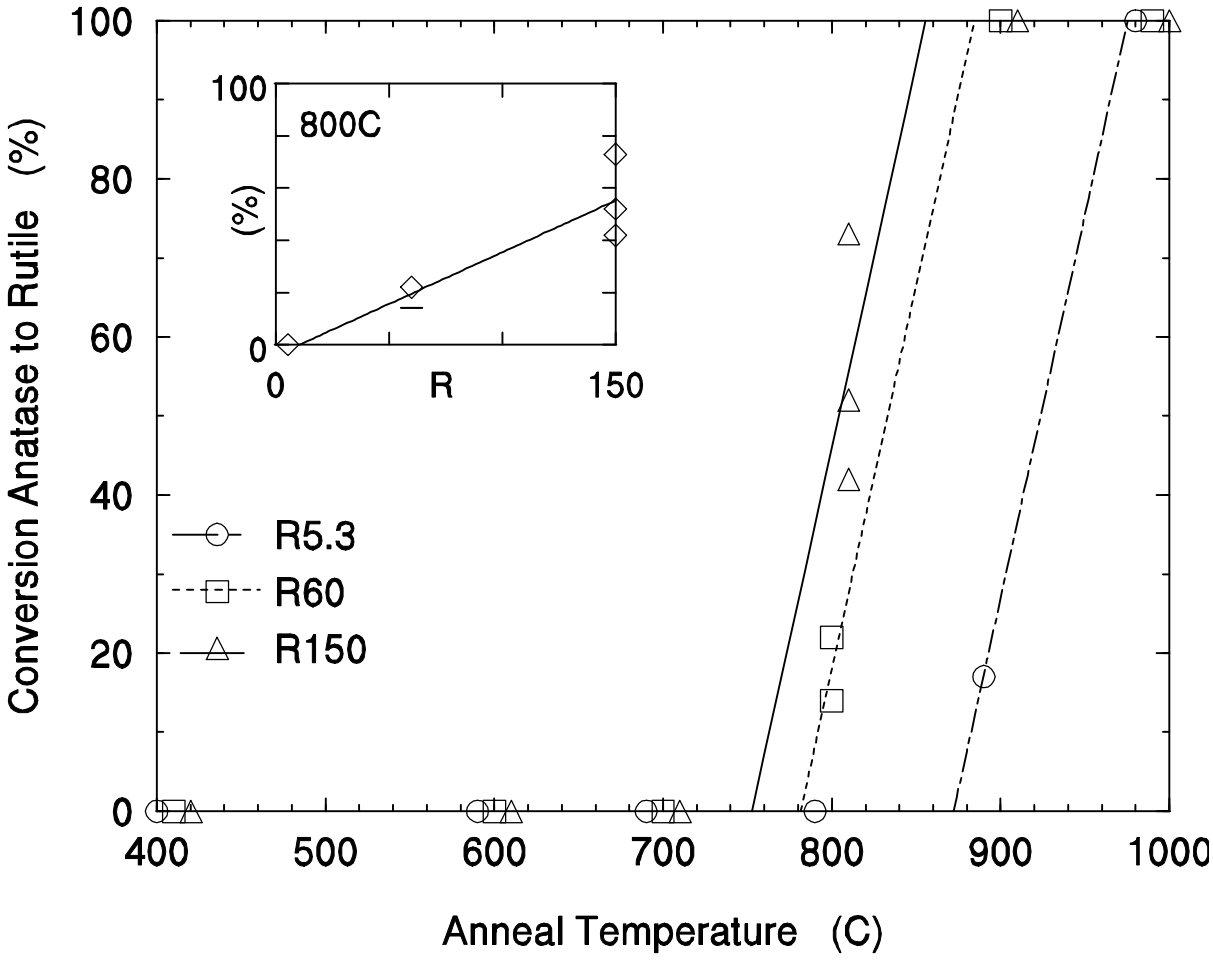

Figure 6.17. Conversion of anatase to rutile as a function of water content, for pellets made out of particles dried out from suspensions with HPC.

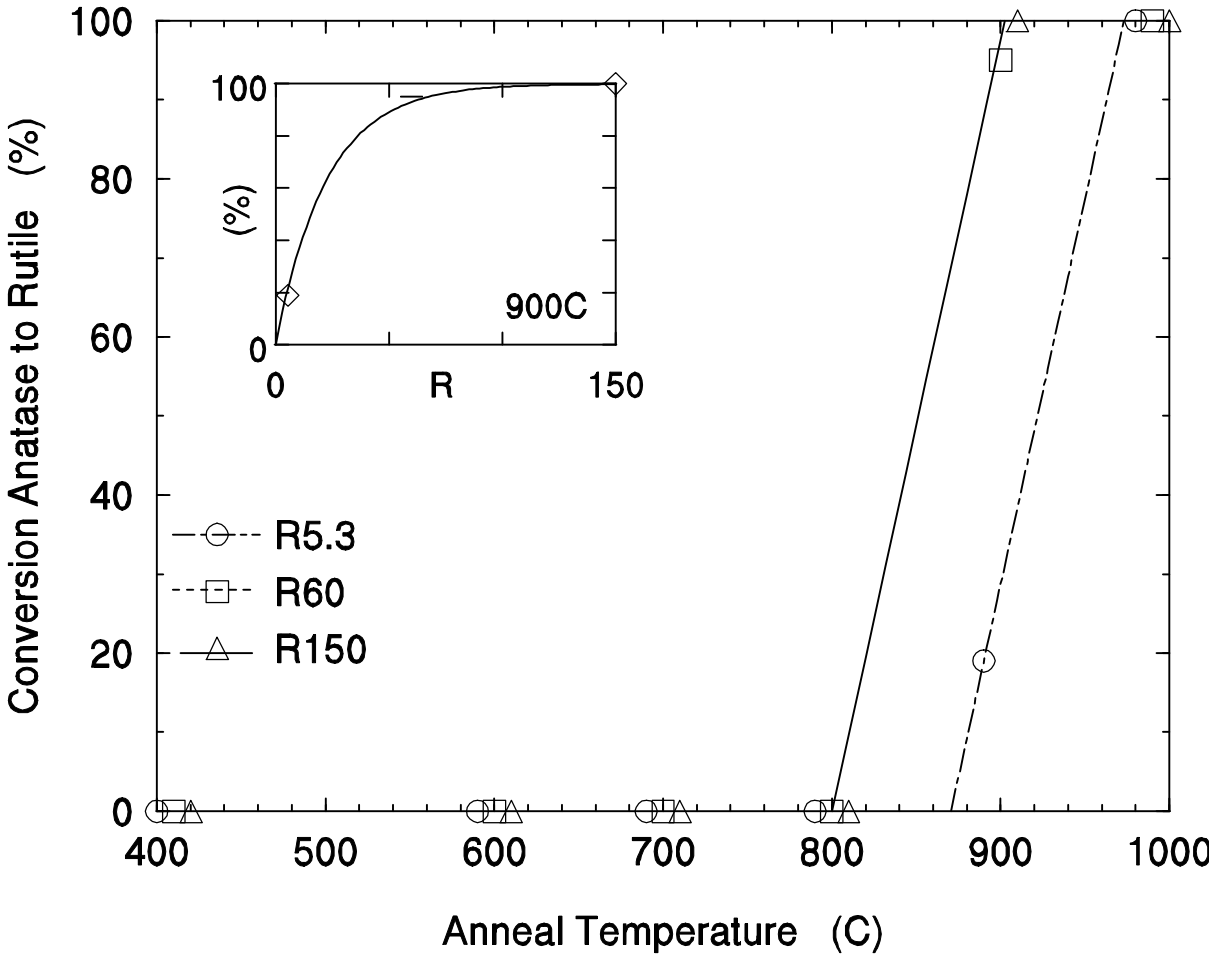

Figure 6.18. Conversion of anatase to rutile as a function of water content, for pellets made out of particles dried out from suspensions without HPC.

CHAPTER SEVEN

7. ELECTRON-ENERGY LOSS STUDIES OF NANOPHASE TITANIA

7.1 Introduction

Electron-energy loss scattering experiments provide information on electronic transitions over a wide frequency range. In the limit of low momentum transfer, information on the optical constants is attainable on samples which would not be suitable for optical measurements. The electron-energy loss spectrum is proportional to the imaginary part of the inverse dielectric function and, unlike optical experiments which only observe dipole transitions, the capabilities in EELS to vary the momentum transfer allows one to observe monopole, quadrupole, and higher order transitions

In an electron-energy loss experiment, an energetic electron beam (80 KeV) passes through a thin film (< 1000 Å) of the material being studied. The electrons on their way through the film may scattered by an angle θ and loose energy ΔE.
Energy and momentum conservation require

$$\Delta E = (\hbar^2 / 2m)(k_0^2 - k_s^2)$$

$$\hbar\vec{q} = \hbar(\vec{k}_0 - \vec{k}_s)$$

where k_0 and k_s are the wave vectors of the incident and scattered electron and q is the momentum transfer to the solid. The wave vector q can be decomposed into a parallel and perpendicular component to k_0 given by

$$q_\perp = k_0 q$$

$$q_{//} = k_0 \frac{\Delta E}{2E_0}$$

where the assumption has been made that the scattered angle and the energy loss are very small.
The transverse momentum is independent of the energy loss and depends only on the scattering angle, whereas the longitudinal momentum is related to the energy loss only.

The purpose of EELS is to obtain the differential cross section for scattering as a function of ΔE, and $q_\perp$. This cross section is given by:[113]

$$\frac{d\Sigma}{d\Delta E d^2 q_\perp} = \left(\frac{e}{pE_0}\right)^2 \frac{\hbar}{q^2} \mathrm{Im}\left(\frac{-1}{e(q,\Delta E)}\right)$$

where ε(q,ΔE) is the complex dielectric function. The optical constants can be obtained from the loss function Im[-1/ε(q,ΔE)], in the long-wavelength limit (q=0), using Kramers-Kronig analysis.

---

[113] S. E. Schnatterly, *Solid State Physics*, (Academic, New York, 1979) vol 34, p. 275.

The main difficulty with EELS experiments is the occurrence of multiple scattering as the electrons pass through the sample which is why it is necessary to work with the thinnest possible sample. Several techniques to remove multiple scattering have been proposed, in this work we use the technique described by Livins, et.al.[114]

We encountered another difficulty applying EELS spectroscopy to the study of titania particles. The particles need a substrate for support. We chose a very thin film of alumina. Because of the double layer composite sample, another source of multiple scattering exists: an electron passing through the composite can scatter in one film and suffer a second scattering in the second film. This type of multiple scattering event made it very difficult to analyze data above 20 eV. We took advantage of the fact that multiple scattering affects the low energy region of the spectra less strongly than the high energy region and developed a simple weighted-subtraction technique that allowed us to have reliable titania EELS spectra below 20 eV.

In this chapter we will present our results on electron diffraction (zero energy loss and variable scattering angle) and electron-energy loss (variable energy loss and variable scattering angle) studies on titania particles which have received: (1) no heat treatment, (2) an annealed at 600°C, (3) and annealed at 1000°C. The anneal temperatures were chosen to transform the as-prepared amorphous titania particles to the anatase and the rutile crystalline phases, respectively.

This chapter is organized as follows. In Sec 7.2 the sample preparation is reviewed and characteristics of the EELS spectrometer are given. The electron diffraction results are given in Sec. 7.3 and the electron energy loss results are found in Sec. 7.4. Also in Sec. 7.4 , the low-energy spectra are analyzed by a parametric model in the energy loss range $\Delta E = 0$ to 12 eV and momentum transfer range $q = 0.1$ Å to 0.9 Å and, in addition, the low-momentum transfer measurements are compared with optical measurements of the absorption edge. Finally, in Sec. 7.5, theoretical calculations by Mo and Ching[115] of $Im(-1/\varepsilon)$ as a function of energy for q=0, are compared with our energy loss measurements and similarities and differences are analyzed.

7.2 Experimental

The preparation of the sol-gel titania powders using a polymer for steric stabilization was described in chapter two. A short summary of the preparation follows. The titania particles were synthesized through the hydrolysis and condensation of titanium tetraethoxide (TEOT) $[Ti(OC_2H_5)_4]$ in the presence of a steric stabilizer, hydroxypropylcellulose (HPC), which

[114] P. Livins, T. Aton, and S. E. Schnatterly, Phys. Rev. B **38**, 5511 (1988).
[115] S-D. Mo and W. Y. Ching, Phys. Rev. B **51**, 13023 (1995).

leads to monodisperse particles.[116] The particle size is controlled through the amount of water used in the reaction. R=[H_2O]/[TEOT] is a measure of the relative water concentration. Suspensions made with R = 150 were used which corresponds to particles of average diameter of 80 nm. The particles were deposited on a TEM molybdenum grid which has been overlaid with a thin layer of aluminum oxide (300 Å in thickness). The deposition is done by spin coating drops of the colloidal suspension on the aluminum oxide-molybdenum grid. After three coatings, a discontinuous island-structure film is obtained. The samples are annealed in argon to prevent substrate oxidation. A Lindberg 54353 three-zone tube furnace is used with 99.998% purity argon flowing through the anneal tube at a partial pressure of 1.2 Torr. Each sample is taken from room temperature to the desired anneal temperature at 20°C min^{-1}, held at the anneal temperature for 2 hr, then slowly cooled back to room temperature. The as-prepared sol-gel titania particles are amorphous (as discussed in chapter Six), annealing to 600°C transform these particles to anatase. A 1000°C anneal temperature transforms titania pellets and powders to rutile, but for island-structure films this transformation was not complete as discussed in chapter six. To study these titania phases, some films were annealed to 600°C and others to 1000°C. The bare substrate (aluminum oxide film) was studied with the same three sample treatments given to the composite films in order to subtract the substrate contribution from the composite spectra.

The electron-energy loss measurements (EELS) were taken with a high resolution transmission electron-energy loss spectrometer similar to the instrument described by Gibbons et. al.[117]. The incident beam energy is 80 KeV and the energy resolution is 0.10 eV (fwhm). The momentum resolution is 0.04 $Å^{-1}$ (fwhm) with a momentum transfer range of 0. to 5.0 $Å^{-1}$. The smallest momentum transfer used in this study was 0.1 $Å^{-1}$ because surface contributions to the loss spectrum overwhelm the bulk contributions at smaller momentum transfer.

7.3 Electron Diffraction Results

The spectrometer can be run at zero energy-loss to measure the electron diffraction at different angles (different momentum-transfer values) to obtain information on the crystal phases present in the sample. Similar measurements can be made with an electron microscope. The electron diffraction results for films annealed at 600°C are shown in Fig. 7.1. The alumina film spectrum shows only broad features characteristic of the amorphous phase. The composite (titania+alumina) film spectrum has some crystalline features, there is a strong broadened peak at 1.8 Å and several barely distinguishable features at 2.6, 3.3, 3.8 and 4.2 Å. Comparing the composite spectrum with the x-ray diffraction from anatase, we conclude that the titania in the annealed film is in the anatase phase. This result is consistent with our infrared results on island-structure films discussed in the previous chapter. The

---

[116] J. H. Jean and T. A. Ring, Colloids and Surfaces **29**, 273 (1988); V. J. Nagpal, J. S. Riffle, and R. M. Davis, Colloids and Surfaces **87**, 25 (1994); V. J. Nagpal, R. M. Davis, and S. B. Desu, J. Mater. Res. **10**, 3068 (1995).

[117] P. C. Gibbons, J. J. Ritsko, and S. E. Schnatterly, Rev. Sci. Instrum. **46**, 1546 (1975).

electron diffraction spectrum of a room-temperature composite film (no annealing) is very similar to the alumina spectrum in Fig. 7.1 confirming the amorphous character of the as-prepared sol-gel titania particles.

The electron diffraction results for alumina and alumina+titania composite films annealed at 1000°C are shown in Fig. 7.2 and 7.3, respectively. Comparing the alumina electron diffraction spectrum with the transition η-alumina x-ray diffraction spectrum, a very good match of peak positions is found. The electron diffraction spectrum of the composite film (Fig. 7.3) displays additional peaks besides those corresponding to η-alumina. These additional peaks match perfectly the rutile x-ray diffraction spectrum shown in Fig. 7.3. This result is somewhat inconsistent with infrared measurements on island-structure films, annealed at 1000°C in argon which showed only anatase features (see chapter six). But those samples were made with a water concentration R = 60, whereas the films made for EELS measurements were made with R = 150. As discussed in chapter six, increasing the water concentration facilitates the anatase to rutile transformation.
The amorphous to crystalline phase transition in the alumina film was also detected in the electron-energy loss (EELS) spectrum. The bulk plasmon peak of the alumina films shifted from 22.3 (no anneal) to 24.8 eV (anneal at 1000°C). This shift is attributed to a change in atomic density due to the crystallization.[118]

7.4 Electron-Energy Loss Results

EELS spectra were taken on alumina films and on composite (alumina+titania) films. A representative experimental result is shown in Fig. 7.4 for samples annealed at 1000°C and for a momentum transfer of 0.7 Å. The predominant feature in both the alumina and composite spectra is the alumina plasmon. In the composite sample, the scattering from the alumina substrate is larger than the scattering from the titania islands because the volume fraction of alumina is much greater than the fraction of titania. Since there is no correlation, in first order, between scattering from the substrate and scattering from the titania islands, the titania spectra is obtained by subtracting the substrate (alumina) from the composite spectra. The relative weight of the two spectra was chosen to minimize the alumina plasmon peak in the subtracted spectra. Multiple scattering in the substrate and titania islands mixes the two spectra in a way which is difficult to disentangle above an energy loss of approximately 20 eV.. At energy losses below the sum of the alumina and titania bandgap (~8 eV and ~3 eV, respectively), the two spectra are not entangled and the subtracted spectrum can be confidently associated with titania. In the region between 11 eV and 20 eV, the subtracted spectra becomes increasingly questionable as the contribution from multiple scattering steadily dominates the spectrum.

Figures 7.5, 7.6 and 7.7 show the titania spectra as a function of energy loss for different momenta corresponding to samples with no anneal (amorphous titania), anneal at 600°C

[118] N. Swanson, Phys. Rev. **165**, 1067 (1968).

(anatase structure), and anneal at 1000°C (rutile structure), respectively. The solid lines are a model fit which will be explained below. The largest peak, lying between 12 eV and 15 eV in all the spectra, is the bulk titania plasmon which is predicted[3] to have an energy of 12 eV. The rough agreement between predicted and measured values of the plasma frequency is evidence that the EELS spectra of titania derived from subtracting the substrate spectrum from the composite spectrum is reasonable. The gross disagreement between measured and predicted spectra above the plasmon peak is due to multiple scattering

There are two other features, besides the bulk titania plasmon, in all three phases and at all momenta transfer and they are a peak at the absorption edge between 4 eV and 7 eV and then a roughly linear increase in intensity between this low energy peak and the plasmon peak. In order to quantify the position and strength of these two features, the low energy spectra has been fit with a parametric model consisting of a linear continuum term which turns on at the energy edge, E_c, plus a Gaussian peak centered at $E_c - E_b$. These two terms have been convoluted with a Gaussian smoothing function of width σ to represent the rounding of sharp features due to intrinsic disorder in the sample and to the effect of the finite energy resolution. The resulting model is:

$$f(e) = C\left\{\frac{e-E_c}{2}\left[erf\left(\frac{e-E_c}{s\sqrt{2}}\right)+1\right]+\frac{s}{\sqrt{2p}}\exp\left[-\left(\frac{e-E_c}{s\sqrt{2}}\right)^2\right]\right\}+b+D\exp\left[-\left(\frac{e-\left(E_c-E_b\right)}{s\sqrt{2}}\right)^2\right]$$

It has six parameters: the continuum edge, E_c, peak position relative to the edge, E_b, the strength of the continuum term, C, the strength of the peak, D, the width of the rounding function, σ, and a constant offset, b.

The parameters derived from fitting the model to the spectra in Figures 7.5-7.7 are given in table 7.1. The fit for amorphous titania (Fig. 7.5) is poor for all momenta (χ^2/N = 4 to 17) primarily because the peak does a poor job of modeling the sharp absorption edge. The fit for anatase (Fig. 7.6) is excellent for all momenta, except q = 0.1 Å where again the sharp edge is difficult to model. The fit for rutile is moderately good for all momenta (χ^2/N = 1.3 to 84) where again the poor fit occurred at q = 0.1 Å where there is a sharp absorption edge. The fit is displayed as a solid line in Figures 7.5-7.7.

Looking at the fitting parameters in Table 7.1, there is no clear trend in the position of the continuum edge, E_c, in the position of the peak relative to the edge, E_b, nor in the strength of the continuum edge relative to the absorption edge peak, D/C. The absolute position of the edge peak, E_c-E_b, is nearly the same for all three phases and is roughly independent of momenta. The width of the smoothing function also does not vary appreciably and there is no clear trend

The absorption edge for all three materials was quite sharp at q = 0.1 Å and was modeled poorly by our smoothed model. If this sharp edge in the q = 0.1 Å spectrum is compared directly in the spectra of the three phases of titania, the gap for anatase and amorphous phases are 0.4±0.2 eV wider than the gap for rutile. These results are in agreement with optical measurements (q=0 $Å^{-1}$) of Tang et.al.[119] who found that the optical gap of anatase was 0.2 eV wider than the rutile gap. The optical gap for amorphous titania has not been reported previously and these measurements indicate that it is the same as the anatase gap.

[119] H. Tang, H. Berger, P. H. Schmid and F. Levy, Sol. State Commun. **92**, 267 (1994).

Table 7.1. Fitting parameters of the low energy side of the electron-energy loss spectra of titania islands, under three annealing conditions: no-anneal (amorphous), anneal at 600°C (anatase) and anneal at 1000°C (rutile). N is the number of points used in the fitting procedure.

Amorphous TiO_2									
q	**C**	**E_c**	**σ**	**b**	**D**	**E_b**	**χ^2/N**	**E_c-E_b**	**D/C**
.1	128.5	.2	.85	-205	426	-5.1	17.3	5.3	3.3
.3	113.5	4.9	.97	46.2	345	-.73	4.21	5.7	3.1
.5	229.5	6.2	.97	3.7	501	.31	9.5	5.9	2.2
1.0	27.34	3.9	.95	46.7	57.9	-1.3	6.6	5.2	2.1
Anatase TiO_2									
q	**C**	**E_c**	**σ**	**b**	**D**	**E_b**	**χ^2/N**	**E_c-E_b**	**D/C**
.1	171.2	4.4	.76	511	556	-.9	1.8	5.3	3.2
.3	42.2	7.0	1.04	64	82	.97	1.	6.1	1.9
.5.	18.4	6.6	.95	58	40	.65	1	5.9	2.2
.7	23.4	6.6	1.34	111	48	.73	.9	5.9	2.1
.9	16.6	3.7	.79	296	50	-2	.7	5.7	3.0
Rutile TiO_2									
q	**C**	**E_c**	**σ**	**b**	**D**	**E_b**	**χ^2/N**	**E_c-E_b**	**D/C**
.1	7876	6.3	1.1	-1600	18600	1.1	84	5.2	2.4
.3	203	7.2	1.2	23	352	1.25	1.3	5.9	1.7
.5	54.4	6.9	1.2	44	96.8	.92	1.8	6.0	2.2
.7	41.3	3.0	1	57	104.6	.16	1.7	5.9	2.5
.9	35.8	4.1	.9	63	88.6	-1.54	3.0	5.6	2.5

The energy loss intensities have been displayed on an arbitrary scale in Figures 7.5 through 7.7. The proportionality constant between the measured energy loss intensity and Im(-1/ε) can be determined in the limit of small momentum transfer using the Kramers-Kronig relation

$$\mathrm{Re}\left(1-\frac{1}{e(E_0)}\right)=\frac{2}{p}P\int_0^\infty \mathrm{Im}\left(-\frac{1}{e(E)}\right)\frac{E}{E^2-E_0^{\,2}}\,dE$$

where Im(-1/ε) is proportional to q^2 times the measured intensity. For E less than the energy gap, Re(1/ε)=1/Re(ε) since Im(ε)=0. Furthermore, Re(ε)=n^2 where n is the index of refraction and is 2.71 for rutile and 2.53 for anatase.[120] The K-K integral is strongly weighted by

[120] *Handbook of Chemistry and Physics*, 68th ed. (CRC Press, Boca Raton, 1987-88), p. B-193.

contributions in the energy range $E \sim E^0$ where multiple scattering is negligible. At high energy, the integrand is in error because of the multiple scattering, but the contribution of this error to the total integral is small because of the 1/E weighting factor. Therefore, the scaling of the measured intensity is quite good and the derived loss function $Im(-1/\varepsilon)$ is accurate below 12 eV. The scaled data for rutile and anatase ($q = 0.1$ Å) is shown in Fig. 7.8. The solid lines are theoretical calculations from Mo and Ching[3] which will be discussed below.

7.5 Discussion of the Low-Energy Electron-Energy Loss Spectra

Mo and Ching[115] have calculated the optical properties ($q = 0$ Å) of rutile, anatase, and brookite using the local density approximation (LDA). This approximation typically underestimates the band gap of insulators by approximately 50%, but generally does a good job of predicting optical spectra above the band gap. Consistent with this generalization, Mo and Ching calculate optical gaps of 1.78 eV and 2.20 eV for rutile (direct gap) and anatase (indirect gap), respectively. The measured optical gaps for these two materials are 3.0 eV and 3.2 eV from both optical measurements[119] and the $q = 0.1$ Å energy loss measurements shown in Fig. 7.8. The agreement is consistent with the typical band gap discrepancies associated with LDA calculations.

A more serious discrepancy between theory and experiment is in the predicted intensity of the loss function between the absorption edge and the bulk plasmon at ~12 eV. A double peak structure is predicted in this energy range with a maximum intensity of order $Im(-1/\varepsilon) \sim 0.2$, whereas the experimental measurement finds a single peak in this energy region which is factors of three to four times larger than the predicted intensity. It is very unlikely that our scaling of the data is off by such a large factor, but even if it were, there is still a factor of three to four discrepancy between the predicted relative intensity of the plasmon peak to low energy peak versus the observed intensity ratio. The same discrepancy exists for rutile and anatase.

The discrepancy in intensity between theory and experiment in the energy region between the optical gap and the bulk plasmon may be due to (1) errors introduced in subtracting the substrate spectrum from the composite spectrum, (2) differences between the angularly averaged loss function of a polycrystalline sample and the loss function of a single crystal calculated for a particular high symmetry direction, (3) differences between the optical properties of islands versus the optical properties of bulk solids, (4) shortcomings of the LDA calculation, (5) excitonic contributions to the loss function. It is possible that option (1) and (2) might give factor of two errors, but not factors of four or five. It is expected that the optical properties of small particles will be different from bulk optical properties when the wavelength of the excitation is less than or comparable to the size of the particle. For these measurements, the effective wavelength is $\lambda = 2\pi/q = 60$ Å which is much smaller than the size of the particles and, therefore, it is expected that we are measuring bulk optical properties. Thus, the most likely explanation of the discrepancy is option (4) or (5) The

problem of distinguishing between band structure effects and excitonic absorption near a band edge is an old one and has not been resolved.

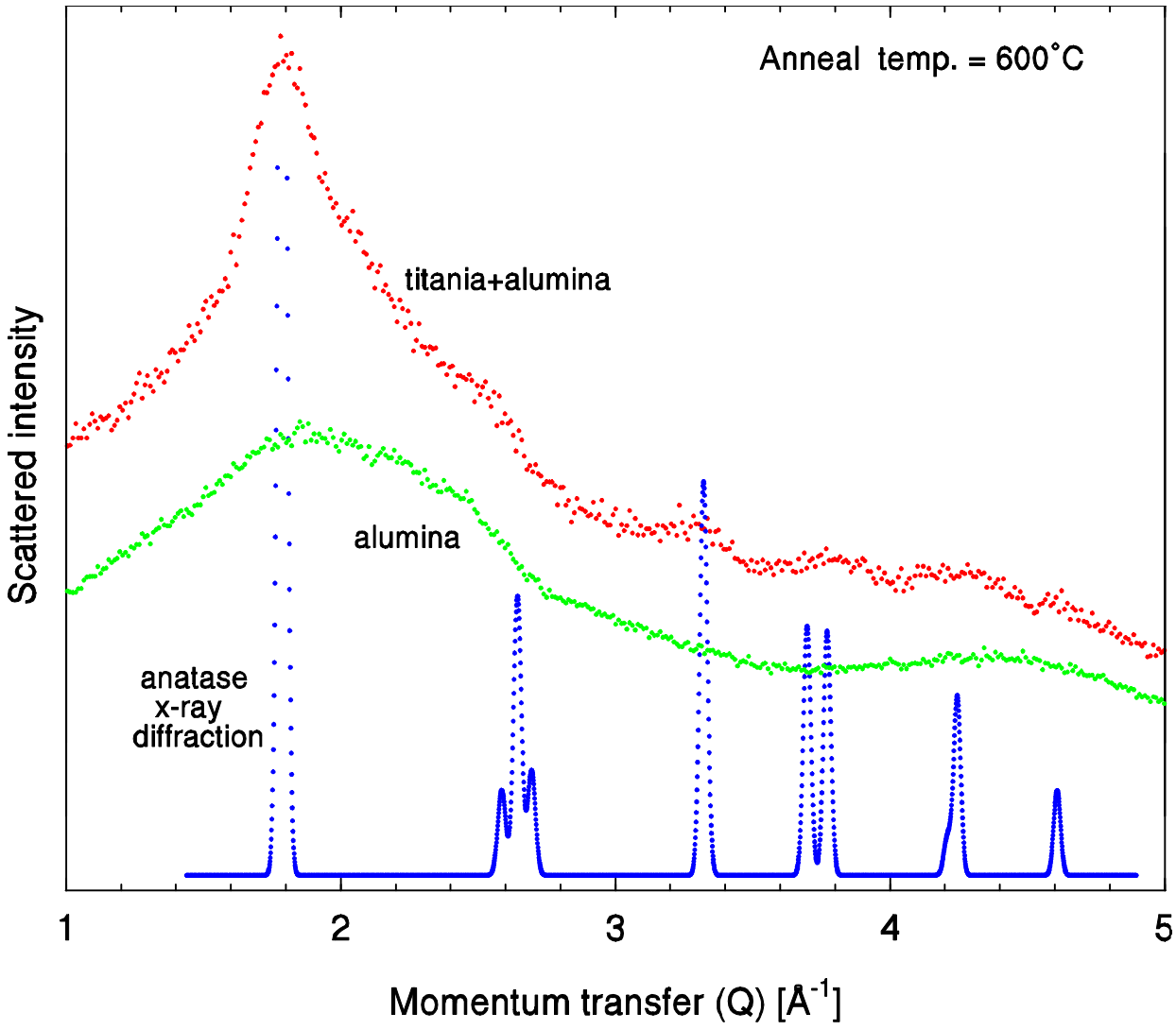

Figure 7.1. Electron diffraction spectra of a composite (alumina+titania) and an alumina films annealed at 600°C. It is also shown the x-ray diffraction spectrum corresponding to anatase TiO_2.

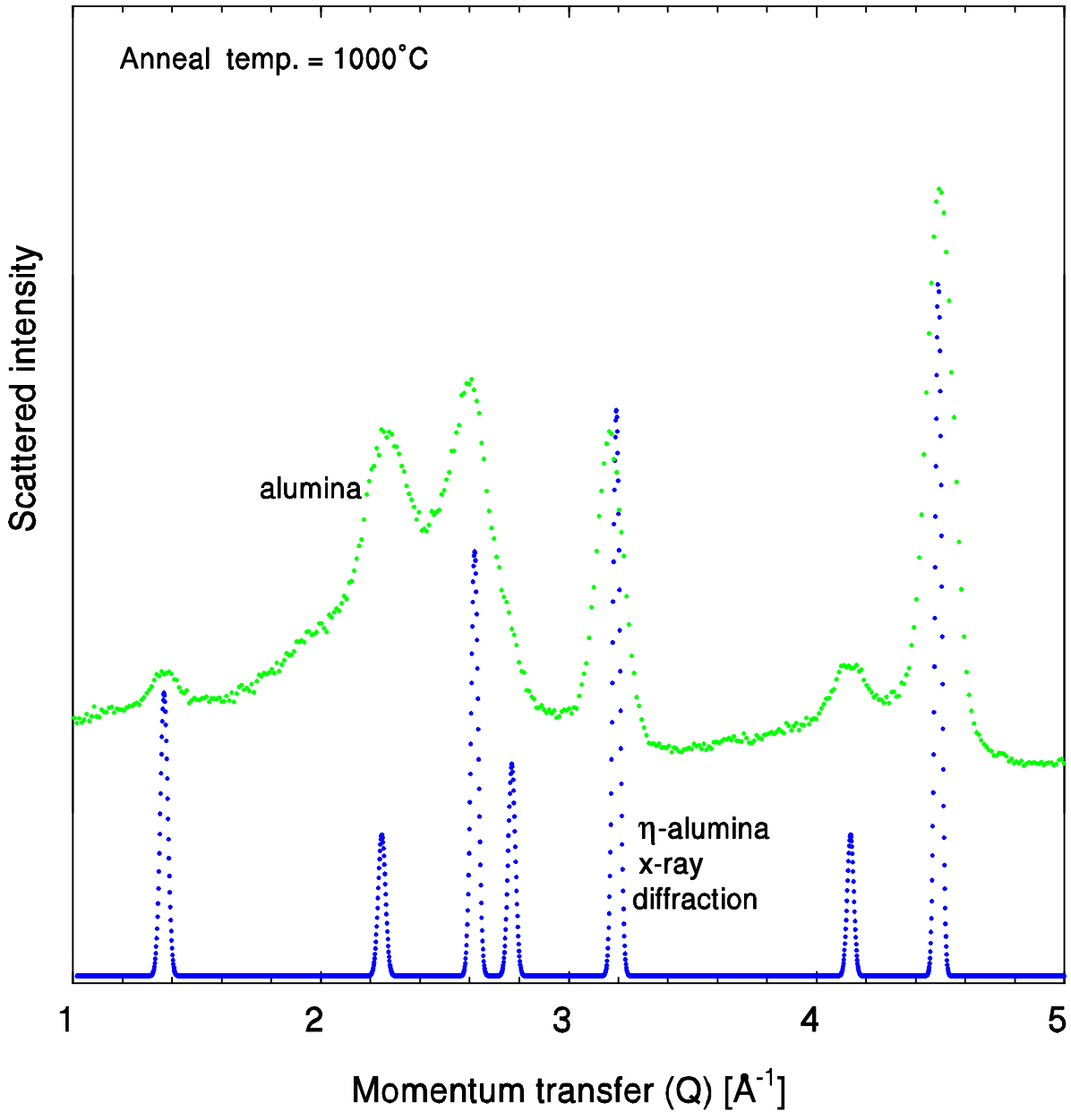

Figure 7.2. Electron diffraction spectra of an alumina film annealed at 1000°C. It is also shown the x-ray diffraction spectrum corresponding to η-alumina.

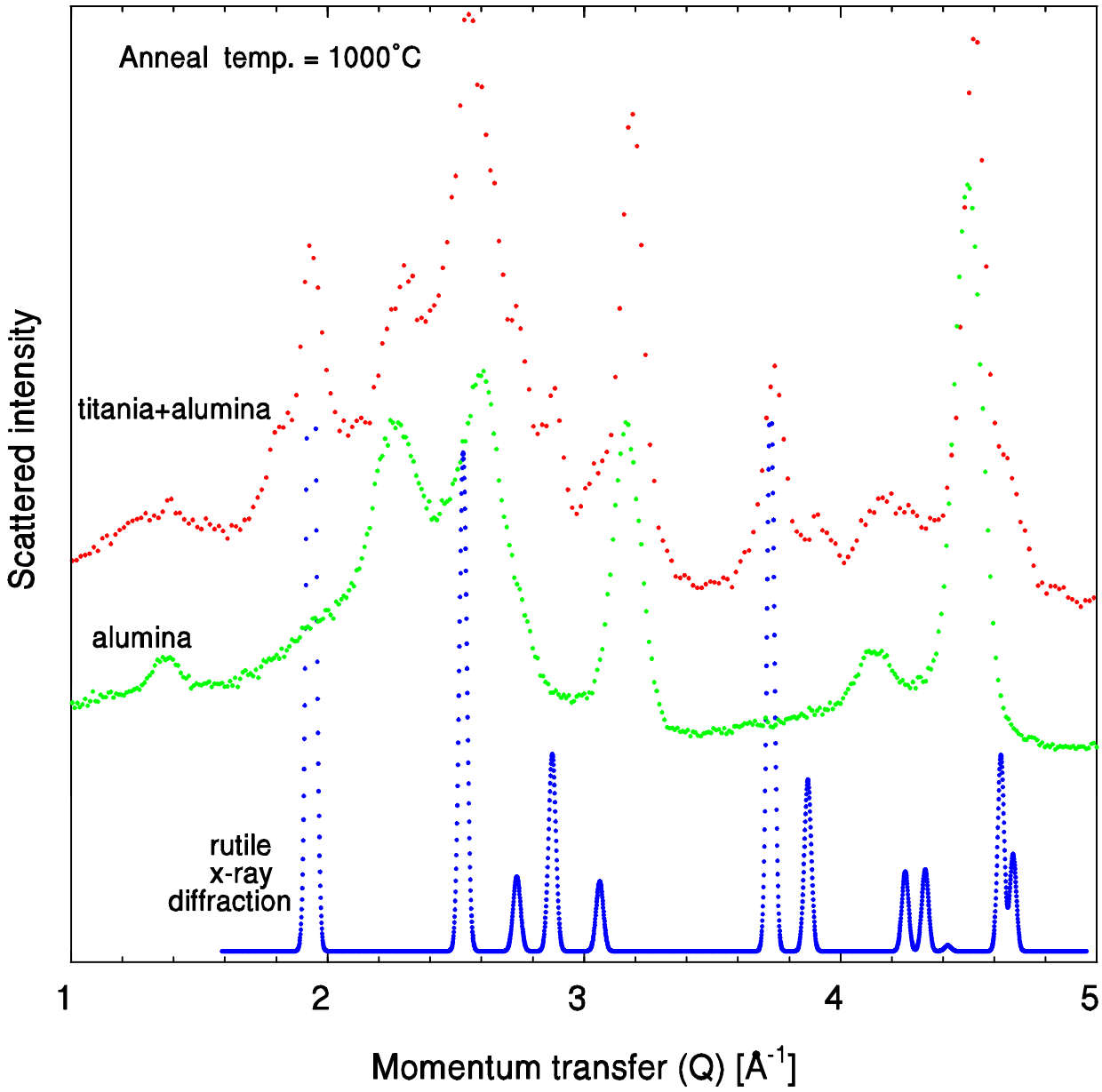

Figure 7.3. Electron diffraction spectra of a composite (alumina+titania) and an alumina films annealed at 1000°C. It is also shown the x-ray diffraction spectrum corresponding to rutile TiO_2.

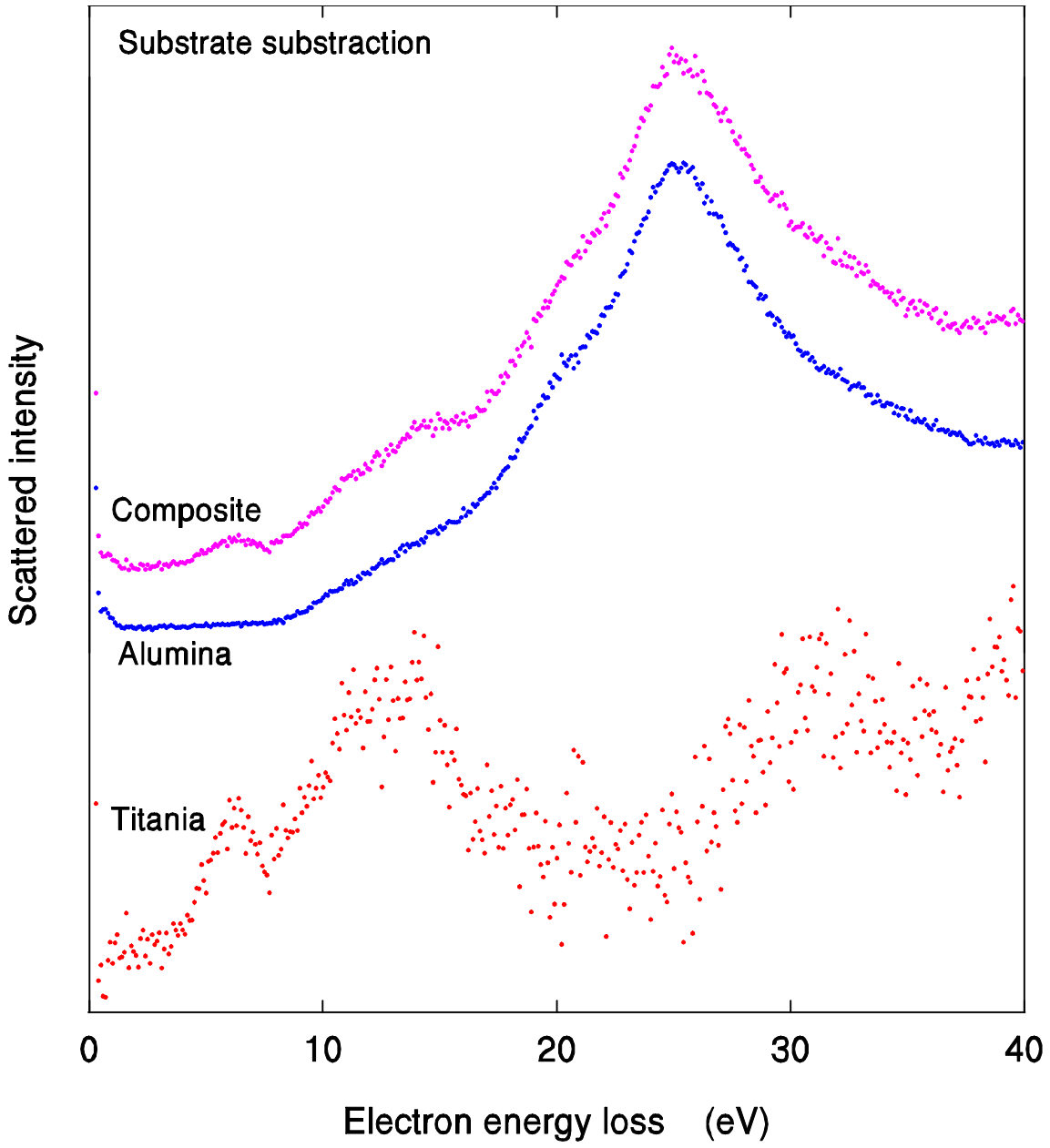

Figure 7.4. Electron-energy loss spectra of a composite and alumina films annealed at 1000°C, with momentum transfer q = 0.7 $Å^{-1}$. The resulting spectrum after the subtraction of the alumina data from the composite spectrum is also shown. This subtracted results corresponds to the EELS spectrum of the island-structure film of rutile TiO_2.

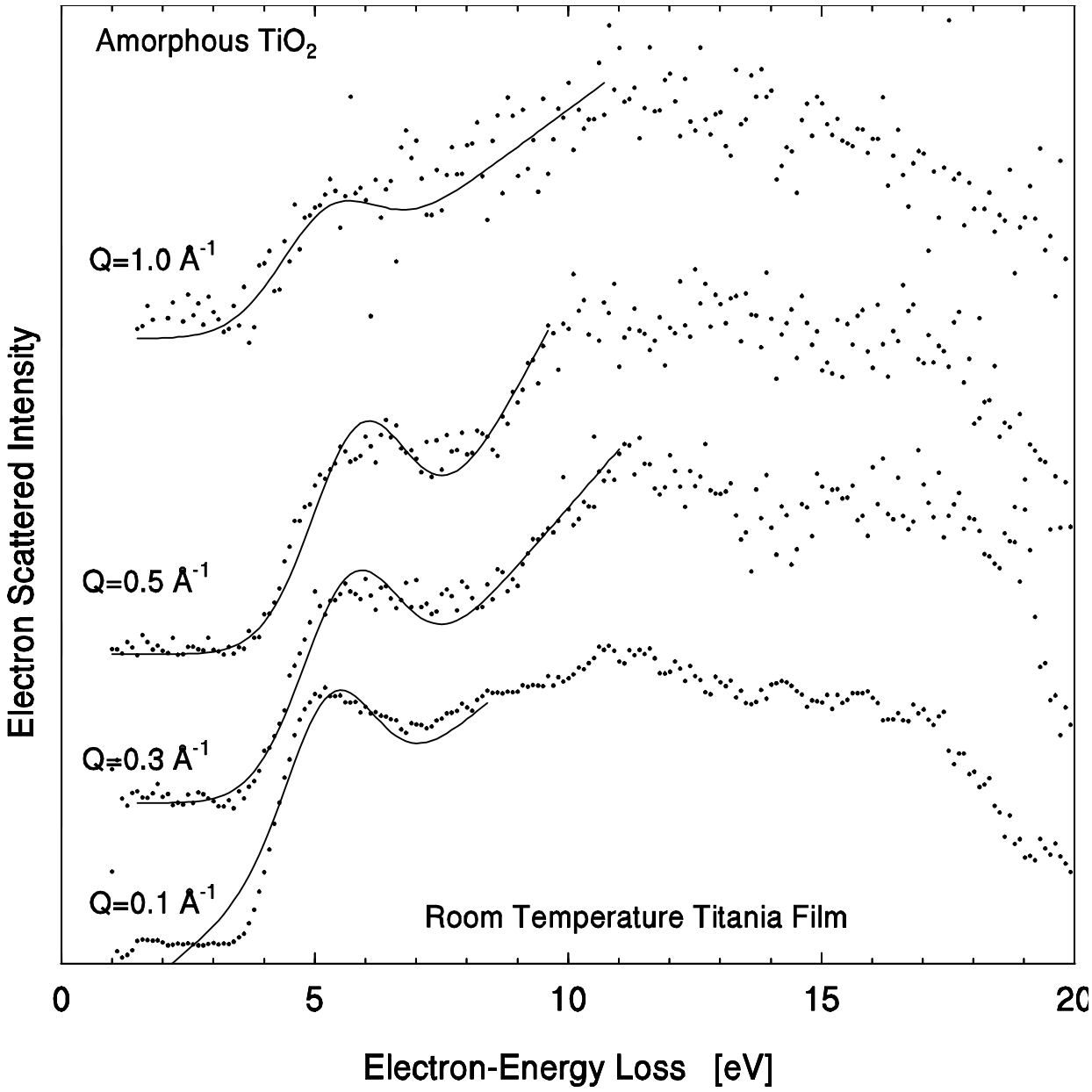

Figure 7.5. EELS spectra of amorphous TiO_2 as a function of momentum transfer. Along with the experimental results, the fitting of the low energy side is also shown.

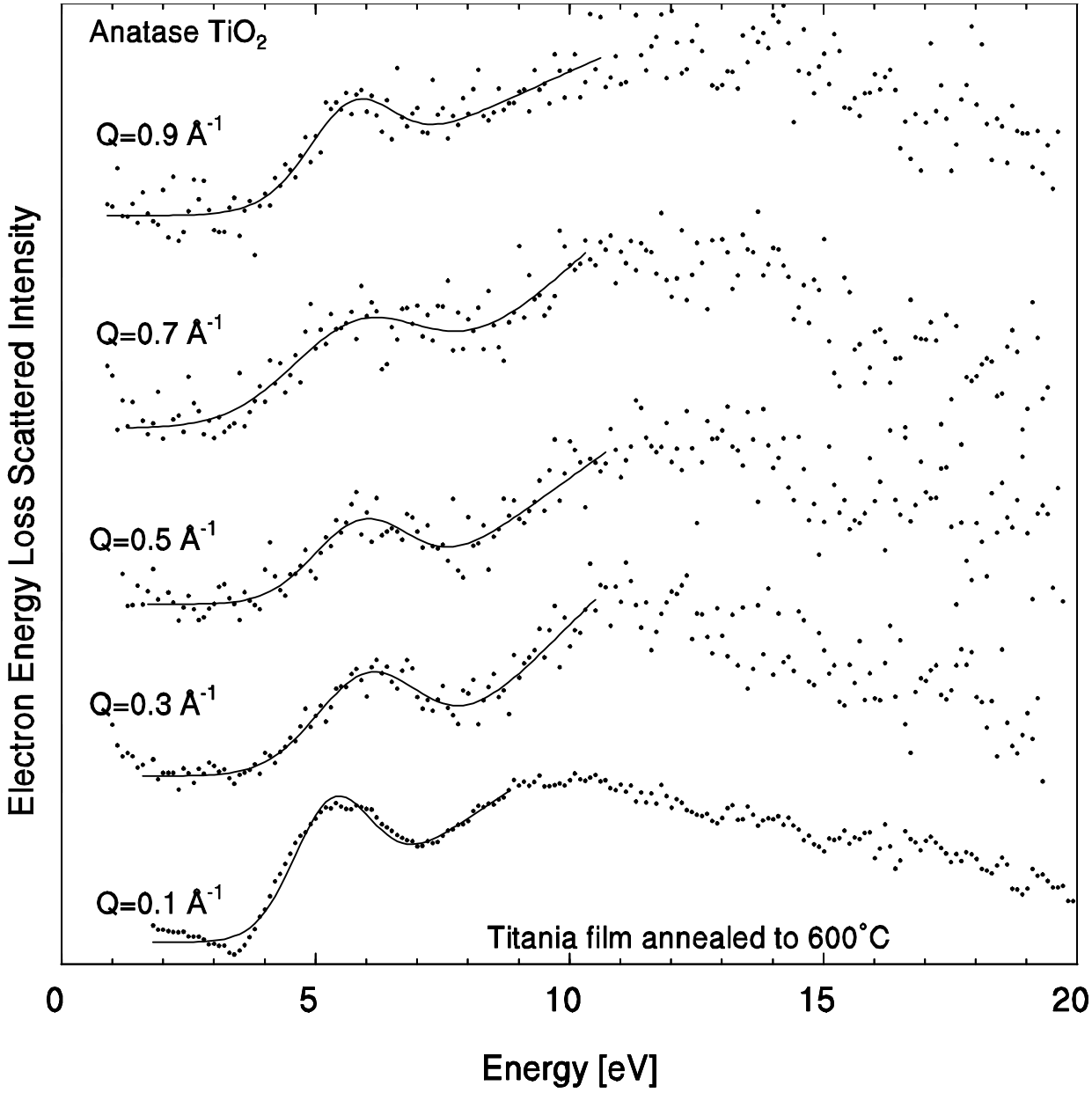

Figure 7.6. EELS spectra of anatase TiO_2 (samples annealed at 600°C) as a function of momentum transfer. Along with the experimental results, the fitting of the low energy side is also shown.

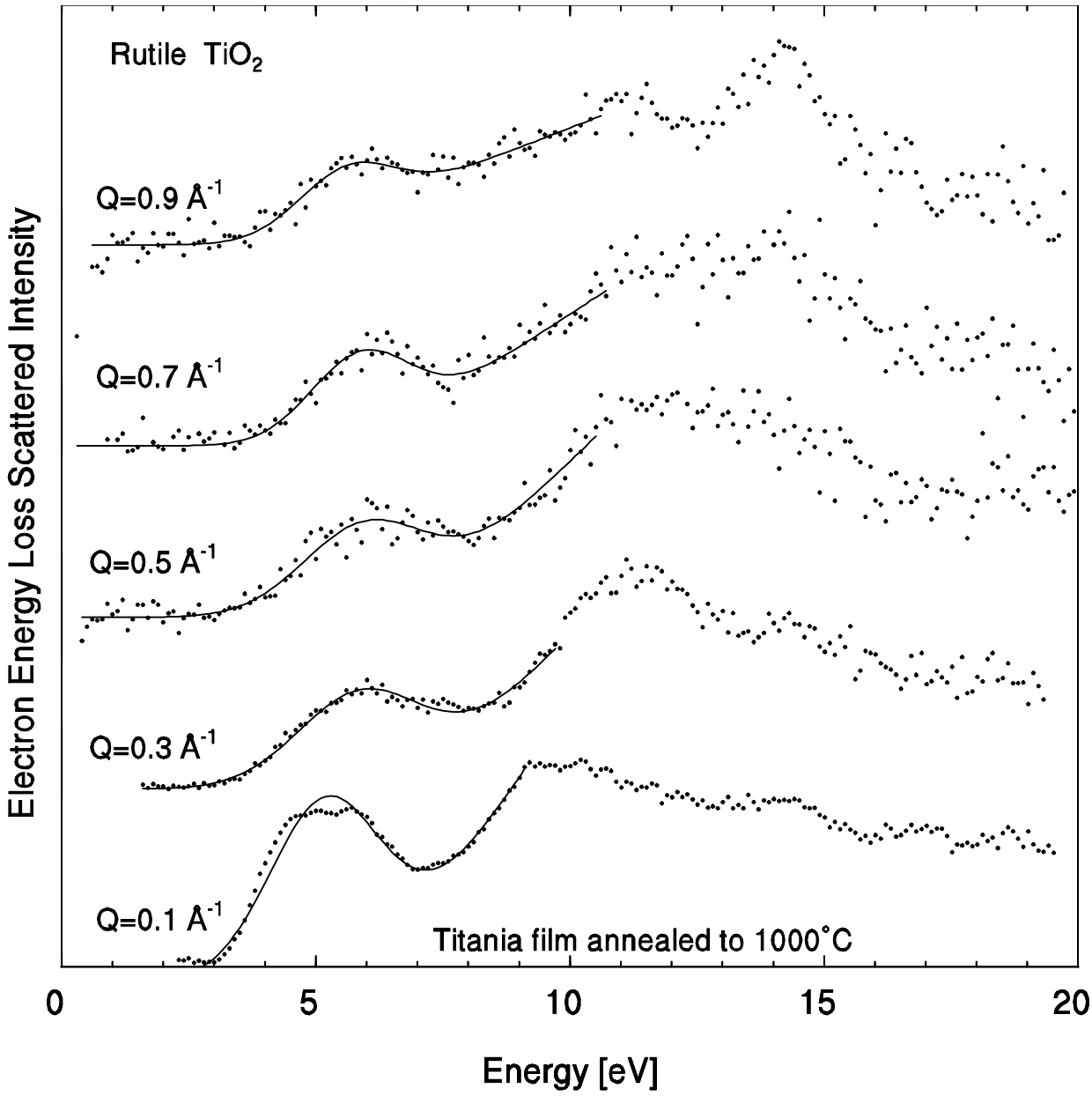

Figure 7.7. EELS spectra of rutile TiO_2 (samples annealed at 1000°C) as a function of momentum transfer. Along with the experimental results, the fitting of the low energy side is also shown.

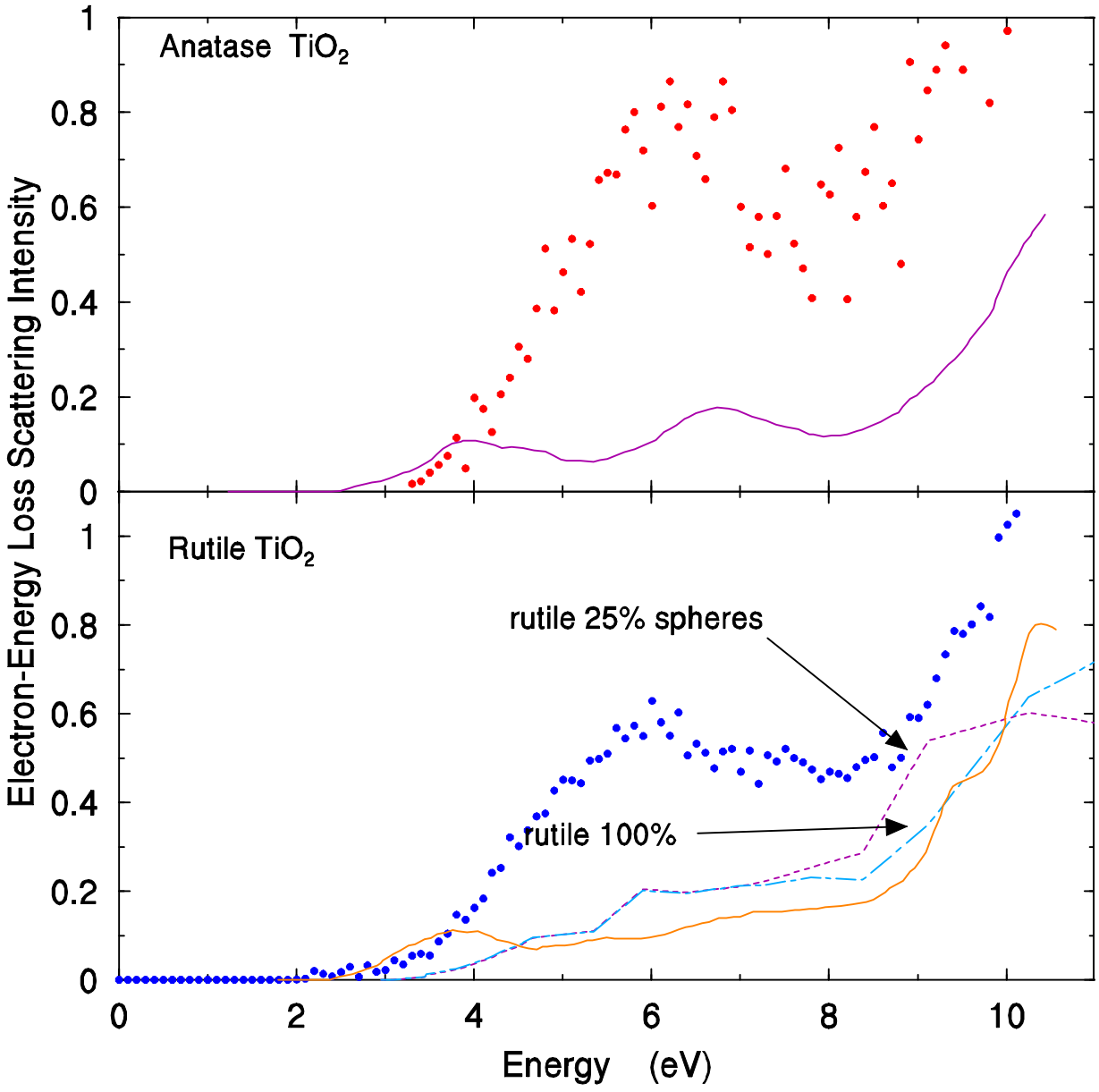

Figure 7.8. Low energy EELS spectra of anatase and rutile TiO_2 taken with momentum transfer q = 0.1. Theoretical calculations of Im(-1/ε) (EELS at q=0) are also shown (solid lines). Optical measurement results from a (100%) rutile sample, and a calculation assuming 25% rutile spheres are also included

CHAPTER EIGHT

8. SUMMARY AND FUTURE DIRECTIONS

Sol-gel titania synthesis and annealing was investigated, primarily using optical techniques, by systematically varying synthesis, sample handling, and annealing variables. The particle synthesis procedure has two main process variables. One relates to the polymer: whether it is absent or present, and, if present, whether it is introduced by the standard method or by the premix method. The other relates to the water concentration used (R), the larger is R, the smaller the particle size. The type of sample prepared from the particles is another process variable related to particle aggregation: whether they are studied in the form of a loose powder, an island-structure film made by spin coating, or a dense pellet made by compression. The final process variables are those which characterize the final thermal treatment: anneal temperature (which varied from room temperature to 1000°C) and anneal atmosphere (air or argon, i.e. an oxygen-containing atmosphere and an inert atmosphere).

In chapter three, I reported effects of most of these variables on the phase transition from anatase to rutile. The particles were characterized using electron microscopy, and the crystal phase concentrations were studied by comparing relative intensities of anatase and rutile Raman peaks. As a byproduct of this work, the Raman intensities were calibrated to yield relative phase concentrations of anatase and rutile. Chapter four presents a more important byproduct of this research. The polarization-dependent far-infrared reflectivity measurements on single crystals of anatase yielded the TO and LO frequencies of the anatase infrared-active phonons. These results for the anatase dielectric functions provided information that was essential for the interpretation of the infrared spectra of pressed pellets (chapter four) and island-structure thin films (chapter six). Because of the polycrystallinity of the titania particles, the surface roughness of the pressed pellets, and the island-structure character of the anatase thin films, effective medium theories were used (along with the single-crystal dielectric functions) to interpret the experimental results. In chapter six, the amorphous to anatase phase-transition studies were reported. Studies were carried out on KBr pellets containing 0.5% (wt/wt) of titania particles which were annealed inside the infrared spectrometer. These in-situ transmission measurements showed the dependence of this transformation on particle size. Infrared transmission and reflection at oblique incidence on anatase continuous films yielded results consistent with the single crystals normal-incidence reflectivity work. Raman and x-ray measurements on titania particles annealed at temperatures ranging from 300 to 800°C are reported in chapter five. The annealing was done in two atmospheres: air (oxygen-containing) and argon (no oxygen). The annealing-induced evolution of the anatase Raman band shape (peak position and linewidth) was interpreted as a stoichiometry effect rather than as a finite size effect of small crystallite size. Chapter seven presented electron energy-loss (EELS) experimental results on annealed titania particles. Electron diffraction was successful in tracking the transformation from amorphous to anatase and rutile. A weighted subtraction technique was used to eliminate the substrate features from EELS spectra. The results provided reliable EELS spectra for the titania particles, for the energies up to 20 eV. The momentum dependence of the EELS spectra

showed that the edge peak position is nearly the same for all phases and is roughly independent of electron momentum.

This study provided some answers for the effect of these process, sample handling, and annealing variables. Some answers were incomplete, needing further study, and new questions were opened. The "premix" method of particle synthesis provided the lowest transformation temperature from anatase to rutile. The only premix samples available were loose powders. It would be interesting to prepare pellets and island-structure films with a wide range of water concentrations to study the effect of particle aggregation and particle size, at a lower temperature range, on the phase transformation temperature. More clues would appear that would help to define the mechanism governing the phase transformation. In our study of finite size versus stoichiometry effects of the Raman spectra of anatase, several options are available to clarify these effects. Some of the argon-annealed powders should be annealed in air, to the same temperatures, to see if the oxygen absorption changes the Raman peak shape and crystallite size. Raman measurements should be carried out on samples annealed to 150, 200, 250°C looking for larger Raman peak shifting and linewidth. In-situ IR absorption measurements, carried out during annealing, determined that from 150°C to 200°C, the anatase phase starts to appear. We suspect that in this anneal region there are very small crystallites, perhaps with sizes as small as those measured in semiconductors and in aluminum hydroxide. Annealing in air and argon will be necessary to discriminate from possible stoichiometry effects. On the other side of the temperature range, dedicated furnaces to carry out in-situ Raman measurement during annealing up to 1000°C are commercially available. The annealing atmosphere can also be controlled. Performing these in-situ Raman measurements on the titania particles would bring more clues to understand the rather fast transformation temperature from anatase to rutile, especially the different factors influencing this transformation temperature. This study, especially in the 700 to 1000°C range, (in this temperature range the rutile phase is present) would help us elucidate the suspected role that the phonon dispersion (available for rutile), the sign and size of the $\nu(k)$ curve near $k=0$, plays in the sensitivity to stoichiometry of a Raman band. There was a small discrepancy in peak position in the oblique incidence experiments on continuous films compared to the peak position predicted from the dielectric function determined from the measurements on anatase single crystals. Running measurements on a set of continuous films with different thicknesses will help define the source of this discrepancy. To clarify our EELS measurements on titania particles, continuous, self supporting thin films of anatase and rutile should be measured. Such self-supporting films would not have any substrate to complicate the experiments, and the signal will be stronger because of the higher density of the film. Techniques such as electron beam evaporation, sputtering, and laser ablation, among others, generate continuous films, and it would be worth trying to see if self-supporting thin films (less than 1000 Å) are possible.

Appendix A Bomem Data Acquisition and Analysis

VG.LIB VGGRAPH (VOLKSGRAPHER) LIBRARY

Most of the programs describe in these appendices make use of the fortran library vgraph.lib to display XY graphs on the screen. This is a public domain software, developed at NIST. It has many features, like zooming, displaying up to 6 curves, saving data from the graph on a (x,y) array that can be used later on in the program. A manual is available in the lab.

DATAM.LIB (DATA HANDLING LIBRARY)

Some programs make use of the fortran library DATAM.LIB. This program has the following subroutines:
INFILE ask for a filename, opens this file for input as unit = 7.
SAVEFILE opens a file for output with unit = 8.
READIN(NPOINTS, X, Y) opens a (x, y)-file and reads in data from x and y arrays.
SAVE(X,Y,NPOINTS) opens a file and saves the x and y arrays as a pair (x, y).
PLOT2(NT1,X1,Y1,NT2,X2,Y2,'LEGEND1','LEGEND2', RIGHTAXIS) displays on the screen two files (x1,y1) and (x2, y2). If rightaxis is .TRUE. the two files will have independent y-scales.
PLOT1(NT, X, Y, "LEGEND") plots a single file.

The program PATCH.BAT is a batch file. It will open, with EDIT, a file called patch.fil. When you are in edit mode, type in first the low energy file and on the second line the high energy file. After closing this file (quitting edit), the batch file calls the file PATCH22.EXE which will perform the patching.

The program AVERAGE1.FOR reduces the number of points of a file, by averaging n (given) consecutive points, and substituting these n points by the average value. First the program asks you to divide the spectrum into regions that will have different number of points to be averaged. To perform this task, the program uses the (s-w-*) sequence. This is the procedure stated by vgraphs to save data from the graph, refer to the manual for details. When you are done with the divisions, the program will ask for the number of points to average in each region.

PATCH.BAT
```
edit patch.fil
c:\rey\ir\patch22
rem **** done ****
```

```
      PROGRAM patch22
c***
c***  declaration of variables
      parameter(ndim=8000,maxcurves=2)
      real x(maxcurves,ndim),y(maxcurves,ndim),w(2*ndim),t(2*ndim)
      real savex(20),savey(20),factor,w1(ndim),t1(ndim)
      integer ncurves,nmax(maxcurves),j,np
      CHARACTER FILNAM*60(2),legend(maxcurves)*30
      character ident*60, answer*1,  return*1
      LOGICAL FILEOk
      dimension card(10)
      common/cdata/savex,savey,ijk
      return = char(013)
c***
c***  Open data files
      write(*,*)' Patching and cutting program'
      write(*,*)
      write(*,*)' To save a point: Use (s) to see the cursor'
      write(*,*)' (w) to see its coordinates and (*) to save them'
      write(*,*)
      write(*,7)ndim,maxcurves
 7    format(' max_number of points per file is '
     &,i5,/,' max_number of files is',i2,/)
      write(*,8)
 8    format(' Enter first low energy file ')
      ncurves = 2
 9    format(i3)
      open(5,file='patch.fil',status='old')
      do i = 1,ncurves
           read(5,'(a12)')filnam(i)
           print*,' file ',i,' = ',filnam(i)
      end do
      close(5)
      do j = 1, ncurves
   50 CONTINUE
  100 FORMAT(A)
      INQUIRE(FILE=FILNAM(j),EXIST=FILEOK)
      IF(FILEOK)THEN
           OPEN(j,FILE=FILNAM(j),STATUS='OLD')
      ELSE
        PRINT *,'File does not exist -- try again.'
        GOTO 50
      ENDIF
```

```
C ***
C *** Read in data.
c ***
      call datain(j,w,t,ndim,np,card,2,1,2,ident)
c       print*, 'np = ',np
      do k = 1, np
           x(j,k) = w(k)
           y(j,k) = t(k)
c          print*,w(k),t(k)
           w(k) = 0.
           t(k) = 0.
      end do
      CLOSE(j)
      nmax(j) = np
      legend(j) = filnam(j)
      end do
      pause
C ***
c --  FIRST LOOK AT FILES
c ***
 400  continue
      call commen(' First look at your files - Hit [ENTER] to continue
     &')
        call legpos(0.67,0.88)
        call plac(0.95,0.05,0.05,.95)
      do j = 1, ncurves
           i1 = j + 1
           call howplt(0,1,i1)
           call rtemy(ndim,maxcurves,nmax(j),x,y,w,t,j)
        call legnd(legend(j))
        call curv(nmax(j),w,t)
      end do
           call nolbox
           call vg
        if (loopin() .eq.1)go to 400
        call newpag
c
c --  DISPLACING FILES UP OR DOWN
c
      answer = 'y'
      write(*,'(a\)')' Do you want to displace any file up or down?
     &(y/n) -> '
      read(*,'(a1)')answer
```

```
    do while (answer .eq. 'y' .or. answer .eq. return)
       ijk = 0
401  continue
    call commen('Choose 2 POINTS away from the intersection')
      call legpos(0.67,0.88)
      call plac(0.95,0.05,0.05,.95)
    do j = 1, ncurves
         i1 = j + 1
         call howplt(0,1,i1)
         call rtemy(ndim,maxcurves,nmax(j),x,y,w,t,j)
      call legnd(legend(j))
      call curv(nmax(j),w,t)
    end do
         call nolbox
         call vg
      if (loopin() .eq.1)go to 401
        call newpag
        if (ijk .gt. 0) then
           factor = savey(2)/savey(1)
           if (savex(1) .le. x(1,nmax(1))) then
              do i =1, nmax(1)
                 y(1,i) = y(1,i)*factor
              end do
           else
              do i =1, nmax(2)
                 y(2,i) = y(2,i)*factor
              end do
           end if
        end if
402  continue
      print*,' Factor -> ',factor
      call commen(' ')
      call legpos(0.67,0.88)
      call plac(0.95,0.05,0.05,.95)
    do j = 1, ncurves
      i1 = j + 1
         call howplt(0,1,i1)
         call rtemy(ndim,maxcurves,nmax(j),x,y,w,t,j)
      call legnd(legend(j))
      call curv(nmax(j),w,t)
    end do
         call nolbox
         call vg
```

```
       if (loopin() .eq.1)go to 402
         call newpag
         write(*,'(a\)')' More displacement? (y/n) -> '
         read(*,'(a1)')answer
      end do
c
c --  PATCHING FILES
C
      answer = 'y'
      do while (answer .eq. 'y')
         ijk = 0
 403  continue
      call commen('PATCHING -- Choose 2 POINTS at intersection')
       call legpos(0.67,0.88)
       call plac(0.95,0.05,0.05,.95)
      do j = 1, ncurves
          i1 = j + 1
          call howplt(0,1,i1)
          call rtemy(ndim,maxcurves,nmax(j),x,y,w,t,j)
       call legnd(legend(j))
       call curv(nmax(j),w,t)
      end do
          call nolbox
          call vg
       if (loopin() .eq.1)go to 403
         call newpag
         if (ijk .gt. 0) then
            factor = savey(2)/savey(1)
            i = 1
            do while (x(1,i) .le. savex(1))
               i = i + 1
            end do
            i1 = i - 1
            i = 1
            do while (x(2,i) .le. savex(1))
               i = i + 1
            end do
            i2 = i - 1
c            print*,factor,i1,i2
c            pause
            if (abs(savey(1)-y(1,i1)) .lt. abs(savey(1)-y(2,i2))) then
               do i =1, i1
                  w(i) = x(1,i)
```

```
                t(i) = y(1,i)*factor
              end do
              i = 1
              do j = i2,nmax(2)
                w(i1+i) = x(2,j)
                t(i1+i) = y(2,j)
                i = i+1
              end do
            else
              do i = 1, i1
                w(i) = x(1,i)
                t(i) = y(1,i)
              end do
              i =1
              do j = i2,nmax(2)
                w(i1+i) = x(2,j)
                t(i1+i) = y(2,j)*factor
                i = i+1
              end do
            end if
            nlmax = i1+i-1
c             print*,nlmax
c             pause
          end if
          call commen(' ')
 404  continue
        call plac(0.95,0.05,0.05,.95)
        call legpos(0.67,0.88)
      do j = 1, ncurves
          i1 = j + 1
          call howplt(0,1,i1)
        call rtemy(ndim,maxcurves,nmax(j),x,y,w1,t1,j)
        call legnd(legend(j))
        call curv(nmax(j),w1,t1)
      end do
        call howplt(0,1,5)
          call curv(nlmax,w,t)
        call nolbox
          call vg
        if (loopin() .eq.1)go to 404
          call newpag
          write(*,'(a\)')' Re-do patching? (y/n) -> '
          read(*,'(a1)')answer
```

```
      end do
c
c --  SAVING PATCHED DATA
C
      write(*,121)
 121  format(' Do you want to save on a file (y/n) ? -> ',\)
      read(*,122)answer
 122  format(A1)
      if (answer .eq. 'y' .or. answer .eq. 'Y') then
           write(*,119)
 119  format(' Output filename? -> ',\)
          read(*,100)filnam(1)
          open(5,file = filnam(1), status = 'unknown')
          do i = 1, nlmax
            write(5,120)w(i),t(i)
          end do
      end if
 120  format(e13.6,1x,e13.6)
      close(5)
      stop
      end
c &&&&&&&&&&&&&&&&&&&&&&&&&&&&&&&&&&
      subroutine vgcurs(x,y)
      real savex(20),savey(20)
      common/cdata/savex,savey,ijk
      ijk = ijk+1
      if (ijk.le.20) then
          savex(ijk) = x
          savey(ijk) = y
      end if
      return
      end
c     &&&&&&&&&&&&&&&&&&&&&&&&&&&&&&&&&&
          subroutine rtemy(ndim,maxcurves,max_frec,x,y,w,t,j)
          real x(maxcurves,ndim),y(maxcurves,ndim),w(ndim),t(ndim)
          integer max_frec
          do i = 1,max_frec
             w(i)=x(j,i)
             t(i) = y(j,i)
c            print*,w(i),t(i)
          end do
          return
          end
```

```
c
c
c*
     SUBROUTINE DATAIN (IDEV,X,Y,NDIM,N,CARD,
    1  ICOL,ICX,ICY,IDENT)
C-----------------------------------------------------------------------
C  This subroutine reads data arrays x and y from a data set containing
C  data columns in free - format.  Description of parameter list:
C
C     IDEV     -     Logical unit no. for input device.
C
C     X        -     Array to contain X-data.
C
C     Y        -     Array to contain Y-data.
C
C     NDIM     -     Dimension of arrays X and Y.
C
C     N        -     Number of data pairs to be computed
C                    by this subroutine.  Reading will
C                    stop if N .EQ. NDIM.
C
C     CARD     -     Auxiliary storage REAL array.  CARD
C                    must be dimensioned at least as large
C                    as the largest column to be read.
C
C     ICOL     -     Column no. of last column to be read.
C                    (i.e. maximum of ICX and ICY).
C
C     ICX      -     No. of column from which X-data is read.
C
C     ICY      -     No. of column from which Y-data is read.
C
C     IDENT    -     BYTE array to contain line to be read.
C
C  NDIM,ICOL,ICX,ICY must be assigned values before DATIN is called.
C  All other parameters are computed by DATIN.
C
C     DATIN stores the first (non-blank) card in IDENT.  If this
C  card does not contain a sentinel in cols. 1 and 2 it then continues
C  to read the first two columns of each succeeding card until it finds
C  one with a '/*'.  This card serves as a sentinel for the numeric data,
C  which is assumed to follow immediately.
C     If end-of-file is reached without finding a '/*' in cols. 1 and 2
```

```
C  then DATIN rewinds to the beginning of the file and starts to read
C  each line as numeric data, counting the lines (points) and skipping
C  those lines which are unintelligible.
C     The numeric data must be written in columns, separated by at
C  least one space/comma.  Otherwise the data format is free.  DATIN
C  continues to read data until either end-of-file is set or the
C  number of data pairs read becomes equal to NDIM.
C
C
C        The file to be read must be opened as Unit #IDEV
C        in calling program.
C
C-----------------------------------------------------------------------
      DIMENSION X (NDIM), Y (NDIM)
      DIMENSION CARD (ICOL)
      CHARACTER*(*) IDENT
      CHARACTER*2 JUNK
C
      BEL = CHAR (7)
C   First look for a '/*' in cols. 1&2; if none present, then reset
C   to the top.
10    READ (IDEV,'(A)',END=2) IDENT
      IF (IDENT .EQ. ' ') GO TO 10
      IF (IDENT(1:2) .EQ. '/*') GO TO 3
1     READ (IDEV,'(A)',END=2) JUNK
      IF (JUNK .EQ. '/*') GO TO 3
      GO TO 1
2     REWIND IDEV
3     K = 0
4     K = K + 1
      IF (K .GT. NDIM) GO TO 5
      READ (IDEV, *, ERR=7, END=5) CARD
      X (K) = CARD (ICX)
      Y (K) = CARD (ICY)
      GO TO 4
5     IF (K .GT. NDIM) WRITE (*,130) BEL,NDIM,NDIM
      N = K - 1
      WRITE (*,'(1H ,A)') IDENT
      WRITE (*,110) N
      RETURN
C  Error-handling portion of code.
7     WRITE (*,120) BEL,K
      K = K - 1
```

```
      GO TO 4
C-------------------------------------------------------------------------
110   FORMAT (' Number of points = ', I5)
120   FORMAT (' ',A1,'?DATIN-W-Unintelligible data in line ', I5,
     1 ' of file.'/' Line skipped: continue reading.')
130   FORMAT (' ',A1,'?DATIN-W-No. of data points exceeds ',I5/
     1 ' Return to main program with first ',I5,' points')
C-------------------------------------------------------------------------
      END
```

```
      PROGRAM average1
c ---  PROGRAM TO AVERAGE EXPERIMENTAL POINTS AND DECREASE DENSITY
C ---  4/96
      PARAMETER (NDIM=10000, NBREAK=20)
      REAL x(NDIM), y(NDIM), xavg(NDIM),yavg(NDIM),savex(20),
     &     savey(20),xbreak(NBREAK)
      INTEGER ntotal, navrg(NBREAK),nbreakp(NBREAK)
      LOGICAL option
      CHARACTER answer*1
      COMMON /cdata/savex,savey,ijk

C ---  READ IN DATA
      call readin(ntotal,x,y)
c
c --- LOOP TO CHOOSE REGIONS OF AVERAGING
      option = .true.
      do while (option)

      ijk = 0
 400  continue
      call commen('Choose breaking points to separate regions with diffe
     &rent averaging value [2 min]')
        call howplt(0,1,2)
        call plac(0.95,0.05,0.05,.95)
        call curv(ntotal,x,y)
           call nolbox
           call vg
        if (loopin() .eq.1)go to 400
      call newpag
c
c ---  FEED-IN NUMBER OF POINTS TO AVERAGE IN EACH REGION
      if (ijk .gt. 0) then
      do i = 1, ijk
         xbreak(i) = savex(i)
      end do
      do i = 1, ijk-1
         write(*,'(a,f8.3,a,f8.3,a\)')'   Number of points to average
     &from ',xbreak(i),' to ',xbreak(i+1),' -> '
         read(*,'(i2)')navrg(i)
      end do
      jmin = 1
      do i = 1, ijk
         j = jmin
```

```
         do while (x(j) .le. xbreak(i) .and. j .lt. ntotal)
            j = j+1
         end do
         jmin = j
         nbreakp(i) = jmin-1
      end do
c
c --- AVERAGING POINTS
      i= 1
      do j = 1, ijk-1
        k = nbreakp(j)
        do while (k .le. nbreakp(j+1) .and. k .le. ntotal)
           xavg(i) = 0.
           yavg(i) = 0.
           do l = 1, navrg(j)
              xavg(i) = xavg(i) + x(k)
              yavg(i) = yavg(i) + y(k)
              k = k+1
           end do
           xavg(i) = xavg(i)/navrg(j)
           yavg(i) = yavg(i)/navrg(j)
           i = i+1
        end do
      end do
      ntotavg = i-1
c
c --- PLOTTING RESULTS
 401  continue
      call commen(' ')
        call howplt(0,1,2)
        call plac(0.95,0.05,0.05,.95)
        call curv(ntotal,x,y)
        call howplt(17,0,3)
        call curv(ntotavg,xavg,yavg)
        call vg
      if (loopin() .eq.1)go to 401
      end if

      write(*,'(a\)')' Do you want to redo? (y/n) -> '
      read(*,'(a1)')answer
      if (answer .eq. 'n' .or. answer .eq. 'N') option = .false.
      end do
      write(*,*)' SAVE AVERAGED FILE '
```

```
      call save(xavg,yavg,ntotavg)

      STOP
      END


c **  ---------------------------------------------------------------
      subroutine vgcurs(x,y)
      real savex(20),savey(20)
      common/cdata/savex,savey,ijk
      ijk = ijk+1
      if (ijk.le.20) then
          savex(ijk) = x
          savey(ijk) = y
      end if
      return
      end
```

Appendix B Wave propagation through stratified media

The programs ENERGYD.FOR performs a calculation of reflectivity and transmission as a function of frequency. The user should provide the thickness, refractive index and absorption coefficient for each layer. The optical parameters (n,k) should be presented as a three column file (w,n,k), i.e. one file per layer. A small file has to be created in advanced that contains general information. It can have any name and it should contain the following parts:

The input file should look like this:

N (Number of films), θ(incident angle), n_0 (ref. index first medium)
thickness film #1
thickness film #2
---
thickness film #N
y or n (whether the last medium has a fixed ref. index or it is provided in a file)
(if yes, provide on this line n_{N+1} ref. index of last medium)
filename film #1 w,n,k
filename film #2 w,n,k
---
filename film #N w,n,k
(if no, above. Provide filename last medium (N+1) w, n,k
Position where to evaluate electric field intensities.

Once this file is created and you have the files with w,n,k for each layer (remember w should be the same in every layer) you can call the energy program.

The program LAYERS2.FOR allows to perform angle scan, depth penetration or film parameter (n, k, thickness) calculations as a function of a chosen free parameter that could be the film thickness, film optical parameters, the incident angle or the penetration depth. The input file should look like this:

N (Number of films)
first media ref. index, 0 0
layer1 ref index, layer 1 abs. Coeff., layer1 thickness
layer2 ref index, layer 2 abs. Coeff., layer2 thickness
…… …….. ……
layerN ref index, layer N abs. Coeff., layerN thickness
last medium ref. index, last medium abs. Coeff., 0
film # to be modified, frequency (cm^{-1}) incoming light, Number points to plot
Position to evaluate electric field intensities, incident angle.

```
      PROGRAM energyd

      parameter(m2 = 21,ndim = 5000,ncurve = 7)
      real zthet(ndim),
     &     n(0:m2),k(0:m2),h(0:m2),w,pi,rs,rp,trs,trp,frs,frp,fts,
     &     ftp,ix,iy,ip,theta,notheta,thetrad,delz,iz,sai,delta,
     &     plot1(ndim),plot2(ndim),plot3(ndim),plot4(ndim),plot5(ndim),
     &     plot6(ndim),plot7(ndim)
      complex*16 nc(0:m2),cosc(0:m2),csqrt,cmplx,identity(2,2)
      integer m,j,ii,noend,iguess,mm,iguess2
      character fname*40,answer*1,legend(ncurve)*30
      common /com1/pi
      common /com2/identity
      data pi/3.14159265/, identity/1.,0.,0.,1./
      print*,'energy scan analysis - R, T, Ix, Iy, Iz, phase'
      print*,' '
  110 format(a40)
      print*,' Filename with "initial" data -> '
      read(*,'(a40)')fname
      open(31,file = fname, status = 'old')
      read(31,*)m,theta,n(0)
      k(0) = 0.
      h(0) = 0.
      h(m+1) = 0.
      thetrad = theta * pi / 180.
      notheta = n(0) * sin(thetrad)
      nc(0) = cmplx(n(0),k(0))
      cosc(0) = csqrt(1 - (notheta/nc(0))**2)
      print*,'Number of films -> ',m
      print*,'Incident angle [deg] -> ',theta
      print*,'refractive index first medium -> ',n(0)
      do while (m .gt. 0)
      do i = 1,m
           read(31,*)h(i)
           print*,'Thickness [um] of film #',i,' -> ',h(i)
      end do
      read(31,'(a1)')answer
      print*,'Is last medium fixed refrac. index ? (y/n) -> ',answer
      if ((answer .eq. 'y') .or. (answer .eq. 'Y')) then
          read(31,*)n(m+1)
          print*,'refractive index last medium -> ',n(m+1)
          k(m+1) = 0.
```

```
          nc(m+1) = cmplx(n(m+1),k(m+1))
          cosc(m+1) = csqrt(1 - (notheta/nc(m+1))**2)
          mm = m
      else
          mm = m+1
      end if
      do i = 1,mm
           read(31,110)fname
           print*,'filename_optical constants-film) #',i,' ->',fname
           open(i,file = fname, status = 'old')
      end do
      m=-m
      end do
c
c --  FOR SINGLE REFLECTION (INTERPHASE)
C
      if (m .eq. 0) then
         mm = 1
        read(31,110)fname
        print*,'filename_optical constants,second medium) ->',fname
        open(mm,file = fname, status = 'old')
      else
         m = -m
      end if
c
c***    z-position for intensities evaluations
c
           read(31,*)z
           print*,'z-position of (Ez*Ez) evaluation [um] -> ',z
           hd = 0.
           j = 0
           if (z .lt. 0.) then
              delz = z
           end if
           do while ((z .ge. hd) .and. (j .ne. m+1))
              j = j+1
              hd = hd + h(j)
           end do
           delz = z - (hd-h(j))

           print*,'what to plot? '
           print*,'rfl-tra and Intensities --> [1]'
           print*,'phase - sai -delta      --> [2]'
```

```
      print*,'Choose option          -->'
      read*,iguess

 i = 0
 do while (.not.eof(1))
        i = i+1
        do l = 1, mm
          read(l,*)w,n(l),k(l)
          nc(l) = cmplx(n(l),k(l))
          cosc(l) = csqrt(1 - (notheta/nc(l))**2)
        end do
        zthet(i) = w

      call calculation(nc,cosc,h,w,notheta,j,delz,m,m2,rs,rp,trs,
&          trp,frs,frp,fts,ftp,ix,iy,iz,ip,sai,delta)

      if (iguess .eq. 1) then
      plot1(i) = rp
      legend(1) = 'p-TM-reflection'
      plot2(i) = rs
      legend(2) = 's-TE-reflection'
      plot3(i) = trp
      legend(3) = 'p-TM-transmition'
      plot4(i) = trs
      legend(4) = 's-TE-transmition'
      plot5(i) = iz
      legend(5) = 'Ez field intensity'
      plot6(i) = iy
      legend(6) = 'Ey field intensity'
      plot7(i) = ix
      legend(7) = 'Ex field intensity'
      else if (iguess .eq. 2) then
      plot1(i) = frp
      legend(1) = 'p-TM-rfl. phase shift'
      plot2(i) = frs
      legend(2) = 's-TE-rfl. phase shift'
      plot3(i) = ftp
      legend(3) = 'p-TM-tra. phase shift'
      plot4(i) = fts
      legend(4) = 's-TE-tra. phase shift'
      plot5(i) = sai
      legend(5) = 'sai = arctan([rp]/[rs])'
      plot6(i) = delta
```

```
        legend(6) = 'delta = delt_rp - delt_rs'
        end if

    end do
    nmax = i

10      continue
        call graph(2,legend(1),nmax,zthet,plot1,ndim)
        call graph(3,legend(2),nmax,zthet,plot2,ndim)
        call vg
        if(loopin() .eq. 1) go to 10
        call newpag

20      continue
        call graph(2,legend(3),nmax,zthet,plot3,ndim)
        call graph(3,legend(4),nmax,zthet,plot4,ndim)
        call vg
        if(loopin() .eq. 1) go to 20
        call newpag

30      continue
        call graph(2,legend(5),nmax,zthet,plot5,ndim)
        call graph(3,legend(6),nmax,zthet,plot6,ndim)
        if (iguess .eq. 1) then
          call graph(4,legend(7),nmax,zthet,plot7,ndim)
        end if
        call vg
        if(loopin() .eq. 1) go to 30
        call newpag

    print*,'Do you want to save any file? [y/n] -> '
    read(*,'(a1)')answer
    iguess2 = 1
    if ((answer .eq. 'y') .or. (answer .eq. 'Y')) then
        do while (iguess2 .ne. 0)
          if (iguess .eq. 1) then
          print*,'p-TM-reflection         ---> [1]'
          print*,'s-TE-reflection         ---> [2] '
          print*,'p-TM-transmition          ---> [3]'
          print*,'s-TE-transmition         ---> [4]'
          print*,'Ez field intensity       ---> [5]'
          print*,'Ey field intensity       ---> [6]'
          print*,'Ex field intensity       ---> [7]'
```

```
print*,'quit                    ---> [0]'
else if (iguess .eq. 2) then
print*,'p-TM-rfl. phase shift    ---> [1]'
print*,'s-TE-rfl. phase shift    ---> [2]'
print*,'p-TM-tra. phase shift    ---> [3]'
print*,'s-TE-tra. phase shift    ---> [4]'
print*,'sai = arctan([rp]/[rs])  ---> [5]'
print*,'delta = delt_rp - delt_rs---> [6]'
print*,'quit                    ---> [0]'
end if
print*,'choose an option -> '
read*,iguess2
if (iguess2 .eq. 0) then
  stop
else
  print*,'output filename -> '
  read(*,'(a12)')fname
  open(9,file = fname, status = 'unknown')
end if
if (iguess2 .eq. 1) then
  do i = 1,nmax
    write(9,*)zthet(i),plot1(i)
  end do
else if (IGUESS2 .eq. 2) then
  do i = 1,nmax
    write(9,*)zthet(i),plot2(i)
  end do
else if (IGUESS2 .eq. 3) then
  do i = 1,nmax
    write(9,*)zthet(i),plot3(i)
  end do
else if (IGUESS2 .eq. 4) then
  do i = 1,nmax
    write(9,*)zthet(i),plot4(i)
  end do
else if (IGUESS2 .eq. 5) then
  do i = 1,nmax
    write(9,*)zthet(i),plot5(i)
  end do
else if (IGUESS2 .eq. 6) then
  do i = 1,nmax
    write(9,*)zthet(i),plot6(i)
  end do
```

```
          else if (IGUESS2 .eq. 7) then
            do i = 1,nmax
              write(9,*)zthet(i),plot7(i)
            end do
          end if
        end do
      else
        stop
      end if

      end
c**************
c
c**************
        subroutine graph(i,legend,nmax,x,y,ndim)
        integer nmax,ndim,i
        real x(ndim),y(ndim)
        character legend*30
        call howplt(0,1,i)
        call legpos(0.67,0.88)
        call legnd(legend)
        call curv(nmax,x,y)
        return
        end
c*********
c*
c*********
      subroutine calculation(nc,cosc,h,w,notheta,j,delz,m,m2,
     &rs,rp,trs,trp,frs,frp,fts,ftp,ix,iy,iz,ip,sai,delta)
      real h(0:m2),w,notheta,pi,delz,sai,delta
     &rs,rp,trs,trp,frs,frp,fts,ftp,ix,iy,iz,ip,hd
      complex*16 tp(20),ts(20),cp(20,2,2),cs(20,2,2),nc(0:m2),cosc(0:m2)
     &,d0s(2,2),djs(2,2),t0s,tjs,d0p(2,2),djp(2,2),t0p,tjp,csqrt,
     &cmplx,crs,crp,cts,ctp,kzjdelz,epjp,epjs,emjp,emjs,ex,ey,ez,cexp,
     &expkzjdelz,conjg
      common /com1/pi
      integer j,m,m2

      call product(nc,cosc,h,w,t0s,t0p,d0s,d0p,djs,djp,tjs,tjp,m,j,m2)

      crs = d0s(2,1)/d0s(1,1)
      cts = t0s/d0s(1,1)
      rs = crs * conjg(crs)
```

```
      trs = real(nc(m+1)*cosc(m+1)/(nc(0)*cosc(0)))*cts*conjg(cts)
      call phase(crs,frs)
      call phase(cts,fts)
      crp = d0p(2,1)/d0p(1,1)
      ctp = t0p/d0p(1,1)
      rp = crp * conjg(crp)
      trp = real(conjg(nc(m+1))*cosc(m+1)/(conjg(nc(0))*cosc(0)))*ctp*co
     &njg(ctp)
      call phase(crp,frp)
      call phase(ctp,ftp)

      delta = frp - frs
      sai = atan2(abs(crp),abs(crs))*180./pi

      kzjdelz = 2*pi*w*nc(j)*cosc(j)*delz/1.e4
      expkzjdelz = cexp(cmplx(-imag(kzjdelz),real(kzjdelz)))

      epjs = expkzjdelz*tjs * djs(1,1)/d0s(1,1)
      emjs = tjs * djs(2,1)/(d0s(1,1)*expkzjdelz)
      epjp = expkzjdelz*tjp * djp(1,1)/d0p(1,1)
      emjp = tjp * djp(2,1)/(d0p(1,1)*expkzjdelz)

      ex = (epjp - emjp) * cosc(j)
      ey = epjs + emjs
      ez = (epjp + emjp) * notheta/nc(j)
      ix = ex * conjg(ex)
      iy = ey * conjg(ey)
      iz = ez * conjg(ez)
      ip = ix + iz

      return
      end
c**********
c
c**********
      subroutine interph(nc1,cosc1,nc2,cosc2,rs,rp,ts,tp)
      complex*16 tp,ts,rp,rs,nc1,nc2,cosc1,cosc2,denp,dens

          denp = nc1*cosc2 + nc2*cosc1
          rp = (-nc1*cosc2 + nc2*cosc1)/denp
          tp = 2*nc1*cosc1/denp
          dens = nc2*cosc2 + nc1*cosc1
          rs = (nc1*cosc1 - nc2*cosc2)/dens
```

```
          ts = 2*nc1*cosc1/dens

      return
      end
c********
c
c********
      subroutine product(nc,cosc,h,w,t0s,t0p,d0s,d0p,djs,djp,tjs,tjp,
     &                   m,j,m2)
      complex*16 d0s(2,2),d0p(2,2),djs(2,2),djp(2,2),t0s,t0p,tjs,tjp,
     &identity(2,2),cs(2,2),cp(2,2),d1s(2,2),d1p(2,2),delta,
     &cexp,csqrt,cmplx,nc(0:m2),cosc(0:m2),ts,tp
      integer m,j,m2
      real pi,w,h(0:m2)
      common /com1/pi
      common /com2/identity

      d0s = identity
      d0p = identity
      t0s = 1.
      t0p = 1.
      tjs = 1.
      tjp = 1.

      do i = 0, m
          if (m-i+1 .eq. j) then
            djs = d0s
            djp = d0p
          end if

          call interph(nc(m-i),cosc(m-i),nc(m+1-i),cosc(m+1-i),cs(1,2),
     &           cp(1,2),ts,tp)
          delta = 2*pi*w*h(m-i)*nc(m-i)*cosc(m-i)/1.e4
c         print*,delta
          cs(2,2) = cexp(cmplx(-imag(delta),real(delta)))
          cp(2,2) = cs(2,2)
          cs(2,1) = cs(1,2)*cs(2,2)
          cp(2,1) = cp(1,2)*cp(2,2)
          cs(1,1) = 1./cs(2,2)
          cp(1,1) = 1./cp(2,2)
          cs(1,2) = cs(1,2)*cs(1,1)
          cp(1,2) = cp(1,2)*cp(1,1)
```

```
          t0s =t0s * ts
          t0p =t0p * tp

          call matprod(cs,d0s,d1s)
          call matprod(cp,d0p,d1p)
          d0s = d1s
          d0p = d1p
          if (m-i+1 .le. j) then
            tjs = tjs * ts
            tjp = tjp * tp
          end if
      end do
      if (j .eq. 0) then
          djs = d0s
          tjs = 1.
          djp = d0p
          tjp = 1.
      end if
      return
      end
c********
c
c********
          subroutine matprod(m1,m2,mm)
          complex*16 m1(2,2),m2(2,2),mm(2,2)
          do i=1,2
            do j=1,2
                mm(i,j)=0.
            end do
          end do
          do i =1,2
            do j=1,2
                do k =1,2
                   mm(i,j)=m1(i,k)*m2(k,j)+mm(i,j)
                end do
            end do
          end do
          return
          end
c*********
c
c*********
      subroutine phase(crs,frs)
```

```
complex*16 crs
real frs
common /com1/pi
if (real(crs) .lt. 1.e-6) then
    frs = 90.

else if (real(crs) .lt. 0.) then
    frs = atan2(imag(crs),real(crs))*180./pi
    frs = frs + 180.
else
    frs = atan2(imag(crs),real(crs))*180./pi
end if
return
end
```

```
      PROGRAM layers2
******          3.8.93
******          r. gonz.
      PARAMETER(m2 = 21,ndim = 2000,ncurve = 6)
      REAL x(ndim),y1(ncurve,ndim),y2(ncurve,ndim),y3(ncurve,ndim),
     &     n(0:m2),k(0:m2),h(0:m2),w,pi,rs,rp,trs,trp,frs,frp,fts,
     &     ftp,ix,iy,ip,theta,notheta,thetrad,delz,iz,sai,delta,
     &     y4(ncurve,ndim),par(ncurve)
      COMPLEX nc(0:m2),cosc(0:m2),csqrt,cmplx,identity(2,2),
     &d0s(2,2),d0p(2,2),djs(2,2),djp(2,2),tjs,tjp,pjs(0:m2),
     &mjs(0:m2),pjp(0:m2),mjp(0:m2)
      integer m,j,ii,noend,iguess,mm,iguess1,mfilm
      character fname*20,answer*1,legend(ncurve)*30,
     $          optiontext(ncurve)*40
      CHARACTER*1 option(6)
      INTEGER nmax,npar
      COMMON /out1/rp,rs,trp,trs,frp,frs,ftp,fts,ix,iy,iz,ip,sai,delta
      COMMON /graphdata/nmax,nfilm,npar,z
      common /com1/pi
      common /com2/identity
      data pi/3.14159265/, identity/1.,0.,0.,1./
      print*,' LAYER SCAN ANALYSIS - R, T, Ix, Iy, Iz, phase'
      print*,' '
      write(*,'(a\)')' Input data filename -> '
      read(*,110)fname
 110  format(a20)
      open(1,file = fname, status = 'old')
      read(1,*)m
      mm = m+1
      do i = 0,mm
          read(1,*)n(i),k(i),h(i)
          print*,n(i),k(i),h(i)
      end do
      read(1,*)mfilm,w,nmax
      print*,'incident light energy [cm-1] -> ',w
      print*,'Number of points to plot (max. 2000) -> ',nmax
      read(1,*)z,theta
           print*,'Incident plane is x-z and  '
           print*,'Outermost reflection surface is x-y plane at z=0'
           print*,'z-position of (Ez*Ez) evaluation [DEFAULT]-> ',z,'[um]'
           print*,'Incident angle (deg) [DEFAULT] -> ',theta
           print*,'*****************'
      nfilm = 1
```

```
************************
*        INDEPENDENT VARIABLE DETERMINATION
************************
      write(*,'(a)')' INDEPENDENT VARIABLE (X-axis)'
      print*,' '
      write(*,'(a)')' Incident angle [deg]              ---> [1]'
      write(*,'(a)')' depth penetration [micron]         ---> [2]'
      write(*,'(a)')' film properties (n,k,d)           ---> [3]'
      print*,' '
      write(*,'(a\)')' Choose and option                ---> '
      read(*,'(a1)')option(1)
      if (option(1).eq.'3') then
          write(*,'(a\)')' film number  ---> '
          read(*,*)nfilm
          print*,' '
          write(*,'(a)')' refractive index of chosen film   ---> [1]'
          write(*,'(a)')' absorption coeff. of chosen film  ---> [2]'
          write(*,'(a)')' Thicknes of chosen film [um]      ---> [3]'
          print*,' '
          write(*,'(a\)')' Choose and option              ---> '
          read(*,'(a1)')option(2)
      end if
      print*,' RANGE '
      write(*,'(a\)')' Initial value   ---> '
      read(*,*)xinitial
      write(*,'(a\)')' Final value     ---> '
      read(*,*)xfinal
      write(*,'(a\)')' Resolution (number of points) [max 3000] -> '
      read(*,*)nmax
      print*,' '
      print*,' '

************************
*     PARAMETER DETERMINATION
************************
      write(*,'(a)')' PARAMETER VARIABLE '
      print*,' '
      write(*,'(a)')' Incident angle [deg]              ---> [1]'
      write(*,'(a)')' depth penetration [micron]         ---> [2]'
      write(*,'(a)')' film properties (n,k,d)           ---> [3]'
c     write(*,'(a)')' Remove a film                     ---> [4]'
      print*,' '
      write(*,'(a\)')' Choose and option                ---> '
```

```
      read(*,'(a1)')option(3)
      if (option(3).eq.'3') then
          write(*,'(a\)')' film number  ---> '
          read(*,*)nfilm
          print*,' '
          write(*,'(a)')' refractive index of chosen film   ---> [1]'
          write(*,'(a)')' absorption coeff. of chosen film  ---> [2]'
          write(*,'(a)')' Thicknes of chosen film [um]      ---> [3]'
          print*,' '
          write(*,'(a\)')' Choose and option               ---> '
          read(*,'(a1)')option(4)
      end if
      print*,' RANGE '
      write(*,'(a\)')' Initial value   ---> '
      read(*,*)parinitial
      write(*,'(a\)')' Final value     ---> '
      read(*,*)parfinal
      write(*,'(a\)')' Number of parameters [max 6] -> '
      read(*,*)npar
      print*,' '
      print*,' '
*************************
*     DEPENDENT VARIABLE DETERMINATION
*************************
      write(*,'(a)')' DEPENDANT VARIABLE '
      print*,' '
      write(*,'(a)')' Reflectance                  ---> [1]'
      write(*,'(a)')' Transmittance                ---> [2]'
      write(*,'(a)')' Electric field intensities     ---> [3]'
      write(*,'(a)')' Phase shifts                 ---> [4]'
      write(*,'(a)')' Psi and Delta                ---> [5]'
      write(*,'(a)')' Sensitivity (Delta Reflectance) ---> [6]'
      print*,' '
      write(*,'(a\)')' Choose and option            ---> '
      read(*,'(a1)')option(5)
      print*,' '
      print*,' '
*********************************
*         CALCULATIONS
*********************************
      if (option(1).eq.'1') then
          optiontext(1) = 'angle scan [deg]'
**************
```

```
*       Angle scan
***************
        if (option(3) .eq. '1') then
           pause 'not possible'
        elseif (option(3) .eq. '2') then
           optiontext(2) = 'Depth variation [um]'
           if (option(5).ne.'6') then
           do l = 0, m+1
                 nc(l) = cmplx(n(l),k(l))
           end do
           do i = 1,npar
                 par(i) = parinitial+(parfinal-parinitial)*(i-1)/
     $           real(npar-1)
                 call depthz(par(i),h,delz,jfilm,m2)
                 do j = 1,nmax
                    x(j)=xinitial+(xfinal-xinitial)*(j-1.)/real(nmax)
                    thetrad = x(j) * pi / 180.
                    notheta = n(0) * sin(thetrad)
                    do l = 0, m+1
                      cosc(l) = csqrt(1 - (notheta/nc(l))**2)
                    end do

                    call calculation(nc,cosc,h,w,notheta,jfilm,delz,
     &                    m,m2,rs,rp,trs,trp,frs,frp,fts,ftp,ix,iy,iz,
     &                    ip,sai,delta)
                    call output1(option(5),y1(i,j),y2(i,j),y3(i,j),
     &                     y4(i,j),optiontext)

                 end do
           end do
          call graphall(option,optiontext,x,y1,y2,y3,y4,par,ncurve,ndim)
           end if

        elseif (option(3) .eq. '3') then
                 if (option(5).ne.'6') then
                 if (option(4).eq.'1' .or. option(4).eq.'2') then
                   call depthz(z,h,delz,jfilm,m2)
                 end if
                 do l = 0, m+1
                   if (l .ne. nfilm) then
                     nc(l) = cmplx(n(l),k(l))
                   end if
                 end do
```

```
                do i = 1,npar
                par(i) = parinitial+(parfinal-parinitial)*(i-1)/
     $          real(npar-1)
                if (option(4) .eq. '1') then
                  nc(nfilm) = cmplx(par(i),k(nfilm))
                  optiontext(2) = 'Refractive index variation'
                else if (option(4) .eq. '2') then
                  nc(nfilm) = cmplx(n(nfilm),par(i))
                  optiontext(2) = 'Absorption coef. variation'
                else if (option(4) .eq. '3') then
                  optiontext(2) = 'Film thickness variation'
                  nc(nfilm) = cmplx(n(nfilm),k(nfilm))
                  h(nfilm) = par(i)
                  call depthz(z,h,delz,jfilm,m2)
                end if
                do j = 1,nmax
                   x(j)=xinitial+(xfinal-xinitial)*(j-1.)/real(nmax)
                   thetrad = x(j) * pi / 180.
                   notheta = n(0) * sin(thetrad)
                   do l = 0, m+1
                     cosc(l) = csqrt(1 - (notheta/nc(l))**2)
                   end do

                   call calculation(nc,cosc,h,w,notheta,jfilm,delz,
     &                  m,m2,rs,rp,trs,trp,frs,frp,fts,ftp,ix,iy,iz,
     &                  ip,sai,delta)
                   call output1(option(5),y1(i,j),y2(i,j),y3(i,j),
     &                   y4(i,j),optiontext)
                end do
                end do
          call graphall(option,optiontext,x,y1,y2,y3,y4,par,ncurve,ndim)
                end if
           end if


       else if (option(1) .eq. '2') then
           optiontext(1) = 'depth profile [um]'
**************
*          Depth scan
**************
           if (option(3) .eq. '2') then
              pause 'not possible'
           elseif (option(3) .eq. '1') then
```

```
      optiontext(2) = 'Incident angle variation'
      if(option(5).eq.'3')then
      do i = 1,npar
        par(i) = parinitial+(parfinal-parinitial)*(i-1)/real(npar-1)
        thetrad = par(i) * pi / 180.
        notheta = n(0) * sin(thetrad)
        do l = 0, m+1
          nc(l) = cmplx(n(l),k(l))
          cosc(l) = csqrt(1 - (notheta/nc(l))**2)
        end do
        do j = 0,m+1
          call productj(nc,cosc,h,w,d0s,d0p,djs,djp,tjs,tjp,m,j,m2)
          pjs(j) =tjs * djs(1,1)/d0s(1,1)
          mjs(j) = tjs * djs(2,1)/d0s(1,1)
          pjp(j) =tjp * djp(1,1)/d0p(1,1)
          mjp(j) = tjp * djp(2,1)/d0p(1,1)
        end do
        htot = 0.
        do ii1 = 0, m+1
          htot = htot + h(ii1)
        end do

        do j = 1, nmax
          zmin= xinitial
          zmax =xfinal
          x(j) = -zmin + (j-1)*(htot+zmin +zmax)/real(nmax)
          call depthz(x(j),h,delz,jfilm,m2)
          call calcdepth(nc,cosc,w,notheta,jfilm,delz,m2,pjs,mjs,
%                 pjp,mjp,y1(i,j),y2(i,j),y3(i,j),y4(i,j))
        end do
      end do
      optiontext(3) = 'X-compt - Electric fied intensity'
      optiontext(4) = 'Y-compt = S-pol - Electric fied intensity'
      optiontext(5) = 'Z-compt - Electric fied intensity'
      optiontext(6) = 'P-pol - Electric fied intensity'
        call graphall(option,optiontext,x,y1,y2,y3,y4,par,ncurve,ndim)
        else
          pause 'not possible'
        end if


      else if(option(3) .eq. '3') then
        if(option(5).eq.'3')then
```

```
      thetrad = theta * pi / 180.
      notheta = n(0) * sin(thetrad)
      do l = 0, m+1
       if (l.ne.nfilm) then
            nc(l) = cmplx(n(l),k(l))
            cosc(l) = csqrt(1 - (notheta/nc(l))**2)
       end if
      end do
     do i = 1,npar
      par(i) = parinitial+(parfinal-parinitial)*(i-1)/real(npar-1)
       if (option(4).eq.'1') then
            optiontext(2) = 'Ref index parameter'
            nc(nfilm) = cmplx(par(i),k(nfilm))
       else if (option(4).eq.'2') then
            optiontext(2) = 'Absorption coef. parameter'
            nc(nfilm) = cmplx(n(nfilm),par(i))
       else if (option(4) .eq. '3') then
            optiontext(2) = 'Film thickness parameter'
            nc(nfilm) = cmplx(n(nfilm),k(nfilm))
            h(nfilm) = par(i)
       end if
       cosc(nfilm) = csqrt(1 - (notheta/nc(nfilm))**2)
      do j = 0,m+1
       call productj(nc,cosc,h,w,d0s,d0p,djs,djp,tjs,tjp,m,j,m2)
       pjs(j) =tjs * djs(1,1)/d0s(1,1)
       mjs(j) = tjs * djs(2,1)/d0s(1,1)
       pjp(j) =tjp * djp(1,1)/d0p(1,1)
       mjp(j) = tjp * djp(2,1)/d0p(1,1)
      end do
      htot = 0.
      do ii1 = 0, m+1
        htot = htot + h(ii1)
      end do

      do j = 1, nmax
       zmin= xinitial
       zmax = xfinal
       x(j) = -zmin + (j-1)*(htot+zmin +zmax)/real(nmax)
       call depthz(x(j),h,delz,jfilm,m2)
       call calcdepth(nc,cosc,w,notheta,jfilm,delz,m2,pjs,mjs,
$            pjp,mjp,y1(i,j),y2(i,j),y3(i,j),y4(i,j))
      end do
     end do
```

```
          optiontext(3) = 'X-compt - Electric fied intensity'
          optiontext(4) = 'Y-compt = S-pol - Electric fied intensity'
          optiontext(5) = 'Z-compt - Electric fied intensity'
          optiontext(6) = 'P-pol - Electric fied intensity'
            call graphall(option,optiontext,x,y1,y2,y3,y4,par,ncurve,ndim)
            else
              pause 'not possible'
            end if
          end if


      else if (option(1) .eq. '3') then
**************
*         Film parameter scan
**************
          pause ' not available yet'
      end if
      STOP
      END
*---------------------------------------------------------------------
*---------------------------------------------------------------------
      SUBROUTINE graphall(option,optiontext,x,y1,y2,y3,y4,par,nc,ndim)
      COMMON /graphdata/nmax,nfilm,npar,z
      REAL x(ndim),y1(nc,ndim),y2(nc,ndim),y3(nc,ndim),y4(nc,ndim),
     $       par(nc)
********************
*         SUB. TO PLOT GRAPHS
********************
      CHARACTER optiontext(nc)*40,option(6)*1
      REAL y(3000)
c      print*,nmax,nfilm,npar
c      pause
          if(option(5) .eq. '3' .or. option(5) .eq. '4') then
            do i = 1,4
 401  continue
      write(*,'(a)')' Parameter values in increasing order'
      write(*,'(6(e10.3,a1))')(par(kk),',',kk=1,npar)
      call plac(0.9,0,0.05,0.95)
      do j = 1, npar
          call howplt(0,j,1)
          if (i.eq.1) then
            call rtemy(nmax,y1,y,j,ndim,nc)
          else if (i.eq.2) then
```

```
          call rtemy(nmax,y2,y,j,ndim,nc)
        else if (i.eq.3) then
          call rtemy(nmax,y3,y,j,ndim,nc)
        else if (i.eq.4) then
          call rtemy(nmax,y4,y,j,ndim,nc)
        end if
          call legpos(0.67,0.72)
          call legnd(char(j+48))
        call curv(nmax,x,y)
    end do
        call nolbox
        call sidtex(optiontext(2),3,optiontext(1),3,optiontext(i+2),3,
   $                ' ',3)
        call vg
        if (loopin() .eq.1)go to 401
        call newpag
        end do
        else
         do i = 1,2
400  continue
    write(*,'(a)')' Parameter values in increasing order'
    write(*,'(6(e10.3,a1))')(par(kk),',',kk=1,npar)
    call plac(0.9,0,0.05,0.95)
    call legpos(0.67,0.72)
    do j = 1, npar
        call howplt(0,j,1)
        if (i.eq.1) then
          call rtemy(nmax,y1,y,j,ndim,nc)
        else if (i.eq.2) then
          call rtemy(nmax,y2,y,j,ndim,nc)
        end if
        call legnd(char(j+48))
        call curv(nmax,x,y)
    end do
        call nolbox
        call sidtex(optiontext(2),3,optiontext(1),3,optiontext(i+2),3,
   $                ' ',3)
        call vg
        if (loopin() .eq.1)go to 400
        call newpag
        end do
        end if
```

```
      RETURN
      END


*-------------------------------------------------------------
*-------------------------------------------------------------
      SUBROUTINE output1(option,y1,y2,y3,y4,optiontext)
      REAL y1,y2,y3,y4
      CHARACTER option*1, optiontext(*)*40
      COMMON /out1/rp,rs,trp,trs,frp,frs,ftp,fts,ix,iy,iz,ip,sai,delta
      if(option .eq. '1') then
          optiontext(3) = 'p-TM-Reflectance'
          optiontext(4) = 's-TE-Reflectance'
          y1 = rp
          y2 = rs
          y3 = 0.
          y4 = 0.
      else if(option .eq. '2') then
          optiontext(3) = 'p-TM-Transmittance'
          optiontext(4) = 's-TE-Transmittance'
          y1 = trp
          y2 = trs
          y3 = 0.
          y4 = 0.
      else if(option .eq. '3') then
          optiontext(3) = 'X-compt - Electric fied intensity'
          optiontext(4) = 'Y-compt = S-pol - Electric fied intensity'
          optiontext(5) = 'Z-compt - Electric fied intensity'
          optiontext(6) = 'P-pol - Electric fied intensity'
          y1 = ix
          y2 = iy
          y3 = iz
          y4 = ip
      else if(option .eq. '4') then
          optiontext(3) = 'p-TM-rfl. phase shift'
          optiontext(4) = 's-TE-rfl. phase shift'
          optiontext(5) = 'p-TM-tra. phase shift'
          optiontext(6) = 's-TE-tra. phase shift'
          y1 = frp
          y2 = frs
          y3 = ftp
          y4 = fts
      else if(option .eq. '5') then
```

```
          optiontext(3) = '|Y = arctan([R_p]/[R_s])'
          optiontext(4) = '|D = |Dphas_R_p - |Dphas_R_s'
          y1 = sai
          y2 = delta
          y3 = 0.
          y4 = 0.
      end if
      RETURN
      END
*-----------------------------------------------------------------
c-----------------------------------------------------------------
      SUBROUTINE rtemy(nmax,y4,y,j,ndim,nc)
      REAL y(ndim),y4(nc,ndim)
c*************
c     TRANSFER DATA FROM MATRIX TO VECTOR
c*************
      do i = 1,nmax
          y(i) = y4(j,i)
      end do
      RETURN
      END
```

Appendix C Factorized Form of the Dielectric Function Fit to IR Reflectivity

Based on the discussion in section 2.3.5 and in chapter four, the following programs were developed. These programs perform a non-linear fit to near-normal reflectivity data using the factorized form of the dielectric function. As an example the program FPSQ31.FOR fits three reflection peaks respectively.

```
      PROGRAM fpsq31
c --  Rey Gonzalez
c --  7.25.95
c --- SIMILAR TO FPSQ3 BUT USING NUM RES ALGORITHM FOR DERIVATIVE
      EXTERNAL funcs3

PARAMETER(NDATA1=3000,MA1=20,MFIT1=20,NCA1=20,MMAX=21,Ndim=3000)
      DIMENSION x(NDATA1),y(NDATA1),sig(NDATA1),a(MA1),covar(NCA1,NCA1),
     &      alpha(NCA1,NCA1),lista(MFIT1),dumm(MMAX),yfit1(ndata1)
      REAL alamda,chisq,ochi,sigout,q
      INTEGER npoints,ndata,icol
      INTEGER*2 i,j,k,l,n,loop
      dimension card(10),energy(ndim),eels(ndim),sigy(ndim)
      character filnam*80, ident*60, lerror*1
      logical fileok
      CHARACTER*35 poflnm
      COMMON /linear/aconst,aslope

      j=0
      alamda=-1.0
      loop=0
      ochi=1.0
      do i = 1, 5
         a(4*i) = 1.
      end do

c**********
c     Read in file  and choose peaks to fit
c**********
  501 CONTINUE
      write(*,5)
 5    format(' What is the name of your data file  -> ',\)
      READ(*,100)FILNAM
```

```
 100 FORMAT(A)
     INQUIRE(FILE=FILNAM,EXIST=FILEOK)
     IF(FILEOK)THEN
          OPEN(3,FILE=FILNAM,STATUS='OLD')
     ELSE
       PRINT *,'File does not exist -- try again.'
       GOTO 501
     ENDIF
     write(*,'(a\)')(' Is error in y_data available? (y/n) -> ')
     read(*,'(a1)')lerror
     if (lerror .eq. 'y' .or. lerror .eq. 'Y') then
        icol = 3
     else
        icol = 2
     end if
     print*,' Please WAIT. Reading in data.....'
     call datain3(3,energy,eels,sigy,ndim,npoints,card,icol,1,2,3,
    $ ident)
     CLOSE(3)
     call peake(energy,eels,sigy,npoints,x,y,sig,ndata,a)
          ma = 13
          nca =13
          mfit = 13
          k = 1
          ochi = 1
          alamda = -1

     do  k=1,MFIT
       lista(k) = k
     end do
c****************
c     NON-LINEAR FIT
C****************
30      call mrqmin(x,y,sig,NDATA,a,MA,lista,MFIT,covar,alpha,NCA,
    &          chisq,funcs3,alamda)
     do  n=1,ndata
       call funcs3(x(n),a,yfit1(n),dumm,MA)
     end do
     call plot2(x,y,yfit1,ndata)
       WRITE(*,'(1X,A,I2,T18,A,F10.4,T43,A,E9.2)') 'Iteration #',K,
    *              'Chi-squared:',CHISQ,'ALAMDA:',ALAMDA
     if (alamda.eq.0.0) then
       ALAMDA=0.0
```

```
      CALL MRQMIN(X,Y,SIG,NDATA,A,MA,LISTA,MFIT,COVAR,ALPHA,
     *              nca,CHISQ,Funcs3,ALAMDA)
      do i = 1, ma
         print*,' ',a(i),'+/-',sqrt(abs(covar(i,i)))
      end do
        q=gammq(0.5*(NDATA-MA),0.5*chisq)
        print*,'CHI-SQ=',chisq, '   N_data-M_paramt= ',ndata-ma
        print*,'PROBABILITY OF GOODNESS OF FIT=',q
        pause
     print*,'ENTER THE NAME OF THE OUTPUT PARAMETER FILE'
     read(*,'(a)') poflnm
        open(unit=8,file=poflnm,status='unknown')
        do 40 l=1,MA
           sigout=sqrt(abs(covar(l,l)))
           write(8,*) a(l),sigout
40       continue
           close(8)
        go to 50

     elseif(abs((chisq-ochi)/ochi).lt.1.0E-5) then
        alamda=0.0
           goto 30
     else
           loop=loop+1
           ochi=chisq
           goto 30
     endif


50      print*,' Wait.... Setting up graph.... '
     do  n=1,ndata
       call funcs3(x(n),a,yfit1(n),dumm,MA)
     end do
     call plot2(x,y,yfit1,ndata)

     stop
     end
**********************************************************************
     SUBROUTINE funcs3(x,a3,y,dyda,MA)
     REAL a3(MA),dyda(MA)
     real  a,b,c,d,f,g,h,m,n,o,p,q,k,w,z,
    &      dydw,dydz,a1,a2,b1,b2,c1,c2
     y=0.
```

```
      a = a3(1)
      b = a3(2)
      c = a3(3)
      d = a3(4)
      f = a3(5)
      g = a3(6)
      h = a3(7)
      m = a3(8)
      n = a3(9)
      o = a3(10)
      p = a3(11)
      q = a3(12)
      k = a3(13)

c     phon1=(b**2-x**2+#i*x*c)/(d**2-x**2+#i*x*f)

c     RE((b**2-x**2+#i*x*c)/(d**2-x**2+#i*x*f))
      a1=
     $(x**4-x**2*(b**2-c*f+d**2)+b**2*d**2)/(x**4+x**2*(f**2-2*d**2)+d**
     $4)

c     IM((b**2-x**2+#i*x*c)/(d**2-x**2+#i*x*f))
      a2=
     $-x*(x**2*(c-f)+b**2*f-c*d**2)/(x**4+x**2*(f**2-2*d**2)+d**4)

c     phonon2=(g**2-x**2+#i*x*h)/(m**2-x**2+#i*x*n)

c     RE((g**2-x**2+#i*x*h)/(m**2-x**2+#i*x*n))
      b1=
     $(x**4-x**2*(g**2-h*n+m**2)+g**2*m**2)/(x**4+x**2*(n**2-2*m**2)+m**
     $4)

c     IM((g**2-x**2+#i*x*h)/(m**2-x**2+#i*x*n))
      b2=
     $-x*(x**2*(h-n)+g**2*n-h*m**2)/(x**4+x**2*(n**2-2*m**2)+m**4)

c     phonon3=(o**2-x**2+#i*x*p)/(q**2-x**2+#i*x*k)

c     RE((o**2-x**2+#i*x*p)/(q**2-x**2+#i*x*k))
      c1=
     $(x**4+x**2*(k*p-o**2-q**2)+o**2*q**2)/(x**4+x**2*(k**2-2*q**2)+q**
     $4)
```

```
c      IM((o**2-x**2+#i*x*p)/(q**2-x**2+#i*x*k))
       c2=
      $x*(x**2*(k-p)-k*o**2+p*q**2)/(x**4+x**2*(k**2-2*q**2)+q**4)


c      DIF((x**4-x**2*(b**2-c*f+d**2)+b**2*d**2)/(x**4+x**2*(f**2-2*d**2)
c     $+d**4),b)
       da1db=
      $2*b*(d**2-x**2)/(x**4+x**2*(f**2-2*d**2)+d**4)

c      DIF((x**4-x**2*(b**2-c*f+d**2)+b**2*d**2)/(x**4+x**2*(f**2-2*d**2)
c     $+d**4),c)
       da1dc=
      $f*x**2/(x**4+x**2*(f**2-2*d**2)+d**4)

c      DIF((x**4-x**2*(b**2-c*f+d**2)+b**2*d**2)/(x**4+x**2*(f**2-2*d**2)
c     $+d**4),d)
       da1dd=
      $2*d*(x**6-x**4*(b**2-2*c*f+2*d**2+f**2)+x**2*(b**2*(2*d**2+f**2)+d
      $**2*(d**2-2*c*f))-b**2*d**4)/(x**4+x**2*(f**2-2*d**2)+d**4)**2

c      DIF((x**4-x**2*(b**2-c*f+d**2)+b**2*d**2)/(x**4+x**2*(f**2-2*d**2)
c     $+d**4),f)
       da1df=
      $x**2*(x**4*(c-2*f)+x**2*(2*b**2*f-c*(2*d**2+f**2)+2*d**2*f)+d**2*(
      $c*d**2-2*b**2*f))/(x**4+x**2*(f**2-2*d**2)+d**4)**2

c      DIF(-x*(x**2*(c-f)+b**2*f-c*d**2)/(x**4+x**2*(f**2-2*d**2)+d**4),b
       da2db=-2*b*f*x/(x**4+x**2*(f**2-2*d**2)+d**4)

c      DIF(-x*(x**2*(c-f)+b**2*f-c*d**2)/(x**4+x**2*(f**2-2*d**2)+d**4),c
       da2dc=x*(d**2-x**2)/(x**4+x**2*(f**2-2*d**2)+d**4)

c      DIF(-x*(x**2*(c-f)+b**2*f-c*d**2)/(x**4+x**2*(f**2-2*d**2)+d**4),d
c     $)
       da2dd=
      $-2*d*x*(x**4*(c-2*f)+x**2*(2*b**2*f-c*(2*d**2+f**2)+2*d**2*f)+d**2
      $*(c*d**2-2*b**2*f))/(x**4+x**2*(f**2-2*d**2)+d**4)**2

c      DIF(-x*(x**2*(c-f)+b**2*f-c*d**2)/(x**4+x**2*(f**2-2*d**2)+d**4),f
c     $)
       da2df=
```

```
     $x*(x**6-x**4*(b**2-2*c*f+2*d**2+f**2)+x**2*(b**2*(2*d**2+f**2)+d**
     $2*(d**2-2*c*f))-b**2*d**4)/(x**4+x**2*(f**2-2*d**2)+d**4)**2

c     DIF((x**4-x**2*(g**2-h*n+m**2)+g**2*m**2)/(x**4+x**2*(n**2-2*m**2)
c    $+m**4),g)
      db1dg=2*g*(m**2-x**2)/(x**4+x**2*(n**2-2*m**2)+m**4)

c     DIF((x**4-x**2*(g**2-h*n+m**2)+g**2*m**2)/(x**4+x**2*(n**2-2*m**2)
c    $+m**4),h)
      db1dh=n*x**2/(x**4+x**2*(n**2-2*m**2)+m**4)

c     DIF((x**4-x**2*(g**2-h*n+m**2)+g**2*m**2)/(x**4+x**2*(n**2-2*m**2)
c    $+m**4),m)
      db1dm=
     $2*m*(x**6-x**4*(g**2-2*h*n+2*m**2+n**2)+x**2*(g**2*(2*m**2+n**2)+m
     $**2*(m**2-2*h*n))-g**2*m**4)/(x**4+x**2*(n**2-2*m**2)+m**4)**2

c     DIF((x**4-x**2*(g**2-h*n+m**2)+g**2*m**2)/(x**4+x**2*(n**2-2*m**2)
c    $+m**4),n)
      db1dn=
     $x**2*(x**4*(h-2*n)+x**2*(2*g**2*n-h*(2*m**2+n**2)+2*m**2*n)+m**2*(
     $h*m**2-2*g**2*n))/(x**4+x**2*(n**2-2*m**2)+m**4)**2

c     DIF(-x*(x**2*(h-n)+g**2*n-h*m**2)/(x**4+x**2*(n**2-2*m**2)+m**4),g
      db2dg=-2*g*n*x/(x**4+x**2*(n**2-2*m**2)+m**4)

c     DIF(-x*(x**2*(h-n)+g**2*n-h*m**2)/(x**4+x**2*(n**2-2*m**2)+m**4),h
      db2dh=x*(m**2-x**2)/(x**4+x**2*(n**2-2*m**2)+m**4)

c     DIF(-x*(x**2*(h-n)+g**2*n-h*m**2)/(x**4+x**2*(n**2-2*m**2)+m**4),m
      db2dm=
     $-2*m*x*(x**4*(h-2*n)+x**2*(2*g**2*n-h*(2*m**2+n**2)+2*m**2*n)+m**2
     $*(h*m**2-2*g**2*n))/(x**4+x**2*(n**2-2*m**2)+m**4)**2

c     DIF(-x*(x**2*(h-n)+g**2*n-h*m**2)/(x**4+x**2*(n**2-2*m**2)+m**4),n
      db2dn=
     $x*(x**6-x**4*(g**2-2*h*n+2*m**2+n**2)+x**2*(g**2*(2*m**2+n**2)+m**
     $2*(m**2-2*h*n))-g**2*m**4)/(x**4+x**2*(n**2-2*m**2)+m**4)**2

c     DIF((x**4+x**2*(k*p-o**2-q**2)+o**2*q**2)/(x**4+x**2*(k**2-2*q**2)
c    $+q**4),o)
      dc1do=2*o*(q**2-x**2)/(x**4+x**2*(k**2-2*q**2)+q**4)
```

```
c     DIF((x**4+x**2*(k*p-o**2-q**2)+o**2*q**2)/(x**4+x**2*(k**2-2*q**2)
c    $+q**4),p)
      dc1dp=k*x**2/(x**4+x**2*(k**2-2*q**2)+q**4)

c     DIF((x**4+x**2*(k*p-o**2-q**2)+o**2*q**2)/(x**4+x**2*(k**2-2*q**2)
c    $+q**4),q)
      dc1dq=
     $2*q*(x**6-x**4*(k**2-2*k*p+o**2+2*q**2)+x**2*(k**2*o**2-2*k*p*q**2
     $+q**2*(2*o**2+q**2))-o**2*q**4)/(x**4+x**2*(k**2-2*q**2)+q**4)**2

c     DIF((x**4+x**2*(k*p-o**2-q**2)+o**2*q**2)/(x**4+x**2*(k**2-2*q**2)
c    $+q**4),k)
      dc1dk=
     $-x**2*(x**4*(2*k-p)+x**2*(k**2*p-2*k*(o**2+q**2)+2*p*q**2)+q**2*(2
     $*k*o**2-p*q**2))/(x**4+x**2*(k**2-2*q**2)+q**4)**2

c     DIF(x*(x**2*(k-p)-k*o**2+p*q**2)/(x**4+x**2*(k**2-2*q**2)+q**4),o)
      dc2do=-2*k*o*x/(x**4+x**2*(k**2-2*q**2)+q**4)

c     DIF(x*(x**2*(k-p)-k*o**2+p*q**2)/(x**4+x**2*(k**2-2*q**2)+q**4),p)
      dc2dp=x*(q**2-x**2)/(x**4+x**2*(k**2-2*q**2)+q**4)

c     DIF(x*(x**2*(k-p)-k*o**2+p*q**2)/(x**4+x**2*(k**2-2*q**2)+q**4),q)
      dc2dq=
     $2*q*x*(x**4*(2*k-p)+x**2*(k**2*p-2*k*(o**2+q**2)+2*p*q**2)+q**2*(2
     $*k*o**2-p*q**2))/(x**4+x**2*(k**2-2*q**2)+q**4)**2

c     DIF(x*(x**2*(k-p)-k*o**2+p*q**2)/(x**4+x**2*(k**2-2*q**2)+q**4),k)
      dc2dk=
     $x*(x**6-x**4*(k**2-2*k*p+o**2+2*q**2)+x**2*(k**2*o**2-2*k*p*q**2+q
     $**2*(2*o**2+q**2))-o**2*q**4)/(x**4+x**2*(k**2-2*q**2)+q**4)**2



      w=a*((a1*b1-a2*b2)*c1-(a1*b2+a2*b1)*c2)
      z=-a*((a1*b1-a2*b2)*c2+(a1*b2+a2*b1)*c1)
c  R= (1-SQRT(w+#i*z))/(1+SQRT(w+#i*z))*((1-SQRT(w-#i*z))/(1+SQRT(w-#i*z
c    $)))
      y=
     $(z**2+w**2-2*w+1)/(SQRT(2)*SQRT(SQRT(z**2+w**2)+w)+SQRT(z**2+w**2)
     $+1)**2

c     DIF((z**2+w**2-2*w+1)/(SQRT(2)*SQRT(SQRT(z**2+w**2)+w)+SQRT(z**2+w
```

```
c    $**2)+1)**2,w)
     dydw=
    $SQRT(2)*((2*(w-1)*SQRT(z**2+w**2)-z**2-w**2+2*w-1)*SQRT(SQRT(z**2+
    $w**2)+w)+SQRT(2)*((w-1)*SQRT(z**2+w**2)-z**2+w*(w-1)))/((SQRT(2)*S
    $QRT(SQRT(z**2+w**2)+w)+SQRT(z**2+w**2)+1)**3*SQRT(z**2+w**2))

c     DIF((z**2+w**2-2*w+1)/(SQRT(2)*SQRT(SQRT(z**2+w**2)+w)+SQRT(z**2+w
c    $**2)+1)**2,z)
     dydz=
    $SQRT(2)*z*(SQRT(2)*SQRT(z**2+w**2)*SQRT(SQRT(z**2+w**2)+w)*(SQRT(z
    $**2+w**2)+1)-SQRT(2)*(z**2+w**2-2*w+1)*SQRT(SQRT(z**2+w**2)+w)+2*w
    $*SQRT(z**2+w**2)+z**2+w**2+2*w-1)/((SQRT(2)*SQRT(SQRT(z**2+w**2)+w
    $)+SQRT(z**2+w**2)+1)**3*SQRT(SQRT(z**2+w**2)+w)*SQRT(z**2+w**2))


     dwda= w/a
     dzda= z/a
     dzdb=a*((da1db*b1-da2db*b2)*c2+(da1db*b2+da2db*b1)*c1)*(-1)
     dzdc=a*((da1dc*b1-da2dc*b2)*c2+(da1dc*b2+da2dc*b1)*C1)*(-1)
     dzdd=a*((da1dd*b1-da2dd*b2)*c2+(da1dd*b2+da2dd*b1)*c1)*(-1)
     dzdf=a*((da1df*b1-da2df*b2)*c2+(da1df*b2+da2df*b1)*c1)*(-1)
     dzdg=a*((a1*db1dg-a2*db2dg)*c2+(a1*db2dg+a2*db1dg)*c1)*(-1)
     dzdh=a*((a1*db1dh-a2*db2dh)*c2+(a1*db2dh+a2*db1dh)*c1)*(-1)
     dzdm=a*((a1*db1dm-a2*db2dm)*c2+(a1*db2dm+a2*db1dm)*c1)*(-1)
     dzdn=a*((a1*db1dn-a2*db2dn)*c2+(a1*db2dn+a2*db1dn)*c1)*(-1)
     dzdo=a*((a1*b1-a2*b2)*dc2do+(a1*b2+a2*b1)*dc1do)*(-1)
     dzdp=a*((a1*b1-a2*b2)*dc2dp+(a1*b2+a2*b1)*dc1dp)*(-1)
     dzdq=a*((a1*b1-a2*b2)*dc2dq+(a1*b2+a2*b1)*dc1dq)*(-1)
     dzdk=a*((a1*b1-a2*b2)*dc2dk+(a1*b2+a2*b1)*dc1dk)*(-1)

     dwdb=a*((da1db*b1-da2db*b2)*c1-(da1db*b2+da2db*b1)*c2)
     dwdc=a*((da1dc*b1-da2dc*b2)*c1-(da1dc*b2+da2dc*b1)*c2)
     dwdd=a*((da1dd*b1-da2dd*b2)*c1-(da1dd*b2+da2dd*b1)*c2)
     dwdf=a*((da1df*b1-da2df*b2)*c1-(da1df*b2+da2df*b1)*c2)
     dwdg=a*((a1*db1dg-a2*db2dg)*c1-(a1*db2dg+a2*db1dg)*c2)
     dwdh=a*((a1*db1dh-a2*db2dh)*c1-(a1*db2dh+a2*db1dh)*c2)
     dwdm=a*((a1*db1dm-a2*db2dm)*c1-(a1*db2dm+a2*db1dm)*c2)
     dwdn=a*((a1*db1dn-a2*db2dn)*c1-(a1*db2dn+a2*db1dn)*c2)
     dwdo=a*((a1*b1-a2*b2)*dc1do-(a1*b2+a2*b1)*dc2do)
     dwdp=a*((a1*b1-a2*b2)*dc1dp-(a1*b2+a2*b1)*dc2dp)
     dwdq=a*((a1*b1-a2*b2)*dc1dq-(a1*b2+a2*b1)*dc2dq)
     dwdk=a*((a1*b1-a2*b2)*dc1dk-(a1*b2+a2*b1)*dc2dk)
```

```
      dyda(1) = dydw*dwda + dydz*dzda
      dyda(2) = dydw*dwdb + dydz*dzdb
      dyda(3) = dydw*dwdc + dydz*dzdc
      dyda(4) = dydw*dwdd + dydz*dzdd
      dyda(5) = dydw*dwdf + dydz*dzdf
      dyda(6) = dydw*dwdg + dydz*dzdg
      dyda(7) = dydw*dwdh + dydz*dzdh
      dyda(8) = dydw*dwdm + dydz*dzdm
      dyda(9) = dydw*dwdn + dydz*dzdn
      dyda(10) = dydw*dwdo + dydz*dzdo
      dyda(11) = dydw*dwdp + dydz*dzdp
      dyda(12) = dydw*dwdq + dydz*dzdq
      dyda(13) = dydw*dwdk + dydz*dzdk

      return
      end
c*****************************************************************

      SUBROUTINE plot2(x,y1,y2,np)
      REAL x(*),y1(*),y2(*)
      call newpag
 400  continue
        call commen(' ')
           call legpos (0.67,0.88)
        call howplt(0,1,2)
        call curv(np,x,y1)
        call howplt(0,1,4)
        call scurv(np,x,y2)
           call vg
      if (loopin() .eq.1)go to 400
      return
      end

c**********
c
c************
      subroutine vgcurs(x,y)
      real savex(20),savey(20)
      common/cdata/savex,savey,ijk
      ijk = ijk+1
      if (ijk.le.20) then
           savex(ijk) = x
           savey(ijk) = y
```

```
      end if
      return
      end

c*****************************************************************
SUBROUTINE DATAIN3 (IDEV,X,Y,SIGY,NDIM,N,CARD,
     1  ICOL,ICX,ICY,ICSIGY,IDENT)
DIMENSION X (NDIM), Y (NDIM) , SIGY (NDIM)
      DIMENSION CARD (ICOL)
      CHARACTER*(*) IDENT
      CHARACTER*2 JUNK
C
      BEL = CHAR (7)
C   First look for a '/*' in cols.; if none present, then reset
C   to the top.
10    READ (IDEV,'(A)',END=2) IDENT
      IF (IDENT .EQ. ' ') GO TO 10
      IF (IDENT(1:2) .EQ. '/*') GO TO 3
1     READ (IDEV,'(A)',END=2) JUNK
      IF (JUNK .EQ. '/*') GO TO 3
      GO TO 1
2     REWIND IDEV
3     K = 0
4     K = K + 1
      IF (K .GT. NDIM) GO TO 5
      READ (IDEV, *, ERR=7, END=5) CARD
      X (K) = CARD (ICX)
      Y (K) = CARD (ICY)
      if (icol .eq. 3) then
         SIGY(K) = CARD(ICSIGY)
      else
         sigy(k) = sqrt(y(k))
      end if
      GO TO 4
5     IF (K .GT. NDIM) WRITE (*,130) BEL,NDIM,NDIM
      N = K - 1
      WRITE (*,'(1H ,A)') IDENT
      WRITE (*,110) N
      RETURN
C  Error-handling portion of code.
7     WRITE (*,120) BEL,K
      K = K - 1
      GO TO 4
```

```
C-----------------------------------------------------------------------
110   FORMAT (' Number of points = ', I5)
120   FORMAT (' ',A1,'?DATIN-W-Unintelligible data in line ', I5,
     1 ' of file.'/' Line skipped: continue reading.')
130   FORMAT (' ',A1,'?DATIN-W-No. of data points exceeds ',I5/
     1 ' Return to main program with first ',I5,' points')
C-----------------------------------------------------------------------
      END
c&&&&&&&&&&&&&&&&&&&&&&&&&&&&&&&&&&&&&&&&&&&&&&&&&&&&&&&&&&&&&&&&&&&&
&
c***********************************************************************
*
c     CHOOSE PEAK TO ANALIZE
C***********************************************************************
**
      SUBROUTINE peake(energy,eels,sigy,npoints,x,y,sig,ndata,a)
      REAL energy(*),eels(*),sigy(*),x(*),y(*),sig(*),a(*),
     &    savex(20),savey(20),xmin,xmax,dydx(2000),dumm(17),yfit1(2000)
      INTEGER ma,option
      LOGICAL first
      CHARACTER ans*1
      COMMON /cdata/savex,savey,ijk

      ma = 17
      ijk = 0
 401  continue
        call commen('    CHOOSE FITTING REGION (z-w-s-*) - 2POINTS
     $or hit [enter] whole range')
        call plac(.95,0.05,0.0,1.)
        call howplt(0,1,3)
        call curv(npoints,energy,eels)
           call vg
           if (loopin() .eq.1)go to 401
           call newpag
c *********
c ***  finding breaking-patching points
c *********
      if (ijk .gt. 0) then
         xmin = savex(1)
         xmax = savex(2)
      else
         xmin = energy(1)
         xmax = energy(npoints)
```

```
    end if
     j = 1
    do i = 1, npoints
     if(energy(i) .ge. xmin .and. energy(i) .le. xmax) then
           x(j) = energy(i)
        y(j) = eels(i)
        sig(j) = sigy(i)
        j = j+1
     end if
    end do
    ndata = j-1
       print*,'data_points to be fitted -> ',ndata
    print*,' '
    call derive(x,y,dydx,ndata)
    ijk = 0
400  continue
     call commen('Choose 8-points with max slope [derivative] ')
     call setgrd(0,1)
     call plac(.95,.05,.05,.95)
     call legpos (0.67,0.88)
     call nolbox
     call legnd('derivative')
     call howplt(0,1,2)
     call curv(ndata,x,dydx)
     call right
     call howplt(0,1,4)
     call legnd('Actual data-right scale')
     call curv(ndata,x,y)
        call vg
    if (loopin() .eq.1)go to 400
    if (ijk .gt. 0) then
       do i = 1,3
          if (savey(2*i-1) .gt. 0) then
             a(4*i) = savex(2*i-1)
             a(4*i-2) = savex(2*i)
          else
             a(4*i) = savex(2*i)
             a(4*i-2) = savex(2*i-1)
          end if
      end do
    end if

    ans = 'y'
```

```
      first = .true.
      do while (ans .eq. 'y' .or. ans .eq. 'Y')
        print*,' Initial guess of fitting parameters '
        do while (first)
        write(*,'(a\)')' Eps infinite -> '
        read(*,*)a(1)
        do i = 1,6
          write(*,'(1x,a,f10.2,t28,a,\)')'frequency -> ',a(2*i),
     $             'damping -> '
          read(*,*)a(2*i+1)
        end do
        first = .false.
        end do
        do while (.not. first)
           print*, ' First guesses trials '
           print*,' '
        do i = 1,6
          write(*,'(1x,i1,a,f10.2,t30,a,f10.2)')i,'-Frequency -> '
     $           ,a(2*i),'damping -> ',a(2*i+1)
        end do
           print*,' '
           write(*,'(a\)')' Choose one to modify -> '
           read(*,'(i1)')option
           write(*,'(a\)')' New value -> '
           read(*,*)a(2*option+1)
           first = .true.
        end do
        first = .false.
        do  n=1,ndata
           call funcs3(x(n),a,yfit1(n),dumm,MA)
        end do
        call plot2(x,y,yfit1,ndata)
       write(*,'(a\)')' Do you want to change damping values (y/n) -> '
        read(*,'(a1)')ans
      end do

      return
      end

c&&&&&&&&&&&&&&&&&&&&&&&&&&&&&&&&&&&&&&&&&&&&&&&&&&&&&&&&&&&&&&&&
      SUBROUTINE derive(x,y,dy,ntotal)
c *** 2.02.96
```

```
      PARAMETER (MAXNP=200)
      INTEGER ntotal,nl,nr,np,ld,m,i,n
      REAL  x(*),y(*),c(MAXNP),dy(*),delx
      CHARACTER option*1

      delx = x(3)-x(2)
      do i = 1,ntotal
         dy(i) = 0
      end do
      print*,' '
      print*,' DERIVATIVE CALCULATION'
      print*,' '
      print*,' X-data has to be equally spaced'
c *** filter parameters
      np = 1
      do while (np .gt. 0)
      write(*,'(a\)')' Number of leftward points? (nl) (try 16) -> '
      read(*,'(i2)')nl
      write(*,'(a\)')' Number of rightward points? (nr) (try 16) -> '
      read(*,'(i2)')nr
      print*, 'np = nl+nr+1'
      np=nl+nr+1
      write(*,'(a\)') 'ld=0 => smooth, ld=1 => deriv, ld=? -> '
      read(*,'(i2)')ld
      write(*,'(a\)')' Order of smoothing polynomial (m) suggested(4) ->
     * '
      read(*,'(i2)')m
      call savgol(c,np,nl,nr,ld,m)
c *** CONVOLUTION LOOP
      do i =nl+1,ntotal-nr
         dy(i)= 0
         do n = 1,nl+1
            dy(i)=dy(i) + c(n)*y(i-n+1)
         end do
         do n = np,nl+2,-1
            dy(i) =dy(i) + c(n)*y(i+np-n+1)
         end do
         if (ld.eq.1) dy(i)=dy(i)/delx
      end do
c --- PLOT RESULTS
101   continue
        call commen(' ')
        call plac(.95,0.05,0.05,0.95)
```

```
  call axcode(0,3,1)
  call legpos(.67,.88)
  call howplt(0,1,3)
  call legnd('Input data')
  call curv(ntotal,x,y)
  call howplt(0,1,4)
  if (ld.eq.1) call right
  call legnd('First derivative')
  call curv(ntotal,x,dy)
  call vg
     if(loopin() .eq. 1) go to 101
call newpag
write(*,'(a\)')' Do you want to redo? (y/n) -> '
read(*,'(a1)')option
if (option .eq. 'n' .or. option .eq. 'N') np = -1
end do

return
END
```

Appendix D Effective Medium Approximation Programs

EMA2.FOR performs the Bruggeman effective medium approximation.
MGEMA1.FOR performs the Maxwell-Garnett effective medium approximation.
TADCRFL1.FOR performs the generalized effective medium approximation for reflectivity experiments.

```
      PROGRAM ema2
c --- Rey Gonzalez
c --- 3.01.96
c --- BRUGGEMAN EFFECTIVE MEDIUM APPROXIMATION
      PARAMETER(NMAX=3000)
      REAL w(NMAX),na(NMAX),ka(NMAX),nb(NMAX),kb(NMAX),eps1p(NMAX),
     &    eps2p(NMAX),eps1n(NMAX),eps2n(NMAX),navgp,kavgp,navgn,kavgn,
     &    savex(20),savey(20),break(20),epsare(NMAX),epsbre(NMAX)
      INTEGER ndata
      COMPLEX epsa, epsb, b, epsavgp, epsavgn, ncp, ncn
      COMMON /cdata/savex,savey,ijk

      print*,' BRUGGEMAN EFFECTIVE MEDIUM APPROXIMATION '
      print*,' '
      print*,' MAKE SURE ALL INPUT PARAMETERS HAVE SAME RANGE AND '
      print*,' SAME STEP SIZE -- PROGRAM DOES NOT CHECK THESE VALUES '
      print*,' '
c --- READ IN OPTICAL PARAMETERS N AND K
      print*,'READ IN (N) OF COMPONENT (A) '
      call readin(ndata,w,na)
      print*,'READ IN (K) OF COMPONENT (A) '
      call readin(ndata,w,ka)
      print*,'READ IN (N) OF COMPONENT (B) '
      call readin(ndata,w,nb)
      print*,'READ IN (K) OF COMPONENT (B) '
      call readin(ndata,w,kb)
      write(*,'(a\)')' Fractional concentration of (A) -> '
      read(*,*)fa
      write(*,'(a\)')' Fractional concentration of (B) -> '
      read(*,*)fb

      ijk = 0
```

```
      do i=1,20
         break(i) = 0.
      end do
      do i = 1, ndata
         epsa = cmplx(na(i)**2-ka(i)**2,2.*na(i)*ka(i))
         epsb = cmplx(nb(i)**2-kb(i)**2,2.*nb(i)*kb(i))
         b= fa*(epsb - 2.*epsa) + fb*(epsa - 2.*epsb)
         epsavgp = (-b + csqrt(b**2+8.*epsa*epsb))/4.
         epsavgn = (-b - csqrt(b**2+8.*epsa*epsb))/4.
         epsare(i) = real(epsa)
         epsbre(i) = real(epsb)
         eps1p(i) = real(epsavgp)
         eps1n(i) = real(epsavgn)
      end do
      print*,' '
      pause 'IN NEXT GRAPH SEE EPSRE_SHAPE - hit [enter] to plot'
      call plot2(ndata,w,epsare,ndata,w,epsbre,'eps-a real     ',
     &    'eps-b real     ',.false.)
      print*,' '
      pause 'IN NEXT GRAPH SAVE CROSSING POINTS!! - hit [enter] to plot'
      call plot2(ndata,w,eps1p,ndata,w,eps1n,'eps1 pos root',
     &    'eps1 neg root',.false.)
      if (ijk .gt. 0) then
         do i =1, ijk
            break(i) = savex(i)
            print*,i,break(i)
         end do
      end if
      print*,' '
      pause ' HIT [ENTER] TO CONTINUE '
      j = 1
      alpha = 1.
      do i = 1, ndata
         if (w(i) .gt. break(j) .and. j.le.ijk) then
            alpha = -1. * alpha
            j = j+1
         end if
c         print*,w(i),alpha
C         pause
         epsa = cmplx(na(i)**2-ka(i)**2,2.*na(i)*ka(i))
         epsb = cmplx(nb(i)**2-kb(i)**2,2.*nb(i)*kb(i))
         b= fa*(epsb - 2.*epsa) + fb*(epsa - 2.*epsb)
         epsavgp = (-b + alpha*csqrt(b**2+8.*epsa*epsb))/4.
```

```
          epsavgn = (-b - alpha*csqrt(b**2+8.*epsa*epsb))/4.
          eps1p(i) = real(epsavgp)
          eps1n(i) = real(epsavgn)
          eps2p(i) = aimag(epsavgp)
          eps2n(i) = aimag(epsavgn)

         ncp = csqrt(epsavgp)
         ncn = csqrt(epsavgn)
         navgp = real(ncp)
         kavgp = aimag(ncp)
          navgn = real(ncn)
          kavgn = aimag(ncn)
          na(i) = navgp
          ka(i) = kavgp
          nb(i) = navgn
          kb(i) = kavgn
       end do


       call plot2(ndata,w,eps1p,ndata,w,eps1n,'eps1 pos root',
      &    'eps1 neg root',.false.)
       call plot2(ndata,w,eps2p,ndata,w,eps2n,'eps2 pos root',
      &    'eps2 neg root',.false.)
       call plot2(ndata,w,na,ndata,w,nb,'n pos root','n neg root',
      &     .false.)
       call plot2(ndata,w,ka,ndata,w,kb,'k pos root','k neg root',
      &     .false.)
       print*,' SAVE N-AVG-POS'
       call save(w,na,ndata)
       print*,' SAVE N-AVG-NEG'
       call save(w,nb,ndata)
       print*,' SAVE K-AVG-POS'
       call save(w,ka,ndata)
       print*,' SAVE K-AVG-NEG'
       call save(w,kb,ndata)

       stop
       end
c*******************************************************
       subroutine vgcurs(x,y)
       real savex(20),savey(20)
       common/cdata/savex,savey,ijk
       ijk = ijk+1
```

```
if (ijk.le.20) then
     savex(ijk) = x
     savey(ijk) = y
end if
return
end
```

```
      PROGRAM MGema1
c --- Rey Gonzalez
c --- 3.01.96
c --- MAXWELL-GARNETT EFFECTIVE MEDIUM APPROXIMATION
      PARAMETER(NMAX=3000)
      REAL w(NMAX),na(NMAX),ka(NMAX),nb(NMAX),kb(NMAX),eps1p(NMAX),
     &    eps2p(NMAX),eps1n(NMAX),eps2n(NMAX),navgp,kavgp,navgn,kavgn,
     &    savex(20),savey(20),break(20),epsare(NMAX),epsbre(NMAX)
      INTEGER ndata
      COMPLEX epsa, epsb, b, epsavgp, epsavgn, ncp, ncn
      COMMON /cdata/savex,savey,ijk

      print*,' MAXWELL-GARNETT EFFECTIVE MEDIUM APPROXIMATION '
      print*,' '
      print*,' MAKE SURE ALL INPUT PARAMETERS HAVE SAME RANGE AND '
      print*,' SAME STEP SIZE -- PROGRAM DOES NOT CHECK THESE VALUES '
      print*,' '
c --- READ IN OPTICAL PARAMETERS N AND K
      print*,'READ IN (N) OF COMPONENT (SPHERES) '
      call readin(ndata,w,na)
      print*,'READ IN (K) OF COMPONENT (SPHERES) '
      call readin(ndata,w,ka)
      print*,'READ IN (N) OF COMPONENT (MATRIX) '
      call readin(ndata,w,nb)
      print*,'READ IN (K) OF COMPONENT (MATRIX) '
      call readin(ndata,w,kb)
      write(*,'(a\)')' Fractional concentration of spheres -> '
      read(*,*)fa
      fb=1. - fa
      write(*,'(a,f8.3)')' Fractional concentration of matrix -> ',fb

      ijk = 0
      do i=1,20
         break(i) = 0.
      end do
      do i = 1, ndata
         epsa = cmplx(na(i)**2-ka(i)**2,2.*na(i)*ka(i))
         epsb = cmplx(nb(i)**2-kb(i)**2,2.*nb(i)*kb(i))
         epsavg = epsb*(epsa*(1+2*fa)+2*epsb*(1-f))
         epsavg = epsavg/(epsa*(1-f) + epsb*(2+f))
         navg(i) = real(csqrt(epsavg))
         kavg(i) = aimag(csqrt(epsavg))
      end do
```

```
      print*,' SAVE N-AVG'
      call save(w,navg,ndata)
      print*,' SAVE K-AVG'
      call save(w,kavg,ndata)

      stop
      end
c*******************************************************
      subroutine vgcurs(x,y)
      real savex(20),savey(20)
      common/cdata/savex,savey,ijk
      ijk = ijk+1
      if (ijk.le.20) then
          savex(ijk) = x
          savey(ijk) = y
      end if
      return
      end
```

```
      PROGRAM tadcRFL1
C----    Rey Gonzalez
C----   March /96
C
C ---    Evaluation of average dielectric function
c         4-parameter dielectric function used to fit experimental
c       titania thin film on Pt or Mo
c
c         To match experimental broadeness, damping constants can be
c         multiplied, large aggregation factors are possible, and
c         particle shape distribution function can be generated
cc
      PARAMETER(m2=3,npeaks = 9,ndim = 5000,ntot = 40,npartc = 5,m21=21)
      REAL energy(ndim),transexp(ndim),transth(ndim),energyth(ndim),
     &       eps1,eps2,w,pi,gpar,gper(ntot),aggr(ntot),
     &      thick,fac3,factortot,widthfactor,
     &       factor(npartc),gpermax(npartc),gperwidth(npartc),
     &       wlopar(npeaks),wtopar(npeaks),gammalopar(npeaks),
     $       gammatopar(npeaks),wloper(npeaks),wtoper(npeaks),
     $       gammaloper(npeaks),gammatoper(npeaks),epsinfpar4,
     $     epsinfper4,lh,dh,ypos,gpertot(5*ntot),aggrtot(5*ntot),
     &      no,hthick(0:m21),notheta,rp,rs,tr
      COMPLEX*16 epsc(0:m2),csqrt,cmplx,epsparn(5*ntot),epspars(5*ntot),
     &      epspern(5*ntot),epspers(5*ntot),partialn,partials,epsavg,nc,
     &       nc1(0:m21),cosc1(0:m21),identity(2,2)
      INTEGER i,nmax,i1,ntypes,npeakpar4,npeakper4,i2,j,k,k1,nmaxtot,
     %        nexp
      CHARACTER fname*40,answer*1,text*12
      common /com1/pi
      common /com2/identity
      data pi/3.14159265/, identity/1.,0.,0.,1./
c**********
c*****          INPUT DATA
C**********
      print*,' Average dielectric constant  '
      print*,' Fit up to 5 particle shape distributions'
      print*,' '
 110  format(a40)
      print*,' Filename with "initial" data -> '
      read(*,'(a40)')fname
      open(31,file = fname, status = 'old')
      do i = 1,2
           read(31,110)fname
```

```
      print*,'file substrate_n&k (1st), exp_data(2nd) ->',fname
      open(i,file = fname, status = 'old')
    end do
    print*,' FOUR PARAMETER DATA '
    read(31,'(i1)')npeakpar4
    read(31,'(i1)')npeakper4
    write(*,'(a,i1)')' Number of parallel phonon modes -> ',npeakpar4
    write(*,'(a,i1)')' Number of perpendc phonon modes -> ',npeakper4
    read(31,*)epsinfpar4
    read(31,*)epsinfper4
    write(*,'(a,f8.4)')' eps infinity parallel  -> ',epsinfpar4
    write(*,'(a,f8.4)')' eps infinity perpendic -> ',epsinfper4
    do i = 1, npeakpar4
        read(31,*)wtopar(i),wlopar(i),gammatopar(i),gammalopar(i)
    end do
    print*,'              PARALLEL MODE '
    print*,'   WTO.        WLO        GAMMATO          GAMMALO '
    do i = 1, npeakpar4
        write(*,*)wtopar(i),wlopar(i),gammatopar(i),gammalopar(i)
    end do
    do i = 1, npeakper4
        read(31,*)wtoper(i),wloper(i),gammatoper(i),gammaloper(i)
    end do
    print*,'              PERPENDICULAR MODE '
    print*,'   WTO.        WLO         GAMMATO         GAMMALO'
    do i = 1, npeakper4
        write(*,*)wtoper(i),wloper(i),gammatoper(i),gammaloper(i)
    end do
c
c ----   TEMPORAL-DATA INPUT
    answer = 'y'
    do while (answer .eq. 'y' .or. answer .eq. 'Y')
    do i = 1,2
       rewind i
    end do
    factortot = 0.
    write(*,'(a \)') ' ENTER incident angle [degrees] ---> '
    read(*,*) theta
    write(*,'(a \)') ' ENTER thicknes [um] ---> '
    read(*,*) thick
    write(*,'(a \)') ' ENTER number of particle types ---> '
    read(*,*) ntypes
    do i1 = 1,ntypes
```

```
      write(*,'(a,i1)')' Data of particles set -> ',i1
      write(*,'(a \)') ' ENTER Aggreg. factor (f) ---> '
      read(*,*) factor(i1)
      write(*,'(a \)') ' ENTER Shape factor <gper> ---> '
      read(*,*) gpermax(i1)
      write(*,'(a \)') ' ENTER gperwidth ---> '
      read(*,*) gperwidth(i1)
      factortot = factortot + factor(i1)
      write(*,'(a)') ' gpar --- (2gper + gpar = 1)  '
      end do
      write(*,'(a\)')' ENTER damping-constants multiplication-factor ->'
      read(*,*)widthfactor
c
c ----   CALCULATIONS
c
c ---    MODIFYING DAMPING CONSTANTS BY A GIVEN FACTOR
            do i2 = 1, npeakpar4
                  gammatopar(i2)=gammatopar(i2)*widthfactor
                  gammalopar(i2)=gammalopar(i2)*widthfactor
            end do
            do i2 = 1, npeakper4
                  gammatoper(i2)=gammatoper(i2)*widthfactor
                  gammaloper(i2)=gammaloper(i2)*widthfactor
            end do
c
c ___   EVALUATING SHAPE DISTRIBUTION FUNCTIONS
           k = 0
           do i1 = 1, ntypes
             call aggrfnct(factor(i1),gpermax(i1),gperwidth(i1),
     &             ntot,nmax,gper,aggr)
             do k1=1,nmax
               k = k+1
               gpertot(k) = gper(k1)
               aggrtot(k) = aggr(k1)
             end do
           end do
           nmaxtot = k
c
c ---   READ IN EXPR DATA AND SUBSTRATE DIELECTRIC CONSTANTS
      j=0
      do while (.not. eof(2))
           j =j+1
           read(2,*)energy(j),transexp(j)
```

```
      end do
      nexp = j
      i = 0
      do while (.not.eof(1))
            i = i+1
            read(1,*)w,eps1,eps2
            energyth(i) = w
            epsc(1) = cmplx(1.,0.)
c
c ----   Evaluation OF 4-PARAMETER dielectric functions
            epsc(2) = cmplx(epsinfpar4,0.)
            epsc(3) = cmplx(epsinfper4,0.)
            do i2 = 1, npeakpar4
                  epsc(2) = epsc(2)*(wlopar(i2)**2-w**2-
     $            cmplx(0.,gammalopar(i2)*w))/(wtopar(i2)**2-w**2-
     $            cmplx(0.,gammatopar(i2)*w))
            end do
            do i2 = 1, npeakper4
                  epsc(3) = epsc(3)*(wloper(i2)**2-w**2-
     $            cmplx(0.,gammaloper(i2)*w))/(wtoper(i2)**2-w**2-
     $            cmplx(0.,gammatoper(i2)*w))
            end do
C
C ---    EVALUATION OF AVERAGE DIELECTRIC FUNCTION
           partialn = 0.
           partials = 0.
           do j = 1, nmaxtot
              gpar = 1-2*gpertot(j)
         call epsilon(epsc(1),epsc(2),gpar,epsparn(j),epspars(j))
         call epsilon(epsc(1),epsc(3),gpertot(j),epspern(j),
     &              epspers(j))
         partialn = aggrtot(j)*(epsparn(j)+2*epspern(j))+partialn
         partials = aggrtot(j)*(epspars(j)+2*epspers(j))+partials
            end do
            fac3 = 3*(1-factortot)
         epsavg = 1. + (fac3*(epsc(1)-1)+partials)/(fac3+partialn)
         nc = csqrt(epsavg)
c          nc= csqrt(epsc(3))
C ---     CALCULATIONS OF REFLECTANCE
          m=1
          hthick(0) = 0.
          no = 1.
          hthick(m) = thick
```

```
        hthick(m+1) = 0.
        nc1(0) = cmplx(no,0.)
        notheta =no*sin(pi*theta/180.)
        nc1(1) = nc
        nc1(2) = cmplx(eps1,eps2)
        do kl = 0,m+1
           cosc1(kl) = csqrt(1.-(notheta/nc1(kl))**2)
        end do
        jk6 = 1
        delz = .001

        call calculation(nc1,cosc1,hthick,w,notheta,jk6,delz,m,m21,
     &         rs,rp,tr,tr,tr,tr,tr,tr,tr,tr,tr,tr,tr,tr)
        transth(i) = rp

      end do
      nmax = i
C
c ----  Reset attenuation parameters
            do i2 = 1, npeakpar4
                  gammatopar(i2)=gammatopar(i2)/widthfactor
                  gammalopar(i2)=gammalopar(i2)/widthfactor
            end do
            do i2 = 1, npeakper4
                  gammatoper(i2)=gammatoper(i2)/widthfactor
                  gammaloper(i2)=gammaloper(i2)/widthfactor
            end do
c
c ----- Plot results on screen
      CALL NEWPAG
      lh = .8
      dh = .04
      ypos = .9
      ypos2 = .25
 1800 CONTINUE
        call axcode(0,3,1)
           CALL PLAC(1.,.3,0.,.85)
      call sidtex('Theory Avg. Dielectric Const.',11,
     $        'Energy [cm^-^1] ',11,'Reflectance',11,' ',0)
      CALL HOWPLT(23,0,1)
      CALL CURV(nexp,energy,transexp)
cc      call right
      CALL HOWPLT(0,1,15)
```

```
      CALL CURV(nmax,energyth,transth)
      CALL VG
           CALL PLAC(.3,0.,0.,.4)
           CALL SIDTEX(' ',11,'g_p_e_r',11,'f_k',11,' ',0)
c          CALL SETGRD(0,1)
           call setlim(1,3,0.,.5)
           CALL HOWPLT(23,0,1)
           CALL CURV(nmaxtot,gpertot,aggrtot)
           CALL VG
           CALL HTEX('Number of',.87,ypos,0.,lh,11)
           CALL HTEX('Particles',.87,ypos-dh,0.,lh,11)
           WRITE(TEXT,2000)ntypes
 2000      FORMAT('   ',I2)
           CALL HTEX(TEXT,.87,ypos-2*dh,0.,lh,1)
           CALL HTEX('Thick-|mm',.87,ypos-4*dh,0.,lh,11)
           WRITE(TEXT,1900)thick
 1900      FORMAT(F8.1)
           CALL HTEX(TEXT,.87,ypos-5*dh,0.,lh,1)
1950       FORMAT(F7.4)
          CALL HTEX('Damping',.87,ypos-7*dh,0.,lh,11)
          CALL HTEX(' Factor ',.87,ypos-8*dh,0.,lh,11)
           WRITE(TEXT,1950)widthfactor
           CALL HTEX(TEXT,.87,ypos-9*dh,0.,lh,1)
        CALL HTEX('Particle  -- Aggreg. factor',
     &      .5,ypos2,0.,lh,11)
          do i11 =1,ntypes
          WRITE(TEXT,1950)factor(i11)
        CALL HTEX(TEXT,.5,ypos2-i11*dh,0.,lh,1)
          end do
 2050      FORMAT(F7.4)
      IF(LOOPIN().EQ.1)GOTO 1800
c
c ---  Saving data
      print*,'Do you want to save this data in a file? (y/n) -> '
      read(*,'(a1)')ans5
      if (ans5 .eq. 'y' .or. ans5 .eq. 'Y') then
           print*,'ENTER THE NAME OF THE OUTPUT  FILE'
           read(*,'(a)') fname
           open(unit=8,file=fname,status='unknown')
           do  i = 1, nmax
          write(8,'(e12.6,a,e12.6)')energyth(i),',',transth(i)
           end do
           close(8)
```

```
      end if
      print*,'Do you want to CHANGE parameters? (y/n) -> '
      read(*,'(a1)')answer
      end do

      stop
      end
c*********************************************************************
          SUBROUTINE epsilon(epsmc,epsc,g,epsn,epss)
        COMPLEX*16 epsmc,epsc,epsn,epss
          REAL g
          epsn = 1/(1+g*((epsc/epsmc)-1))
          epss = (epsc - 1) * epsn
          return
          end

c*********************************************************************
*
      SUBROUTINE transmittance(nc,w,d,tabsr)
c
c     SUBROUTINE TO COMPUTE TRANSMITANCE, NORMAL INCIDENCE
c
      REAL d,w,pi,tabsr,beta
      COMPLEX etha,nc,tabs,cmplx,cexp,conjg
      pi = 3.141592654
      beta = 2*pi*d*1.e-4
          etha = cexp(cmplx(-aimag(nc),real(nc))*w*beta)
          tabs = log(4*nc)+cmplx(-aimag(nc),real(nc))*w*beta-
     $          log((nc+1)**2-((1-nc)*etha)**2)
          tabsr =-tabs-conjg(tabs)
      return
      end
c ************************************************************
      SUBROUTINE aggrfnct(factormax,gpermax,gperwidth,ntot,nmax,
     &                        gper,aggr)
C
c --- sub to generate particle distribution-function
c
      REAL factormax,gpermax,gperwidth,a,b,gper(ntot),aggr(ntot),k
      INTEGER i,nmax
c
      k = 0.
      b = .86*gperwidth
```

```
a = gpermax - 1.2247*b
delg = 3*gperwidth/34
g0 = gpermax - 1.5*gperwidth
i1 = 0
do i = 1, 34
     param = g0 + delg*(i+2)
     if (param .ge. 0. .and. param .le. 0.5)  then
        i1 = i1 +1
        gper(i1) = param
        aggr(i1) = (gper(i1) - a)**3*exp(-((gper(i1)-a)/b)**2)
        k = k + aggr(i1)
     end if
end do
nmax =  i1
k = factormax/k
do i = 1,nmax
       aggr(i) = k*aggr(i)
end do
return
end
```

Appendix E Dilor XY Raman Spectrometer Data Acquisition

Three programs are needed:
NEFIT1.FOR calculates the correction factors (slope, and y-intercept) to calibrate the frequency data. Input files are the *.PKS obtained from LabCalc after doing a fit to spectrum.
NECOR.BAT, calls NICOR1.FOR and corrects, at once, all the files subject to the calibration determined for that set of measurements.

```
      PROGRAM nefit1
c --  Rey Gonzalez
c --  4.28.95

      PARAMETER (ndim = 1500, npt =50,npol=3)
      REAL tpc(ndim),temp(ndim),newdata(ndim),center(npt),height(npt),
     $     left(npt),right(npt),newcent(npt),
     $     x,yold,ynew,delx,nepeaks(15),q,ynn(npt),sigy(npt)
      LOGICAL fileok, test
      CHARACTER filnam*12,infil*12,nfilnam*12,ofilnam*12,name*6
      CHARACTER letter*1,junk*80
      INTEGER i, ndata,j,k,npeaks, oldi, ngauss,npremove
      DATA nepeaks/162.1637,172.225,178.9011,218.769,237.099,243.3714,
     $257.2534,286.6786,329.3925,560.7665,584.1387,676.1503,712.3833,
     $720.0556,918.5472/

      write(*,'(a\)')' *.prn file_name [6 char. otherwise redefine] -> '
      read(*,'(a)')filnam
      I=0
  160 CONTINUE
      I=I+1
      LETTER=FILNAM(I:I)
      IF(I.LE.LEN(FILNAM).AND.LETTER.NE.' '.AND.LETTER.NE.'.')GOTO 160
      NAMLEN=I-1
      NAME=FILNAM(1:NAMLEN)
      NFILNAM =name//'.prn'
      ofilnam =name//'.pks'
      OPEN(3,FILE=NFILNAM,STATUS='OLD')
      OPEN(4,FILE=OFILNAM,STATUS='new')
c
c --  Create one file out of 4 input_files
      do i1 = 1,4
```

```
        infil =name//char(i1+48)//'.pks'
        INQUIRE(FILE=infil,EXIST=FILEOK)
        WRITE(*,'(1x,A)')INFIL
         IF(FILEOK)THEN
          OPEN(7,FILE=infil,STATUS='OLD')
         ELSE
           PRINT *,'File does not exist -- try again.'
           stop
         ENDIF
         read(7,'(a)')junk
         read(7,'(a)')junk
         i=1
         read(7,*)center(i),height(i),left(i),right(i)
         do while (abs(right(i)) .gt. 1.e-5)
            i = i+1
            read(7,*)center(i),height(i),left(i),right(i)
         end do
         ngauss = i-1
         close(7)
         do j = 1, ngauss
           write(4,*)center(j),height(j),left(j),right(j)
         end do
      end do
c
c --  Find peak centers
      rewind 4
      i= 1
      do while (.not. eof(4))
         i = i+1
         read(4,*)center(i),height(i),left(i),right(i)
      end do
      ngauss = i-1
      close(4)
      i=0
      do while (.not. eof(3))
      i=i+1
      read(3,*)temp(i),tpc(i)
      end do
      close(3)
      ndata = i
***************
*         Calculations
****************
```

```
 do i = 1,ndata
      newdata(i)=0.
      call gaussum1(temp(i),newdata(i),center,height,left,right,
$         ngauss,npt)
 end do

 oldi = 1
 i = 1
 j = 1
 do while (i+1 .lt. ndata)
  i=oldi
      do while (newdata(i+1) .le. newdata(i) .and. i+1 .le. ndata)
         i = i+1
  end do
      k = i
      do while (newdata(i+1) .gt. newdata(i) .and. i+1 .le. ndata)
         i = i+1
  end do

      if (i+1 .le. ndata) then
        test = .true.
      else
        test = .false.
      end if

      do while (test)
        test = .false.
    oldi = i+1
        k1 =oldi
        x = temp(i-1)
        delx = (temp(i) - temp(i-1))/30.
        yold = newdata(i-2)
        ynew = newdata(i-1)
        do while(ynew .gt. yold)
          yold = ynew
          x = x + delx
          call gaussum1(x,ynew,center,height,left,right,ngauss,npt)
        end do
        newcent(j) = x - delx
  end do
      j = j+1
 end do
 npeaks = j-2
```

```
      if (npeaks .gt. 15) then
         print*,' Ne_peaks:'
         do i = 1,10
            print*,i,nepeaks(i)
         end do
         print*,' Peaks found: '
         do i = 1,npeaks
            print*,i,newcent(i)
         end do
         write(*,'(a\)')' Give peak_number to remove -> '
         read(*,'(i2)')npremove
         do i =npremove, npeaks-1
            newcent(i) = newcent(i+1)
         end do
         npeaks = npeaks -1
      end if
c
c --  Linear fit with Raman Ne_calibrated peaks
c      open(8,file='test',status='unknown')
      do i = 1,npeaks
         print*,newcent(i),nepeaks(i)
c          write(8,*)newcent(i),nepeaks(i)
      end do
      pause
c      close(8)
      call fit(newcent,nepeaks,npeaks,sigy,0,a,b,siga,sigb,chi2,q)
      do i = 1, npeaks
         ynn(i) = a + b*newcent(i)
      end do
101    continue
       write(*,'(1x,a,f12.6)')'chi-squared -> ',chi2
       write(*,'(1x,a,f12.6)')'Q -> ',q
          write(*,'(1x,e12.6,a,e10.4)')a,'  +-',siga
          write(*,'(1x,e12.6,a,e10.4)')b,'  +-',sigb
       call plac(.8,0.,0.1,0.9)
       call howplt(17,0,3)
       call curv(npeaks,newcent,nepeaks)
          call nolbox
       call howplt(0,1,4)
       call curv(npeaks,newcent,ynn)
       call vg
          if(loopin() .eq. 1) go to 101
      call newpag
```

```
      stop
      end


*%%%%%%%%%%%%%%%%%%%%%%%%%%%%%%%%%%%%%%%%%%%%%%%%%%%%%%%%%%%%%%%%%%%%%%%
**********************************************************************
      SUBROUTINE gaussum1(x,y,center,height,left,right,ngauss,npt)
      REAL x,y, center(npt),height(npt),left(npt),right(npt)
      INTEGER ngauss, j
      y = 0.
      do j =1,ngauss
            y = y + height(j)*exp(-((x-center(j))*1.665/
     $              (right(j)-left(j)))**2)
      end do
      return
      end
```

NECOR.BAT

```
REM:  THIS FILE CORRECTS "DILOR XY" FILES
REM:  USING NE SPECTRUM AS REFERENCE
REM:
pause files must be IN the directory of conversion
DIR *.PRN >FDIR.LIS
c:\rey\raman\necor1
ERASE FDIR.LIS
rem: ERASE *.
```

```
      PROGRAM necor1
      PARAMETER(ndim=3000)
      REAL x(ndim),y(ndim),card(10)
      INTEGER ndata
      CHARACTER LETTER*1,NAME*60, ident*60
      LOGICAL FILEOK
*
       CHARACTER*3 TEST,TYPE
       CHARACTER*12 INFIL,OUTFIL
       CHARACTER*1 C1,C2,C3,C4,C5,C6,C7,C8
c***
*
       OPEN(1,FILE='FDIR.LIS')
          READ(1,*)
          READ(1,*)
          READ(1,*)
          READ(1,*)
          READ(1,*)
*
       TEST='PRN'
       TYPE='PRN'
c********
c     Read in slope and y-intercept  to correct x-axis
c********
      write(*,'(a\)')' Slope -> '
      read(*,*)slope
      write(*,'(a\)')' Y-intecept -> '
      read(*,*)yintercept
c**************
```

```
*
555   CONTINUE
      READ(1,1000)C1,C2,C3,C4,C5,C6,C7,C8,TYPE
      IF(TYPE.NE.TEST)go to 102
      IF(C8.NE.' ') GO TO 10
      IF(C7.NE.' ') GO TO 20
      IF(C6.NE.' ') GO TO 30
      IF(C5.NE.' ') GO TO 40
      IF(C4.NE.' ') GO TO 50
      IF(C3.NE.' ') GO TO 60
      IF(C2.NE.' ') GO TO 70
      IF(C1.NE.' ') GO TO 80

10    INFIL=C1//C2//C3//C4//C5//C6//C7//C8//'.prn'
        OUTFIL=C1//C2//C3//C4//C5//C6//C7//C8//'.prn'
      GOTO 100
20    INFIL=C1//C2//C3//C4//C5//C6//C7//'.prn'
        OUTFIL=C1//C2//C3//C4//C5//C6//C7//'.prn'
      GOTO 100
30    INFIL=C1//C2//C3//C4//C5//C6//'.prn'
        OUTFIL=C1//C2//C3//C4//C5//C6//'.prn'
      GOTO 100
40    INFIL=C1//C2//C3//C4//C5//'.prn'
        OUTFIL=C1//C2//C3//C4//C5//'.prn'
      GOTO 100
50    INFIL=C1//C2//C3//C4//'.prn'
        OUTFIL=C1//C2//C3//C4//'.prn'
      GOTO 100
60    INFIL=C1//C2//C3//'.prn'
        OUTFIL=C1//C2//C3//'.prn'
      GOTO 100
70    INFIL=C1//C2//'.prn'
        OUTFIL=C1//C2//'.prn'
      GOTO 100
80    INFIL=C1//'.prn'
        OUTFIL=C1//'.prn'
*
100   CONTINUE
c***  Open data files
     print*,' '
     print*,' Correcting energy values according to Ne-spectrum'
501   continue
     INQUIRE(FILE=infil,EXIST=FILEOK)
```

```
      WRITE(*,'(1x,A12\)')INFIL
      IF(FILEOK)THEN
        OPEN(5,FILE=infil,STATUS='unknown')
      ELSE
        PRINT *,'File does not exist -- try again.'
          GOTO 501
      ENDIF
      I=0
  150 CONTINUE
      I=I+1
      LETTER=infil(I:I)
      IF(I.LE.LEN(infil).AND.LETTER.NE.' '.AND.LETTER.NE.'.')GOTO 150
      NAMLEN=I-1
      NAME=infil(1:NAMLEN)
C
C --- Read in data.
      call datain(5,x,y,ndim,ndata,card,2,1,2,ident)
      CLOSE(5)
c
c --- X-axis correction
      do i = 1 , ndata
         x(i) = yintercept + slope * x(i)
      end do
c
c --- Save data
      WRITE(*,'(A13)')outfil
      open(6,file=outfil,status='unknown')
      do j = 1, ndata
        write(6,1001)x(j),y(j)
      end do
      close(6)
*
500    GOTO 555
*
1000   FORMAT(8A1,1X,A3)
1001   format(f9.2,',',e12.5)
*
102     STOP
        END
```

Appendix F Electron Energy-Loss Program

A user-friendly program was develop to perform the data analysis of EELS spectra. EELSA1.FOR performs the low energy extrapolation, the q^2 dependence correction, the scaling based on known values of the dielectric function, the multiple scattering correction and the KK to calculate the optical parameters.

```
      PROGRAM EELSA1
c************
c*************
      PARAMETER (ndim = 1000)
      REAL xfinal(ndim),yfinal(ndim),g1(ndim),g1s(ndim),itmult(ndim)
      character  ans2*1,ans3*1

c**********
c     MAIN MENU
c**********
      ans3 = 'y'
      do while (ans3 .eq. 'y' .or. ans3 .eq. 'Y')
      print*,' '
      print*,'  EELS DATA ANALYSIS'
      print*,' '
      print*,'  Zero energy extrapolation ---> [1]'
      print*,'  Q-dependance - Kinemat    ---> [2]'
      print*,'  Normalizing - Scaling     ---> [3]'
      print*,'  Multp._Scatt. - Itermult  ---> [4]'
      print*,'  Re(1/eps), Eps1, Eps2     ---> [5]'
      print*,'  Quit                      ---> [6]'
      print*,' '
      write(*,'(a\)')'  Choose an option -> '
      read(*,'(a1)')ans2
      print*,' '

            if (ans2 .eq. '1' ) then
              call zeep(xfinal,yfinal,ntotal)
            else if (ans2 .eq. '2' ) then
              call kinemats(xfinal,yfinal,ntotal,g1)
            else if (ans2 .eq. '3') then
              call scales(xfinal,g1,ntotal,g1s)
            else if (ans2 .eq. '4') then
              call imes(xfinal,g1s,ntotal,itmult)
            else if (ans2 .eq. '5') then
              call kkes(xfinal,itmult,ntotal)
```

```
          else if (ans2 .eq. '6') then
             ans3 = 'n'
          end if
       end do

      stop
      end
c&&&&&&&&&&&&&&&&&&&&&&&&&&&&&&&&&&&&&&&&&&&&&&&&&&&&&&&&&&&&&&&
&
*     KK-ANALYSIS
*****************************************************************
      SUBROUTINE kkes(x,y,ndata)
      REAL x(*),y(*)
      REAL rinveps(1000),iinveps(1000),
     &   e(1000),ppint,psint,intinf,reps(1000),ieps(1000),denom
      INTEGER ndata,i,j,k,m,n
      REAL a(1000),b(1000),c,pi,x1,x2
      CHARACTER*35 repsflnm,iepsflnm,flnm
      CHARACTER ans5*1
      PARAMETER (PI=3.141593)

      call readin(ndata,x,y)
*****************************************************************************
*CALCULATE THE SLOPE AND INTERCEPT FOR EACH SET (X1,X2,Y1,Y2)
*****************************************************************************
      do 20 i=1,ndata-1
       a(i)=(x(i+1)*y(i)-x(i)*y(i+1))/(x(i+1)-x(i))
       b(i)=(y(i+1)-y(i))/(x(i+1)-x(i))
20     continue

*****************************************************************************
*CALCULATE THE INTERPOLATION TO INFINITY CONSTANT 'C'.
*****************************************************************************
      c=y(ndata)*x(ndata)**3.0
      print*,'INTERPOLATION CONSTANT FOR 1/(E^3)=',c
      print*,'ENTER ENERGY [en] and REAL(1/EPS[en]) )'
      read*,e0,rinvepe0
*****************************************************************
*     CALCULATING A NEW SCALING FACTOR AFTER GOING THROUGH
ITERMUTE
*****************************************************************
      call kke(x,y,sum,ndata,e0)
```

```
      if (e0 .gt. 1.e-7) then
         z = e0/x(ndata)
         intinf=-(c/(2.0*e0**3.0))*log((1-z)*exp(2*z)/(1+z))
      else
         intinf=c/(3.0*x(NDATA)**3.0)
      end if
        re1epse0kk=1-2.0*(sum+intinf)/pi
     print*,' Re(1/eps(Eo)) -> ',rinvepe0
     print*,' Re(1/eps(Eo))_kk -> ',re1epse0kk
     print*,' Wait for calculations ....'
*********************************************************************
*'J' SELECTS THE DATA POINT AND 'K' LOOPS THE INTEGRAL. INTINF IS THE
*CONTRIBUTION TO THE INTEGRAL FROM THE LAST DATA POINT TO INFINITY.
*********************************************************************
     do 40 j=1,ndata-1
      rinveps(j)=0.
      e(j)=(x(j+1)+x(j))/2.0
      do 30 k=1,ndata-1
       x1=x(k)
       x2=x(k+1)
       if((e(j).lt.x1).or.(e(j).gt.x2)) then
        rinveps(j)=rinveps(j)+ppint(x1,x2,a(k),b(k),e(j))
       else
        rinveps(j)=rinveps(j)+psint(x1,x2,a(k),b(k),e(j))
       endif
30     continue
      z = e(j)/x(ndata)
      intinf=-(c/(2.0*e(j)**3.0))*log((1-z)*exp(2*z)/(1+z))
      rinveps(j)=1.0-(rinveps(j)+intinf)*2/pi
c      print*,'energy = ',e(j),'intinf = ',intinf
40    continue
*********************************************************************
*CONVERT REAL AND IMAG.(1/EPS) TO THE REAL AND IMAG. PARTS OF EPS.
*********************************************************************
     do 50 m=1,ndata-1
      iinveps(m)=(y(m+1)+y(m))/2.0
      denom=1.0/(rinveps(m)**2.0+iinveps(m)**2.0)
      reps(m)=denom*rinveps(m)
      ieps(m)=denom*iinveps(m)
50    continue

*********************************************************************
*WRITE REAL AND IMAG. (EPS) TO THE FILES.
```

```
**************************************************************************
105   continue
         call commen(' ')
       call sidtex(' ',1,'Energy [eV]',1,' ',1,' ',1)
         call legpos(0.67,0.88)
         call legnd('MSdata=Imag[eps(inf)/eps]')
         call howplt(0,1,2)
       call curv(ndata,x,y)
         call legnd('Real[1/eps]')
         call howplt(0,1,6)
       call curv(ndata-1,e,rinveps)
       call nolbox
       call vg
         if(loopin() .eq. 1) go to 105
     call newpag
106   continue
         call commen(' ')
       call sidtex(' ',1,'Energy [eV]',1,' ',1,' ',1)
         call legpos(0.67,0.88)
         call legnd('Real[eps/eps(inf)]')
         call howplt(0,1,2)
       call curv(ndata-1,e,reps)
         call legnd('Imag[eps/eps(inf)]')
         call howplt(0,6,3)
       call curv(ndata-1,e,ieps)
         call nolbox
         call vg
         if(loopin() .eq. 1) go to 106
     call newpag

     print*,'Do you want to save this data in a file? (y/n) -> '
     read(*,'(a1)')ans5
     if (ans5 .eq. 'y' .or. ans5 .eq. 'Y') then
     print*,'ENTER THE OUTPUT FILE NAME FOR REAL(EPS/EPS(INF))'
     read(*,'(a)') repsflnm
     print*,'ENTER THE OUTPUT FILE NAME FOR IMAG.(EPS/EPS(INF))'
     read(*,'(a)') iepsflnm
     print*,'ENTER THE OUTPUT FILE NAME FOR REAL (1/eps)'
     read(*,'(a)') flnm
     open(unit=7,file=repsflnm,status='unknown')
     open(unit=8,file=iepsflnm,status='unknown')
     open(unit=9,file=flnm,status='unknown')
     do 60 n=1,ndata-1
```

```
      write(7,*) e(n),reps(n)
      write(8,*) e(n),ieps(n)
      write(9,*) e(n),rinveps(n)
60    continue
     end if
     close(7)
     close(8)
     close(9)

     return
     end
c#####################################################################
c*    MULTIPLE SCATTERING CORRECTIONS
**********************************************************************
     SUBROUTINE imes(energy,g1,ndata,itmult)
     REAL energy(*),g1(*),itmult(*),g2(1000),g3(1000),g1fix(1000),
    &    g1sum,g2sum,g3sum,g1kk,g2kk,g3kk,beta,gama,a,c,wp2,reps,e0
     INTEGER i,k,l,ndata,imax,m

     call readin(ndata,energy,g1)
     write(*,'(a \)') ' ENTER THE PLASMA FREQ SQUARED(IN eV)--->'
     read(*,*) wp2
     write(*,'(a\)')' ENTER ENERGY [en] and REAL(1/EPS[en]) )'
     read(*,*)e0,rinvepe0
     reps = 1 - rinvepe0
     write(*,'(a \)') ' ENTER MAX NUM OF ITERS--->'
     read(*,*) imax
     print*,'  '
     print*,' Wait for calculations .... '
     m=0
     gama = 5.
     do ijk = 1,ndata
        g1fix(ijk) = g1(ijk)
     end do
**********************************************************************
**********************************************************************
     do while ((abs(gama).gt.1.E-04).and.(m.lt.imax))
     m=m+1

*calculate the sum rule for g1
     call sumrule(energy,g1,g1sum,ndata)

*calculate the e0. kk integral for g1
```

```
      call kke(energy,g1,g1kk,ndata,e0)
*************************************************************************
*************************************************************************
*calculate g2
      do 30 k=1,ndata
           g2(k)=0.
           do 20 l=1,k-1
             g2(k)=g2(k)+(g1(k+1-l)*g1(l)+g1(k-l)*g1(l+1))*
     &          (energy(k+1-l)-energy(k-l))/2.
20         continue
30     continue

*calculate the sum rule for g2
      call sumrule(energy,g2,g2sum,ndata)

*calculate the e=0. kk integral for g2
      call kke(energy,g2,g2kk,ndata,e0)
*************************************************************************
*************************************************************************
*calculate g3
      do 50 k=1,ndata
           g3(k)=0.
           do 40 l=1,k-1
             g3(k)=g3(k)+(g2(k+1-l)*g1(l)+g2(k-l)*g1(l+1))*
     &          (energy(k+1-l)-energy(k-l))/2.
40         continue
50     continue

*calculate the sum rule for g3
      call sumrule(energy,g3,g3sum,ndata)

*calculate the e=0. kk integral for g3
      call kke(energy,g3,g3kk,ndata,e0)
*************************************************************************
*************************************************************************
      call findgta(g1sum,g1kk,g2sum,g2kk,g3sum,g3kk,g1(ndata),
     &  g2(ndata),g3(ndata),beta,gama,a,c,wp2,reps,energy(ndata),e0)
      write(*,'(a)') ' FINISHED ITERATION #'
      write(*,*) m
      if (c.lt.0.) then
        print*,' Extrapolation to infinity NEGATIVE - STOP '
        do ijk = 1, ndata
           itmult(ijk) = g1(ijk)
```

```
        end do
        pause
105     continue
          call commen(' ')
       write(*,'(1x,a,e12.5,1x,a,e12.5)') ' BETA -> ',beta,
      $ ' GAMMA -> ',gama
       write(*,'(1x,a,e12.5,1x,a,e12.5)') ' A    -> ',a,
      $ ' C     -> ',c
          call plac(.85,0.,0.05,0.95)
          call legpos(0.67,0.74)
          call legnd('Scaled data ')
          call howplt(0,1,2)
          call curv(ndata,energy,g1fix)
          call legnd('Multp. scattr. correction')
          call howplt(0,1,3)
        call curv(ndata,energy,itmult)
        call nolbox
        call vg
        if(loopin() .eq. 1) go to 105
      call newpag
        call save(energy,itmult,ndata)
        return
      endif

      if((abs(gama).gt.1.E-04).and.(m.lt.imax)) then
           do 60 i=1,ndata
           g1(i)=a*(g1(i)-gama*g2(i)/2.+3.*gama**2.*g3(i)/8.)
60       continue
      endif
      end do

      do  i=1,ndata
        itmult(i)=a*(g1(i)-gama*g2(i)/2.+3.*gama**2.*g3(i)/8.)
      end do
      pause
104   continue
          call commen(' ')
      write(*,'(1x,a,e12.5,1x,a,e12.5)') ' BETA -> ',beta,
      $ ' GAMMA -> ',gama
       write(*,'(1x,a,e12.5,1x,a,e12.5)') ' A    -> ',a,
      $ ' C     -> ',c
          call plac(.85,0.,0.05,0.95)
          call legpos(0.67,0.74)
```

```
          call legnd('Scaled data ')
          call howplt(0,1,2)
          call curv(ndata,energy,g1fix)
          call legnd('Multp. scattr. correction')
          call howplt(0,1,3)
        call curv(ndata,energy,itmult)
        call nolbox
        call vg
           if(loopin() .eq. 1) go to 104
      call newpag
      call save(energy,itmult,ndata)

      return
      end
c%%%%%%%%%%%%%%%%%%%%%%%%%%%%%%%%%%%%%%%%%%%%%%%%%%%%%%%%%%%%%%%%%%%%%%%
c*    SCALING - KK AT A SINGLE ENERGY
**********************************************************************
      SUBROUTINE scales(x,y,ndata,ys)
      REAL x(*),y(*),scale,e0,rinvepe0,c,sum,intinf,z,ys(*)
      PARAMETER (PI=3.141593)

      call readin(ndata,x,y)
      print*,'ENTER ENERGY [en] and REAL(1/EPS[en]) )'
      read*,e0,rinvepe0

**********************************************************************
***
*CALCULATE THE INTERPOLATION TO INFINITY CONSTANT 'C'.
**********************************************************************
****
      c=y(ndata)*x(ndata)**3.0
      print*,'INTERPOLATION CONSTANT FOR 1/(E^3)=',c

**********************************************************************
***
*'KKE' LOOPS THE INTEGRAL. INTINF IS THE
*CONTRIBUTION TO THE INTEGRAL FROM THE LAST DATA POINT TO INFINITY.
**********************************************************************
****
      call kke(x,y,sum,ndata,e0)

       if (e0 .gt. 1.e-7) then
          z = e0/x(ndata)
```

```
          intinf=-(c/(2.0*e0**3.0))*log((1-z)*exp(2*z)/(1+z))
        else
          intinf=c/(3.0*x(NDATA)**3.0)
        end if
         scale=(1-rinvepe0)*PI/(2.0*(sum+intinf))
           print*,'THE SCALE FACTOR IS=',scale

      do i = 1, ndata
         ys(i) = y(i)*scale
      end do
      call save(x,ys,ndata)

      return
      end
c&&&&&&&&&&&&&&&&&&&&&&&&&&&&&&&&&&&&&&&&&&&&&&&&&&&&&&&&&&&&&&&&
c     KINEMAT - Q_DEPENDANCE CALCULATIONS
**********************************************************************
      SUBROUTINE kinemats(xfinal,yfinal,ntotal,g1)
      REAL xfinal(*),yfinal(*),g1(*),mom,momres,e0,kinfact1

      call readin(ntotal,xfinal,yfinal)
      write(*,'(a \)') ' ENTER THE MOMENTUM TRANSFER--->'
      read(*,*) mom
      write(*,'(a \)') ' ENTER THE MOMENTUM RESOLUTION--->'
      read(*,*) momres
      write(*,'(a \)') ' ENTER THE BEAM ENERGY IN keV--->'
      read(*,*) e0

*calculate g1 by dividing the data by the kinematic factor
      do j=1,ntotal
        g1(j)=yfinal(j)/kinfact1(xfinal(j),mom,momres,e0)
      end do
      write(*,'(a)') ' G1 HAS BEEN CALCULATED'
      call save(xfinal,g1,ntotal)

      return
      end

c$$$$$$$$$$$$$$$$$$$$$$$$$$$$$$$$$$$$$$$$$$$$$$$$$$$$$$$$$$$$$$$$$$
c**********************************************************************
c*     ZERO ENERGY EXTRAPOLATION
c**********************************************************************
      SUBROUTINE zeep(xfinal,yfinal,ntotal)
```

```
      external fpoly
      parameter (npt=200, npol=3,ndim=1000)
      real x(npt),y(npt),sigy(npt),a(npol),cvm(npol,npol),u(npt,npol),
     $        v(npol,npol),w(npol),xnn(npt),ynn(npt),xerrs(npt)
      REAL xfinal(*),yfinal(*),energy(ndim),eels(ndim),
     &     savex(60),savey(60)
      INTEGER npoints,ntotal
      CHARACTER  answer*1
      common /cdata/savex,savey,ijk
C
c*** READ IN EXPERIMENTAL DATA
C
      call readin(npoints,energy,eels)
C **********
c *** plotting curve
c ***********
      delx = energy(2)-energy(1)
      print*,' Del-x -> ',delx
      print*,' If delx is zero, break program and remove double data'
      pause
      answer = 'y'
      do while (answer .eq. 'y' .or. answer .eq. 'Y')
      ijk = 0
 400  continue
      write(*,*)' '
      write(*,*)'    To choose fitting region use (s) to see the cursor'
      write(*,*)'    (w) to see its coordinates and (*) to save them'
           call plac(.85,0.,0.05,0.95)
           call howplt(0,1,2)
           call curv(npoints,energy,eels)
           call nolbox
           call vg
           if (loopin() .eq.1)go to 400
           call newpag
c *********
c ***  finding breaking-patching points
c *********
      if (ijk .gt. 0) then
            do i = 1 , ijk
            xmin = savex(1)
            xmax = savex(2)
            write(*,*)savex(i),savey(i)
            end do
```

```
      end if
      j = 1
      do i =1,npoints
          if(energy(i) .ge. xmin .and. energy(i) .le. xmax) then
             x(j) = energy(i)
             y(j) = eels(i)
             sigy(j) = sqrt(eels(i))
             j = j+1
             print*,x(j-1),y(j-1),sigy(j-1)
          end if
      end do
      ndata = j-1
           write(*,'(a\)')' Do you want to add an extra point to fit?
     &(y/n) -> '
      read(*,'(a1)')ans2
           if (ans2 .eq. 'y' .or. ans2 .eq. 'Y') then
           ndata = ndata+1
           do i = 1, ndata-1
             x(ndata-i+1) = x(ndata-i)
             y(ndata-i+1) = y(ndata-i)
             sigy(ndata-i+1) = sigy(ndata-i)
           end do
           write(*,'(a\)')'extra energy value [eV] -> '
           read(*,*)x(1)
           write(*,'(a\)')'extra eels value [cps] -> '
           read(*,*)y(1)
           sigy(1) = sqrt(y(1))
           end if
           print*,'ndata -> ',ndata
C          pause
C*********
c         Fitting 2nd order polynomial
c*********
      write(*,'(a\)')'Linear [1] or quadratic [2] fit? -> '
      read(*,*)npol1
      npol1 = npol1+1
      mp = ndata
      np = npol1
      call svdfit(x,y,sigy,ndata,a,npol1,u,v,w,mp,np,chisq,fpoly,npt)
      call svdvar(v,npol1,np,w,cvm,npol1)
      xnn(1) = 0.
      call function(xnn(1),ynn(1),a,npol1,p,fpoly)
           if (ynn(1) .lt. 0.) then
```

```
            ynn(1) = 0.
          end if
      i=1
      do while(abs(xnn(i)-x(2)) .ge. .05)
          i = i+1
          xnn(i) = xnn(i-1) + delx
          call function(xnn(i),ynn(i),a,npol1,p,fpoly)
          if (ynn(i) .lt. 0.) then
            ynn(i) = 0.
          end if
      end do
      do j = 2, ndata
          xnn(i) = x(j)
          call function(xnn(i),ynn(i),a,npol1,p,fpoly)
          xerrs(j) = 0.
          i= i+1
      end do
      ndatanew = i-1
      pause
      ijk = 0
101   continue
      write(*,*)'    CHOOSE PATCHING POINT with z-w-s-* sequence'
          write(*,'(1x,a,f12.6)')'chi-squared -> ',chisq
          do i = 1,npol1
             write(*,'(1x,e12.6,a,e10.4)')a(i),'  +-',sqrt(cvm(i,i))
          end do
          call plac(.85,0.,0.05,0.95)
          call howplt(0,1,2)
          call curv(npoints,energy,eels)
          call nolbox
          call howplt(9,0,1)
          call errbar(ndata,x,y,xerrs,sigy,0,1)
          call howplt(0,1,3)
          call scurv(ndatanew,xnn,ynn)
          call vg
          if(loopin() .eq. 1) go to 101
      call newpag
c *********
c ***  finding patching point
c *********
      if (ijk .gt. 0) then
           xmid = savex(1)
           write(*,*)savex(1),savey(1)
```

```
      end if
      i = 1
      do while (xnn(i) .le. xmid)
            xfinal(i) = xnn(i)
            yfinal(i) = ynn(i)
            i = i+1
      end do

      do j = 1,npoints
           if (energy(j) .gt. xmid) then
             xfinal(i) = energy(j)
             yfinal(i) = eels(j)
             i = i+1
            end if
      end do
      ntotal = i - 1
102   continue
           call howplt(0,1,3)
           call curv(npoints,energy,eels)
           call howplt(0,1,2)
           call curv(ntotal,xfinal,yfinal)
           call vg
           if(loopin() .eq. 1) go to 102
      call newpag
      call save(xfinal,yfinal,ntotal)
      print*,'Do you want to REDO extrapolation? (y/n) -> '
      read(*,'(a1)')answer
      end do

      return
      end
c$$$$$$$$$$$$$$$$$$$$$$$$$$$$$$$$$$$$$$$$$$$$$$$$$$$$$$$$$$$$$$$$$$$$$$$$$$$
*     READ IN DATA
*************************************************************************
      SUBROUTINE readin(ntotal,x,y)
      REAL x(*),y(*),card(10)
      CHARACTER filnam*12,ident*60
      LOGICAL fileok

      if (ntotal .le. 1) then
   50 CONTINUE
      write(*,5)
 5    format(' Filename with input data  -> ',\)
```

```
      READ(*,100)filnam
  100 FORMAT(A)
      INQUIRE(FILE=FILNAM,EXIST=FILEOK)
      IF(FILEOK)THEN
           OPEN(3,FILE=FILNAM,STATUS='OLD')
      ELSE
        PRINT *,'File does not exist -- try again.'
        GOTO 50
      ENDIF
      call datain(3,x,y,1000,ntotal,card,2,1,2,ident)
      CLOSE(3)
      end if

      return
      end

c&&&&&&&&&&&&&&&&&&&&&&&&&&&&&&&&&&&&&&&&&&&&&&
*     SAVE DATA
*************************************************************
      SUBROUTINE save(xfinal,yfinal,ntotal)
      REAL xfinal(*), yfinal(*)
      INTEGER ntotal
      CHARACTER filnam*12, ans5*1

      print*,'Do you want to save this data in a file? (y/n) -> '
      read(*,'(a1)')ans5
      if (ans5 .eq. 'y' .or. ans5 .eq. 'Y') then
          print*,'ENTER THE NAME OF THE OUTPUT  FILE'
          read(*,'(a)') filnam
          open(unit=8,file=filnam,status='unknown')
          do  i = 1, ntotal
            write(8,'(e12.6,a,e12.6)')xfinal(i),',',yfinal(i)
          end do
          close(8)
      end if

      return
      end
Ccccccccccccccccccccccccccccccccccccccccccccccccccccccccccccccccccccccccc
      subroutine vgcurs(x,y)
      real savex(60),savey(60)
      common/cdata/savex,savey,ijk
      ijk = ijk+1
```

```
      if (ijk.le.20) then
          savex(ijk) = x
          savey(ijk) = y
      end if
      return
      end

c*************
c
c************

      SUBROUTINE FPOLY(X,P,NP)
      DIMENSION P(NP)
      P(1)=1.
      DO 11 J=2,NP
        P(J)=P(J-1)*X
11    CONTINUE
      RETURN
      END

c**************
c
c**************
      subroutine function(x,y,a,np,p,fpoly)
      dimension a(np),p(np)
      call fpoly(x,p,np)
      y = 0.
      do i = 1, np
          y = y + a(i)*p(i)
      end do
      return
      end
c*************
c
c************
      SUBROUTINE DATAIN (IDEV,X,Y,NDIM,N,CARD,
     1  ICOL,ICX,ICY,IDENT)
      DIMENSION X (*), Y (*)
      DIMENSION CARD (ICOL)
      CHARACTER*(*) IDENT
      CHARACTER*2 JUNK
C
      BEL = CHAR (7)
```

```
C   First look for a '/*' in cols. 1&2; if none present, then reset
C   to the top.
10    READ (IDEV,'(A)',END=2) IDENT
      IF (IDENT .EQ. ' ') GO TO 10
      IF (IDENT(1:2) .EQ. '/*') GO TO 3
1     READ (IDEV,'(A)',END=2) JUNK
      IF (JUNK .EQ. '/*') GO TO 3
      GO TO 1
2     REWIND IDEV
3     K = 0
4     K = K + 1
      IF (K .GT. NDIM) GO TO 5
      READ (IDEV, *, ERR=7, END=5) CARD
      X (K) = CARD (ICX)
      Y (K) = CARD (ICY)
      GO TO 4
5     IF (K .GT. NDIM) WRITE (*,130) BEL,NDIM,NDIM
      N = K - 1
      WRITE (*,'(1H ,A)') IDENT
      WRITE (*,110) N
      RETURN
C  Error-handling portion of code.
7     WRITE (*,120) BEL,K
      K = K - 1
      GO TO 4
C-------------------------------------------------------------------------
110   FORMAT (' Number of points = ', I5)
120   FORMAT (' ',A1,'?DATIN-W-Unintelligible data in line ', I5,
     1 ' of file.'/' Line skipped: continue reading.')
130   FORMAT (' ',A1,'?DATIN-W-No. of data points exceeds ',I5/
     1 ' Return to main program with first ',I5,' points')
C-------------------------------------------------------------------------
      END
```

Vita

Reinaldo J. Gonzalez

Reinaldo (Rey) Jose Gonzalez was born on February 27, 1961 in Quito, Ecuador (South America). He earned a Bachelor of Science degree in Physics in April 1985, from Escuela Politecnica Nacional (Quito, Ecuador). From 1984 to 1988, he worked as an Assistant Professor at Escuela Politecnica Nacional. He earned a Master of Science degree in Physics in December 1990, and a Ph. D. in Materials Physics in July 1996, from Virginia Tech.